The Power Inversion Adaptive Array

by

C C Ko

A Doctoral Thesis

Submitted in partial fulfilment of the requirements
for the award of

Doctor of Philosophy of the Loughborough University of Technology

September 1981

Supervisor: Dr J E Hudson
Department of Electrical and Electronic Engineering

ABSTRACT

After the brief review on adaptive array processing, three fairly separate topices on the power inversion adaptive array are treated in this thesis. The first topic is the behaviour of a narrowband array using the stochastic gradient descent algorithm, with the environment assumed to rotate at constant velocity in the $\sin\theta$ domain. Conditions for steady state weight deviations and output power deterioration from optimal values due to the nonstationary environment are derived and are then used to determine the maximum scan rate of a radar sidelobe canceller. The second topic is the jamming rejection capability of a broadband array using tapped delay line processing. The results obtained are used for designing the tap spacing and number of taps of the delay lines as well as assessing, in terms of the number of variable weights, the relative advantage of the alternative broadband processing method using several narrowband array processors. The frequency distortions at various directions introduced by rejecting the jammers are also studied qualitatively. The third topic is the convergence behaviour of the broadband array when the stochastic gradient descent algorithm is employed. Comparison with the alternative broadband processing method is again given. A simple transformation preprocessor, independent of the external environment and capable of improving the convergence behaviour of using tapped delay line processing, is also derived.

ACKNOWLEDGEMENT

I would like to thank Dr J E Hudson for valuable discussion and criticisms as well as arranging the contract with the Royal Aircraft Establishment. I would also like to thank Prof J W R Griffiths for initially offering me the studentship.

TABLE OF CONTENTS

CHAPTER 1 REVIEW OF ADAPTIVE ARRAY PROCESSING

Before the development of chapter 2, this chapter will first give a brief review on adaptive array processing in general so as to form a framework for the three topics treated on the subject in this thesis. In the review, no attempt has been made to include all the possible references. This is due to the large number of related publications and furthermore, many detailed aspects in adaptive array processing, especially in connection with practical implementation, have not been studied or are still being actively researched at the time of writing.

The review is organized as follows. Section 1.1 discusses adaptive array processing in the framework of array processing. Section 1.2 traces the origin of adaptive array processing. Section 1.3 then classifies the important developments from three fundamental concerns in adaptive array processing. Section 1.4 discusses the "controls" commonly employed for achieving the adaptive processing. Finally, section 1.5 describes some experimental adaptive arrays and recent studies regarding more detailed aspects.

1.1 Within the Framework of Array Processing

In the context of signal processing, a receiving array is a number of transducing elements spatially distributed in a region, termed the aperture. The array output is formed by summing the weighted element outputs. Two common reasons for using a number of array elements are: (a) the aperture is too large to be fully filled so that sampling in the spatial domain is necessary and (b) the directional, frequency or other characteristics of the entire system have to be varied from time to time and this can easily be achieved by varying the element weights.

In conventional array synthesis[1,2], the weights are designed a priori, perhaps using optimization procedures, with regard to the look direction, beamwidth, average sidelobe level, component accuracies and/or other similar parameters. The method obviously leads to pre-determined array responses that may not match the actual operating environment which is seldom known precisely a priori and is often time-varying. However, the performance of the conventional array is usually adquate when the interferences are roughly isotropically distributed. In the other extreme, array performance is most probably inadquate in situations where there are strong deliberate or accidental jammers whose leakage powers, even through the sidelobes, would increase the array output noise power to unacceptable level. Therefore, with the advent of high power ECM systems in recent years, increasing interest has been directed to the use of complex adaptive array processing techniques to improve performance.

Best array performance is obtained by employing the weights which maximize the performance criterion in question, subject to the feasible measurements and a priori knowledge regarding the environment. This is often referred to as "optimum array processing" in the literature. Obviously, if the environment is time-varying, the optimal weights are also time-varying so that in a practical realization, the weights have to be updated by an algorithm using the most recent measurements and a priori knowledge concerning the environment. This is "adaptive array processing". Due to the nonzero settling time of the adaptive algorithm as well as the replacement of old by new measurements in a stochastic environment, an adaptive array is never able to achieve optimum weighting in a nonstationary and most probably, even stationary en-

vironment. However, the array is able to track the changing environment and most likely maintains near-optimum performance. Other side benefits, such as compensation for component inaccuracies and transducer distortion effects, can also be obtained. Introductory material for adaptive array processing can be found in [3-8].

1.2 Origin

Historically, the concept of adaptive array processing was first conceived in the retordirective antenna arrays invented by Van Atta[9] and developed by others[10,11] in the early 1950's and 1960's. Adaptivity in these arrays refers to the use of adaptive phase-cohering circuits so that a self-phased beam can be focused at a signal at unknown direction or position, provided that the element input noises are uncorrelated with one another. If this condition is satisfied, performance enhancement is obtained. In cases of severe jamming where the element input noises are highly correlated, however, there is no inherent adaptive protection.

The use of adaptive processing for rejecting interferences to improve performance then originated in the middle 1960's in many diverse fields. Some of the early initiative was taken in the radar sidelobe canceller of Howells[12], the adaptive filters and antenna arrays of Widrow[13-15], the adaptive equalizer of Lucky[16], the works by Byn[17], Mermoz[18] and Shor[19] on sonar arrays and the works by Capon[20] and Lacoss[21] on seismic arrays. Since these early systems were proposed, the development of adaptive array processing, especially in the area of communication antenna arrays, has been rapid and numerous papers have been appearing on the subject.

1.3 Classifications of Important Developments

To outline the important developments briefly and systematically, the various adaptive arrays of general interest in the literature are now classified into categories according to: (a) the way the a priori knowledge about the signal is utilized, (b) the adaptive algorithm and its implementation and (c) the performance criterion. From the discussion of section 1.1, these are the most fundamental concerns in adaptive array processing.

1.3.1 Classification (a) - the way the signal a priori knowledge is utilized

Adaptive arrays can be divided roughly into three categories in this section. The a priori knowledge about the signal is used to generate a reference input, highly correlated with the signal but almost uncorrelated with the interferences, in the early adaptive antenna arrays proposed by Widrow[11]. Thus, by adjusting the weights so that the array output approaches the reference input in a mean square sense, the interferences are rejected while the signal is preserved. Obviously, these arrays are of interest if the reference input can easily be derived as, for example, in coded communication systems.

In contrast, the adaptive arrays derived by Griffiths[22] and Frost[23] from that of Widrow as well as the early seismic arrays studied by Lacoss[21] require a priori knowledge about the signal direction and possibly, the shape of the signal power density spectrum for formulating constraints on the weights to preserve the signal while minimizing array output power to reject the interferences. In [23], for instance, the weights are subject to a set of hard linear equality constraints so that the frequency

response at the look direction is pre-determined and do not vary with the updating of the weights. The term "hard constraint" is coined relative to the term "soft constraint" which means a constraint that can be violated with the amount of violation proportional to the "forces" set up in the algorithm forcing the weights to satisfy the constraint. One early difficulty in employing simple schemes like that just described is the cancellation of the signal even if there are slight mismatches between the actual signal characteristics, for example, direction[24], and that assumed to be known and used by the array. The problem is overcome by using additional constraints[25-27] to decrease the sensitivity of the array towards such mismatches. This type of arrays is of most interest in radar, sonar and seismology where, apart from the direction, the signal structure is seldom known in detail a priori.

Lastly, the power inversion array, suggested by Zahm[28] and Compton[29], only requires the signal power to be small for its operation. The array functions by the phenomenon that if optimum weighting is used, the output power component due to a jammer decreases roughly linearly with increase in the jammer's power. In situations where there are only two jammers, inversion of jammer power ratio or "power inversion" is obtained. Thus, acquisition of a weak signal in the presence of strong jammers is possible even without any other a priori knowledge about the signal. Having the simplest structure, the power inversion array is most attractive when the signal is weak or can easily be filtered out, as in frequency hopping systems. The early radar sidelobe canceller[12] as well as later developments of the canceller by Appleba-

um[30] and Brennan[31] can be regarded as a special form of power inversion array with a carefully designed quiesent response.

1.3.2 Classification (b) - the adaptive algorithm and its implementation

With the adaptive algorithm, the weights will be updated and converge towards the optimal values. The convergence behaviour of the weights and the other parameters of interest is clearly one important characteristic of the algorithm. Note that due to the stochastic nature of the environment and the essential replacement of old by new datas used in every algorithm to track the environment, the weights will not converge exactly to the optimal values but will undergo stochastic processes in the steady state, even in stationary environments[13,32]. First used by Widrow[13], "misadjustment" is a measure of the increase in output noise power due to the stochastic processes of the weights and is another important characteristic of the algorithm used. Not surprisingly, faster or better convergence behaviour can be achieved only at the expense of increasing misadjustment and vice versa, unless a superior algorithm can be employed. Evidently, in comparing the convergence behaviour from using various algorithms, the misadjustment should be kept constant.

Especially in the early adaptive arrays[12,15,19,21], the stochastic gradient descent algorithm has received the most interest so far. Analogue implementation with correlation loops and digital implementation have been proposed. The algorithm, however, has the disadvantage that the convergence behaviour is dependent on the external environment and can be very slow in some situations of severe jamming. Better convergence behaviour can be

obtained at the cost of changing the basic structure with various modifications, including hard-limiting[33], modifications of feedback loops[32,34] and the use of preprocessors[35]. On the other hand, simpler, cheaper but slower implementation can be achieved by using perturbation techniques[36] in conjuction with search algorithms[37-39].

All these algorithms are sometimes referred to as closed-loop algorithms, in contrast to open-loop algorithms which do not use the array output and hence do not have any feedback loop. These latter more complex algorithms are much faster but require higher computation rates and with no feedback loop, have lost most of the side benefits of compensating for nonideal component characteristics. They are thus of most interest in sonar, seismology or radar when due to the low data rate, all-digital array processing is possible and component inaccuracy is not a problem. The algorithms based on the inversion of the sampled covariance matrix[40], Woodbury identity[41] and Kalman filtering[42] as well as that discussed in [43] are some well known open-loop algorithms.

Of course, both closed- and open-loop algorithms can be employed together so that some of the advantages of both types of algorithms are obtained. An example is the algorithm based on the Newton-Raphson[44] procedure.

1.3.3 Classification (c) - the performance criterion

Since the performance criterion depends on the signal characteristics and the purpose of the array, the classification here, being widely used in the literature, is closely related to that of subsection 1.3.1.

In the arrays proposed by Widrow[15] and Griffiths[22], the

performance criterion is minimum mean square error. This corresponds, in the former arrays, with the minimization of mean square error between the reference input and the array output to reject interferences and is the reason for the terminology "LMS (Least Mean Square) algorithm" used by Widrow to refer to the use of the stochastic gradient descent algorithm in his array.

In association with arrays employing constraints, another widely used criterion is constrained minimization of output power. This refers to the minimization of output power to reject the interferences while the signal is preserved by the constraints. When simple linear look direction constraints are used, the optimal weights resulting from this criterion are the same as those from the criteria of maximum likelihood and maximum likelihood ratio. The array is therefore sometimes said to use the latter two criteria in such cases. Similar to Widrow, Frost [23] introduced the terminology "CLMS (constrained LMS) algorithm" to refer to using the stochastic gradient descent algorithm in his simple linear look direction constrained array.

The last widely used criterion, especially in radar arrays [12,30,31], is maximum signal to noise power ratio.

In [8,45,46], all these criteria are discussed, compared and shown to define very similar optimal weights, especially when the array is narrowband.

1.4 Controls for achieving the Adaptive Processing

In almost all adaptive arrays investigated in the literature, the control of the processing for the element inputs has been achieved by using quadrature/complex weighting or variable

gain tapped delay lines[15]. When the array is narrowband, full control of the array response can be obtained by using, behind each element, quadrature weights or with negligible difference, a 2-tap delay line with a quarter wavelength spacing at the centre frequency. When the array is broadband, however, the tapped delay lines should theoretically have infinite numbers of taps if full control is required. Alternatively, the array frequency band can be divided into an infinite number of "frequency bins", with the element inputs within the frequency bins being processed in parallel by using an infinite number of similar narrowband array processors. Of course, in practice, the number of taps and narrowband processors will be finite and should be as small as possible.

Other methods of controlling the processing in adaptive arrays are of course possible. In narrowband arrays, full control can also be achieved by using amplitude and phase weighting behind each element. Amplitude only[47] and phase only[48] weighting can also be used when the number of elements is large so that full control is cumbersome and not essential. Some techniques for reducing the number of weights without seriously impairing performance are discussed in [49,50]. Furthermore, control of the processing via the Nolen beamforming[35,51] and Davies null steering[52] networks is also possible and can lead to better convergence behaviour. In broadband arrays, control of the processing based on the architecture of adaptive lattice filters [53] has also attracted interest recently. Finally, note that though the discussion in previous sections was addressed principally to the two common processing structures of the last paragraphs, the fundamental concepts of adaptive array optimality are

applicable to all methods of controlling the processing. However, the detailed aspects, for example, implementations of algorithms, may well be very different for different processing structures.

1.5 Experimental Arrays and Detailed Aspects

Because of the intensive research in adaptive array processing in the past two decades, most of the fundamental theoretical concepts in the subject have been formulated. Recent publications therefore incline towards more detailed aspects or discussing experimental arrays. Some of the important published works in these areas will now be briefly discussed.

Two of the earliest experimental adaptive arrays based on reference inputs were described by Reigler [54] and Susan [55]. The latter array, though not very successful, was for use at UHF television stations and employed a perturbation algorithm. The former was a 2-element LMS array intended for RF communication purpose and was one of the earliest to demonstrate practically the advantages and feasibility of adaptive array processing. A similar more realistic 4-element array was subsequently described by Compton [56] who later modified it for use in PN-coded spread spectrum communication systems [57]. The fundamental characteristics of the LMS array were verified in these experiments which also led to the recognition of two practical difficulties: multiplier offset voltage [58] and reference loop phase shift [59]. The use of artifical noise [60] was suggested to overcome the former problem. Associated with arrays using reference inputs, some other detailed aspects studied include the grating nulls due to dif-

ferent element directional patterns[61], weight errors[62] and the bandwidth of a 2-element tapped delay line broadband array[63].

With regard to arrays using constraints, Griffiths[64] discussed an experimental application of the CLMS and his P-vector algorithms in an HF radar array. Furthermore, Giraudon[65] discussed an experimental sonar array based on the Gram-Schmidt orthogonization procedure, whereas Windram[66] discussed a successful perturbation array for use at UHF television stations. The advantages of adaptive array processing were again illustrated from these experiments. With respect to more detailed studies, the accuracies required for D/A and A/D convertors, used in some closed-loop arrays before analogue weighting and open-loop arrays for digitizing element inputs respectively, were investigated by Hudson[67]. The performance deterioration resulted from various distortion effects and component inaccuracies was studied by Vural[68] and Cox[69].

The performance with respect to signal direction error of 2-element arrays using constraints, reference input and the principle of power inversion was compared by Compton[70].

In connection with many open-loop algorithms, the precision requirements for estimating the covariance matrix and subsequent computing of the optimal weights were discussed by Reed[40], Nitzberg[71] and Boroson[72].

The bandwidth of a narrowband Applebaum array was studied by Mayhan[73] with regard to antenna distortion and channel mismatch effects.

In the field of RF at large, the choice of various implementations at present depends very much on the available device

technologies. Some general discussion in this area was given by Doctor[74] and Masenten[75].

Finally, Compton[76] presented an overview of research on adaptive antenna arrays for communication purpose in the Ohio State University.

CHAPTER 2 INTRODUCTION

This thesis ic concerned with three fairly separate topics on the power inversion array[28,29]. Each topic is properly introduced, discussed and concluded in each of chapters 3-5. After the brief review on adaptive array processing in the last chapter, the power inversion array of interest will first be discussed in more detail before the three topics are briefly introduced in this chapter.

2.1 The Power Inversion Array

In a general M-element power inversion array, the channel gain for one of the elements is held constant at unity, whereas those for the other elements are adaptively controlled, without any constraint, to minimize output power. This results in the phenomenon of power inversion mentioned in subsection 1.3.1. Intuitively, the purpose of having one element with constant processing gain is to prevent the trivial condition in which all the elements have zero processing gains and the output power is truly minimized at zero. Of course, regarding the input from the constant gain element as the reference input, the power inversion array can be viewed as a special case of Widrows' arrays[15] which use reference inputs. Furthermore, the power inversion array can also be considered as one using constraints[25], the constraints being on the processing of the constant gain element.

The main advantage of the power inversion array over the other types of adaptive arrays lies in its simplicity. The simplicity is obtained since no inherent mechanism is used in the adaptive processing to preserve the signal. The array is therefore

of most interest in applications where the signal is small or can easily be filtered out before the adaptive processing so that the array, when attempting to reject the interferences by minimizing output power, is not responding to and so will not reject the signal. Uses of the power inversion array can thus be envisaged in, for example, spread spectrum systems where the signal's power is around or below receiver noise power, radar systems where no target return is present over most of the time and frequency hopping systems where the signal can easily be filtered out.

In communication applications, the array usually has identical elements with isotropic directional responses in the plane of interest. Furthermore, adjacent elements are usually spaced by the order of half a wavelength at the centre frequency. When used in radar, however, the power inversion array usually takes the form of a sidelobe canceller[30]. The element with constant processing gain is now a well-designed high-directivity antenna pointing towards the target returns, while the other elements are usually isotropic in the plane of interest with antenna gains roughly equal to the sidelobe gain of the high-directivity antenna. Moreover, adjacent element spacings are usually very much greater than half a wavelength at the centre frequency.

The power inversion array concerned in this thesis is shown in fig.2.1. As indicated, the M-element array is linear and equally spaced by d, with the end element on the left having constant unity processing gain. The reason for using the linear equally spaced array is simplicity and popularity, though many derivations in this thesis can easily be extended to arrays with other geometries. The reason for choosing one of the end elements but not the

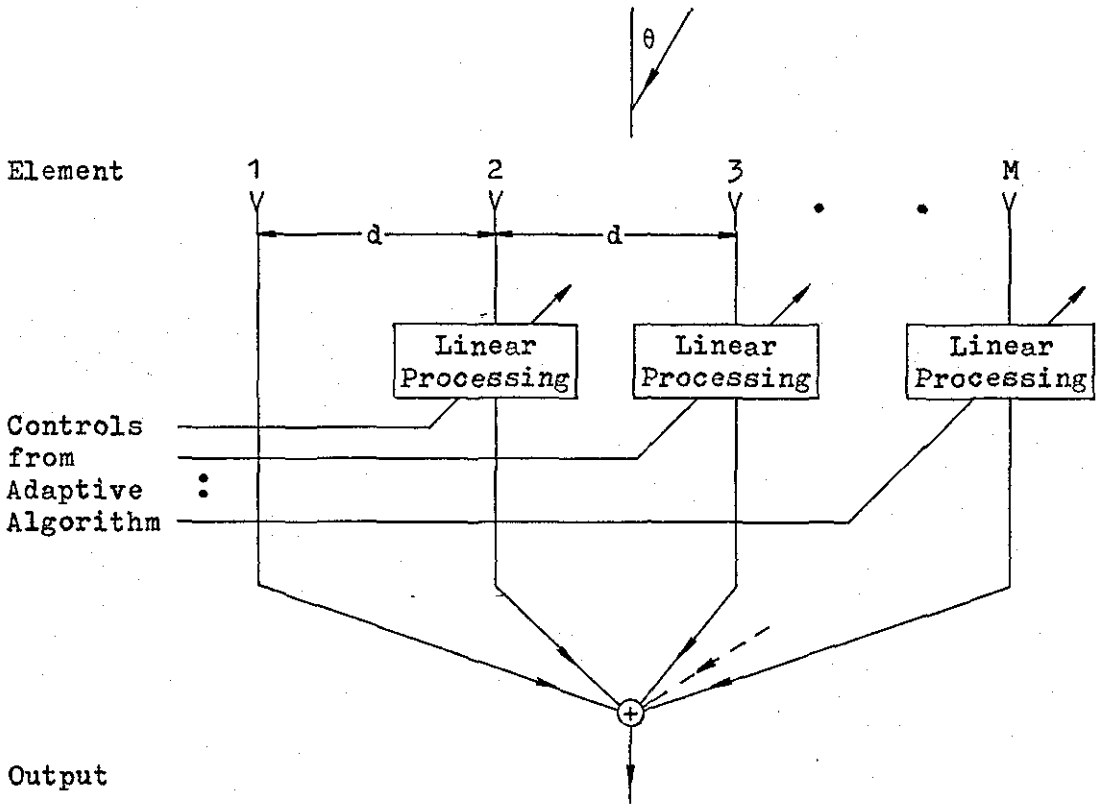

Fig.2.1 The power inversion array concerned in this thesis.

others to have constant processing gain is that if this is not so, the array may not be able to utilize its M-1 spatial degrees of freedom to reject M-1 directional jammers in certain situations. Consider, for example, a 3-element narrowband array in an environment consisting of only 2 directional jammers. If the directions of the jammers are such that the centre element has to have zero processing gain for the two jammers to be nulled together, then obviously, if the centre element has constant unity processing gain, the array cannot null the two jammers together. The array concerned is intended for communication purpose and thus, for simplicity, all the elements are assumed to be identical with isotropic directional responses in the plane of interest, except in section 3.10 where under the conditions discussed there, some of the results derived are applied directly to the sidelobe canceller.

Furthermore, without loss of generality, all the simulation results in this thesis will be for the element spacing of half a wavelength at the centre frequency.

For simplicity again, the array is assumed to be in an environment consisting of only N independent directional jammers and receiver noise. For proper operation, the number of elements is assumed to be greater than the number of jammers. The nth jammer's power and direction (initial direction in the rotating environment of chapter 3) will be denoted by s_n and θ_n respectively, the convention for measuring direction being indicated by θ in fig.2.1. Receiver noise is assumed to be independent between elements and of power s_0. When the array is broadband, bandpass filtering is assumed to be used so that all the power density spectrums are zero outside the array frequency band from $(1-B/2)f_0$ to $(1+B/2)f_0$ where f_0 is the centre frequency and B the array relative bandwidth. For convenience, the array frequency band and relative bandwidth will simply be referred to as the band and bandwidth respectively. Note that because of the bandpass filtering, receiver noise will, in addition, be taken as having a flat power density spectrum across the whole band. The signal, assumed to be weak or filtered out before the adaptive processing, is neglected in this thesis which is not concerned with the behaviour or effects of all signal parameters. The discussion in the last and this paragraphs gives the usual assumptions made regarding the power inversion array and its operating environment and will be used in this thesis. Of course, there are also other assumptions associated with each topic and these will be discussed in the appropriate chapters. Note that for convenience, some of the symbols and terminologies

used in this thesis may have different meanings at different places. In cases where ambiguity arises, however, clarification will be given.

2.2 The Three Topics

To the knowledge of the author, the three topics concerned have not been studied before in the literature and the investigations presented in this thesis are original. Although the thesis treats only the array discussed in the last section, many of the problems investigated and proposal suggested are also relevant in adaptive array processing in general.

The first topic treated in chapter 3 concerns the behaviour and performance of the narrowband power inversion array in a nonstationary environment. For simplicity and mathematical tractability, the array is assumed to employ the widely used stochastic gradient descent algorithm and the nonstationarity is modelled by the jammers rotating with equal angular velocities in the $\sin\theta$ domain. The practical significance of the nonstationarity is clearly that it corresponds roughly to the situation when the array is moved or rotated. The main reason for the study is that due to mathematical difficulties, the behaviour and performance of adaptive arrays have always been investigated assuming the environment is stationary, although the prime use of adaptive arrays is clearly to track time-varying environments. The main objective of the study is thus to provide insight in the latter situations.

Chapters 4 and 5 discuss two topics connected with the broadband implementation of the power inversion array. The two usual methods of achieving broadband adaptive array processing are by using several similar narrowband array processors in parallel or

by employing tapped delay lines[15]. The use of tapped delay lines, since first proposed, has not yet been studied in detail and the relative advantages of the two methods still remain unresolved. Chapter 4 investigates the ability of the tapped delay line power inversion array to reject jammers so that the tap spacing and number of taps required of the delay lines can be determined. Comparison with the other broadband processing method can then be made in terms of the number of variable weights needed. Chapter 5 investigates the convergence behaviour of the tapped delay line array so that comparison with that using the other broadband processing method can be made. The widely used stochastic gradient descent algorithm is assumed to be employed. In subsequent analysis, a transformation preprocessor depending only on the array parameters is derived and shown to lead to better convergence behaviour of the tapped delay line array.

CHAPTER 3 THE POWER INVERSION ARRAY IN THE ROTATING ENVIRONMENT

3.1 Introduction

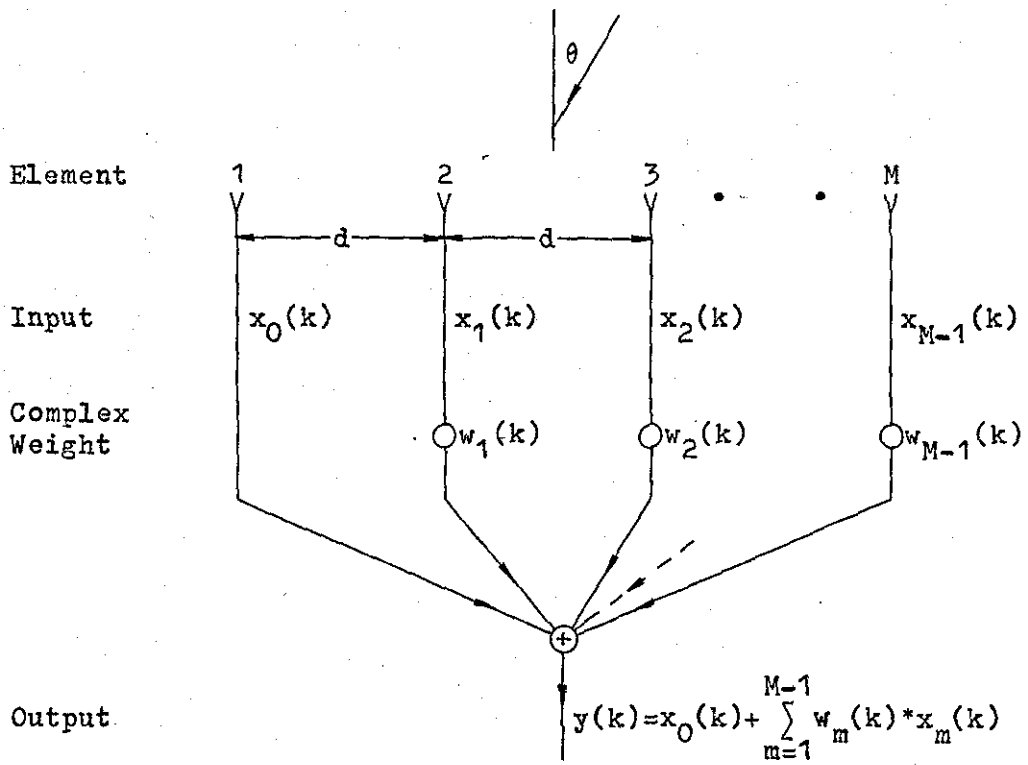

Fig.3.1 Narrowband power inversion array using complex weights.

This chapter investigates the behaviour of the narrowband power inversion[28,29] array in a nonstationary environment. Fig. 3.1 shows the narrowband array of interest. In addition to the assumptions of section 2.2, the array is assumed to employ complex weights, with the widely used stochastic gradient descent algorithm for updating. Furthermore, the jammers in the external environment are assumed to rotate with equal angular velocities in the $\sin\theta$ domain. These assumptions concerning the array and nonstationarity are made mainly because of simplicity and mathematical tractability, although as discussed below, they are physically maeaningful as well.

Due to mathematical tractability, almost all previous eval-

uations of adaptive algorithms and arrays have been based on the assumption that the operating environment is stationary. The theories and results derived using this assumption are relevant just after abrupt changes occur in the environment, as when the array is first switched on. However, when the movement of the jammers relative to the array is smooth and continuous, the assumption clearly does not apply. The main objective of the investigation is therefore to provide insight in the latter situation, when the stochastic gradient descent algorithm is employed on the narrowband power inversion array.

A related study by Widrow on the nonstationary characteristics of the adaptive LMS filter is given in [77]. The nonstationarity concerned in [77] for the adaptive filter, however, is different from that in the adaptive array situation. In [77], the nonstationarity is characterized by the optimal weights which are assumed to undergo stationary random processes uncorrelated with the stationary random process of the input. In the case of the adaptive array, the random input processes are nonstationary and determine also the random optimal weight processes.

The relative movement of the jammers can be due to the actual motions of the jammers and/or the motion of the array itself. The former situation can obviously be very complicated, since usually, each jammer can move independent of all the others. However, in applications like scanning radars or airborne communication systems where the arrays are mobile, it can be speculated that, since the jammers and arrays are normally separated by long distances, the motions of the arrays will be more significant than that of the jammers. Obviously, as smooth motion of the array

corresponds roughly to a rotation of the environment, the investigation is relevant in many practical situations.

This chapter is organized as follows. In section 3.2, the notations, terminologies and basic formulations associated with the algorithm and the array are discussed in general terms. The behaviour of the array in stationary environments is then studied in section 3.3 to introduce the usual methods used in analysing adaptive arrays and enable comparisons to be made later. Investigation in the rotating environment is given in sections 3.4-3.10. Following the mathematical formulation of the environment in section 3.4, the average weights and output power in the steady state are solved, in sections 3.5 and 3.6 respectively, and discussed in general terms. To complete the general discussion, section 3.7 discusses the transient convergence behaviour of the array to the steady state. The more interesting steady state behaviour is then studied in more detail in section 3.8 by solving some of the equations explicitly and using simulation results for the single-jammer situation. Similarly, section 3.9 discusses the multi-jammer situation. A direct application of the results to determine the maximum scan rate limitation of a radar sidelobe canceller is given in section 3.10 as a practical example. Conclusions are drawn in section 3.11.

Finally, the principal derivations and deductions of this chapter were published in [78].

3.2 Preliminary Discussion and Fundamental Formulations

In this section, the notations, terminologies and fundamental formulations associated with the stochastic gradient descent algorithm on the array of interest are discussed. The discussion

will be general and all the results and formulations are applicable to all stationary and nonstationary environments.

Firstly, using the notation in fig.3.1, the input vector X(k) and weight vector W(k) will be defined in this chapter as

$$X(k)^T = [x_1(k)^* \; x_2(k)^* \cdots x_{M-1}(k)^*] \tag{3.1a}$$

and

$$W(k)^T = [w_1(k)^* \; w_2(k)^* \cdots w_{M-1}(k)^*] \tag{3.1b}$$

where k, T and * denote the kth sampling instant, complex conjugate transpose and complex conjugate respectively. Note that since complex weights are used, complex variables are employed. Also, for simplicity, discrete rather than continuous time formulation is used. Clearly, from the definitions in (3.1) and fig.3.1, the array output is

$$y(k) = x_0(k) + W(k)^T X(k). \tag{3.2}$$

From (3.2), the output power for the weight vector W(k) is

$$\begin{aligned} s_W(k) &= \overline{y(k)^* y(k)} \\ &= s_x(k) + W(k)^T R_0(k) + R_0(k)^T W(k) + W(k)^T R(k) W(k) \end{aligned} \tag{3.3}$$

where

$$s_x(k) = \overline{x_0(k)^* x_0(k)}, \tag{3.4a}$$

$$R_0(k) = \overline{x_0(k)^* X(k)}, \tag{3.4b}$$

$$R(k) = \overline{X(k) X(k)^T} \tag{3.4c}$$

and the overbar denotes ensemble average. Among the second order input statistics of (3.4), R(k) will be referred to as the covariance matrix, in accordance with usual terminology. It can be shown[31] that the gradients of the output power with respect to the weights are given by the gradient vector

$$\nabla_W(k) = 2R_0(k) + 2R(k)W(k) \tag{3.5}$$

which is obviously the same as

$$\nabla_W(k) = 2\overline{y(k)*X(k)}. \tag{3.6}$$

Therefore, to minimize the output power to reject the jammers, the output must be uncorrelated with the input vector so that the gradient vector is zero. Clearly, this is in accordance with Wiener filter theory. The optimal weight vector for minimum output power is thus, from (3.5),

$$W_{opt}(k) = -R(k)^{-1}R_0(k). \tag{3.7}$$

Substituting this into (3.3) gives the minimum or optimal output power as

$$\begin{aligned} s_{opt}(k) &= s_x(k) - R_0(k)^T R(k)^{-1} R_0(k) \\ &= s_x(k) + R_0(k)^T W_{opt}(k). \end{aligned} \tag{3.8}$$

Evidently, from (3.7), the optimal weight vector depends on the second order input statistics of the environment. To maintain good performance in nonstationary environments, the adaptive array therefore has to periodically make measurements regarding the environment and utilize the information via an algorithm to update the weights. In discrete time formulation, the stochastic gradient descent algorithm used for this purpose can be written as

$$W(k+1) = W(k) - \alpha y(k)*X(k) \tag{3.9}$$

where α is a positive constant, termed the feedback factor for the algorithm. From (3.6), the weight vector adjustment per sampling period can be seen to be a stochastic approximation of the gradient vector, scaled by minus the feedback factor to be in the dir-

ection of decreasing output power. Thus, on average at least, the algorithm, which is obviously named after these features, is always attempting, by adjusting the weights, to minimize the output power to reject the jammers.

Using (3.2) and (3.9), all the statistics concerning the behaviour of the array can be derived, at least theoretically, once the statistical properties of the inputs are specified. For ease of analysis, the inputs at different sampling instants are commonly and will be assumed to be independent. Since, from (3.9), the present weights depend only on inputs at previous sampling instants, this assumption clearly leads to the important independence of the inputs and weights at the same sampling instant.

The average weight vector is obviously one of the statistics of interest. With the weights and inputs at the same sampling instant being independent, its behaviour can be found by taking the ensemble average of (3.9) giving

$$\begin{aligned}\overline{W(k+1)} &= \overline{W(k)} - a\overline{y(k)^{*}X(k)} \\ &= \overline{W(k)} - a[\overline{X(k)X(k)^{T}W(k)} + \overline{x_{0}(k)^{*}X(k)}] \\ &= [I - aR(k)]\overline{W(k)} - R_{0}(k). \end{aligned} \tag{3.10}$$

Evidently, the average weight vector at any sampling instant can be calculated from this recursive equation using the second order input statistics and initial weight vector.

The other statistics of interest are the various components of the average output power. By taking the ensemble average of $y(k)^{*}y(k)$ and again using the independence of the inputs and weights at the same sampling instant, the average output power is

$$s(k) = \overline{y(k)^{*}y(k)}$$

$$= \overline{x_0(k)*x_0(k)} + \overline{W(k)^T x_0(k)*X(k)}$$

$$+ \overline{x_0(k)X(k)^T W(k)} + \overline{W(k)^T X(k)X(k)^T W(k)}$$

$$= s_x(k) + \overline{W(k)}^T R_0(k) + R_0(k)^T \overline{W(k)} + \overline{W(k)^T R(k) W(k)}. \qquad (3.11)$$

Note that this is the actual ensemble average output power and is different from the output power of (3.3). The latter is obviously for a "particular" and hence deterministic weight vector and thus, is applicable for a particular sample of the weight vector process. Defining $\Delta W(k)$ as

$$\Delta W(k) = W(k) - \overline{W(k)} \qquad (3.12)$$

so that

$$\overline{\Delta W(k)} = 0 \qquad (3.13)$$

and using the mathematical theorem

$$\mathrm{tr}(A^T B) = \mathrm{tr}(B^T A) \qquad (3.14)$$

for two matrices A and B of the same dimensions, (3.11) becomes

$$s(k) = s_y(k) + s_{wt}(k) \qquad (3.15)$$

where

$$s_y(k) = s_x(k) + \overline{W(k)}^T R_0(k) + R_0(k)^T \overline{W(k)} + \overline{W(k)}^T R(k) \overline{W(k)} \qquad (3.16)$$

and

$$s_{wt}(k) = \overline{\Delta W(k)^T R(k) \Delta W(k)} = \mathrm{tr}[R(k) \overline{\Delta W(k) \Delta W(k)^T}]. \qquad (3.17)$$

Clearly, the average output power is separated into two positive components. $s_{wt}(k)$ is the component due to the noisiness of the weights about their average values resulting from the algorithm replacing, effectively, old with new inputs. For convenience, this will be referred to as weight variance noise. In contrast,

being equal to the output power of (3.3) if the particular weight vector W(k) is replaced by the average weight vector $\overline{W(k)}$, $s_y(k)$ is the component resulting from the average weight vector. Clearly, it will be equal to the average output power if there is no weight variance. Thus, for convenience, the term output power will henceforth be used to mean $s_y(k)$. By substituting (3.7) and (3.8) into (3.16), the output power becomes

$$s_y(k) = s_{opt}(k) + [\overline{W(k)} - W_{opt}(k)]^T R(k)[\overline{W(k)} - W_{opt}(k)]. \quad (3.18)$$

Obviously, with $s_{opt}(k)$ as the minimum output power possible, the second term is the component of output power due to the difference or "lag" of the average from the optimal weight vector. This lag results from the finite convergence rate of the algorithm so that for instance, perfect tracking of the optimal weights in nonstationary environments is not achieved, even on average in the steady state. From (3.18), the output power is expressed, in addition to the covariance matrix, in terms of the optimal output power, optimal and average weight vectors. Since the behaviour of these, as specified in (3.7), (3.8) and (3.10), depends only on the second order input statistics, the behaviour of the output power is also given from only the second order input statistics. In contrast, the weight variance noise of (3.17) depends also on the weight covariance matrix $\overline{\Delta W(k)\Delta W(k)^T}$ in addition to the covariance matrix.

To find the behaviour of the weight covariance matrix and hence, that of the weight variance noise, (3.10) is subtracted from (3.9) yielding, after substituting (3.7) and (3.12),

$$\Delta W(k+1) = \Delta W(k) - \alpha y(k)^* X(k) + \alpha R(k)[\overline{W(k)} - W_{opt}(k)]. \quad (3.19)$$

Post-multiplying both sides with their own complex conjugate tra-

anspose and taking ensemble average, this is shown in appendix 3.12.1 to give rise to

$$\overline{\Delta W(k+1)\Delta W(k+1)^T} = \overline{\Delta W(k)\Delta W(k)^T} + a^2\overline{y(k)^*y(k)X(k)X(k)^T} \qquad (3.20)$$
$$- a^2R(k)[\overline{W(k)} - W_{opt}(k)][\overline{W(k)} - W_{opt}(k)]^TR(k)$$
$$- aR(k)\overline{\Delta W(k)\Delta W(k)^T} - a\overline{\Delta W(k)\Delta W(k)^T}R(k).$$

Theoretically, this is a recursive equation from which the weight covariance matrix at any sampling instant can be calculated from the statistics of the inputs. However, the equation is obviously very complex and in particular, fourth order statistics are involved in the second term. To decompose this term, the inputs are commonly and will be assumed to be zero mean complex Gaussian[79] random processes so that all fourth order input statistics can be expressed in terms of second order statistics by using the mathematical theorem

$$\overline{z_1^*z_2z_3^*z_4} = (\overline{z_1^*z_2})(\overline{z_3^*z_4}) + (\overline{z_1^*z_4})(\overline{z_2^*z_3}) \qquad (3.21)$$

for four zero mean complex Gaussian random variables z_1, z_2, z_3 and z_4. Using this theorem, (3.20) is then shown in appendix 3.12.2 to become

$$\overline{\Delta W(k+1)\Delta W(k+1)^T} = \overline{\Delta W(k)\Delta W(k)^T} \qquad (3.22)$$
$$+ a^2[s_y(k) + s_{wt}(k)]R(k) + a^2R(k)\overline{\Delta W(k)\Delta W(k)^T}R(k)$$
$$- aR(k)\overline{\Delta W(k)\Delta W(k)^T} - a\overline{\Delta W(k)\Delta W(k)^T}R(k).$$

This slightly simplified recursive equation, in which only second order input statistics are involved, can be used in conjuction with (3.17) to derive expressions for the weight variance noise.

Summarizing, the stochastic gradient descent algorithm has

been formulated mathematically on the narrowband power inversion array in this section. Because of the algorithm and the stochastic environment, the average output power consists of: (a) weight variance noise which is due to the variances of the weights about their average values and (b) output power which results from the average weights and is composed of the optimal output power plus a component due to the lagging of the average from the optimal weights. By using the common simplifying assumptions, general equations for determining the behaviour of the average weight vector and the various components of the average output power were derived.

3.3 Behaviour in Stationary Environments

Before studying the rotating environment, the behaviour of the array in stationary environments will first be investigated by using the formulations of the last section. Comparison can then be made later and the usual analysis in adaptive array processing can be introduced.

In stationary environments, all the input statistics are time-independent. The second order input statistics of (3.4) can thus be written as

$$s_x(k) = s_x, \tag{3.23a}$$

$$R_0(k) = R_0 \tag{3.23b}$$

and

$$R(k) = R. \tag{3.23c}$$

Using (3.7) and (3.8), the optimal weight vector and output power then become

$$W_{opt}(k) = W_{opt} = -R^{-1}R_0 \tag{3.24}$$

and

$$s_{opt}(k) = s_{opt} = s_x - R_0^T R^{-1} R_0 \tag{3.25}$$

which are also time-independent.

To study the behaviour of the average weight vector, (3.24) is substituted into (3.10) yielding

$$\overline{W(k+1)} - W_{opt} = [I - aR][\overline{W(k)} - W_{opt}]. \tag{3.26}$$

With W(0) denoting the initial weight vector, this implies

$$\overline{W(k)} = W_{opt} + [I - aR]^k[W(0) - W_{opt}]. \tag{3.27}$$

Using the polar decomposition

$$R = \sum_{m=1}^{M-1} h_m H_m H_m^T \tag{3.28}$$

where h_m, m=1,··,M-1, is the mth largest eigenvalue of R with H_m as the corresponding normalized eigenvector, (3.27) can be written as

$$\overline{W(k)} = W_{opt} + \sum_{m=1}^{M-1} e_m(k) H_m \tag{3.29}$$

where $e_m(k)$ is the component of $\overline{W(k)}-W_{opt}$, the average weight vector lag, in the direction of H_m and converges according to

$$e_m(k) = (1 - ah_m)^k e_m(0). \tag{3.30}$$

Evidently, in stationary environments, the average weight vector will eventually converge to the optimal weight vector. Specifically, if the average weight vector lag is expressed in component form with H_m as the mth of the M-1 basis vectors, then the mth component $e_m(k)$ will converge, independent of the other components, to zero exponentially with a time constant of $-1/\ln|1-ah_m|$ sampl-

ing period. Obviously, the convergence is subject to $|1-\alpha h_m|$ being less than unity or since the sum of all the eigenvalues is equal to the trace of the covariance matrix,

$$\alpha < \frac{2}{trR}. \tag{3.31}$$

Due to weight variance noise, the feedback factor will be shown later to be limited to well below this bound. αh_m will thus be much smaller than unity and the time constant for the convergence of $e_m(k)$ can be approximated by

$$\tau_m = \frac{-1}{\ln|1 - \alpha h_m|} \approx \frac{1}{\alpha h_m} \text{ sampling period.} \tag{3.32}$$

By substituting (3.25), (3.28) and (3.29) into (3.18), the behaviour of the output power is easily expressed as

$$s_y(k) = s_{opt} + \sum_{m=1}^{M-1} h_m |e_m(k)|^2. \tag{3.33}$$

Obviously, the output power converges eventually to the optimal output power, with convergence behaviour also described by that of $e_m(k)$. Specifically, the difference between the output and optimal output power is given by the sum of M-1 components, the mth component having power $h_m|e_m(0)|^2$ initially and converging exponentially to zero with a time constant twice that of (3.32).

After the transient convergence period or in the steady state in stationary environments, the average weight vector will be equal to the optimal weight vector and with the output power given by the optimal output power, the average output power will compose of only the optimal output power plus weight variance noise. In these circumstances, (3.17) and (3.22) for determining the weight variance noise become

$$s_{wt}(k) = \overline{tr[R\Delta W(k)\Delta W(k)^T]} \tag{3.34}$$

and

$$\overline{\Delta W(k+1)\Delta W(k+1)^T} = \overline{\Delta W(k)\Delta W(k)^T} \tag{3.35}$$
$$+ a^2[s_{opt} + s_{wt}(k)]R + a^2\overline{R\Delta W(k)\Delta W(k)^T R}$$
$$- a\overline{R\Delta W(k)\Delta W(k)^T} - a\overline{\Delta W(k)\Delta W(k)^T}R.$$

Evidently, the weight covariance matrix and weight variance noise will become time-independent in the steady state as k tends towards infinite. Therefore with k=∞ denoting steady state, (3.34) and (3.35) become

$$s_{wt}(\infty) = tr[\overline{R\Delta W(\infty)\Delta W(\infty)^T}] \tag{3.36}$$

and

$$\overline{R\Delta W(\infty)\Delta W(\infty)^T} + \overline{\Delta W(\infty)\Delta W(\infty)^T}R = \tag{3.37}$$
$$a[s_{opt} + s_{wt}(\infty)]R + a\overline{R\Delta W(\infty)\Delta W(\infty)^T}R.$$

Clearly, solving for the steady state weight variance noise from these two equations is still not easy. However, useful tight bounds for the noise can be obtained by taking the trace of (3.37) and using (3.36). This gives, after using also (3.14),

$$(2 - atrR)s_{wt}(\infty) = as_{opt}trR + atr[\overline{R^2\Delta W(\infty)\Delta W(\infty)^T}]. \tag{3.38}$$

Using (3.36) again and the mathematical theorem

$$a_{min}trB \leq tr(AB) \leq a_{max}trB \tag{3.39}$$

for two positive definite hermitian matrices A and B with a_{min} and a_{max} as the smallest and largest eigenvalues of A respectively, the steady state weight variance noise is then easily seen to be bounded in the inequality

$$\frac{atrR}{2 - a(trR + h_{M-1})} \leq \frac{s_{wt}(\infty)}{s_{opt}} \leq \frac{atrR}{2 - a(trR + h_1)}. \tag{3.40}$$

Clearly, for finite steady state weight variance noise, at least the denominator of the lower bound has to be greater than zero. This implies that the condition of (3.31) for the convergence of the output power and average weight vector will always be satisfied.

The term "misadjustment" was first introduces by Widrow [13] as a measure of weight variance noise, relative to optimal output power, in the steady state in stationary environments. In this thesis, misadjustment is defined in more general terms as

$$M_{wt} = \frac{\text{steady state weight variance noise}}{\text{steady state output power}} \qquad (3.41)$$

so that it is still applicable in the rotating environment to be discussed. In stationary environments where the optimal and steady state output powers are equal, the misadjustment so defined agrees with that in [13] and is clearly within the bounds of (3.40). In almost all applications, the misadjustment desired is small, of the order of 10% say. The misadjustment can then be approximated, from (3.40), by

$$M_{wt} \approx \frac{\alpha \mathrm{tr} R}{2} \qquad (3.42)$$

which implies that the feedback factor is well below the bound of (3.31) as mentioned.

From (3.32) and (3.42), increasing the feedback factor can be seen to lead to shorter time constants, hence faster convergence, at the expense of higher misadjustment and vice versa. By substituting (3.42) into (3.32) the convergence time constant is

$$\tau_m \approx \frac{\mathrm{tr} R}{2 M_{wt} h_m} \text{ sampling period.} \qquad (3.43)$$

Evidently, since the sum of all the eigenvalues is equal to the trace of the covariance matrix, slower transient convergence, at

constant misadjustment, is associated with larger spread of the eigenvalues. This, in turn, is known to be associated with situations where the jammers are closed together and/or have large range of powers. Finally, as the weight variance noise is relatively small during the transient convergence period, the convergence behaviour of the average output power will be roughly equal to that of the output power. In addition to being difficult to analyze, the behaviour of the weight variance noise during the transient convergence period is therefore not of interest and thus is commonly and will not be discussed.

Summarizing, using the formulations of the last section, the behaviour of the array in stationary environments has been investigated in this section. In such environments, the output power and average weights will converge to the optimal values in the steady state as sums of exponentially decaying components with time constants inversely proportional to the eigenvalues of the covariance matrix. As given by (3.43), the time constants are also inversely proportional to the misadjustment defined by (3.41), illustrating the dilemma between fast convergence and high weight variance noise. Moreover, slow convergence is associated with large spread of eigenvalues and will be the case when the jammers are closed together and/or have large range of powers.

3.4 Formulation of the Rotating Environment

Having analyzed the behaviour of the array in stationary environments, similar investigation in the nonstationary rotating environment will now be started by formulating the environment mathematically in this section.

In an arbitrary nonstationary environment, study of the beh-

aviour of the array by solving analytically (3.10), (3.22) and the other associated equations will not be possible because of mathematical difficulties. However, by assuming that all the jammers in the environment rotate with equal angular velocities in the $\sin\theta$ domain, the nonstationary second order input statistics have particularly simple forms and thus at least some theoretical analysis can be expected to be possible. Mathematically, (3.4) is easily seen to have the form

$$s_x(k) = s_x, \tag{3.44a}$$

$$R_0(k) = F^k R_0 \tag{3.44b}$$

and

$$R(k) = F^k R (F^k)^T = F^k R F^{-k} \tag{3.44c}$$

where

$$F = \text{dia}(e^{j\Delta\Phi}, e^{2j\Delta\Phi}, \cdots, e^{(M-1)j\Delta\Phi}), \tag{3.44d}$$

$$\Delta\Phi = \frac{2\pi d f_0}{c} \cdot \text{angular velocity in the } \sin\theta \text{ domain} \tag{3.44e}$$

and c is the wave velocity. The initial second order statistics at k=0, given by s_x, R_0 and R, will be assumed to be the same as that given by (3.23) in stationary environments so that the results obtained in the rotating and stationary environments can be compared. Clearly, in the second order statistics formulated, the rotation of the jammers is described in terms of only the time-varying matrix F^k with $\Delta\Phi$ giving the rate of rotation. Note that $\Delta\Phi$ can also be defined, equivalent to (3.44e), as the change in element to element phase of inputs per sampling period due to the rotation of the jammers. For convenience, this will be referred to as jammer phase rate. Obviously, the main concern of the study is to

investigate the variation of the behaviour of the array as the jammer phase rate varies.

3.5 Average Weight Vector in the Steady State

With the second order input statistics elegantly formulated, the steady state behaviour of the array appears intuitively and and will be shown to be well defined. Specifically, this section will be concerned with the general derivations and discussion of the steady state average weight vector, while similar investigation of the steady state average output power will be given in the next section. For convenience, the average weight vector in the steady state will be referred to as the steady state weight vector, although even in the steady state, the weight vector is still a set of random processes.

Using (3.7), the optimal weight vector in the rotating environment is

$$W_{opt}(k) = F^k W_{opt} = -F^k R^{-1} R_0. \qquad (3.45)$$

Note that, with F^k as the first and only time-varying factor, the directional pattern obtained using this weight vector rotates in synchronization with the jammers. This is because, for an observer rotating with the same velocities as the jammers so that the jammers always appear to arrive from their initial directions, the optimal directional pattern observed will be given by pre-multiplying the optimal weight vector by F^{-k} and thus also appears to be stationary. For convenience, the term directional pattern will henceforth be used in this chapter to mean that observed by the rotating observer and so given by the "de-rotated" weight vector obtained from pre-multiplying the weight vector concerned by F^{-k}.

Due to the finite convergence rate of the algorithm, the optimal weight vector is not expected to be attained even on average in the steady state in the rotating environment. However, it seems reasonable to assume that, similar to the optimal weight vector, the steady state weight vector also gives rise to stationary directional pattern:

$$W_s(k) = F^k W_s \tag{3.46}$$

where the subscript s denotes steady state. Substituting (3.46), (3.10) in the rotating environment becomes

$$F^{k+1} W_s = F^k (I - \alpha R) W_s - \alpha F^k R_0 \tag{3.47}$$

which leads to

$$W_s = (R + \frac{F - I}{\alpha})^{-1} R_0. \tag{3.48}$$

Obviously, this time-independent solution for W_s proves the consistency of assumption (3.46).

With the initial environment represented by N jammers of powers s_n, n=1,··,N, at directions θ_n plus receiver noise of power s_0, the initial second order input statistics can be expressed in more physical terms as

$$s_x(0) = s_x = \sum_{n=0}^{N} s_n = s_0 + G^T \Lambda G, \tag{3.49a}$$

$$R_0(0) = R_0 = \sum_{n=1}^{N} s_n Q_n = Q \Lambda G \tag{3.49b}$$

and

$$R(0) = R = s_0 I + \sum_{n=1}^{N} s_n Q_n Q_n^T = s_0 I + Q \Lambda Q^T \tag{3.49c}$$

where

$$Q = [Q_1 \; Q_2 \; \cdots \; Q_N], \tag{3.49d}$$

$$Q_n^T = [e^{-j\Phi_n} \; e^{-2j\Phi_n} \; \cdots \; e^{-(M-1)j\Phi_n}], \tag{3.49e}$$

$$\Phi_n = \frac{2\pi d f_0 \sin\theta_n}{c}, \tag{3.49f}$$

$$G^T = \underbrace{[1 \; 1 \; \cdots \; 1]}_{N} \tag{3.49g}$$

and

$$\Lambda = \text{dia}(s_1, s_2, \cdots, s_N). \tag{3.49h}$$

Obviously, in (3.49a-c), the terms with suffix n=1,··,N give the second order statistics due to the nth of the N jammers, while the terms with suffix 0 give those due to receiver noise. Using the matrix inversion theorem

$$(A + C^T B C)^{-1} = A^{-1} - A^{-1}C^T(CA^{-1}C^T + B^{-1})^{-1}CA^{-1} \tag{3.50}$$

for three compatible matrices A, B and C, (3.45) and (3.46) are then shown in appendix 3.12.3 to become

$$W_{opt}(k) = F^k W_{opt} = -F^k(s_0 I)^{-1}Q[Q^T(s_0 I)^{-1}Q + \Lambda^{-1}]^{-1}G \tag{3.51}$$

and

$$W_s(k) = F^k W_s = -F^k D^{-1}Q(Q^T D^{-1}Q + \Lambda^{-1})^{-1}G \tag{3.52}$$

where

$$D = s_0 I + \frac{F - I}{a}$$

$$= s_0 I + \text{dia}\left(\frac{e^{j\Delta\Phi} - 1}{a}, \frac{e^{2j\Delta\Phi} - 1}{a}, \cdots, \frac{e^{(M-1)j\Delta\Phi} - 1}{a}\right). \tag{3.53}$$

Since the jammer phase rate will be small, D can be approximated by

$$D \simeq s_0 I + \frac{j\Delta\Phi}{a}\text{dia}(1, 2, \cdots, M-1). \tag{3.54}$$

Clearly, (3.52) for the steady state weight vector can be obtained from (3.51) for the optimal weight vector by replacing $s_0 I$ with D. Therefore, from (3.54), the steady state weights can be deduced to

start to deviate from their optimal values when the jammer phase rate has increased to the critical value of

$$\Delta\Phi = \frac{as_0}{M-1} \tag{3.55}$$

so that the largest element deviation in D from s_0 is equal to s_0.

3.6 Average Output Power in the Steady State

In addition to the average weight vector, the other statistics of most concern in the steady state are the various components of the average output power. These will now be discussed in this section.

Substituting (3.45) into (3.8), the optimal output power in the rotating environment is

$$s_{opt}(k) = s_{opt} = s_x - R_0^T R^{-1} R_0 = s_x + R_0^T W_{opt} \tag{3.56}$$

which is time-independent. In more physical terms, this is shown in appendix 3.12.4, using (3.49) and (3.51), to be

$$s_{opt} = s_0(1 + \|W_{opt}\|) + \sum_{n=1}^{N} \frac{|[\{Q^T(s_0 I)^{-1} Q + \Lambda^{-1}\}^{-1} G]_n|^2}{s_n} \tag{3.57}$$

where, with $\|A\|$ and $[A]_n$ as the Euclidean norm $A^T A$ and the nth element of the vector A respectively, the first term is the optimal output power component due to receiver noise, while the nth of the N terms under the summation is the component due to the nth jammer.

Substituting (3.46) into (3.16), the steady state output power in the rotating environment is

$$s_y(\infty) = s_x + W_s^T R_0 + R_0^T W_s + W_s^T R W_s \tag{3.58}$$

which is also time-independent. Again, as discussed in appendix 3.12.4, this can be expressed, using (3.49) and (3.52), in more physical terms as

$$s_y(\infty) = s_0(1 + \|W_s\|) + \sum_{n=1}^{N} \frac{|[(Q^T D^{-1} Q + \Lambda^{-1})^{-1} G]_n|^2}{s_n} \qquad (3.59)$$

where the first term is the steady state output power component due to receiver noise, while the nth term under the summation is the component due to the nth jammer. For convenience, these components of the steady state output power due to the jammers and receiver noise will be referred to as residue powers. Comparing (3.57) and (3.59) indicates that the output power, unlike that in stationary environments, is not equal to and hence greater than the optimal output power even in the steady state.

Intuitively, in accordance with faster convergence behaviour in stationary environments, the array appears to be less vulnerable to the rotation of the jammers if the feedback factor and hence the critical jammer phase rate of (3.55) is increased. However, as in stationary environments, the feedback factor is limited by the desired amount of steady state weight variance noise which will now be derived using the same analysis as in stationary environments. In the rotating environment, (3.17) and (3.22) for determining the weight variance noise become, after using (3.14),

$$s_{wt}(k) = \mathrm{tr}[R F^{-k} \overline{\Delta W(k) \Delta W(k)^T} F^k] \qquad (3.60)$$

and

$$F[F^{-k-1} \overline{\Delta W(k+1) \Delta W(k+1)^T} F^{k+1}] F^{-1} = F^{-k} \overline{\Delta W(k) \Delta W(k)^T} F^k \qquad (3.61)$$
$$+ a^2 [s_y(k) + s_{wt}(k)] R + a^2 R[F^{-k} \overline{\Delta W(k) \Delta W(k)^T} F^k] R$$
$$- aR[F^{-k} \overline{\Delta W(k) \Delta W(k)^T} F^k] - a[F^{-k} \overline{\Delta W(k) \Delta W(k)^T} F^k] R.$$

Evidently, the matrix $F^{-k} \overline{\Delta W(k) \Delta W(k)^T} F^{-k}$ is the weight covariance matrix after de-rotating the weight vector. Clearly, as k tends towards infinity in the steady state so that the output power

attains its constant steady state value, the de-rotated weight covariance matrix and weight variance noise, as given by (3.60) and the recursive equation of (3.61), will become time-independent, though this implies that the actual weight covariance matrix will be time-varying. Thus, taking the trace of (3.61) and using (3.14) and (3.60) gives

$$(2 - \alpha \mathrm{tr}R)s_{wt}(\infty) = \alpha s_y(\infty)\mathrm{tr}R + \alpha \mathrm{tr}[R^2 F^{-k} \overline{\Delta W(k)\Delta W(k)^T} F^k] \qquad (3.62)$$

where k tends towards infinity. Note that (3.60) and (3.62) have the same forms as the corresponding equations (3.36) and (3.38) respectively in stationary environments. Hence, using the same arguments for deriving (3.40) from (3.36) and (3.38) as well as the definition for misadjustment in (3.41), (3.60) and (3.62) lead to

$$\frac{\alpha \mathrm{tr}R}{2 - \alpha(\mathrm{tr}R + h_{M-1})} \leq M_{wt} = \frac{s_{wt}(\infty)}{s_y(\infty)} \leq \frac{\alpha \mathrm{tr}R}{2 - \alpha(\mathrm{tr}R + h_1)}. \qquad (3.63)$$

Thus, for small misadjustment, the misadjustment can again be approximated, using (3.49c,e), by

$$M_{wt} \approx \frac{\alpha \mathrm{tr}R}{2} = \frac{\alpha(M-1)}{2} \sum_{n=0}^{N} s_n \qquad (3.64)$$

which is clearly the same as (3.42) in stationary environments.

From the discussion in the last two paragraphs, the array obviously has better performance if the environment is stationary. Note that as used here and henceforth in this chapter, array performance refers to the ability of the array to reject the jammers as measured by the average output power in the steady state. Thus, array performance deterioration refers to where the steady state average output power has increased significantly above the

optimal value. Evidently, with roughly the same misadjustment as in stationary environments, performance deterioration in the rotating environment is the result of significant increase in steady state output power due to the lag of the steady state from the optimal weight vector. Any increase in steady state output power is, of course, a combination of: (a) increase in receiver noise residue power due to increase in the Euclidean norm of the steady state weight vector and/or (b) increase in jammers' residue powers due to the inability of the array to track the rotating jammers. As expected intuitively and to be demonstrated in later sections, the receiver noise residue power do not change much as the jammer phase rate increases and thus, significant increase in steady state output power or performance deterioration is the result of the latter factor. Since the only difference between the terms in (3.57) and (3.59) associated with the same jammer is in the matrices D and $s_0 I$, the jammers' residue powers can be deduced, similar to the steady state weight vector, to start increasing from their optimal values when the jammer phase rate has increased to the critical value of (3.55). However, note that (3.55) only gives the jammer phase rate at which the steady state weights and jammers' residue powers start to deviate from their optimal values. As will be explained more clearly in later sections, performance deterioration usually starts at jammer phase rate much greater than the critical value of (3.55).

By substituting (3.64), (3.55) becomes

$$\Delta\Phi \simeq \frac{2M_{wt}}{(M-1)^2}\left(\sum_{n=0}^{N}\frac{s_n}{s_0}\right)^{-1} = \frac{2M_{wt}}{(M-1)^2 ENR} \qquad (3.65)$$

where ENR denotes the element to receiver noise power ratio.

Clearly, the critical jammer phase rate for steady state weight and jammers' residue power deviations is roughly proportional to misadjustment and inversely proportional to the ENR. This agrees with the intuitive thought that the ability of the array to track the rotating jammers will improve if either the feedback factor is increased at the expense of higher misadjustment or corresponding to a decrease in ENR, the jammers' powers are decreased so that the accuracies required of the nulls in tracking the jammers can be decreased. The critical jammer phase rate of (3.65) is also roughly proportional to the square of the number of elements. Intuitively, this is because when the number of elements increases, both the misadjustment and the rate of change of the environment seen by the array, measured from the end elements say, increase.

Summarizing, the steady state behaviour of the array in the rotating environment, as derived and discussed generally in this and the last sections, was found to be well-defined. Specifically, the optimal output power, steady state output power and weight variance noise are time-independent with both the optimal and steady state weight vectors defining stationary directional patterns. Furthermore, the critical jammer phase rate of (3.55) was derived for deviation of steady state weights and jammers' residue powers from optimal values. However, apart from the weight variance noise, the other statistics concerned, as given by (3.51), (3.52), (3.57) and (3.59), cannot be expressed in more explicit forms unless some simplifying assumptions are made regarding the environment so that some of the matrices in these equations have special properties. This will be done in sections 3.8 and 3.9

where more insight can be obtained.

3.7 Transient Convergence Behaviour

Before the more detailed investigation of sections 3.8 and 3.9, this section will complete the general discussion by studying briefly the transient convergence behaviour of the average weight vector and output power. Note that for the same reason as in stationary environments, the behaviour of the weight variance noise in the transient convergence period will not be discussed.

The transient convergence behaviour of the average weight weight vector can be found by subtracting (3.47) from (3.10). Using (3.46) then gives

$$\overline{W(k+1)} - W_s(k+1) = F^k(I - \alpha R)F^{-k}[\overline{W(k)} - W_s(k)]. \qquad (3.66)$$

To find the condition for the convergence of the average weight vector, both sides are pre-multiplied by their own complex conjugate transpose yielding

$$\|\overline{W(k+1)} - W_s(k+1)\| = [\overline{W(k)} - W_s(k)]^T F^k(I - \alpha R)^2 F^{-k} \cdot [\overline{W(k)} - W_s(k)]. \qquad (3.67)$$

With H_m, m=1,··,M-1, as the normalized eigenvector associated with the mth largest eigenvalue h_m of R, the corresponding eigenvalue and normalized eigenvector of $F^k(I-\alpha R)^2F^{-k}$ are obviously $(1-\alpha h_m)^2$ and F^kH_m respectively. Thus, (3.67) is easily seen to be bound by

$$\|\overline{W(k+1)} - W_s(k+1)\| \leq \underset{m}{\text{Max}}\{(1 - \alpha h_m)^2\}[\overline{W(k)} - W_s(k)] \qquad (3.68)$$

where $\underset{z}{\text{Max}}\{f(z)\}$ specifies the maximum value of the function f(z) with respect to z. Therefore, the convergence of the average weight vector is guaranteed if as in stationary environments, $|1-\alpha h_m|$ is less than unity or since the sum of all the eigenvalues of R

is equal to its trace,

$$\alpha < \frac{2}{trR}. \tag{3.69}$$

Again, as in stationary environments, this will be satisfied since for finite weight variance noise, the denominator in the lower bound of (3.63) has to be positive.

To further investigate the transient convergence behaviour of the average weight vector, the recursive equation of (3.66) is easily seen to give rise to

$$F^{-k}[\overline{W(k)} - W_s(k)] = [F^{-1}(I - \alpha R)]^k[W(0) - W_s(0)] \tag{3.70}$$

where W(0) is the initial weight vector. With l_m and P_m denoting its mth eigenvalue and the corresponding eigenvector respectively, the matrix $F^{-1}(I-\alpha R)$ can be decomposed as

$$F^{-1}(I - \alpha R) = PLP^{-1} \tag{3.71}$$

where

$$L = dia(l_1, l_2, \cdots, l_{M-1}) \tag{3.72}$$

and

$$P = [P_1\ P_2 \cdots P_{M-1}]. \tag{3.73}$$

(3.70) then becomes

$$F^{-k}[\overline{W(k)} - W_s(k)] = PL^kP^{-1}[W(0) - W_s(0)] \tag{3.74}$$

where the l.h.s. is obviously the de-rotated lag of the average from the steady state weight vector. If this de-rotated average weight vector lag is written in component form as

$$F^{-k}[\overline{W(k)} - W_s(k)] = \sum_{m=1}^{M-1} p_m(k)P_m \tag{3.75}$$

where P_m is the mth basis vector, the mth component $p_m(k)$ is eas-

ily seen from (3.72), (3.73) and (3.74) to converge according to

$$p_m(k) = \lambda_m^k p_m(0). \tag{3.76}$$

To relate the eigenvalues and eigenvectors of $F^{-1}(I-\alpha R)$ to those of R, $F^{-1}(I-\alpha R)$ can be approximated by

$$F^{-1}(I - \alpha R) \simeq (I - \alpha R) - j\Delta\Phi \mathrm{dia}(1, 2, \cdots, M-1)(I - \alpha R) \tag{3.77}$$

as $\Delta\Phi$ will be small. With the last term being a perturbation matrix for the hermitian matrix $I-\alpha R$, the eigenvalues and eigenvectors of $F^{-1}(I-\alpha R)$ can be found by using the perturbation methods discussed by Wilkinson[80]. Specifically, in a first order approximation, the eigenvectors of $F^{-1}(I-\alpha R)$ is roughly equal to the corresponding eigenvectors of $I-\alpha R$ and hence R:

$$P_m \simeq H_m. \tag{3.78}$$

Furthermore, the first order approximation for the mth eigenvalue of $F^{-1}(I-\alpha R)$ is $H_m^T F^{-1}(I-\alpha R)H_m$. Using (3.77), this is

$$\lambda_m \simeq [1 - j\Delta\Phi H_m^T \mathrm{dia}(1, 2, \cdots, M-1)H_m](1 - \alpha h_m) \tag{3.79}$$

which is equal to $1-\alpha h_m$, the mth eigenvalue of $I-\alpha R$, plus an imaginary perturbed component between $-j\Delta\Phi$ and $-(M-1)j\Delta\Phi$ that of $1-\alpha h_m$.

With the eigenvalue and eigenvector relations of (3.78) and (3.79), the transient convergence behaviour of the average weight vector as described by (3.75) and (3.76) is obviously very similar to that by (3.29) and (3.30) in stationary environments. Specifically, if the de-rotated lag of the average from the steady state weight vector is expressed in component form with P_m or roughly H_m as the mth of the M-1 basis vectors, then the mth component $p_m(k)$ will converge, independent of the other components, to zero exponentially with a time constant of $-1/\ln|\lambda_m|$ sampling period. Si-

nce $(M-1)\Delta\Phi$ and αh_m will be much smaller than unity, this time constant is, from (3.79),

$$\tau_m \simeq \frac{-1}{\ln|1 - \alpha h_m|} \simeq \frac{1}{\alpha h_m} \text{ sampling period} \tag{3.80}$$

which is obviously the same as (3.32) in stationary environments. Note that since l_m is complex, the phase of $p_m(k)$ can be seen from (3.76) to be rotating constantly by the phase of l_m per sampling period. This is clearly not so in stationary environments where the phase of the corresponding component $e_m(k)$ does not change.

To investigate the transient convergence behaviour of the output power, (3.18) can be expressed more conveniently as

$$\begin{aligned} s_y(k) &= s_{opt}(k) + [\overline{W(k)} - W_s(k) + W_s(k) - W_{opt}(k)]^T R(k) \\ &\quad \cdot [\overline{W(k)} - W_s(k) + W_s(k) - W_{opt}(k)] \\ &= s_{opt}(k) + [W_s(k) - W_{opt}(k)]^T R(k)[W_s(k) - W_{opt}(k)] \\ &\quad + [\overline{W(k)} - W_s(k)]^T R(k)[\overline{W(k)} - W_s(k)] \\ &\quad + 2\mathrm{Re}\{[\overline{W(k)} - W_s(k)]^T R(k)[W_s(k) - W_{opt}(k)]\}. \end{aligned} \tag{3.81}$$

Clearly, the first two terms together give the steady state output power as the other terms tend towards zero when the steady state is approached and the average becomes the steady state weight vector. Thus, substituting (3.45) and (3.46), (3.81) becomes

$$\begin{aligned} s_y(k) &= s_y(\infty) + [\overline{W(k)} - W_s(k)]^T F^k R F^{-k} [\overline{W(k)} - W_s(k)] \\ &\quad + 2\mathrm{Re}\{[\overline{W(k)} - W_s(k)]^T F^k R(W_s - W_{opt})\} \end{aligned} \tag{3.82}$$

which gives, after further substituting (3.75) and (3.76),

$$\begin{aligned} s_y(k) &= s_y(\infty) + \sum_{m,n=1}^{M-1} [p_m(0)^* p_n(0) P_m^T R P_n](l_m^* l_n)^k \\ &\quad + \sum_{m=1}^{M-1} 2\mathrm{Re}\{[p_m(0)^* P_m^T R(W_s - W_{opt})](l_m^*)^k\}. \end{aligned} \tag{3.83}$$

Obviously, since P_m is an eigenvector of $F^{-1}(I-\alpha R)$ but not R, the square-bracketed factors will not be exactly zero in general. Therefore, different from that in stationary environments, the transient convergence behaviour of the output power to the steady state value is described in (3.83) as the sum of many time-varying terms, each term representing a sinusoid whose envelope converges exponentially to zero. With initial powers given by the square-bracketed factors in (3.83), the sinusoids have frequencies given by the moduli of the phases of $l_m^* l_n$, $n=1,\cdots,m$, and l_m^* per sampling period, while the corresponding time constants of the envelops are $-1/\ln|l_m^* l_n|$ and $-1/\ln|l_m|$ sampling period. Using the same arguments for deriving (3.80) from (3.79), the time constants are roughly $1/\alpha(h_m+h_n)$ and $1/\alpha h_m$ respectively. Clearly, the longest time constant is $1/\alpha h_{M-1}$ and from the discussion in section 3.4, is roughly twice the corresponding value in stationary environments. If the jammer phase rate is small so that the steady state approaches the optimal weight vector and P_m tends towards the mth eigenvector of R, the sinusoids with nonzero frequencies, that is, except those corresponding to l=m, are easily seen from (3.83) to have initial powers approaching zero. Clearly, the above description for the transient convergence of the output power will then become that in stationary environments.

In summary, during the transient convergence period, the average weight vector, after de-rotating, converges in roughly the same way as in stationary environments. The output power, however, converges in more complicated fashion as a sum of many exponentially decaying sinusoidal components. Nevertheless, for small jammer phase rate, only the components with zero frequency are dominant and the convergence behaviour is roughly that in statio-

nary environments. In any case, the convergence time constants are still roughly inversely proportional to the feedback factor and the eigenvalues of the covariance matrix. Therefore, the dilemma that increasing the feedback factor leads to faster transient convergence and better steady state tracking ability but at the expense of higher misadjustment can be deduced. Furthermore, as in stationary environments, slow convergence is evidently associated with large spread of eigenvalues and will be the case when the jammers are closed together and/or have large range of powers.

3.8 Single-Jammer Situation

Having generally investigated the behaviour of the array in the last three sections, this and the next sections will be concerned with obtaining more insight on the more interesting steady state behaviour by examining some typical simulation results and analytically, by making some realistic simplifying assumptions about the environment so that the important equations derived can be expressed more explicitly. Specifically, this section will investigate the single-jammer situation.

When only one jammer is present, the matrices Λ, G, Q, $Q^T(s_0 I)^{-1}Q$ and $Q^T D^{-1}Q$ can be seen from (3.49d,e,g,h) and (3.53) to be given simply by s_1, 1, Q_1, $(M-1)s_1/s_0$ and $tr(D^{-1})$ respectively. Thus, (3.51), (3.52), (3.57) and (3.59) become

$$W_{opt}(k) = F^k W_{opt} = \frac{-s_1 F^k Q_1}{(M-1)s_1 + s_0}, \tag{3.84}$$

$$W_s(k) = F^k W_s = \frac{-s_1 F^k D^{-1} Q_1}{1 + s_1 tr(D^{-1})}, \tag{3.85}$$

$$s_{opt} = s_0(1 + \|W_{opt}\|) + s_1\left[\frac{s_0}{(M-1)s_1 + s_0}\right]^2 \qquad (3.86)$$

$$= s_0\left\{1 + \frac{(M-1)s_1^2}{[(M-1)s_1 + s_0]^2}\right\} + s_1\left[\frac{s_0}{(M-1)s_1 + s_0}\right]^2$$

and

$$s_y(\infty) = s_0(1 + \|W_s\|) + \frac{s_1}{|1 + s_1 tr(D^{-1})|^2}. \qquad (3.87)$$

Being the component of optimal output power due to the jammer, the second term of (3.86) is roughly inversely proportional to the jammer's power and is usually much smaller than the fairly constant first term due to receiver noise. This illustrates the power inversion property and the ability of the array to suppress the optimal output power components due to strong jammers to well below optimal output power. Included in both (3.85) and (3.87), the important factor $[1+s_1 tr(D^{-1})]^{-1}$ is, from (3.54),

$$[1 + s_1 tr(D^{-1})]^{-1} \simeq [1 + \sum_{m=1}^{M-1} \alpha s_1(\alpha s_0 + jm\Delta\Phi)^{-1}]^{-1}. \qquad (3.88)$$

Clearly, this cannot be further simplified unless assumptions are made regarding the relative magnitudes of αs_0, αs_1 and $\Delta\Phi$. Since the cases of most interest correspond to where the jammer's power is greater than receiver noise power, the three most interesting and usual assumptions for simplifying (3.88) are

$$(M-1)\alpha s_1 \gtrsim \alpha s_0 \gtrsim (M-1)\Delta\Phi, \qquad (3.89)$$

$$\ln(2M-1)\alpha s_1 \gtrsim 2\Delta\Phi \gtrsim 4\alpha s_0 \qquad (3.90)$$

and

$$\Delta\Phi \gtrsim 2\ln(2M-1)\alpha s_1 \gtrsim \alpha s_0 \qquad (3.91)$$

where the numerical factors 2, 4, M-1 and ln(2M-1) are sufficient

for deriving approximate explicit solutions for (3.85) and (3.87). The significance of and the results obtained under these assumptions will now be discussed.

Under assumption (3.89), the jammer phase rate is below the critical value of (3.55) for steady state weight and jammers' residue power deviations from optimal values. The assumption therefore corresponds to the case where the jammer is rotating too slowly to give rise to any significant change in array behaviour and performance. Specifically, (3.85) and (3.87) are shown, using Maclaurin's theorem and neglecting second and higher order terms, in appendix 3.12.5 to become

$$W_s(k) \approx \frac{-s_1 F^k}{(M-1)s_1 + s_0}\left[I + \frac{j\Delta\Phi}{\alpha s_0}\mathrm{dia}\left(\frac{M-2}{2}, \frac{M-4}{2}, \cdots, \frac{2-M}{2}\right)\right]Q_1 \qquad (3.92)$$

and

$$s_y(\infty) \approx s_0\left\{1 + \frac{(M-1)s_1^2}{[(M-1)s_1 + s_0]^2}\right\} + s_1\left[\frac{s_0}{(M-1)s_1 + s_0}\right]^2. \qquad (3.93)$$

Note that second and higher order terms is used in this chapter to mean those relative to the first and so the largest term of the series concerned. Comparing (3.84) and (3.92) shows that the mth of the M-1 steady steady state weights is composed of the corresponding optimal weight plus a perturbed component. Relative to the optimal weight, the perturbed component is at phase quadrature and has relative magnitude of roughly $|(M/2-m)\Delta\Phi/\alpha s_0|$. The maximum relative magnitude is hence roughly $M\Delta\Phi/2\alpha s_0$ or 1/2 at the critical jammer phase rate of (3.55) which is clearly physically relevant. Regarding the steady state output power of (3.93), the first and second terms due to receiver noise and the jammer respectively are obviously equal to the corresponding components

of the optimal output power of (3.86) in this case.

Next, under assumption (3.91), (3.85) and (3.87) are shown in appendix 3.12.7, using the same analysis as deriving (3.92) and (3.93) in appendix 3.12.5, to be

$$W_s(k) \approx \frac{j\alpha s_1 F^k}{\Delta\Phi}\{[1 + \frac{j\ln(2M-1)\alpha s_1}{\Delta\Phi}]\mathrm{dia}(1, \frac{1}{2}, \cdots, \frac{1}{M-1}) + \frac{j\alpha s_0}{\Delta\Phi}\mathrm{dia}(1, \frac{1}{4}, \cdots, [\frac{1}{M-1}]^2)\}Q_1 \qquad (3.94)$$

and

$$s_y(\infty) \approx s_0[1 + \frac{2(M-1)}{M}(\frac{\alpha s_1}{\Delta\Phi})^2] + s_1. \qquad (3.95)$$

Obviously, as the jammer phase rate increases, the steady state weights tend towards zero. Furthermore, as the first term of (3.95) due to receiver noise decreases towards receiver noise power, the steady state output power becomes that due to the first element of the array. Evidently, as implied in (3.91), for jammer phase rate greater than $2\ln(2M-1)\alpha s_1$ and αs_0, the jammer is moving too fast to be tracked so that in accordance with intuitive thought, the adaptive array tends towards adopting a policy of nonadaptation. Note that this case is not physically unrealistic. In multi-jammer situations, the inequality $\Delta\Phi \backslash 2\ln(2M-1)\alpha s_1$ implied by (3.91) can be satisfied as the feedback factor may be limited by the presence of other considerably stronger jammers to much smaller value than when only one jammer is present.

Finally, the intermediate and most interesting case under assumption (3.90) will now be discussed. Again, using the same analysis as deriving (3.92) and (3.93) in appendix 3.12.5, (3.85) and (3.87) are shown in appendix 3.12.6 to be

$$W_s(k) \approx \frac{-F^k}{\ln(2M-1)}\{[1 - \frac{j\alpha s_1}{\ln(2M-1)\alpha s_1} - \frac{j2(M-1)\alpha s_0}{M\ln(2M-1)\Delta\Phi}] \qquad (3.96)$$

$$\cdot \operatorname{dia}(1, \frac{1}{2}, \cdots, \frac{1}{M-1}) - \frac{j\alpha s_0}{\Delta\Phi}\operatorname{dia}(1, \frac{1}{4}, \cdots, [\frac{1}{M-1}]^2)\, Q_1$$

and

$$s_y(\infty) \simeq s_0\{1 + \frac{2(M-1)}{M[\ln(2M-1)]^2}\} + s_1[\frac{\Delta\Phi}{\ln(2M-1)\alpha s_1}]^2. \qquad (3.97)$$

Obviously, the steady state weight vector is very different from the optimal one given by (3.84). Regarding the steady state output power, both the first and second terms of (3.97) due to receiver noise and the jammer respectively are easily seen to be greater than the corresponding components of the optimal output power of (3.86). Specifically, the jammer's residue power increases in proportion to the square of jammer phase rate and over the range of jammer phase rate specified by (3.90), can increase from $4s_1[s_0/\ln(2M-1)\alpha s_1]^2$ to $s_1/4$. Clearly, the lower bound is not very much greater than the optimal output power component due to the jammer in (3.86), while the upper bound is only 6dB below the jammer's power or residue power after the array has adopted the nonadaptation policy. Evidently, assumption (3.90) corresponds to the case where the tracking ability of the array is deteriorating significantly. Note that, with $\ln(2M-1)\alpha s_1 \geq 4s_0$ implied by (3.90), the increase in receiver noise residue power can be seen by comparing the first terms of (3.86) and (3.97) to be of the order of 10% or less of the optimal output power. Therefore, as mentioned, significant increase in steady state output power is due to the increase in jammer's residue power resulting from degradation in the tracking ability of the array. Very loosely, it can be considered that the steady state output power will start to increase significantly and the array performance will start to deteriorate if the jammer phase rate is increased above the

critical value of

$$\Delta\Phi = \ln(2M-1)\alpha(s_0 s_1)^{1/2} \qquad (3.98)$$

at which the jammer's residue power is roughly equal to receiver noise power. Of course, as used in [77], a more precise approach to find the condition for performance deterioration is first to determine the optimal feedback factor so that the steady state average output power is minimized. Assuming the optimal feedback factor is to be used, the condition can then be derived by specifying an acceptable increase, which will be of the order of weight variance noise, of the steady state average above the optimal output power. Essentially, the critical jammer phase rate found from this approach will correspond to where the jammer's residue power is at a value depending on misadjustment, optimal output power and other related parameters. Obviously, the replacement of this threshold value by simply receiver noise power leads to (3.98). Thus, being proportional to only the square root of receiver noise power which will not be very different from this threshold value, the critical jammer phase rate of (3.98) will be roughly equal to that obtained via the more precise approach mentioned and for simplicity, will be used in the investigation.

As a demonstrating example, fig.3.2 shows the variation of steady state behaviour with jammer phase rate for a 4-element array with -20dB receiver noise power and feedback factor of 0.0005. Having 0dB power, the jammer is chosen to arrive from 0° initially so that the space vector Q_1, from (3.49e,f), has unity elements. Figs.3.2a and b show the variation of the real and imaginary parts respectively of the elements of the steady state weight vector after de-rotating or ignoring the time-varying factor

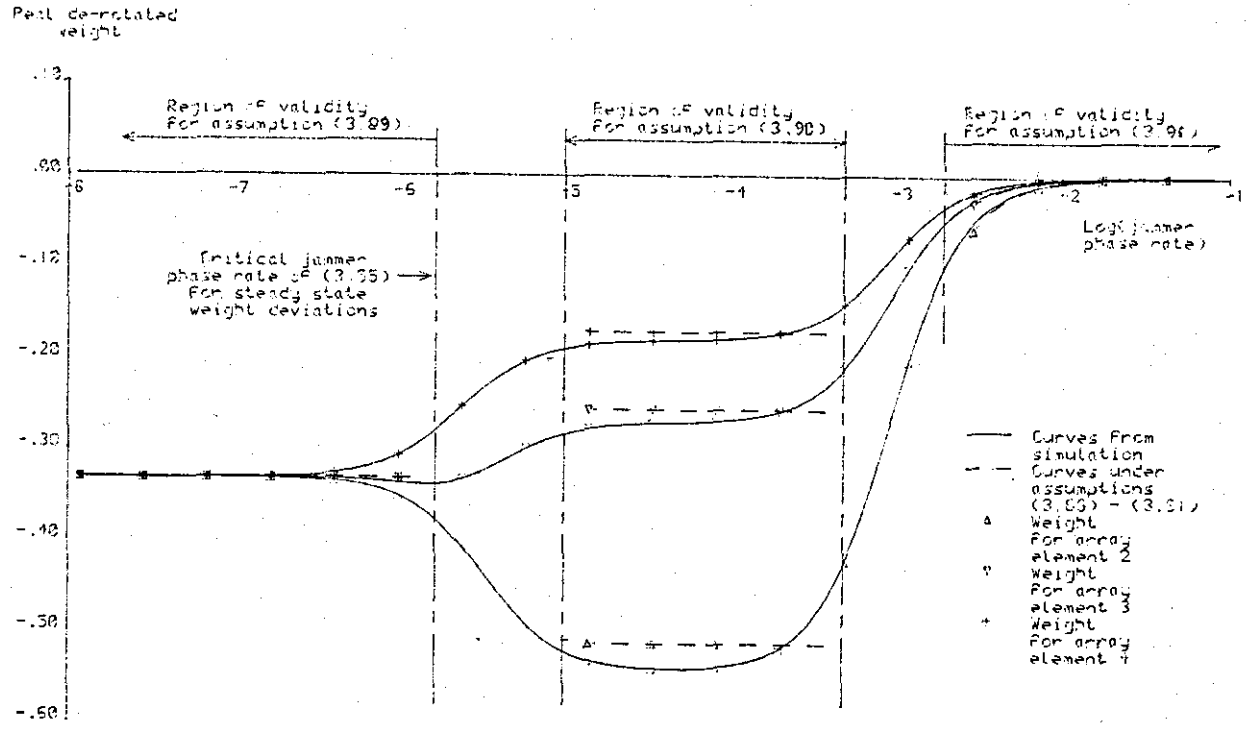

Fig.3.2a Real parts of the de-rotated steady state weights

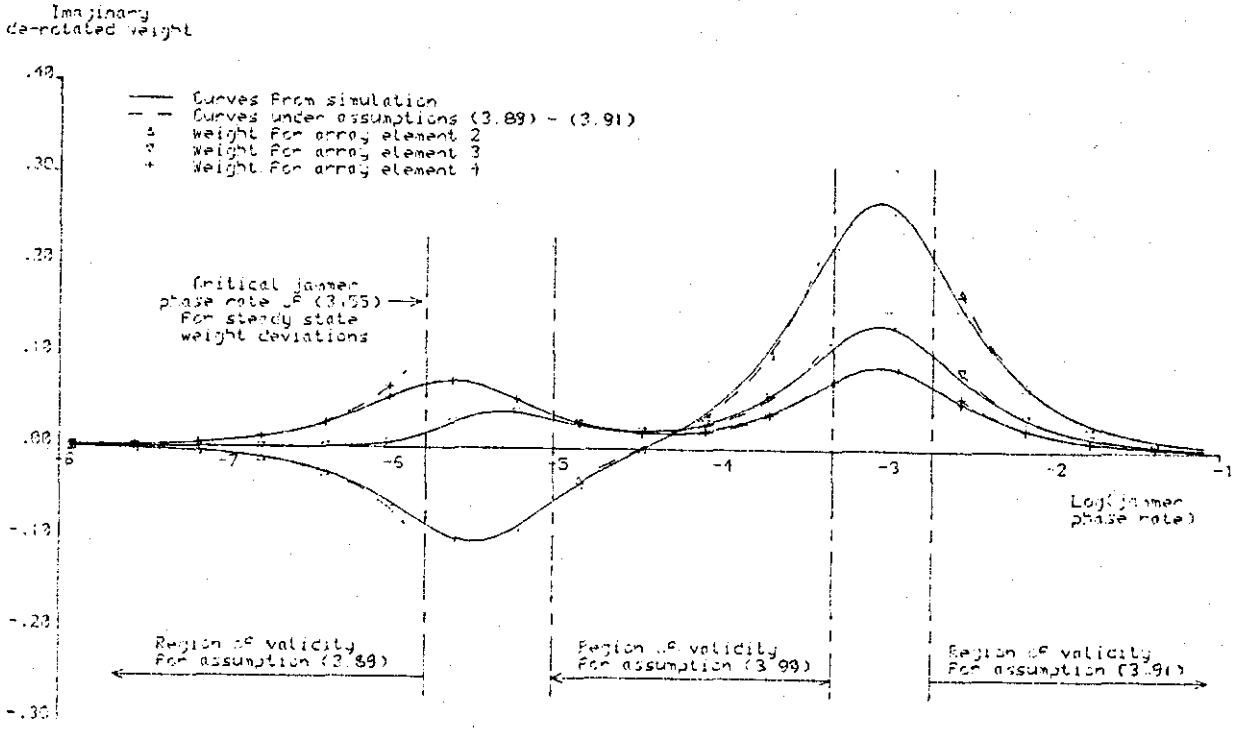

Fig.3.2b Imaginary parts of the de-rotated steady state weights

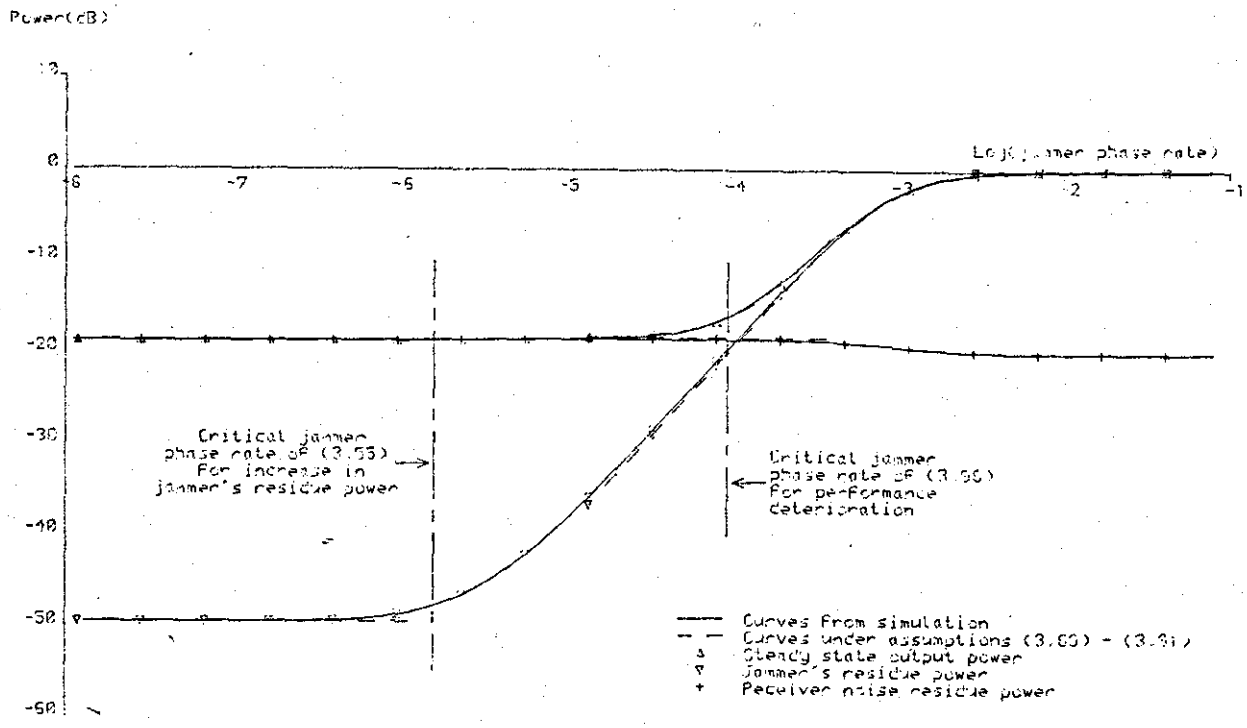

Fig.3.2c Steady state output power and its components

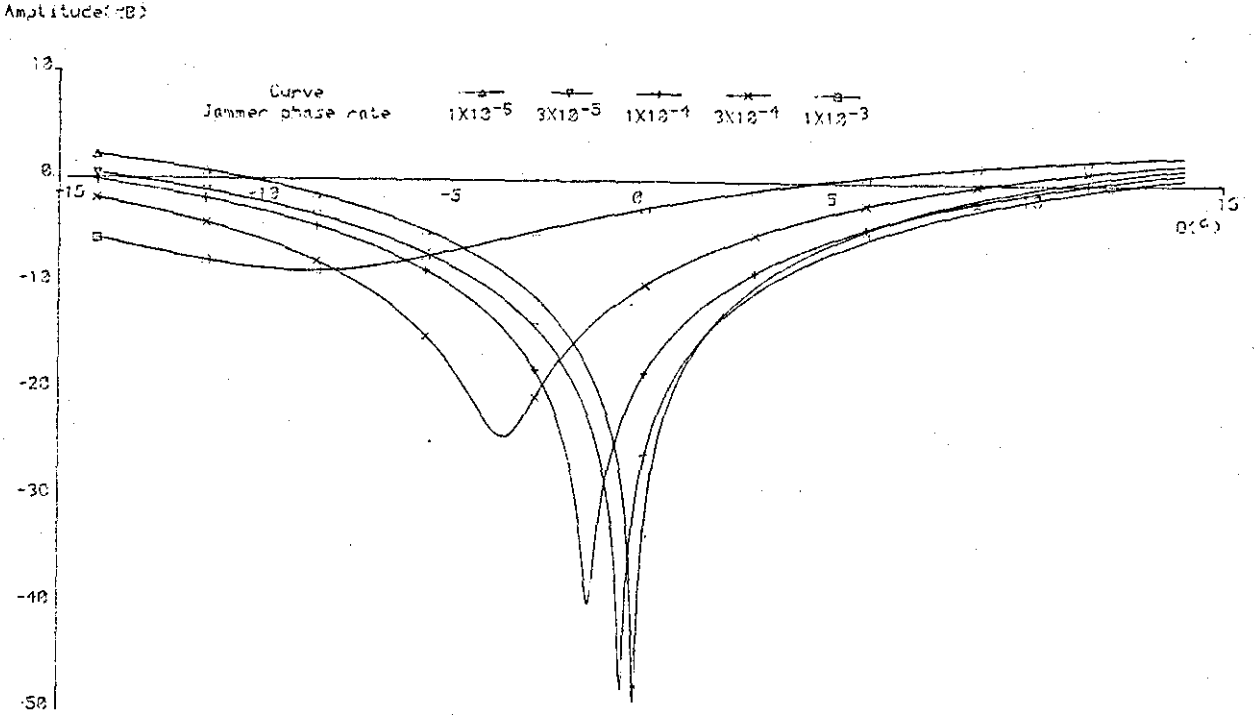

Fig.3.2d Steady state directional pattern

Fig.3.2 Variation of steady state behaviour with jammer phase rate for a single-jammer situation. The array has 4 elements, -20dB receiver noise power and feedback factor of 0.0005, whereas the jammer has power 0dB and arrives from 0° initially.

F^k. Regions of jammer phase rate for the validity of the three assumptions of (3.89)-(3.91) are shown, in addition to the critical jammer phase rate of (3.55) for steady state weight deviations. Solid and broken lines are used for curves due to simulation and those obtained from analytic results derived under the three assumptions respectively. Obviously, good agreement can be seen between the two sets of curves. Note that the purpose of using the very small feedback factor of 0.0005 is to present the case under assumption (3.91). Fig.3.2c shows the variation of the steady state output power and its components. The two dashed lines drawn on the figure correspond to the critical jammer phase rates of (3.55) and (3.98). Again, the broken curves are due to the analytic results derived and can be seen to agree well with the corresponding solid simulation curves. From figs.3.2a-c, the steady state weights and jammer's residue power can be seen to start to deviate from their optimal values as the jammer phase rate increases above the critical value of (3.55), illustrating its physical relevance. Furthermore, as the jammer phase rate increases further, the receiver noise residue power do not vary much, though the steady state weights change considerably. In contrast, the jammer's residue power curve increases with gradient of 20dB per decade, in accordance with the proportionality to the square of jammer phase rate discussed under assumption (3.90), and gives rise to significant increase in steady state output power, hence performance deterioration, at roughly the critical jammer phase rate of (3.98) whose physical relevance is thus also illustrated. As the jammer phase rate increases still further, the steady state weights can be seen to tend towards zero eventually, resulting in the jammer's and receiver noise residue power

curves to level off at the jammer's and receiver noise powers respectively. Note that from (3.55) and (3.98), the two critical jammer phase rates have ratio of $M\ln(2M-1)(s_1/s_0)^{1/2}$, which increases as the number of elements and the jammer to receiver noise power ratio increase, and are very different in this example. This difference can be seen from fig.3.2c to be due to the suppression of the jammer's residue power to approximately 30dB below optimal output power at very small jammer phase rate. Fig.3.2d shows the variation of the steady state directional pattern obtained from the steady state weight vector. The pattern corresponding to the smallest jammer phase rate is essentially the same as when the jammer is not moving. As the jammer phase rate increases, the depth of the null obviously decreases and its position shifts to the left. These changes can also be seen to accelerate with increase in jammer phase rate. Note that since the jammer is moving in the direction of increasing θ, the shifting of the null towards the left represents a lag of the null behind the jammer.

3.9 Multi-Jammer Situation

In this section, the more detailed investigation on the steady state behaviour of the array will be continued by studying the multi-jammer situation. Computer simulation will be used, but first, the important results in the single-jammer situation will be extended analytically.

As mentioned, expressing (3.52) and (3.59) in more explicit forms is not possible without making simplifying assumptions about the environment. In the multi-jammer situation, the most useful assumption is obviously that the space vectors Q_n, $n=1,\cdots,N$, for the jammers satisfy the orthogonal relation of

$$Q_n^T D^{-1} Q_m = 0, \quad m=1,\cdots,N\neq n, \tag{3.99}$$

so that from (3.49d,e,f) and (3.53), the matrix $Q^T D^{-1} Q$ is simply $tr(D^{-1})I$. Thus, (3.52) and (3.59) become, after using (3.49d,g,h) as well,

$$W_s(k) = F^k W_s = \sum_{n=1}^{N} \frac{-s_n F^k D^{-1} Q_n}{1 + s_n tr(D^{-1})} \tag{3.100}$$

and

$$s_y(\infty) = s_0(1 + \|W_s\|) + \sum_{n=1}^{N} \frac{s_n}{|1 + s_n tr(D^{-1})|^2}. \tag{3.101}$$

Clearly, with assumption (3.99), the steady state weight vector is given by the sum of N component vectors with forms as (3.85). Specifically, the nth component vector is the steady state weight vetcor from considering only the nth jammer in a single-jammer situation. The same is true for the second term of (3.101), the total jammer residue power, which is composed of N components having forms as the jammer's residue power in (3.87). Evidently, all the discussion regarding the steady state weight vector and jammer's residue power in section 3.8 on the single-jammer situation is also applicable, by considering each jammer separately and independent of the others, in this simplified multi-jammer situation.

Corresponding to assumption (3.90) in the single-jammer situation, consider now the most interesting case expressed by

$$\ln(2M-1)\alpha \underset{n}{Min}\{s_n\} \gg 2\Delta\Phi \gg 4\alpha s_0 \tag{3.102}$$

when, with $\underset{z}{Min}\{f(z)\}$ denoting the minimum value of the function $f(z)$ with respect to z, the tracking ability for all the jammers is deteriorating considerably. Since, in this case, the jammers'

residue powers have the same form as the second term of (3.97) under assumption (3.90) in the single-jammer situation, (3.101) becomes

$$s_y(\infty) \approx s_0(1 + \|W_s\|) + \left[\frac{\Delta\Phi}{a\ln(2M-1)}\right]^2 \sum_{n=1}^{N} \frac{1}{s_n}. \qquad (3.103)$$

As will be illustrated later from simulation results, with the change in receiver noise residue power being relatively small, significant increase in steady state output power is the result of increase in jammers' residue powers. Therefore, with the same reason for deriving (3.98) in the single-jammer situation, array performance can be considered to start deteriorating when the jammer phase rate is increased above the critical value of

$$\Delta\Phi = a\ln(2M-1)\left(\sum_{n=1}^{N} \frac{1}{s_0 s_n}\right)^{-1/2} \qquad (3.104)$$

at which the total jammer residue power is approximately equal to receiver noise power. Using (3.64) to eliminate the feedback factor, this becomes

$$\Delta\Phi \approx \frac{2\ln(2M-1)M_{wt}}{M-1}\left(\sum_{n=1}^{N} s_n\right)^{-1}\left(\sum_{n=1}^{N} \frac{1}{s_0 s_n}\right)^{-1/2} \qquad (3.105)$$

and is dependent on the individual jammers' powers. In practical applications, the individual jammers' powers are most probably not known, although the total jammer power can be calculated from the measured element power. For a given total jammer power, (3.105) is easily seen to be minimized if the environment is composed of one strong jammer with as many weak jammers as possible. Furthermore, the weak jammers' powers should be as small as possible, but of course, should also be above the minimum value, s_{min}, so that the array still suffers performance deterioration if it is

unable to track the weak jammers. With s_{min} being much smaller than the strong jammer's power and the maximum number of weak jammers being M-2 when all the degrees of freedom of the array are fully utilized, the minimum value of (3.105) is approximately

$$\Delta\Phi \approx \frac{2\ln(2M-1)M_{wt}(s_0 s_{min})^{1/2}}{(M-1)(M-2)^{1/2}}\left(\sum_{n=1}^{N} s_n\right)^{-1}. \qquad (3.106)$$

To very roughly obtained a more useful expression for the "safety" jammer phase rate below which the array performance will not deteriorate regardless of the distribution of the jammers' powers, s_{min} can be equated to s_0 yielding

$$\Delta\Phi \approx \frac{2\ln(2M-1)M_{wt}}{(M-1)(M-2)^{1/2}ENR}. \qquad (3.107)$$

Obviously, the equating of s_{min} to s_0 for deriving the safety jammer phase rate is very similar to the equating of the total jammer residue power in (3.103) to s_0 for deriving the critical jammer phase rate of (3.104). However, the whole discussion in this paragraph is based on the assumption of (3.102) which implies that s_{min} is greater than $4s_0/\ln(2M-1)$ and thus may not equal s_0. Despite this inconsistancy, (3.107) will still be used in this chapter, as (3.106) is proportional to only the square root and thus fairly insensitive to the variation of s_{min}. Furthermore, if the array is able to track only the strong jammer, it seems reasonable that the increase in steady state output power of $(M-2)s_0$ due to the weak jammers can be regarded as approaching the minimum for performance deterioration. Note that the safety jammer phase rate of (3.107) is very similar to the critical jammer phase rate of (3.65) for steady state weight and jammers' residue power deviations from optimal values. Specifically, the ratio of the former

to the latter is $(M-1)(M-2)^{-1/2}\ln(2M-1)$ which depends only on the number of elements and is less than 10 for arrays with less than 11 elements.

Having extended the important results obtained in the single-jammer situation, it should be noted that the orthogonal relation of (3.99), on which the whole discussion is based, will not be satisfied if Q_n and D have the forms as given in (3.49e) and (3.53) respectively. Despite this shortcoming, many deductions obtained will be shown, mainly by computer simulation, to be still valid, particularly if the array has extra degrees of freedom and the jammers are far apart. In any case, using (3.49d), the steady state weight vector of (3.52) can be written in general as

$$W_s(k) = \sum_{n=1}^{N} \frac{-g_n s_n F^k D^{-1} Q_n}{1 + s_n \mathrm{tr}(D^{-1})} \qquad (3.108)$$

where

$$g_n = [\frac{1}{s_n} + \mathrm{tr}(D^{-1})]\,[(Q^T D^{-1} Q + \Lambda^{-1})^{-1} G]_n. \qquad (3.109)$$

Obviously, except that each of the component vectors is now weighted by a complex scalar, (3.108) is the same as (3.100) which is obtained after assuming (3.99).

To obtain more insight, the multi-jammer situation will now be further investigated by using some typical simulation results. Fig.3.3a shows graphs of steady state output power and its components against jammer phase rate for a 4-element array with -40dB receiver noise power and feedback factor of 0.05. Two jammers of powers 0 and -20dB arrive initially from 10° and 40° respectively. The power inversion property of the array can be seen from the difference between the two solid jammers' residue power curves

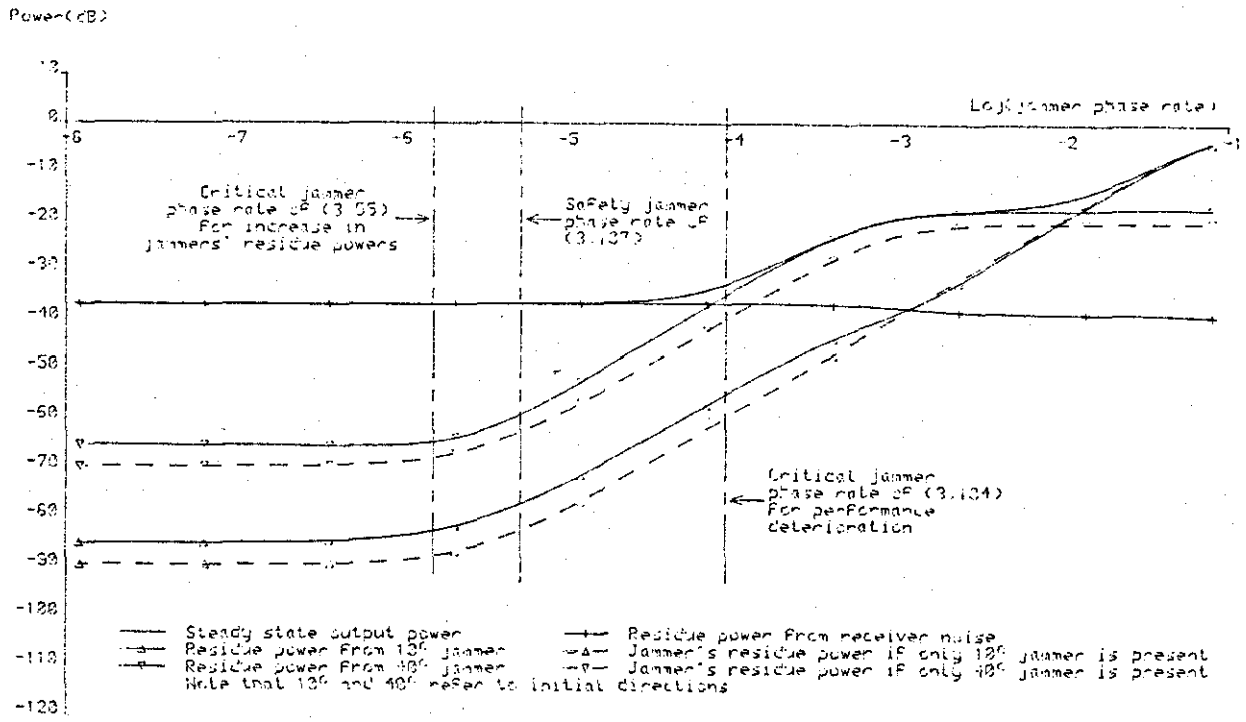

Fig.3.3a Steady state output power and its components

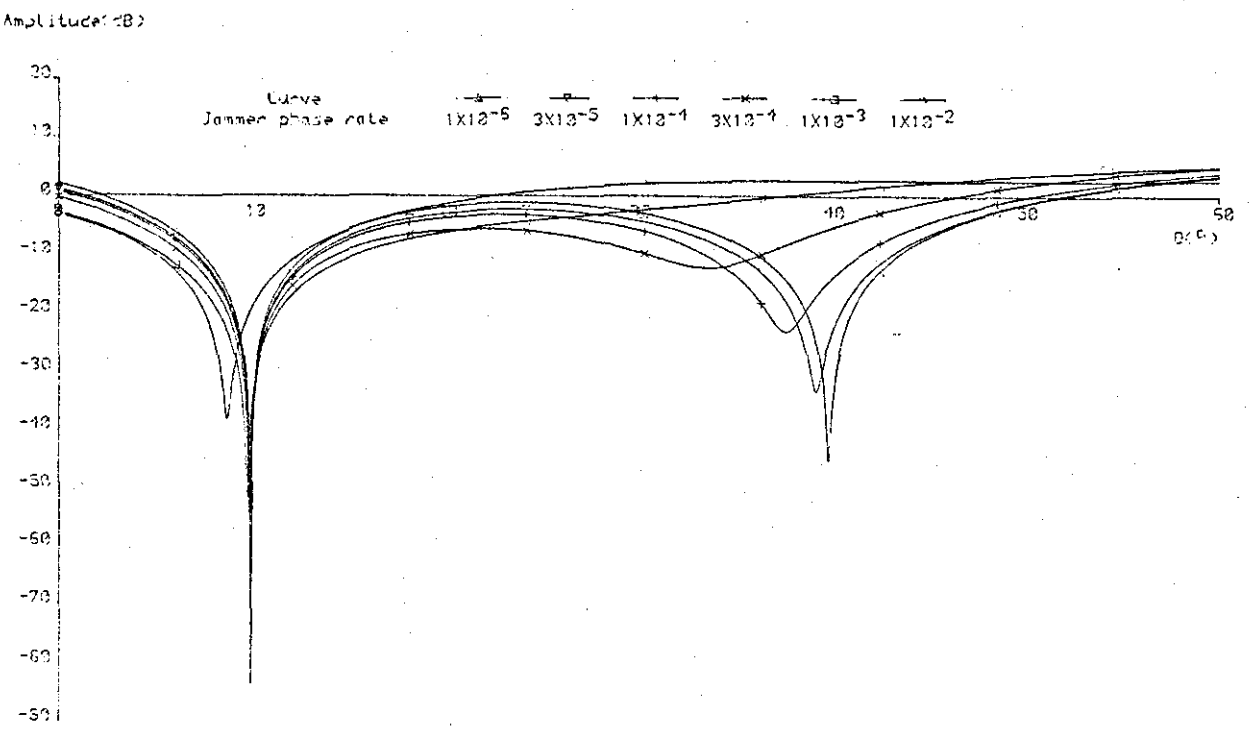

Fig.3.3b Steady state directional pattern

Fig.3.3 Variation of steady state behaviour with jammer phase rate for a 4-element array with -40dB receiver noise and feedback factor of 0.05. Two jammers of powers 0 and -20dB arrive initially from 10° and 40° respectively. This is one typical example where the jammers are far apart and the array has extra degrees of freedom.

before they start to increase. This gives the ratio of the weak to the strong jammers' residue powers when the array has near-optimal behaviour as approximately 20dB and hence, roughly equal to the ratio of the strong to the weak jammers' powers. Also shown in fig.3.3a in broken lines are the variation of the jammers' residue powers when only one of the jammers is present. The slight difference between these broken curves with the corresponding solid curves obtained when both jammers are present illustrates that the two-jammer situation here is roughly a linear combination of two single-jammer situations. For clarity, the term residue powers will be used to refer to those obtained when all the jammers are present, unless stated otherwise. As shown in the figure, the dashed lines indicate the important theoretical jammer phase rates of (3.55), (3.104) and (3.107). Clearly, the jammers' residue power curves start to increase simultaneously at around the critical jammer phase rate of (3.55). As the jammer phase rate increases, these curves attain gradients of about 20dB per decade, corresponding to the jammers' residue powers being roughly proportional to the square of jammer phase rate. However, with virtually no change in receiver noise residue power, the array performance deteriorates only until the weak jammer's residue power curve has increased to where it is about to meet the steady state output power curve which, as a result, increases significantly at around the critical jammer phase rate of (3.104). As the jammer phase rate increases further, the steady state output power curve then follows the increase and later levelling off of the weak jammer's residue power curve. Note that this levelling off of the curve at around the weak jammer's power of -20dB implies that the

array is no longer able to track and null the weak jammer. Still further increase in jammer phase rate then causes the strong jammer's residue power curve to increase above the weak jammer's residue power curve so that the steady state output power curve finally follows the former curve. Note that roughly after the array performance has deteriorated, the receiver noise residue power starts to decrease and eventually approaches the receiver noise power of -40dB, indicating that the weight vector norm is decreasing and the array is tending towards adopting the nonadaptation policy. Clearly, in this scenario, the critical jammer phase rates of (3.55) and (3.104) are physically relevant, though the safety jammer phase rate of (3.107) is quite conservative. Fig.3.3b shows the variation of steady state directional pattern with jammer phase rate in this scenario. Evidently, the behaviour of the nulls (decreasing in depths and lagging behind the jammers) as the jammer phase rate increases is the same as that in the single-jammer situation of fig.3.2d. Also, as expected, the null for the weak jammer disappears first, at the jammer phase rate corresponding to where its residue power curve in fig.3.3a starts to level off at -20dB. Fig.3.4 shows the same set of curves as fig.3.3a, using also the same scenario but with the weak jammer having -30 instead of -20dB power. Obviously, all the general comments and description regarding fig.3.3a also apply to this figure. However, due to the decrease in the weak jammer's power, the intermediate levelling off of the steady state output power is lengthened and at a lower value. Array performance deterioration now begins at smaller jammer phase rate and the safety jammer phase rate of (3.107) is approached. Fig.3.5 shows the same set of curves as

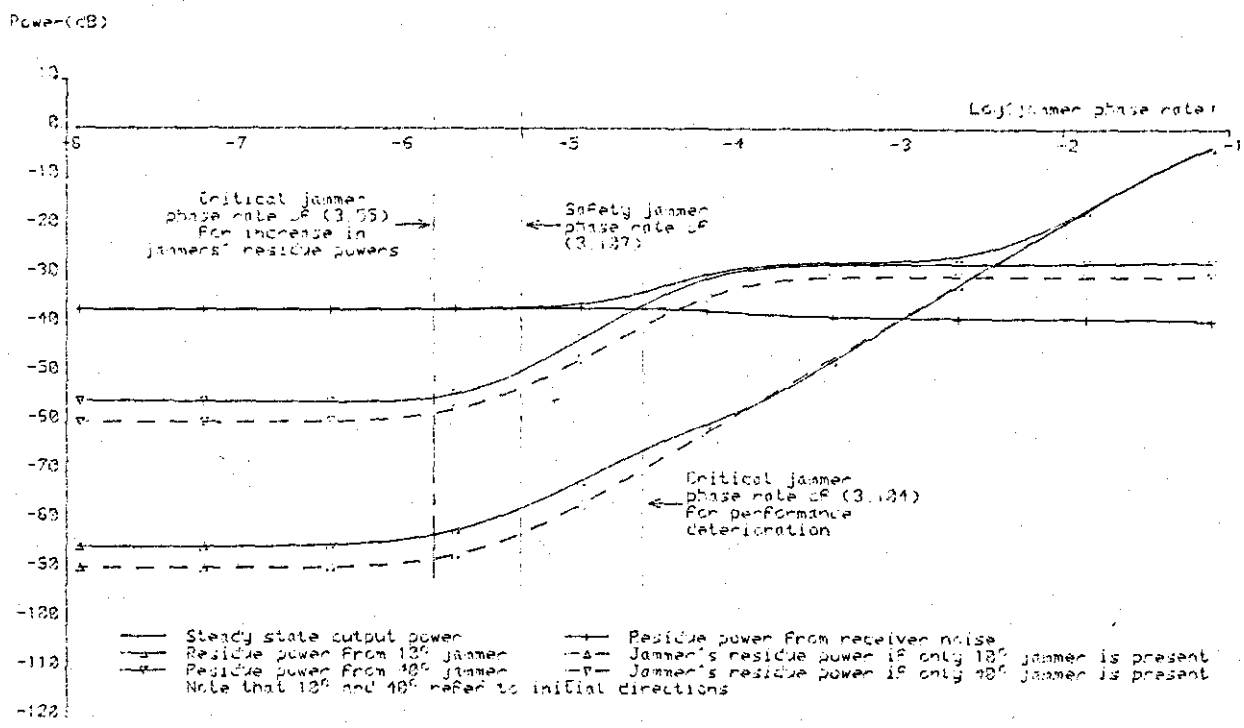

Fig.3.4 Variation of steady state output power and its components with jammer phase rate for the situation of fig.3.3 except that the weaker jammer now has -30dB power. Comparing with fig.3.3a shows the effect of decreasing the weaker jammer's power.

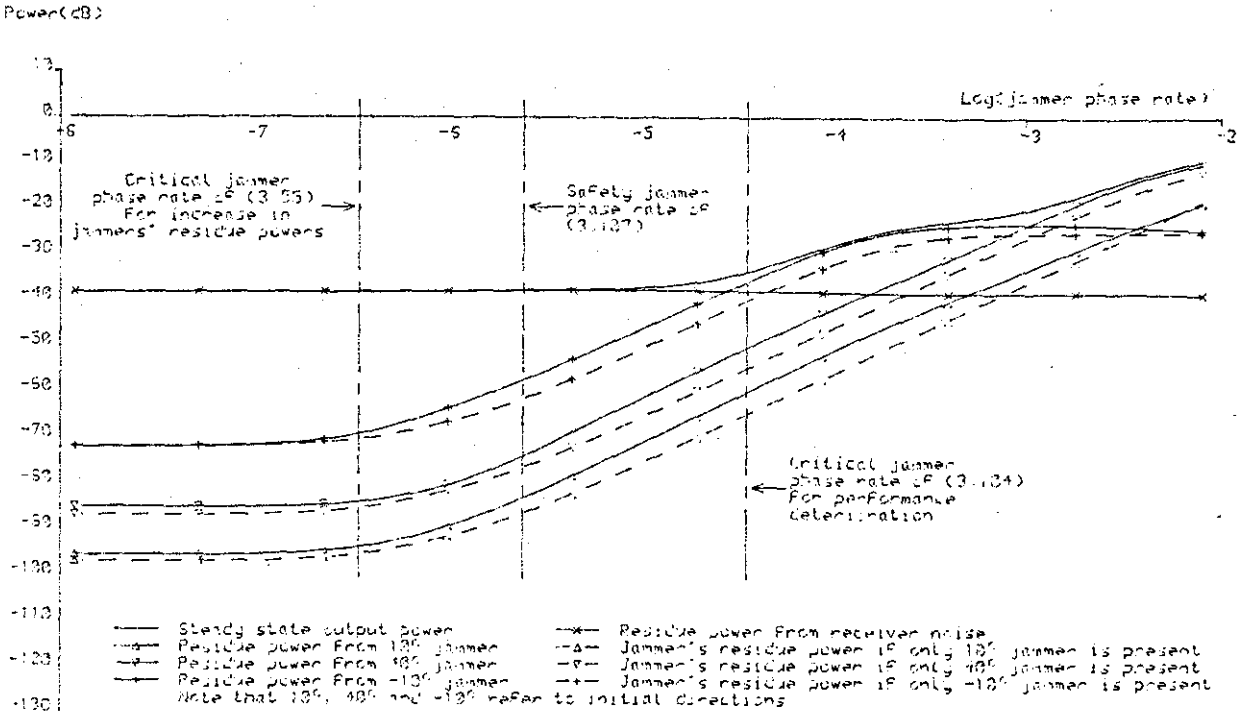

Fig.3.5 Variation of steady state output power and its components with jammer phase rate for a 8-element array with -40dB receiver noise and feedback factor of 0.025. Three jammers of powers 0, -10 and -25dB arrive initially from 20°, 40° and -10° respectively. This more complex example is again typical of that when the jammers are far apart and the array has extra degrees of freedom.

fig.3.3a, but for a more complex 8-element, 3-jammer situation with -40dB receiver noise power and feedback factor of 0.025. The three jammers, of powers 0, -10 and -25dB, arrive initially from 20°, 40° and -10° respectively. Again, the independence of the jammers' residue powers, the relevance of the critical jammer phase rates of (3.55) and (3.104) as well as the general remarks regarding fig.3.3a are demonstrated even in this more complex scenario. In general, the scenarios studied by figs.3.3-3.5 represent examples in which the jammers are far apart and the array has extra degrees of freedom. In these situations, the theoretical deductions discussed under assumption (3.99) has been found to be valid and applicable, at least approximately.

Fig.3.6a shows the same set of curves as fig.3.3a except that the two jammers now arrive from 10° and 13° initially and both have powers -3dB. This scenario is one typical example when the array has extra degrees of freedom but the jammers are close together. By comparison, the steady state output power and its components have the same behaviour as that of fig.3.3a apart from two differences. Firstly, for very large jammer phase rate after performance deterioration, the residue power curve due to the jammer at initially 13° decreases in gradient while that for the other jammer has a notch. Secondly, even for smaller jammer phase rate, the jammers' residue power curves are very much greater, though by roughly a constant margin, than the corresponding broken ones when only one of the jammers is present. Obviously, because of this, performance deterioration starts at jammer phase rate which is much smaller than the critical value of (3.104) and approaches, though not yet reached, the safety value of (3.107). The rather complex behaviour of the jammers' residue power curves

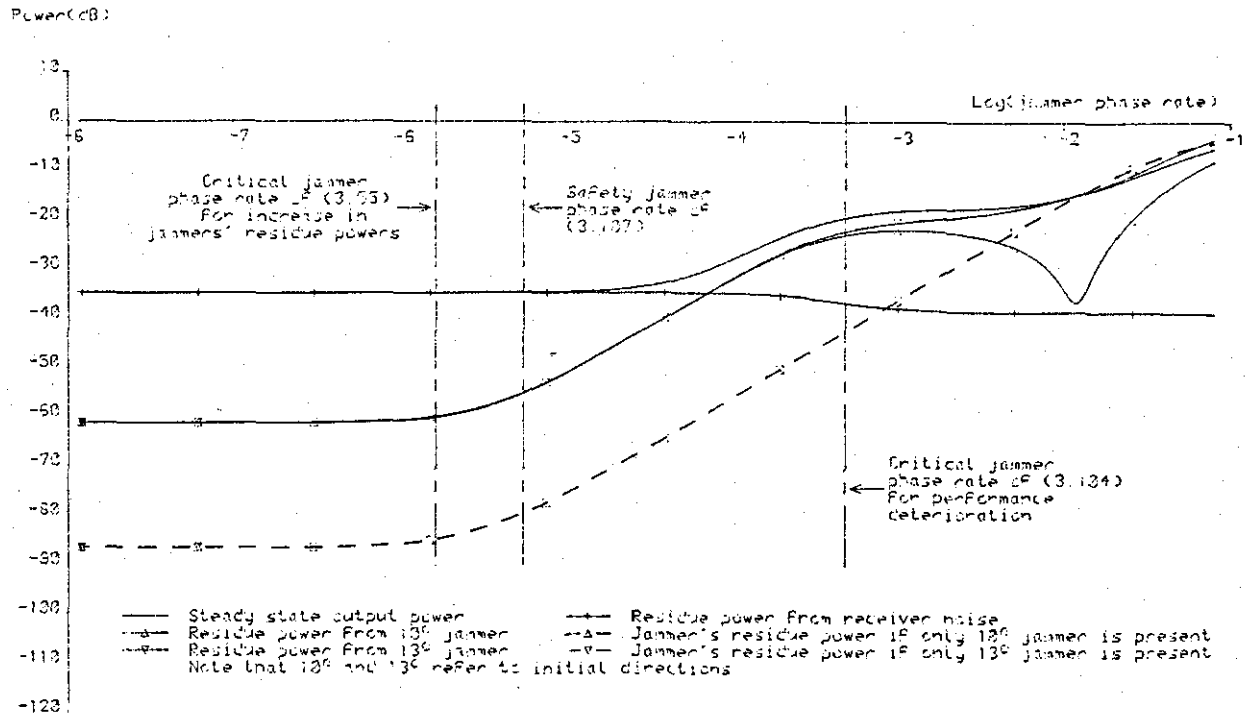

Fig.3.6a Steady state output power and its components

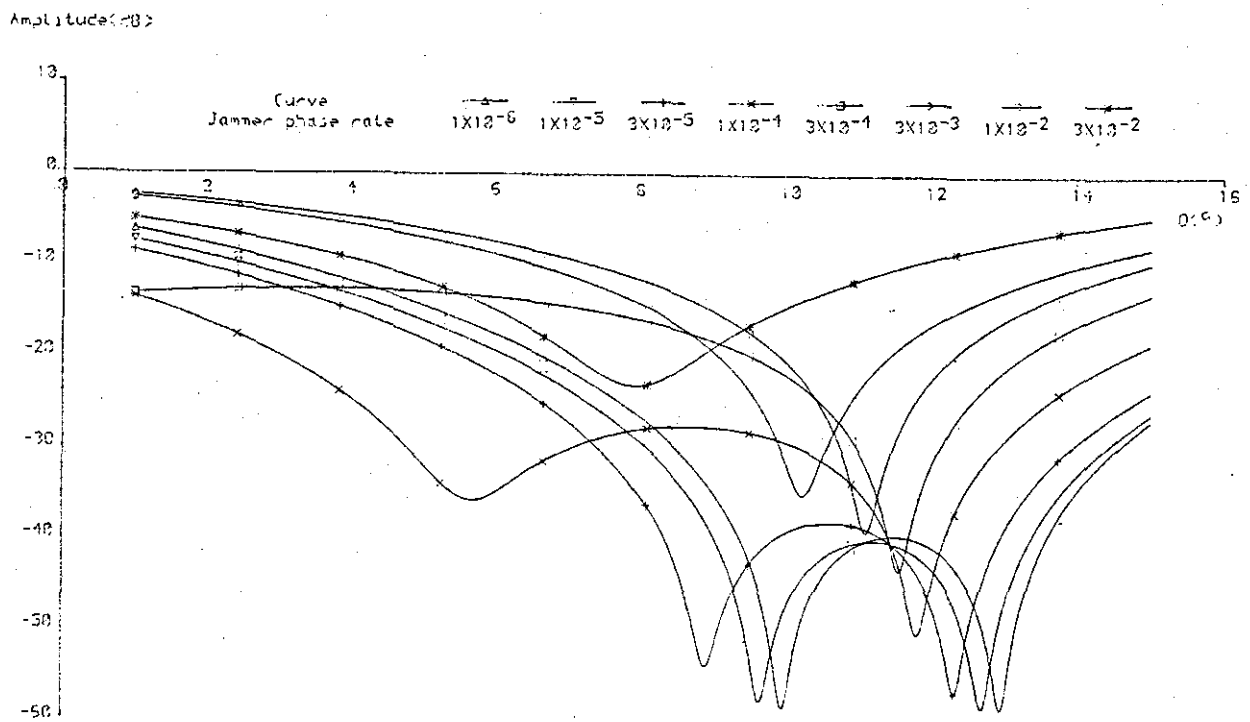

Fig.3.6b Steady state directional pattern

Fig.3.6 Variation of steady state behaviour with jammer phase rate for the array of fig.3.3 when two jammers, both of powers -3dB, arrive initially from 10° and 13°. This is one typical example where the jammers are closed together but the array still has extra degrees of freedom.

mentioned for large jammer phase rate can be better understood from the variation of steady state directional pattern with jammer phase rate shown in fig.3.6b in this situation. As the jammer phase rate increases above the critical value of (3.55), the movements (decreasing in depths and shifting to the left) of the two nulls relative to the corresponding jammers are roughly equal and correspond to the 20dB per decade gradient of the jammers' residue power curves in fig.3.6a. Further increase in jammer phase rate then causes performance deterioration after which the null at initially 10° starts to shift relatively faster to the left and disappears first while the other null is about half way between the two jammers. Intuitively, since the array is not able to form two nulls to track the jammers, it uses all its degrees of freedom to form one null in the middle of the two closely spaced jammers. As the jammer phase rate increases still further, this null shifts to the left and decreases in depth relatively slowly until it has passed the jammer at initially 10°, accounting for the decrease in gradients of the jammers' residue power curves. Obviously, when this null shifts pass the jammer at initially 10°, the residue power due to this jammer first decreases and then increases, resulting in the notch observed in the corresponding residue power curve.

Fig.3.7 shows the same set of curves as fig.3.3a, using, again, the same array but with three jammers of powers 0, -10 and -20dB arriving initially from 20°, 40° and 70° respectively. This is one typical example when the jammers are far apart but the array has no extra degree of freedom. Note that the behaviour of the steady state output power and residue powers is essentially the same as that of fig.3.6a. In particular, when the weakest

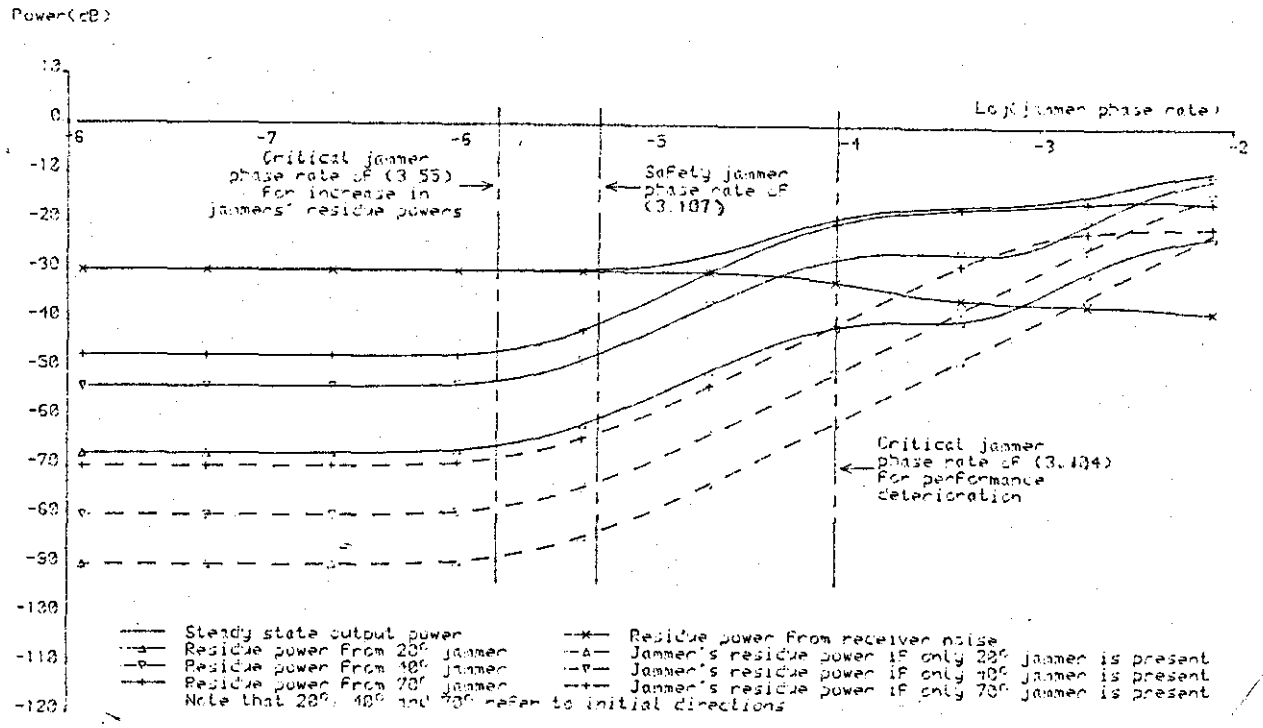

Fig.3.7 Variation of steady state output power and its components with jammer phase rate for the array of fig.3.3 when three jammers, of powers 0, -10 and -20dB, arrive initially from 20°, 40° and 70° respectively. This is one typical example where the jammers are far apart but the array has no extra degree of freedom.

jammer's residue power curve starts to level off at around -20dB indicating that the array is no longer able to track this jammer, the array uses its two degrees of freedom initially for rejecting this jammer to reject the other two jammers instead, resulting in the intermediate levelling off of their residue power curves. This behaviour is virtually the same as the formation of one null between the jammers in the situation of fig.3.6 and is also slightly noticeable in figs.3.3a, 3.4 and 3.5. Many other scenarios in which the jammers are far apart/closed together and/or the array has/has no extra degrees of freedom have been studied. The results obtained will not be presented as no new characteristic concerning the array behaviour is observed.

One important observation from all the simulation results

is that if the jammers' residue power curves are increasing with jammer phase rate, they always tend to increase with gradients of roughly 20dB per decade. In particular, for jammer phase rate above roughly the critical value of (3.55) but before any of the jammers' residue power curves levels off or decreases, the curves always increase with gradient of about 20dB per decade. This can be explained theoretically by examining the matrix factor $(Q^T D^{-1} Q + \Lambda^{-1})^{-1}$ in (3.59). Using (3.49d,e,h) and (3.54), the (p,q) element of the N·N matrix $Q^T D^{-1} Q + \Lambda^{-1}$ is

$$[Q^T D^{-1} Q + \Lambda^{-1}]_{pq} = \begin{cases} \frac{1}{s_p} + \sum_{n=1}^{N} \frac{1}{s_0 + jm\Delta\Phi/a}, & p=q \\ \sum_{n=1}^{N} \frac{e^{jn(\Phi_q - \Phi_p)}}{s_0 + jm\Delta\Phi/a}, & p\neq q \end{cases} \quad . \qquad (3.110)$$

Clearly, for $\Delta\Phi$ greater than as_0 but much smaller than $a\underset{n}{\text{Min}}\{s_n\}$, this is roughly inversely proportional to $\Delta\Phi$ and thus the matrix $(Q^T D^{-1} Q + \Lambda^{-1})^{-1}$ is roughly proportional to $\Delta\Phi$. Evidently, in such cases, all the terms under the summation in (3.59) are roughly proportional to the square of jammer phase rate and hence, all the jammers' residue power curves increase with about 20dB per decade gradients.

Summarizing the deductions obtained in the detailed discussion of this and the last sections, array performance deterioration from significant increase in steady state output power has been found to be the result of increase in jammers' residue powers. As the jammer phase rate increases, the jammers' residue powers begin to increase simultaneously at the critical jammer phase rate of (3.55), where the steady state weights also start to deviate from their optimal values, and soon become proportional to the square of jammer phase rate. As the jammer phase rate increases further

so that some of the jammers' residue powers become increasing less rapidly, the jammers' residue powers may start having complex behaviour which has to be accounted for by the shifting of nulls and the switching of degrees of freedom of the array from nulling weak to strong jammers. However, when the jammers are far apart and the array has extra degrees of freedom, the behaviour of the jammers' residue powers are quite independent and simple and roughly equal to that obtained in single-jammer situations when the corresponding jammers are present on their own. As a result, array performance deterioration starts at around the critical jammer phase rate of (3.104) which is usually much greater than the actual value in other situations. Finally, because of the ability of the array to suppress the strong jammers' residue powers, before they increase, to well below optimal output power, array performance deterioration usually starts at jammer phase rate much greater than the critical value of (3.55). However, there exists "worst" situations where the safety jammer phase rate of (3.107), being the minimum of (3.104) and closed to the critical value of (3.55) which is obviously the lowest upper bound before performance deterioration, is approached. From the simulation results examined, such worst situations are associated with scenarios in which: (a) the range of the jammers' powers is large and/or (b) the jammers are close together and/or the array has no extra degree of freedom. Clearly, the first two circumstances are also associated with situations when the array has slow transient convergence behaviour in the rotating and stationary environments.

3.10 Maximum Scan Rate Limitation of the Radar Sidelobe Canceller

The differences between the radar sidelobe canceller and the

power inversion array of fig.3.1 have been discussed in section 2.2. Obviously, in terms of the second order input statistics, the former is the same as the latter if, in addition to both having the same geometries: (a) corresponding to element 1 in fig.3.1, the high gain antenna in the radar sidelobe canceller is designed to have uniform sidelobe level, (b) all the jammers are in the sidelobes of the high gain antenna, which is a case of most interest, (c) the high gain antenna and the other elements, which are isotropic with the same antenna gains as the sidelobe gain of the high gain antenna, have equal receiver noise power and (d) the target returns in the look direction of the high gain antenna are small enough to be neglected. Provided these conditions are satisfied, all the results derived can be applied directly to the sidelobe canceller if it is further assumed that the constant rotational speed of the radar does not change the deductions significantly.

Thus, under the assumptions of the last paragraph, the safety jammer phase rate of (4.107) can be used directly to determine the maximum scan rate limitation of the radar sidelobe canceller. Consider an example of a 5-element, 20 wavelength spacing canceller with 10% misadjustment operating in a 40dB ENR environment. The safety jammer phase rate of (3.107) is then given by $4\cdot10^{-6}$ rad. per sampling period or 8 rad. per second if the radar has a wavelength of 1MHz and Nyquist sampling at 2MHz is used. Assuming further a scan sector of 180° so that as θ varies from -90° to 90°, the total change in element to element phase Φ, given by $2\pi df_0\sin\theta/c$, is 80π rad., the maximum scan rate is obviously limited to about $8/80\pi$ or 1/30 scan per second.

3.11 Conclusion

Having analyzed the array behaviour in stationary environments, the nonstationary rotating environment was formulated elegantly in terms of the rate of rotation, the jammer phase rate, in this chapter. The steady state behaviour was then solved implicitly in general terms and found to be well defined. In particular, the weight variance noise, steady state and optimal output powers are time-independent, while the steady state and optimal weights define directional patterns which rotate in synchronization with the jammers. Furthermore, the steady state weights and jammers' residue powers start to deviate from their optimal values at the critical jammer phase rate of (3.55). Regarding the transient convergence behaviour, the average weights converge in similar manner as in stationary environments, though the output power may converge in more complicated fashion in, for example, having many more time constants. Theoretically and by using simulation results, the more interesting steady state behaviour was studied in more detail in the single-jammer situation, leading to the derivation of the critical jammer phase rate of (3.98) for array performance deterioration. Similarly, when the jammers are far apart and the array has extra degrees of freedom, the multi-jammer situation was found to be roughly a linear combination of single-jammer situations and the critical jammer phase rate of (3.104), with a minimum value given by the safety jammer phase rate of (3.107), was obtained for performance deterioration. In other situations, the steady state behaviour may be more complex and have to be explained by the shifting of nulls and the switching of degrees of freedom from nulling weak to strong jammers.

Furthermore, performance deterioration now usually starts at jammer phase rate much greater than the critical value of (3.104), though still below the safety value of (3.107). In any case, because of the ability of the array to suppress the strong jammers' residue powers to well below optimal output power for small jammer phase rate, performance deterioration usually begins at jammer phase rate much greater than the critical value of (3.55). However, when (a) the jammers are closed together and/or (b) the jammers have large range of powers and/or (c) the array has no extra degree of freedom, the safety jammer phase rate of (3.107), being closed to the critical value of (3.55), may be approached. Lastly, as an application example, using the safety jammer phase rate of (3.107), the maximum scan rate of a 5-element sidelobe canceller was found to be limited to about 1/30 scan per second.

3.12 Appendix

3.12.1 Derivation of (3.20)

Post-multiplying both sides of (3.19) with their own complex conjugate transposes and taking ensemble average gives

$$\begin{aligned}\overline{\Delta W(k+1)\Delta W(k+1)^T} &= \overline{\Delta W(k)\Delta W(k)^T} + a^2\overline{y(k)^*y(k)X(k)X(k)^T} \\ &+ a^2R(k)[\overline{W(k)} - W_{opt}(k)][\overline{W(k)} - W_{opt}(k)]^TR(k) \\ &- a^2\overline{y(k)^*X(k)}[\overline{W(k)} - W_{opt}(k)]^TR(k) \\ &- a^2R(k)[\overline{W(k)} - W_{opt}(k)]\overline{y(k)X(k)^T} \\ &- a\overline{y(k)^*X(k)\Delta W(k)^T} - a\overline{y(k)\Delta W(k)X(k)^T} \\ &+ aR(k)[\overline{W(k)} - W_{opt}(k)]\overline{\Delta W(k)^T} + a\overline{\Delta W(k)}[\overline{W(k)} - W_{opt}(k)]^TR(k).\end{aligned} \tag{3A.1}$$

Since the weights are independent of the inputs at the same sampling instant, the ensemble average of $y(k)^*X(k)$ is

$$\overline{y(k)*X(k)} = \overline{x_0(k)*X(k)} + \overline{X(k)X(k)^T W(k)}$$
$$= R_0(k) + R(k)\overline{W(k)}$$
$$= R(k)[\overline{W(k)} - W_{opt}(k)] \qquad (3A.2)$$

where $W_{opt}(k)$ is given by (3.7). Similarly, with $\Delta W(k)$ defined by (3.12), the ensemble average of $y(k)*X(k)\Delta W(k)^T$ is

$$\overline{y(k)*X(k)\Delta W(k)^T} = \overline{x_0(k)*X(k)\Delta W(k)^T} + \overline{X(k)X(k)^T W(k)\Delta W(k)^T}$$
$$= R_0(k)\overline{\Delta W(k)^T} + \overline{R(k)W(k)\Delta W(k)^T}$$
$$= R_0(k)\overline{\Delta W(k)^T} + R(k)\overline{W(k)}[\overline{\Delta W(k)^T}] + R(k)\overline{\Delta W(k)\Delta W(k)^T}. \qquad (3A.3)$$

Finally, substituting (3A.2) and (3A.3) into (3A.1) and using (3.13) then easily yields (3.20).

3.12.2 Derivation of (3.22)

Since, at any sampling instant, the inputs are complex Gaussian random variables independent of the weights, the ensemble average of the (p,q) element of the (M-1)·(M-1) matrix $y(k)*y(k)X(k)X(k)^T$ is, using (3.21) and ignoring the time index k for convenience,

$$\overline{[y*yXX^T]}_{pq} = \overline{(x_0^* + X^T W)(x_0 + W^T X)[X]_p[X^*]_q}$$
$$= \overline{x_0^* x_0 x_q^* x_p} + 2\mathrm{Re}\{\sum_{m=1}^{M-1} (\overline{w_m})\overline{x_m^* x_0 x_q^* x_p}\}$$
$$+ \sum_{m,n=1}^{M-1} (\overline{w_n^* w_m})\overline{x_m^* x_n x_q^* x_p}$$
$$= (\overline{x_0^* x_0})(\overline{x_q^* x_p}) + (\overline{x_0^* x_p})(\overline{x_q^* x_0})$$
$$+ 2\mathrm{Re}\{\sum_{m=1}^{M-1} (\overline{w_m})(\overline{x_m^* x_0})(\overline{x_q^* x_p}) + (\overline{w_m})(\overline{x_m^* x_p})(\overline{x_q^* x_0})\}$$
$$+ \sum_{m,n=1}^{M-1} (\overline{w_n^* w_m})(\overline{x_m^* x_n})(\overline{x_q^* x_p}) + (\overline{w_n^* w_m})(\overline{x_m^* x_p})(\overline{x_q^* x_n})$$
$$= s_x[R]_{pq} + [R_0]_p[R_0^*]_q + \overline{W^T R W}[R]_{pq} \qquad (3A.4)$$

$$+ 2\mathrm{Re}\{\sum_{m=1}^{M-1} [\bar{W}]_m [R_0^*]_m [R]_{pq} + [\bar{W}]_m [R]_{pm} [R_0^*]_q\}$$
$$+ \sum_{m,n=1}^{M-1} [R]_{nq} \overline{[WW^T]}_{mn} [R]_{pm}.$$

Clearly, the ensemble average of $y(k)^*y(k)X(k)X(k)^T$ is

$$\overline{y(k)^*y(k)X(k)X(k)^T} = R_0(k)R_0(k)^T + R(k)\overline{W(k)W(k)^T}R(k) \qquad (3A.5)$$
$$+ R(k)\overline{W(k)}R_0(k)^T + R_0(k)\overline{W(k)}^T R(k)$$
$$+ [s_x(k) + \overline{W(k)^T R(k) W(k)} + R_0(k)^T\overline{W(k)} + \overline{W(k)}^T R_0(k)]R(k).$$

Substituting (3.12) and using (3.11) and (3.13) then gives

$$\overline{y(k)^*y(k)X(k)X(k)^T} = s(k)R(k) + R(k)\overline{\Delta W(k)\Delta W(k)^T}R(k) \qquad (3A.6)$$
$$+ [R_0(k) + R(k)\overline{W(k)}][R_0(k) + R(k)\overline{W(k)}]^T.$$

Using (3.7) and (3.15), this becomes

$$\overline{y(k)^*y(k)X(k)X(k)^T} = [s_y(k) + s_{wt}(k)]R(k) \qquad (3A.7)$$
$$+ R(k)[\overline{W(k)} - W_{opt}(k)][\overline{W(k)} - W_{opt}(k)]^T R(k)$$
$$+ R(k)\overline{\Delta W(k)\Delta W(k)^T}R(k)$$

which, if substituted into (3.20), obviously gives rise to (3.22).

3.12.3 Derivation of (3.51) and (3.52)

By substituting (3.49b,c), (3.45) becomes

$$W_{opt}(k) = F^k W_{opt} = -F^k(s_0 I + Q\Lambda Q^T)^{-1}Q\Lambda G. \qquad (3A.8)$$

Using (3.50), this can be manipulated to give (3.51) as follows.

$$W_{opt}(k) = -F^k\{(s_0 I)^{-1} - (s_0 I)^{-1}Q[Q^T(s_0 I)^{-1}Q + \Lambda^{-1}]^{-1}Q^T(s_0 I)^{-1}\}Q\Lambda G$$
$$= -F^k(s_0 I)^{-1}Q\{[Q^T(s_0 I)^{-1}Q + \Lambda^{-1}]^{-1}[Q^T(s_0 I)^{-1}Q + \Lambda^{-1}]$$
$$- [Q^T(s_0 I)^{-1}Q + \Lambda^{-1}]^{-1}Q^T(s_0 I)^{-1}Q\}\Lambda G$$
$$= -F^k(s_0 I)^{-1}Q[Q^T(s_0 I)^{-1}Q + \Lambda^{-1}]^{-1}G. \qquad (3A.9)$$

Similarly, by substituting (3.48) and (3.49b,c), (3.46) becomes

$$W_s(k) = F^k W_s = -F^k(D + Q\Lambda Q^T)^{-1}Q\Lambda G \tag{3A.10}$$

where

$$D = s_0 I + \frac{F - I}{a} \tag{3A.11}$$
$$= s_0 I + \text{dia}\left(\frac{e^{j\Delta\Phi} - 1}{a}, \frac{e^{2j\Delta\Phi} - 1}{a}, \cdots, \frac{e^{(M-1)j\Delta\Phi} - 1}{a}\right).$$

Clearly, (3A.11) is the same as (3.53) and using the same manipulation which leads to (3A.9) on (3A.10) results in (3.52).

3.12.4 Derivation of (3.57) and (3.59)

The optimal output power component due to the nth of the N jammers is obviously given by (3.3) with W(k) being equal to $W_{opt}(k)$ and the second order input statistics replaced by their components due to only the nth jammer. Thus, from (3.49a-c), this optimal output power component is

$$s_n[1 + W_{opt}(k)^T F^k Q_n + (F^k Q_n)^T W_{opt}(k) + W_{opt}(k)^T F^k Q_n \tag{3A.12}$$
$$\cdot (F^k Q_n)^T W_{opt}(k)] = s_n|1 + (F^k Q_n)^T W_{opt}(k)|^2.$$

With $W_{opt}(k)$ given by (3.51), this becomes

$$s_n|1 + (F^k Q_n)^T W_{opt}(k)|^2 \tag{3A.13}$$
$$= s_n|1 - Q_n{}^T(s_0 I)^{-1}Q[Q^T(s_0 I)^{-1}Q + \Lambda^{-1}]^{-1}G|^2.$$

Defining K_n as

$$K_n = \text{dia}(\underbrace{0, 0, \cdots, 0}_{n}, 1, \underbrace{0, 0, \cdots, 0}_{N-n}) \tag{3A.14}$$

and using (3.49e,g,h), (3A.13) becomes

$$s_n|1 + (F^k Q_n)^T W_{opt}(k)|^2 = s_n|Q_n{}^T(s_0 I)^{-1}Q[Q^T(s_0 I)^{-1}Q + \Lambda^{-1}]^{-1}G$$
$$- G^T K_n[Q^T(s_0 I)^{-1}Q + \Lambda^{-1}][Q^T(s_0 I)^{-1}Q + \Lambda^{-1}]^{-1}G|^2$$
$$= s_n|G^T K_n \Lambda^{-1}[Q^T(s_0 I)^{-1}Q + \Lambda^{-1}]^{-1}G|^2$$
$$= \frac{|[\{Q^T(s_0 I)^{-1}Q + \Lambda^{-1}\}^{-1}G]_n|^2}{s_n}. \tag{3A.15}$$

Using (3.51), the optimal output power component due to receiver noise is clearly

$$s_0[1 + W_{opt}(k)^T W_{opt}(k)] = s_0(1 + W_{opt}{}^T W_{opt}) = s_0(1 + \|W_{opt}\|) \qquad (3A.16)$$

where $\|A\|$ is the Euclidean norm of the vector A. Combining (3A.15) and (3A.16) then gives rise to (3.57). Similarly, (3.59) is obtained by applying the same arguments discussed for $W_{opt}(k)$ to $W_s(k)$ of (3.52).

3.12.5 Derivation of (3.92) and (3.93)

With the inequality $\alpha s_0 \gg (M-1)\Delta\Phi$ implied by (3.89), the summation in (3.88) can be approximated by using Maclaurin's theorem and neglecting second and higher order terms as

$$\sum_{m=1}^{M-1} \alpha s_1(\alpha s_0 + jm\Delta\Phi)^{-1} = \frac{s_1}{s_0}\sum_{m=1}^{M-1}(1 + \frac{jm\Delta\Phi}{\alpha s_0})^{-1} \simeq \frac{s_1}{s_0}\sum_{m=1}^{M-1}(1 - \frac{jm\Delta\Phi}{\alpha s_0}) = \frac{(M-1)s_1 - js_1(M-1)M\Delta\Phi/2\alpha s_0}{s_0}. \qquad (3A.17)$$

Thus, (3.88) becomes

$$[1 + s_1 tr(D^{-1})]^{-1} \simeq [\frac{(M-1)s_1 + s_0 - js_1(M-1)M\Delta\Phi/2\alpha s_0}{s_0}]^{-1} = \frac{s_0}{(M-1)s_1 + s_0}\{1 - \frac{js_1(M-1)M\Delta\Phi}{2\alpha s_0[(M-1)s_1 + s_0]}\}^{-1}. \qquad (3A.18)$$

Obviously, from (3.89), the imaginary term has magnitude less than unity. Hence, further use of Maclaurin's theorem with (3.89) and neglecting second and higher order terms gives

$$[1 + s_1 tr(D^{-1})]^{-1} \simeq \frac{s_0}{(M-1)s_1 + s_0}\{1 + \frac{js_1(M-1)M\Delta\Phi}{2\alpha s_0[(M-1)s_1 + s_0]}\} \simeq \frac{s_0(1 + jM\Delta\Phi/2\alpha s_0)}{(M-1)s_1 + s_0}. \qquad (3A.19)$$

By substituting (3.54) and (3A.19), the mth of the M-1 elements of

W_s, as given in (3.85), is thus

$$[W_s]_m \simeq \frac{-s_1[Q_1]_m}{(M-1)s_1 + s_0}\left(1 + \frac{jM\Delta\Phi}{2as_0}\right)\left(1 + \frac{jm\Delta\Phi}{as_0}\right)^{-1}. \qquad (3A.20)$$

Using Maclaurin's theorem with $as_0 \gg (M-1)\Delta\Phi$ again and neglecting second and higher order terms then yields

$$[W_s]_m \simeq \frac{-s_1[Q_1]_m}{(M-1)s_1 + s_0}\left(1 + \frac{jM\Delta\Phi}{2as_0}\right)\left(1 - \frac{jm\Delta\Phi}{as_0}\right)$$

$$\simeq \frac{-s_1[Q_1]_m}{(M-1)s_1 + s_0}\left[1 + \left(\frac{M}{2} - m\right)\frac{j\Delta\Phi}{as_0}\right] \qquad (3A.21)$$

which, with (3.85), obviously gives rise to (3.92).

With Q_1 given by (3.49e), the Euclidean norm of W_s, from (3A.21), is

$$\|W_s\| \simeq \frac{(M-1)s_1^2}{[(M-1)s_1 + s_0]^2}. \qquad (3A.22)$$

Note that if exact manipulation is used to find the Euclidean norm from (3A.21), a second order term will result from the first order term in (3A.21). However, since second and higher order terms have been neglected in (3A.21) and thus the Euclidean norm found from this equation cannot be more accurate than a first order approximation, the second order term is neglected and (3A.22) results. Similarly, the modulus square of $[1+s_1\mathrm{tr}(D^{-1})]^{-1}$, from (3A.19), is

$$|[1 + s_1\mathrm{tr}(D^{-1})]^{-1}|^2 \simeq \left[\frac{s_0}{(M-1)s_1 + s_0}\right]^2. \qquad (3A.23)$$

Clearly, substituting (3A.22) and (3A.23) into (3.87) leads to (3.93).

3.12.6 Derivation of (3.96) and (3.97)

Using Maclaurin's theorem with the inequality $\Delta\Phi \ll as_0$ implied

by (3.90) and neglecting second and higher order terms, the summation in (3.88) can be approximated by

$$\sum_{m=1}^{M-1} as_1(as_0 - jm\Delta\Phi)^{-1} = \sum_{m=1}^{M-1} \left(\frac{as_1}{jm\Delta\Phi}\right)\left(1 + \frac{as_0}{jm\Delta\Phi}\right)^{-1}$$

$$\simeq \sum_{m=1}^{M-1} \left(\frac{as_1}{jm\Delta\Phi}\right)\left(1 - \frac{as_0}{jm\Delta\Phi}\right) = \frac{as_1}{j\Delta\Phi}\left(\sum_{m=1}^{M-1}\frac{1}{m}\right) + \frac{a^2 s_0 s_1}{\Delta\Phi^2}\left(\sum_{m=1}^{M-1}\frac{1}{m^2}\right)$$

$$\simeq \frac{\ln(2M-1)as_1}{j\Delta\Phi} + \frac{2(M-1)a^2 s_0 s_1}{M\Delta\Phi^2}. \qquad (3A.24)$$

By substitution, (3.88) becomes

$$[1 + s_1 tr(D^{-1})]^{-1} \simeq \frac{j\Delta\Phi}{\ln(2M-1)as_1}\left[1 + \frac{2j(M-1)as_0}{M\ln(2M-1)\Delta\Phi} + \frac{j\Delta\Phi}{\ln(2M-1)as_1}\right]^{-1}. \qquad (3A.25)$$

From (3.90), both the second and third terms can be seen to have magnitudes less than 1/2. Therefore, using Maclaurin's theorem and neglecting second and higher order terms gives (3A.25) as

$$[1 + s_1 tr(D^{-1})]^{-1} \simeq \frac{j\Delta\Phi}{\ln(2M-1)as_1}\left[1 - \frac{2j(M-1)as_0}{M\ln(2M-1)\Delta\Phi} - \frac{j\Delta\Phi}{\ln(2M-1)as_1}\right]. \qquad (3A.26)$$

By substituting (3.54) and (3A.26), the mth of the M-1 elements of W_s, as given in (3.85), is thus

$$[W_s]_m \simeq \frac{-[Q_1]_m}{m\ln(2M-1)}\left[1 - \frac{j\Delta\Phi}{\ln(2M-1)as_1} - \frac{2j(M-1)as_0}{M\ln(2M-1)\Delta\Phi}\right] \cdot \left(1 + \frac{as_0}{jm\Delta\Phi}\right)^{-1}. \qquad (3A.27)$$

Using Maclaurin's theorem with $\Delta\Phi \backslash as_0$ and neglecting second and higher order terms then yields

$$[W_s]_m \simeq \frac{-[Q_1]_m}{m\ln(2M-1)}\left[1 - \frac{j\Delta\Phi}{\ln(2M-1)as_1} - \frac{2j(M-1)as_0}{M\ln(2M-1)\Delta\Phi}\right]\left(1 + \frac{jas_0}{m\Delta\Phi}\right)$$

$$\simeq \frac{-[Q_1]_m}{m\ln(2M-1)}\left\{1 - \frac{j\Delta\Phi}{\ln(2M-1)as_1} - \frac{jas_0}{\Delta\Phi}\left[\frac{2(M-1)}{M\ln(2M-1)} - \frac{1}{m}\right]\right\} \qquad (3A.28)$$

which, together with (3.85), obviously gives rise to (3.96).

With the same arguments as in deriving (3A.22), the Euclidean norm of W_s, from (3A.28), is

$$\|W_s\| \simeq \frac{1}{[\ln(2M-1)]^2}\left(\sum_{m=1}^{M-1}\frac{1}{m^2}\right) \simeq \frac{2(M-1)}{M[\ln(2M-1)]^2} \qquad (3A.29)$$

in a first order approxiamtion. Similarly, the modulus square of $[1+s_1 tr(D^{-1})]^{-1}$ is, from (3A.26),

$$|[1 + s_1 tr(D^{-1})]^{-1}|^2 \simeq [\frac{\Delta\Phi}{\ln(2M-1)as_1}]^2. \qquad (3A.30)$$

Clearly, substituting (3A.29) and (3A.30) into (3.87) leads to (3.97).

3.12.7 Derivation of (3.94) and (3.95)

By substituting (3A.24) which is derived under the inequality $\Delta\Phi \backslash as_0$, also implied in (3.91), (3.88) becomes

$$[1 + s_1 tr(D^{-1})]^{-1} \simeq [1 + \frac{\ln(2M-1)as_1}{j\Delta\Phi} + \frac{2(M-1)a^2 s_0 s_1}{M\Delta\Phi^2}]^{-1}. \qquad (3A.31)$$

Because of (3.91), the second and third terms can easily be seen to have magnitudes less than 1/2. Hence, using Maclaurin's theorem and neglecting second and higher order terms gives (3A.31) as

$$[1 + s_1 tr(D^{-1})]^{-1} \simeq 1 - \frac{\ln(2M-1)as_1}{j\Delta\Phi}. \qquad (3A.32)$$

By substituting (3.54) and (3A.32), the mth of the M-1 elements of W_s, as given in (3.85), is then

$$[W_s]_m \simeq \frac{jas_1[Q_1]_m}{m\Delta\Phi}[1 + \frac{j\ln(2M-1)as_1}{\Delta\Phi}](1 + \frac{as_0}{jm\Delta\Phi})^{-1}. \qquad (3A.33)$$

Using Maclaurin's theorem with $\Delta\Phi \backslash as_0$ again and neglecting second and higher order terms gives

$$[W_s]_m \simeq \frac{jas_1[Q_1]_m}{m\Delta\Phi}[1 + \frac{j\ln(2M-1)as_1}{\Delta\Phi} + \frac{jas_0}{m\Delta\Phi}] \qquad (3A.34)$$

which, with (3.85), obviously gives rise to (3.94).

With the same arguments as in deriving (3A.22), the Euclidean norm of W_s, from (3A.28), is

$$\|W_s\| \approx \left(\frac{as_1}{\Delta\Phi}\right)^2 \left(\sum_{m=1}^{M-1} \frac{1}{m^2}\right) \approx \frac{2(M-1)}{M}\left(\frac{as_1}{\Delta\Phi}\right)^2 \qquad (3A.34)$$

in a first order approximation. Similarly, the modulus square of $[1+s_1 tr(D^{-1})]^{-1}$, from (3A.32), is

$$|[1 + s_1 tr(D^{-1})]^{-1}|^2 \approx 1. \qquad (3A.35)$$

Substituting (3A.34) and (3A.35) into (3.87) then gives rise to (3.95).

CHAPTER 4 THE JAMMING REJECTION CAPABILITY OF THE BROADBAND TAPPED DELAY LINE POWER INVERSION ARRAY

4.1 Introduction

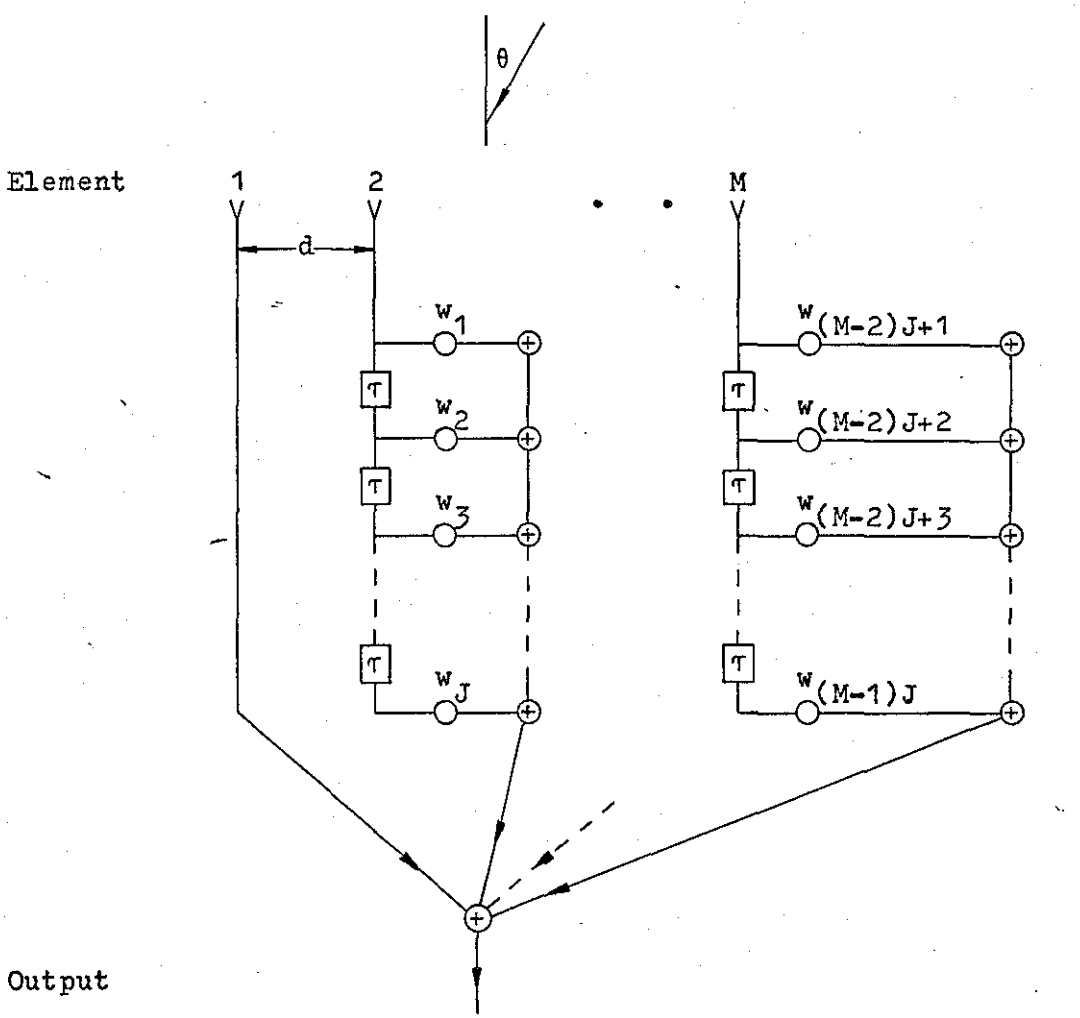

Fig.4.1 The broadband tapped delay line power inversion array.

Fig.4.1 shows the broadband tapped delay line power inversion [28,29] array concerned. It is obtained from fig.2.1 by replacing the processing behind each element with a tapped delay line having J taps and equal tap spacing τ. (The use of tapped delay line processing in broadband adaptive arrays was first suggested by Widrow [15]. Another broadband processing method is to divide the whole band into several equal divisions and use one narrowband array processor to process the array inputs within each division.

Thus, the broadband adaptive array becomes several similar narrowband adaptive arrays in parallel. For convenience, the term "alternative broadband processing" will be used to refer to this processing method which, together with tapped delay line processing, are the two most discussed processing techniques in broadband adaptive arrays.) Practically, the tap spacing used will not be greater than $1/4f_0$. For simplicity, this will be assumed so in the experimental study in this chapter. Since the objective of the power inversion array is to minimize output power, the weights w_m, $m=1,\cdots,(M-1)J$, in the figure will be optimal if the corresponding output power s_y is at the minimum value of s_{opt}, the optimal output power. Two most obvious observations on the use of tapped delay line processing on the power inversion array are: (a) As with increasing the number of elements, if the number of taps increases, the optimal output power will not increase and most probably decreases. However, the amount by which it decreases will also decrease with increasing number of taps since obviously, the optimal output power cannot be less than receiver noise power. (b) Since the optimal output power will evidently increase with the bandwidth, so will the number of taps required if the optimal output power is to be kept roughly constant at a useful level.

With any signal processing system, it is of interest to know the variation of the best performance obtainable in various situations. This is particularly true for the array concerned here as well as for other systems employing tapped delay line processing, because from such information, the tap spacing and number of taps required can be determined for a certain designed bandwidth. Then, the bandwidth under which the use of 2-tap delay line or with negligible difference, quadrature weighting will be adequate

can be determined. Thus, it is possible to determine the number of narrowband processors required if the alternative broadband is used instead of tapped delay line processing. Furthermore, the relative advantage, in terms of the number of variable weights required, of the two broadband processing techniques can be compared. In this chapter, the best performance obtainable from the array concerned will be investigated, both theoretically in a qualitative manner and quantitatively using simulation results, in terms of the jamming rejection capability, in various situations. The investigation will be slightly biased towards situations where the best performance obtainable is "worse", as the results obtained will be applied for the mentioned practical purposes and designs which will be based on assuming that the best performance obtainable is to be adequate under all the possible environments. Since the jamming rejection capability, to be discussed shortly, is a measure averaged over the entire band, this chapter will eventually also study, qualitatively from simulation results, the distortion in frequency response at various directions due to rejecting the jammers.

In this chapter, the jamming rejection capability will be used in synonymous with the more technical term "Jammer Gain (JG)", defined as

$$\text{Jammer Gain} = \frac{\text{optimal output power assuming no receiver noise}}{\text{element power assuming no receiver noise}}. \qquad (4.1)$$

Clearly, this is also the ratio of the component of output power from all the jammers to the total jammer power if the array utilizes all its ability to reject the jammers. This is therefore a measure of the ultimate ability of the array to reject the jammers. Since the power inversion array has the objective of minimi-

zing output power to reject the jammers, it is most appropriate to measure the best performance obtainable, which will be referred to as the performance henceforth in this chapter for convenience, by using the optimal output to receiver noise power ratio (ONR). Instead, as mentioned in the last paragraph, the JG will be used for this purpose because: (a) The ONR depends on one more parameter than does the JG. Specifically, corresponding to the jammer to receiver noise power ratios on which the ONR depends, the JG depends on the jammer power ratios. (b) Despite this, given the JG and element to receiver noise power ratio (ENR), it is possible to roughly estimate the ONR and so determine if significant improvement in ONR can be obtained by, say, increasing the number of taps. As will be explained in more detail in section 4.7, if the ENR is much greater than -JG in dB, the ONR will be roughly equal to -JG in dB and substantial improvement in ONR will be possible. On the contrary, if the ENR is less than -JG in dB, then most probably, the ONR will not be much greater than unity and substantial improvement in ONR not possible. With the JG as the performance measure, the worst performance for a given array is obviously measured by the Maximum Jammer Gain (MJG), given by

$$\text{Maximum Jammer Gain} = \begin{array}{l}\text{maximum value of JG over the domain}\\ \text{of number of jammers, jammers' direc-}\\ \text{tions, jammer power ratios and shapes}\\ \text{of jammers' power density spectrums.}\end{array} \quad (4.2)$$

Clearly, in addition to the JG, the MJG will be of particular interest in this chapter since, as implied in the discussion in the last paragraph, the practical applications to be discussed will be with respect to the worst performance in the worst environment.

Regarding other detailed studies with similar objectives in the literature, Rodgers and Compton[63] first investigated the

performance of employing tapped delay line processing in broadband adaptive arrays. The study was based on a 2-element LMS array [15]. The investigation by Mayhan [73] was more general, but was concerned with only narrowband arrays. The results in both studies, though useful, are not applicable to the broadband power inversion array of interest here.

This chapter is organized as follows. Section 4.2 investigates the JG theoretically for small bandwidth by expressing the autocorrelation functions of the jammers' power density spectrums in power series of bandwidth. Although only qualitative deductions are obtained, the derivation is general and can easily be extended to other similar systems using tapped delay line processing. Sections 4.3, 4.4 and 4.5 then study, in a more detailed and quantitative manner using simulation results, the JG of the 2-, 3- and multi-element arrays respectively. Some of the theoretical deductions are verified and the three sections will be based on the assumption that all the jammers have flat power density spectrums across the whole band. The situations when this assumption does not hold are then similarly but briefly studied in section 4.6. In section 4.7, the results obtained are applied to the practical applications mentioned. Section 4.8 discusses qualitatively using simulation results the frequency distortion introduced by rejecting the jammers. Conclusions are drawn in section 4.9.

Finally, the principal derivations and deductions of this chapter were published in [81].

4.2 Theoretical Derivation

In this section, the JG will be studied theoretically by assuming small bandwidth and expanding the autocorrelation funct-

ions of the jammers' power density spectrums in power series of bandwidth. The results derived, though mainly qualitative in nature, are useful for providing valuable insight and explaining many of the quantitative simulation results obtained. Furthermore, most of the derivation can easily be extended to other similar tapped delay line processing systems.

4.2.1 Autocorrelation functions

To start off the investigation, the autocorrelation functions of the jammers' power density spectrums will be expanded in power series of bandwidth in this subsection. In accordance with the assumptions concerning the environment in section 2.2, fig.4.2a shows the power density spectrum $S_n(f)$ of the nth of the N jammers

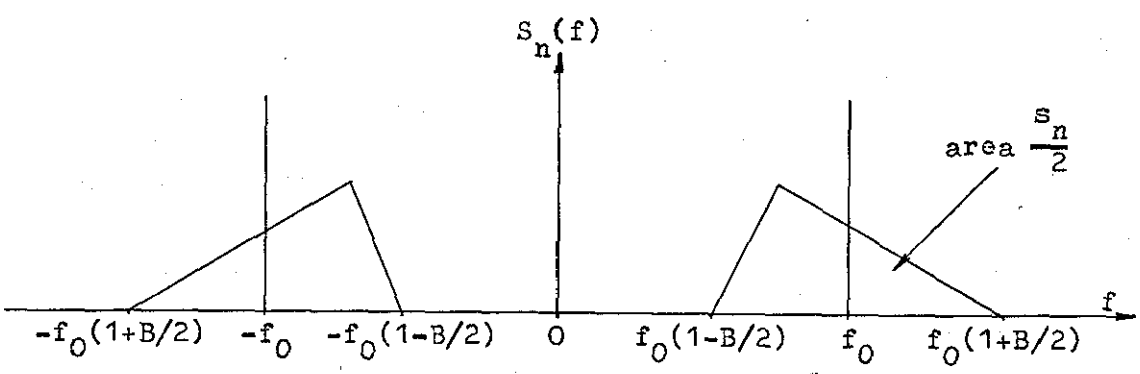

Fig.4.2a The nth jammer's power density spectrum $S_n(f)$

Fig.4.2b The spectrum $S_{0n}(f)$ corresponding to the nth jammer's power density spectrum $S_n(f)$

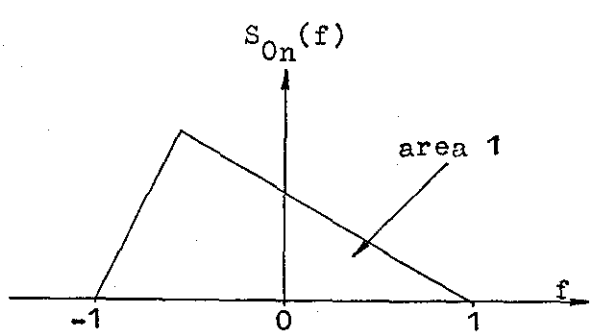

Fig.4.2 The power density spectrum $S_n(f)$ and spectrum $S_{0n}(f)$ corresponding to the nth jammer. The spectrum $S_{0n}(f)$ gives the shape of the power density spectrum.

with power s_n and arriving from direction θ_n. The shape of this power density spectrum is depicted by the spectrum $S_{On}(f)$ of fig. 4.2b with unity power and extending from f=-1 to f=1. For convenience and clarity, the term "spectrum" will henceforth be used in this thesis to mean the shape of the associated power density spectrum which depends also on the bandwidth and the corresponding jammers' or receiver noise power. From fig.4.2, the power density spectrum $S_n(f)$ is obviously related to the spectrum $S_{On}(f)$ by

$$S_n(f) = \frac{s_n}{Bf_0}\left[S_{On}\left(\frac{2f - 2f_0}{Bf_0}\right) + S_{On}\left(\frac{-2f - 2f_0}{Bf_0}\right)\right]. \qquad (4.3)$$

The autocorrelation function $R_n(t)$ of the power density spectrum is therefore

$$\begin{aligned} R_n(t) &= \int_{-\infty}^{\infty} S_n(f) e^{j2\pi ft} df \\ &= \frac{s_n}{2}\int_{-1}^{1} S_{On}(f)\left[e^{j2\pi f_0 t(1+Bf/2)} + e^{-j2\pi f_0 t(1+Bf/2)}\right] df \\ &= s_n \int_{-1}^{1} S_{On}(f)\cos\left[2\pi f_0 t\left(1 + \frac{Bf}{2}\right)\right] df. \end{aligned} \qquad (4.4)$$

Expanding the factor $\cos[2\pi f_0 t(1+Bf/2)]$ in power series of bandwidth as

$$\begin{aligned} \cos\left[2\pi f_0 t\left(1 + \frac{Bf}{2}\right)\right] &= \cos 2\pi f_0 t \cos \pi Bf_0 tf - \sin 2\pi f_0 t \sin \pi Bf_0 tf \\ &= \cos 2\pi f_0 t + \frac{(\pi Bf_0 tf)^2}{2!}\cos(2\pi f_0 t + \pi) + \frac{(\pi Bf_0 tf)^4}{4!}\cos(2\pi f_0 t \\ &\quad + 2\pi) + \cdots + (\pi Bf_0 tf)\cos\left(2\pi f_0 t + \frac{\pi}{2}\right) + \frac{(\pi Bf_0 tf)^3}{3!}\cos\left(2\pi f_0 t \right. \\ &\quad \left. + \frac{3\pi}{2}\right) + \cdots \\ &= \sum_{p=0}^{\infty} \frac{(\pi Bf_0 tf)^p}{p!}\cos\left(2\pi f_0 t + \frac{p\pi}{2}\right), \end{aligned} \qquad (4.5)$$

(4.4) then becomes

$$R_n(t) = s_n \sum_{p=0}^{\infty} M_{pn} \frac{(\pi Bf_0 t)^p}{p!}\cos\left(2\pi f_0 t + \frac{p\pi}{2}\right) \qquad (4.6)$$

where

$$M_{pn} = \int_{-1}^{1} S_{On}(f) f^p df, \quad p=0,\cdots,\infty. \tag{4.7}$$

As given, M_{pn} is the pth moment of the spectrum $S_{On}(f)$ about the origin and thus, is proportional to the pth derivative of the autocorrelation function of this spectrum at the origin. Evidently, (4.6) is essentially a Maclaurin series expansion.

4.2.2 Output power component due to the nth jammer

Having expanded the autocorrelation functions of the jammers' power density spectrums in power series of bandwidth, the component of output power due to the nth of the N jammers will now be derived in this subsection as a sum of square terms by using the expansion.

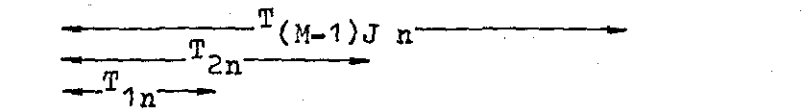

Fig.4.3 The equivalent filter for the nth jammer. To the jammer, the array is equivalent to this filter.

To the nth jammer, the array of fig.4.1 is equivalent to a general tapped delay line transversal filter, to be referred to as the nth jammer's equivalent filter for convenience, as shown in fig.4.3. As indicated, T_{mn}, $m=1,\cdots,(M-1)J$, is the total time delay from the input to the tapping point for the mth weight and can have any, including negative, value depending on the jammer's direction and tap spacing. Note that for clarity, the term "tap spacing" always refers to that of the tapped delay lines employed

in the array and not to those of the equivalent filters. Defining T_{0n} and w_0 as

$$T_{0n} = 0 \tag{4.8}$$

and

$$w_0 = 1 \tag{4.9}$$

for notational convenience, the output power component due to the nth jammer is, from the equivalent filter, clearly

$$s_{yn} = \sum_{m,l=0}^{(M-1)J} w_m w_l R_n(T_{mn} - T_{ln}). \tag{4.10}$$

From (4.6) and using the binomial expansion, the factor $R_n(T_{mn} - T_{ln})$ is

$$\begin{aligned} R_n(T_{mn} - T_{ln}) &= s_n \sum_{p=0}^{\infty} \frac{M_{pn}(\pi B f_0)^p}{p!} \cos[2\pi f_0(T_{mn} - T_{ln}) + \tfrac{\pi p}{2}](T_{mn} - T_{ln})^p \\ &= s_n \sum_{p=0}^{\infty} \frac{M_{pn}(\pi B f_0)^p}{p!} \cos[2\pi f_0(T_{mn} - T_{ln}) + \tfrac{\pi p}{2}] \\ &\quad \cdot \sum_{q=0}^{p} (-1)^q \binom{p}{q} T_{mn}^{p-q} T_{ln}^{q} \\ &= s_n \sum_{p=0}^{\infty} \sum_{q=0}^{p} \frac{M_{pn}(\pi B f_0)^p}{q!(p-q)!} T_{mn}^{p-q} T_{ln}^{q} \\ &\quad \cdot \cos[2\pi f_0(T_{mn} - T_{ln}) + \tfrac{\pi}{2}(p - 2q)]. \end{aligned} \tag{4.11}$$

Using the mathematical theorem

$$\sum_{z_1=0}^{\infty} \sum_{z_2=0}^{z_1} f(z_1, z_2) = \sum_{z_1, z_2=0}^{\infty} f(z_1 + z_2, z_2), \tag{4.12}$$

where $f(z_1, z_2)$ is a function of the indices z_1 and z_2, (4.11) becomes

$$\begin{aligned} R_n(T_{mn} - T_{ln}) &= s_n \sum_{p,q=0}^{\infty} \frac{M_{p+q\ n}(\pi B f_0)^{p+q}}{p!q!} T_{mn}^{p} T_{ln}^{q} \\ &\quad \cdot \cos[2\pi f_0(T_{mn} - T_{ln}) + \tfrac{\pi}{2}(p - q)] \end{aligned}$$

$$= s_n \sum_{p=0}^{\infty} \frac{(\pi B f_0 T_{mn})^p}{p!} \cos(2\pi f_0 T_{mn} + \frac{\pi p}{2}) \qquad (4.13)$$

$$\cdot \sum_{q=0}^{\infty} \frac{(\pi B f_0 T_{ln})^q}{q!} \cos(2\pi f_0 T_{ln} + \frac{\pi q}{2}) M_{p+q\ n}$$

$$+ s_n \sum_{p=0}^{\infty} \frac{(\pi B f_0 T_{mn})^p}{p!} \sin(2\pi f_0 T_{mn} + \frac{\pi p}{2})$$

$$\cdot \sum_{q=0}^{\infty} \frac{(\pi B f_0 T_{ln})^q}{q!} \sin(2\pi f_0 T_{ln} + \frac{\pi q}{2}) M_{p+q\ n}.$$

Substituting this into (4.10), the output power component due to the nth jammer is therefore

$$s_{yn} = s_n \sum_{p,q=0}^{\infty} M^0_{pqn} (w_{cpn} w_{cqn} + w_{spn} w_{sqn}) \qquad (4.14)$$

where

$$w_{cpn} = \sum_{m=0}^{(M-1)J} w_m (B f_0 T_{mn})^p \cos(2\pi f_0 T_{mn} + \frac{\pi p}{2}), \quad p=0,\cdots,\infty, \qquad (4.15)$$

$$w_{spn} = \sum_{m=0}^{(M-1)J} w_m (B f_0 T_{mn})^p \sin(2\pi f_0 T_{mn} + \frac{\pi p}{2}) \qquad (4.16)$$

and

$$M^0_{pqn} = \frac{\pi^{p+q}}{p!q!} M_{p+q\ n}, \quad q=0,\cdots,\infty. \qquad (4.17)$$

Evidently, w_{cpn} and w_{spn} are linear combinations of the weights and proportional to B^p, with the suffix c and s signifying the cosine and sine factors respectively.

In matrix form, (4.14) can be written as

$$s_{yn} = s_n \left(\begin{bmatrix} w_{c0n} \\ w_{c1n} \\ \vdots \end{bmatrix}^T \begin{bmatrix} M^0_{00n} & M^0_{01n} & \cdots \\ M^0_{10n} & M^0_{11n} & \\ \vdots & & \end{bmatrix} \begin{bmatrix} w_{c0n} \\ w_{c1n} \\ \vdots \end{bmatrix} \right. \qquad (4.18)$$

$$\left. + \begin{bmatrix} w_{s0n} \\ w_{s1n} \\ \vdots \end{bmatrix}^T \begin{bmatrix} M^0_{00n} & M^0_{01n} & \cdots \\ M^0_{10n} & M^0_{11n} & \\ \vdots & & \end{bmatrix} \begin{bmatrix} w_{s0n} \\ w_{s1n} \\ \vdots \end{bmatrix} \right)$$

where T denotes transpose, Since M^0_{pqn}, from (4.17), satisfies

$$M^0_{pqn} = M^0_{qpn}, \tag{4.19}$$

the matrices in (4.18) with M^0_{pqn} as elements are symmetrical and can be decomposed as

$$\begin{bmatrix} M^0_{00n} & M^0_{01n} & \cdot & \cdot \\ M^0_{10n} & M^0_{11n} & & \\ \cdot & & & \\ \cdot & & & \end{bmatrix} = \frac{1}{M^0_{00n}} \begin{bmatrix} M^0_{00n} \\ M^0_{10n} \\ \cdot \\ \cdot \end{bmatrix} \begin{bmatrix} M^0_{00n} \\ M^0_{10n} \\ \cdot \\ \cdot \end{bmatrix}^T + \begin{bmatrix} 0 & 0 & 0 & \cdot & \cdot \\ 0 & M^1_{11n} & M^1_{12n} & \cdot & \cdot \\ 0 & M^1_{21n} & M^1_{22n} & & \\ \cdot & \cdot & & & \\ \cdot & \cdot & & & \end{bmatrix} \tag{4.20}$$

where

$$M^1_{pqn} = M^1_{qpn} = M^0_{pqn} - \frac{M^0_{p0n} M^0_{q0n}}{M^0_{00n}}, \quad p,q=1,\cdot\cdot,\infty. \tag{4.21}$$

Obviously, the decomposition depends on M^0_{00n} being nonzero. That this is so can be seen from (4.7) and (4.17) which give M^0_{00n} as unity. However, to decompose the last term of (4.20) in the same way, it is necessary to investigate the possible values that M^1_{11n} may take. Deleting all except the first two rows and columns of (4.20) gives

$$\begin{bmatrix} M^0_{00n} & M^0_{01n} \\ M^0_{10n} & M^0_{11n} \end{bmatrix} = \frac{1}{M^0_{00n}} \begin{bmatrix} M^0_{00n} \\ M^0_{10n} \end{bmatrix} \begin{bmatrix} M^0_{00n} \\ M^0_{10n} \end{bmatrix}^T + \begin{bmatrix} 0 & 0 \\ 0 & M^1_{11n} \end{bmatrix}. \tag{4.22}$$

Consider now the quadratic form obtained from the l.h.s.:

$$\begin{bmatrix} z_1 \\ z_2 \end{bmatrix}^T \begin{bmatrix} M^0_{00n} & M^0_{01n} \\ M^0_{10n} & M^0_{11n} \end{bmatrix} \begin{bmatrix} z_1 \\ z_2 \end{bmatrix} = \sum_{p,q=0}^{1} z_p z_q M^0_{pqn}. \tag{4.23}$$

Using (4.7) and (4.17), this becomes

$$\begin{aligned} \sum_{p,q=0}^{1} z_p z_q M_{pqn} &= \sum_{p,q=0}^{1} \frac{\pi^{p+q} z_p z_q}{p!q!} \int_{-1}^{1} S_{0n}(f) f^{p+q} df \\ &= \int_{-1}^{1} \left[\sum_{p=0}^{1} \frac{(\pi f)^p z_p}{p!} \right]^2 S_{0n}(f) df. \end{aligned} \tag{4.24}$$

Clearly, this is non-negative. Furthermore, since the square factor can only be zero (without z_1 and z_2 being zero together) at one frequency at most, the quadratic form will be positive definite unless the jammer's spectrum is composed of only one discrete narrowband component:

$$S_{On}(f) = d(f - f_1) \tag{4.25}$$

where $d(\cdot)$ is the delta function and f_1 gives the frequency of the narrowband component. In this special case, M^O_{pqn}, $p,q=0,\cdots,\infty$, is given, from (4.7) and (4.17), by

$$M^O_{pqn} = \frac{\pi^{p+q}}{p!q!}\int_{-1}^{1} d(f - f_1) f^{p+q} df = \frac{(\pi f_1)^{p+q}}{p!q!} \tag{4.26}$$

and thus, (4.20) becomes simply

$$\begin{bmatrix} M^O_{00n} & M^O_{01n} & \cdot & \cdot \\ M^O_{10n} & M^O_{11n} & & \\ \cdot & & & \\ \cdot & & & \end{bmatrix} = \begin{bmatrix} \frac{(\pi f_1)^0}{0!} \\ \frac{(\pi f_1)^1}{1!} \\ \cdot \\ \cdot \end{bmatrix} \begin{bmatrix} \frac{(\pi f_1)^0}{0!} \\ \frac{(\pi f_1)^1}{1!} \\ \cdot \\ \cdot \end{bmatrix}^T \tag{4.27}$$

which implies that the last term in (4.20) is zero. Apart from this special case, M^1_{11n} will be positive since the quadratic form of (4.24) and hence (4.22) are positive definite. Therefore, the same decomposition for the l.h.s. can be applied to the last term of (4.20) yielding

$$\begin{bmatrix} M^O_{00n} & M^O_{01n} & \cdot & \cdot \\ M^O_{10n} & M^O_{11n} & & \\ \cdot & & & \\ \cdot & & & \end{bmatrix} = \frac{1}{M^O_{00n}} \begin{bmatrix} M^O_{00n} \\ M^O_{10n} \\ \cdot \\ \cdot \end{bmatrix} \begin{bmatrix} M^O_{00n} \\ M^O_{10n} \\ \cdot \\ \cdot \end{bmatrix}^T + \frac{1}{M^1_{11n}} \begin{bmatrix} 0 \\ M^1_{11n} \\ M^1_{21n} \\ \cdot \\ \cdot \end{bmatrix} \begin{bmatrix} 0 \\ M^1_{11n} \\ M^1_{21n} \\ \cdot \\ \cdot \end{bmatrix}^T \tag{4.28}$$

$$+ \begin{bmatrix} 0 & 0 & 0 & 0 & \cdot & \cdot \\ 0 & 0 & 0 & 0 & \cdot & \cdot \\ 0 & 0 & M^2_{22n} & M^2_{23n} & \cdot & \cdot \\ 0 & 0 & M^2_{32n} & M^2_{33n} & & \\ \cdot & \cdot & \cdot & & & \\ \cdot & \cdot & \cdot & & & \end{bmatrix}$$

where

$$M^2_{pqn} = M^2_{qpn} = M^1_{pqn} - \frac{M^1_{p1n} M^1_{q1n}}{M^1_{11n}}, \quad p,q=2,\cdots,\infty. \tag{4.29}$$

Clearly, the same arguments for investigating M^1_{11n} can be applied to M^2_{22n} to determine if the last term of (4.28) can be similarly decomposed. As to be expected, the deduction is that the last term will be zero if the jammer's spectrum consists of only two discrete narrowband components. Otherwise, M^2_{22n} will be positive and further decomposition can be performed. Evidently, the entire arguments can be applied repetitively so that eventually, (4.20) becomes a sum of dyads:

$$\begin{bmatrix} M^0_{00n} & M^0_{01n} & \cdots \\ M^0_{10n} & M^0_{11n} & \\ \vdots & & \end{bmatrix} = \sum_{u=0}^{\infty} \frac{1}{M^u_{uun}} \begin{bmatrix} 0 \\ 0 \\ \vdots \\ 0 \\ M^u_{uun} \\ M^u_{u+1\ un} \\ \vdots \end{bmatrix} \begin{bmatrix} 0 \\ 0 \\ \vdots \\ 0 \\ M^u_{uun} \\ M^u_{u+1\ un} \\ \vdots \end{bmatrix}^T \tag{4.30}$$

where M^u_{pqn}, $u=1,\cdots,\infty$, $p,q=u,\cdots,\infty$, can be obtained from the recursive equation

$$M^u_{pqn} = M^u_{qpn} = M^{u-1}_{pqn} - \frac{M^{u-1}_{p\ u-1\ n} M^{u-1}_{q\ u-1\ n}}{M^{u-1}_{u-1\ u-1\ n}} \tag{4.31}$$

and M^u_{uun} is positive. Of course, if the jammer's spectrum is composed of only a number, say S, of discrete narrowband components, only the first S dyads in (4.30) will be present and the index u range from only 0 to S-1. Considering this as a special case in the remaining derivation in this section, (4.18) becomes, by substituting (4.30),

$$s_{yn} = \sum_{u=0}^{\infty} \frac{s_n}{M^u_{uun}} [(\sum_{p=u}^{\infty} M^u_{pun} w_{cpn})^2 + (\sum_{p=u}^{\infty} M^u_{pun} w_{spn})^2] \qquad (4.32)$$

which gives the output power component due to the nth jammer as a sum of non-negative square terms.

4.2.3 Jammer Gain

Having decomposed the output power component due to the nth of the N jammers as a sum of square terms, this subsection will study the JG using the decomposition and assuming small bandwidth.

From (4.32), the output power, with no receiver noise, is

$$s_y = \sum_{u=0}^{\infty} \sum_{n=1}^{N} \frac{s_n}{M^u_{uun}} [(\sum_{p=u}^{\infty} M^u_{pun} w_{cpn})^2 + (\sum_{p=u}^{\infty} M^u_{pun} w_{spn})^2]. \qquad (4.33)$$

With w_{cun}, u=0,··,∞, and w_{sun} proportional to B^u, this is essentially a power series of bandwidth. Obviously, if the bandwidth tends towards zero, the output power will be dominated by the terms with the least power of bandwidth and will be smaller when this least power of bandwidth is larger. Thus, with w_{cun} and w_{sun} being linear combinations of the weights, the optimal weights must be such that this least power of bandwidth is as large as possible. Consider, therefore, the output power of (4.33) being represented by terms proportional to $B^{2(U-1)}$ or less, U=1,··,∞:

$$s_y = \sum_{u=0}^{U-1} \sum_{n=1}^{N} \frac{s_n}{M^u_{uun}} [(\sum_{p=u}^{U-1} M^u_{pun} w_{cpn})^2 + (\sum_{p=u}^{U-1} M^u_{pun} w_{spn})^2]. \qquad (4.34)$$

Clearly, if the 2NU linear equations on the weights,

$$w_{cun} = w_{sun} = 0, \quad u=0,··,U-1, \quad n=1,··,N, \qquad (4.35)$$

are not all satisfied, (4.34) will not be zero and the output power will not be proportional to more than $B^{2(U-1)}$ for small band-

width. On the contrary, if the weights satisfy these 2NU equations, (4.34) will be zero and thus, the output power, from (4.33), will be given by

$$s_y = \sum_{u=0}^{\infty} \sum_{n=1}^{N} \frac{s_n}{M^u_{uun}} \left(\sum_{p=U}^{\infty} M^u_{pun} w_{cpn} \right)^2 + \left(\sum_{p=U}^{\infty} M^u_{pun} w_{spn} \right)^2 \qquad (4.36)$$

and will be proportional to at least B^{2U}. Therefore, if V is such that the weights can satisfy the 2NV equations of

$$w_{cun} = w_{sun} = 0, \quad u=0,\cdots,V-1, \quad n=1,\cdots,N, \qquad (4.37)$$

but cannot satisfy the 2N(V+1) equations of

$$w_{cun} = w_{sun} = 0, \quad u=0,\cdots,V, \quad n=1,\cdots,N, \qquad (4.38)$$

simultaneously, the output power can be proportional to B^{2V} but cannot be proportional to more than B^{2V}, implying that the optimal output power will be proportional to B^{2V}. Since there are (M-1)J weights, V is normally given by

$$V = \left\lfloor \frac{(M-1)J}{2N} \right\rfloor \qquad (4.39)$$

where $\lfloor z \rfloor$ is the smallest integer larger than or equal to z. In a functional form, the optimal output power at zero receiver noise and for small bandwidth is thus

$$s_{opt} = f(M,J,\tau,N,\{s_n\},\{\theta_n\},\{M_{pn}\})B^{2\lfloor (M-1)J/2N \rfloor} \qquad (4.40)$$

where $f(z_1,z_2,\cdots,z_Z)$ denotes a function of the parameters z_1, z_2, $\cdots$ and z_Z, while $\{s_n\}$, $\{\theta_n\}$ and $\{M_{pn}\}$ give the sets of jammers' powers, directions and spectrums respectively. By substituting (4.40) into (4.1), the JG for small bandwidth is hence

$$JG = f(M,J,\tau,N,\{\frac{s_n}{s_N}\},\{\theta_n\},\{M_{pn}\})B^{2\lfloor (M-1)J/2N \rfloor} \qquad (4.41)$$

where $\{s_n/s_N\}$ is the set of jammer power ratios and for convenie-

nce, will be taken to have elements s_1/s_N, s_2/s_N, $\cdots$ and s_{N-1}/s_N.

Examining (4.41), the factor $B^{2\lfloor(M-1)J/2N\rfloor}$ is most interesting because it relates the array performance to bandwidth, the number of jammers and the number of degrees of freedom. Since, for small bandwidth, it is the dominating factor in the equation, the following qualitative deductions can be made. (a) Variation of tap spacing gives rise to relatively small change in performance as compared with varying the number of taps in which the index of the dominating factor changes. (b) As discussed earlier, better performance is generally obtained from increasing the number of degrees of freedom. Of course, better performance will also result if the number of jammers is decreased such that the index of the dominating factor is increased, although intuitively, this is expected to be so even when the index does not change. In any case, the change in performance due to changes in the number of jammers and/or degrees of freedom will be more significant if the index changes as a result. (c) The performance improvement from increase in the index becomes less as the bandwidth, the base of the dominating factor, increases. (d) Since the number of jammers will not be greater than the number of spatial degrees of freedom, the minimum value for the index is $2\lfloor J/2\rfloor$ and is obviously associated with situations where the performance is worse. In particular, from (4.2) and (4.41), the MJG is

$$\text{MJG} = f(M,J,\tau)B^{2\lfloor J/2\rfloor} \qquad (4.42)$$

for small bandwidth. (e) The inefficiency, in terms of the number of weights required, of the odd-tap array in worse situations where the index has the minimum value of $2\lfloor J/2\rfloor$ is obvious as increasing the number of taps of an even-tap array by one leads to the same index.

In the derivation of (4.40), it is essential that, with V given by (4.39), the weights are able to satisfy (4.37) but not (4.38). As mentioned, this is normally the case. The other two rare possibilities will now be discussed. The first possibility is that the weights are able to satisfy, not only (4.37), but also (4.38). Obviously, the optimal output power will now be proportional to more than $B^{2L(M-1)J/2NJ}$, hence implying better performance. Situations associated with this possibility include those in which all the jammers can be perfectly nulled as, for instance, when there is only one jammer arriving from broadside. Such situations can clearly be included in (4.41) as special cases where the function f(M,J,··) is zero. Other situations associated with this possibility will be pointed out in later sections when discussing simulation results. The second possibility is that with (4.39) giving V, the 2NV equations of (4.37) are inconsistent and so cannot be satisfied simultaneously. Clearly, the optimal output power will now be proportional to less than $B^{2L(M-1)J/2NJ}$, implying performance deterioration. This possibility is associated with the trivial situations where the number of jammers exceeds the number of spatial degrees of freedom so that the output power of (4.33) cannot be equal to zero even if only the terms proportional to B^0 are present as when all the jammers' spectrums consist only of discrete narrowband components at the centre frequency. As an example of non-trivial situations associated with this possibility, consider a 4-tap array in a 2-jammer environment. From (4.41), the JG is proportional to $B^{2(M-1)}$, which is usually the case. However, with c denoting the wave velocity, if one of the jammers arrives from the direction

$$\theta = -\sin^{-1}\left(\frac{c\tau}{d}\right) \qquad (4.43)$$

so that, from fig.4.1, the time delay of the input due to this jammer at the mth of the M elements relative to that at the first element is $(M-1)\tau$, then the equivalent filter of fig.4.3 for this jammer will become the one shown in fig.4.4. Clearly, the equivalent filter, which normally has $4(M-1)$ separate tapping points, is now degenerated into one with only $M+2$ separate tapping point-

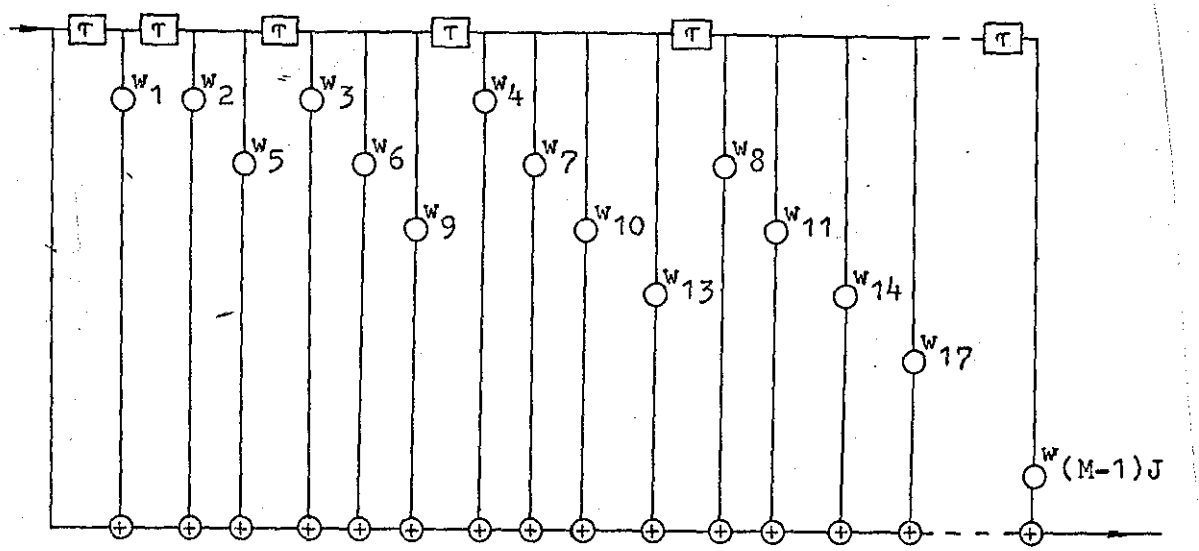

Fig.4.4 The equivalent filter for a jammer arriving from $\sin^{-1}(c\tau/d)$ when the array has 4 taps.

s, meaning that at most $M+2$ degrees of freedom can be directed towards rejecting this jammer. By considering the terms in (4.33) associated with only the nth of the N jammers and using the arguments that followed, the output power component due to the nth jammer can easily be seen to be proportional to B^{2U} if and only if

$$w_{cun} = w_{sun} = 0, \quad u=0,\cdots,U-1, \qquad (4.44)$$

which normally requires $2U$ degrees of freedom. Evidently, for the JG to be proportional to $B^{2(M-1)}$, $2(M-1)$ degrees of freedom are usually needed per jammer. Hence, if $2(M-1)$ is greater than $M+2$ or M is greater than 4, it is most probably that the JG will not

be proportional to $B^{2(M-1)}$ but instead proportional to $B^{2\lfloor(M+2)/2\rfloor}$, because even with the maximum of M+2 degrees of freedom directed towards rejecting the jammer from the direction of (4.43), the output power component due to this jammer is proportional to only $B^{2\lfloor(M+2)/2\rfloor}$ at most. Generally, it has been found that only if C, given by

$$C = \begin{array}{l}\text{minimum value of numbers of separate tapping points of the jammers' equivalent filters, not counting the filters whose input points coincide with some of the tapping points} \\ = \text{minimum value of numbers of degrees of freedom that can be directed towards each of the jammers, neglecting the jammers that can be perfectly nulled individually because the input points of the associated equivalent filters coincide with some of the tapping points,}\end{array} \quad (4.45)$$

is less than 2V as when M is greater than 4 in the example just discussed, the 2NV equations of (4.37) can be and are most probably inconsistent. The JG will then be limited by the maximum number of degrees of freedom that can be directed towards rejecting the jammers giving rise to C and so proportional to $B^{2\lfloor C/2\rfloor}$. Note that as expressed in (4.45), the evaluation of C excludes tha jammers that can be perfectly nulled individually. This is obviously because if the maximum numbers of degrees of freedom that can be directed to reject these jammers are used, the output power components due to these jammers will be zero and so the JG cannot be limited by these jammers. In other words, these jammers cannot lead to the inconsistency of the 2NV equations of (4.37). However, as implied in the general statement, there are also a few other situations where, with C less than 2V, the JG is proportional to more than $B^{2\lfloor C/2\rfloor}$ and hence, better performance than expected results. In particular, one situation where the 2NV equations of (4.37) are still consistent despite 2V is greater than C will be

pointed out in section 4.4.

From the considerations of the last paragraph, the JG of (4.41) should be more precisely written as

$$JG = \begin{cases} f(M,J,\tau,N,\{\frac{s_n}{s_N}\},\{\theta_n\},\{M_{pn}\})B^{2\lfloor(M-1)J/2N\rfloor}, & 2\lfloor\frac{(M-1)J}{2N}\rfloor \leq C \\ f(M,J,\tau,N,\{\frac{s_n}{s_N}\},\{\theta_n\},\{M_{pn}\})B^{2\lfloor C/2\rfloor}, & 2\lfloor\frac{(M-1)J}{2N}\rfloor > C \end{cases} \tag{4.46}$$

except for a few situations in which the index of the dominating factor is greater than the values given and the performance is better. From (4.45) and fig.4.1, the minimum value for C is easily seen to be M+J-2 when the environment includes a jammer arriving from the direction of (4.43) so that the associated equivalent filter has the same structure as that of fig.4.4. Thus, from (4.46),

maximum value of JG over the domain of jammers' directions, spectrums and jammer power ratios (4.47)

$$= \begin{cases} f(M,J,\tau,N)B^{2\lfloor(M-1)J/2N\rfloor}, & 2\lfloor\frac{(M-1)J}{2N}\rfloor \leq M+J-2 \\ f(M,J,\tau,N)B^{2\lfloor(M+J-2)/2\rfloor}, & 2\lfloor\frac{(M-1)J}{2N}\rfloor > M+J-2 \end{cases}$$

Evidently, when the number of elements greatly exceeds the number of jammers, there exists many worse situations in which the index of the dominating factor $2\lfloor(M+J-2)/2\rfloor$ is much smaller than $2\lfloor(M-1)J/2N\rfloor$, that obtained if the number of elements is roughly equal to the number of jammers, keeping the total number of weights $(M-1)J$ constant. Thus, if the maximum number of jammers to be anticipated is much smaller than the number of elements, the tapped delay line array of fig.4.1 can be very inefficient in terms of the number of weights required unless the array structure is modified by using, for example, different tap spacings and numbers of taps for the delay lines so that the minimum value for C is increased.

These modifications will not be investigated.

Finally, note that for simplicity, all the discussion so far in this subsection has been without regard to the situations mentioned in the last subsection when some of the jammers' spectrums are composed of only finite numbers of discrete narrowband components. Clearly, since the output power in these cases will still be given by (4.33) except that the index u now ranges from zero to some finite values for such jammers, all the above analysis and arguments are easily extended to these few situations. In particular, the index of the dominating factor in these cases is easily seen to be not smaller than that in the corresponding general situations discussed above. Evidently, (4.46) can be considered as applicable generally, except for a few special situations where the index of the dominating factor has larger value.

Summarizing, by expressing the autocorrelation functions of the jammers' power density spectrums in power series of bandwidth which is then assumed to be small, the JG has been derived to have the form of (4.46), with C given by (4.45). Normally, the condition $2L(M-1)J/2NJ \leq C$ is valid and the array devotes $2L(M-1)J/2NJ$ degrees of freedom to reject each jammer, resulting in the JG being proportional to $B^{2L(M-1)J/2NJ}$. However, because of the fairly symmetrical processing structure of fig.4.1, it may also happen that the array is not able to direct $2L(M-1)J/2NJ$ degrees of freedom towards rejecting the jammer should it arrive from certain directions so that many of tapping points of the associated equivalent filter of fig.4.3 coincide. The JG in such cases, specified by $2L(M-1)J/2NJ > C$, is proportional to only $B^{2LC/2J}$. In addition to the usual situations, there are also a few other special situations, for example, when some of the jammers' spectrums con-

sist of only a few discrete narrowband components, in which the index of the dominating factor in (4.46) has smaller value and the performance is hence better. Lastly, although the deductions in (a)-(e) are derived from (4.41), they are obviously worded to be applicable in general.

4.3 Two-Element Array

Having investigated the JG theoretically but qualitatively in the last section, the quantitative study of the JG by using simulation results will now be started. First, the 2-element array will be discussed in this section, with the 3- and multi-element arrays to be discussed in the next two sections. The discussion in the three sections will be based on the assumption that all the jammers' spectrums are flat. Note that for convenience, flat spectrum means flat across the whole band. The assumption is of course for reducing the dimension of the investigation, although the spectrums assumed obviously have practical significance. Thus, since the jammers do not normally know the array frequency band precisely, the best jamming source may be a wideband noise over the entire suspected frequency band. Hence, the jammer's spectrum with respect to the array after bandpass filtering will then be roughly flat over the whole band, especially if the bandwidth is small. In addition, it also appears intuitively plausible that the jammers' spectrums assumed will lead to worse performance which as mentioned in section 4.1, is of more interest. Nevertheless, some simulation examples with other jammers' spectrums will be discussed in section 4.6. As may be expected, the principal results obtained there are very similar to those of this and the next two sections.

For the 2-element array, N is equal to only 1 and from (4.45), C is equal to J. Thus, (4.47) becomes simply

$$JG = f(J,\tau,\theta_1)B^{2\lfloor J/2 \rfloor}. \qquad (4.48)$$

Some typical simulation results obtained for examining and verifying this as well as some of the theoretical deductions in the last section will now be presented and discussed for the 2-element array.

For general discussion as well as to verify the $B^{2\lfloor J/2 \rfloor}$ dependence, figs.4.5-4.7 show graphs of JG against jammer's direction at bandwidths of 5, 10, 20 and 40%. The tap spacing used is $1/4f_0$ and the number of taps being 2, 3 and 4 for figs.4.5, 4.6 and 4.7 respectively. All the graphs indicate that better performance results when the jammer's direction is positive. Furthermore, the difference in JG for positive and negative jammers' directions becomes more pronounced as the number of taps increases. This can be explained by referring to the jammer's equivalent filter of fig.4.8, easily obtained from the array of fig.4.1. Clearly, if the jammer arrives from a positive direction, the tapping points are "nearer" to the input point and consequently, better performance results. In particular, for $\sin\theta_1$ less than 1 and such that

$$u\tau = \frac{d\sin\theta_1}{c} \qquad (4.49)$$

where u equals 0, 1, ·· or J-1, the input point will coincide with one of the tapping points. Perfect nulling will then be possible and is depicted by the dips at the jammers' directions of 0°, 30° and 90° in all the curves. In contrast, when the jammer's direction is negative, all the curves flatten to plateaus which can be

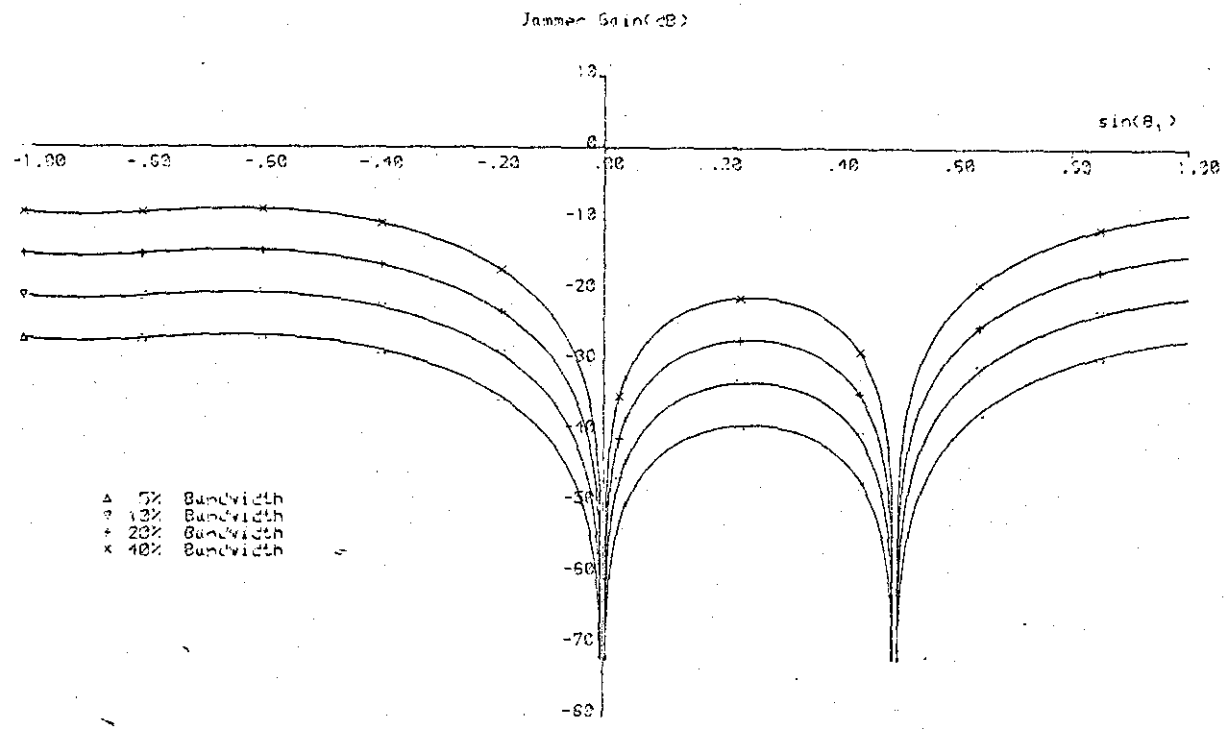

Fig.4.5 Graphs of JG against jammer's direction at bandwidths of 5, 10, 20 and 40% for a 2-element, 2-tap array with $1/4f_0$ tap spacing.

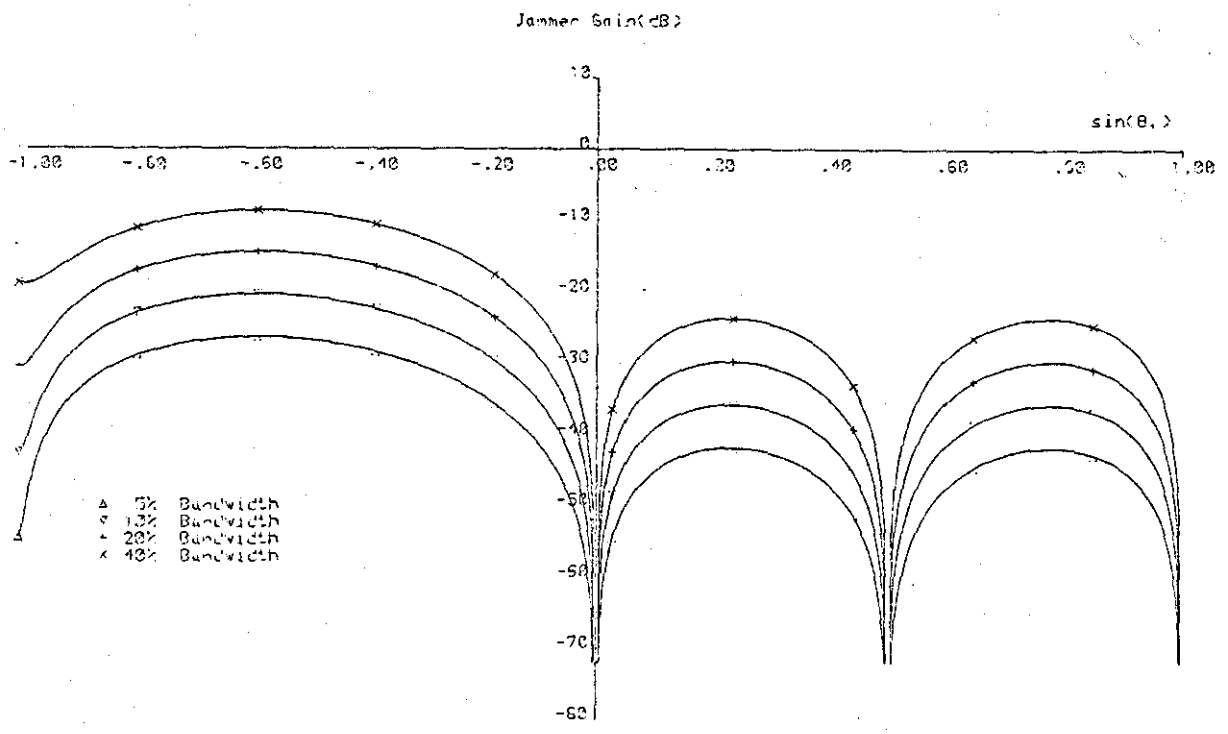

Fig.4.6 Graphs of JG against jammer's direction at various bandwidths obtained for the situations of fig.4.5 but with the array having 3 taps.

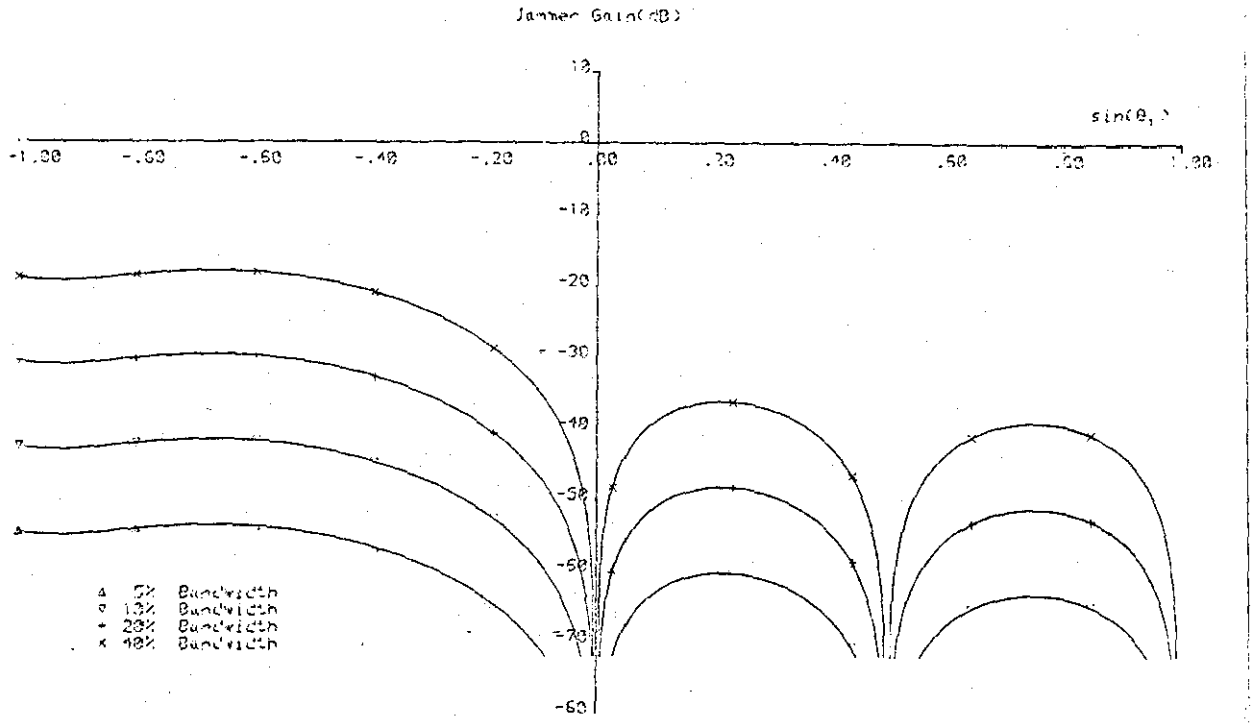

Fig.4.7 Graphs of JG against jammer's direction at various bandwidths obtained for the situations of fig.4.5 but with the array having 4 taps.

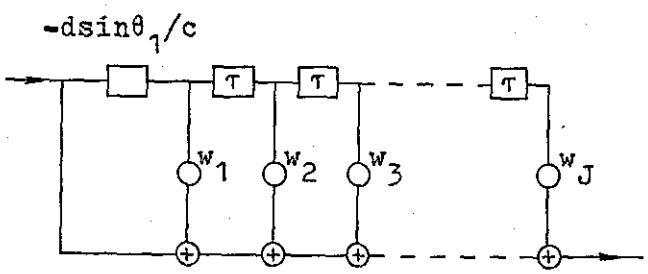

Fig.4.8 The jammer's equivalent filter when the array has only 2 elements.

regarded as regions of worse performance. The B^2 dependence for the 2-tap array can be seen from the 6dB difference between adjacent curves, with bandwidths differing by a factor of 2, in fig. 4.5. Similarly, the B^4 dependence for the 4-tap array can be seen from the 12dB difference between adjacent curves in fig.4.7. Likewise, the curves in fig.4.6 for the 3-tap array show the B^2 dependence except at jammer's direction closed to -90°. At this direction, adjacent curves differ by 12dB and by comparing with fig.4.7, the JG actually equals that of the 4-tap array. This is one of the special situations where the index of the dominating

factor in (4.46) has larger values and so better performance results. Specifically, with V given by (4.39), this situation is one in which the (M-1)J weights are able to satisfy, not only (3.37), but also (3.38). From figs.4.5-4.7 and other similar results, the $B^{2LJ/2J}$ dependence has been found to be valid, apart from a few special cases like the one just discussed, for bandwidth up to about 40%. For larger bandwidth, it has been found that the spacing between adjacent curves decreases and thus, the performance does not deteriorate as rapidly as predicted by (4.48).

To study the variation of performance with number of taps, fig.4.9 shows graphs of JG against jammer's direction for arrays with 2-6 taps at 20% bandwidth and $1/4f_0$ tap spacing. The general characteristics of the curves are obviously as discussed. In the regions of worse performance, the curves for the even-tap arrays are equally spaced by the same amount as that for the odd-tap arrays. Furthermore, the curves for the 3- and 5-tap arrays are only slightly below those for the 2- and 4-tap arrays respectively, except for jammer's direction near to -90° and 90°. For the reason discussed in the last paragraph, the 3- and 5-tap arrays have the same JG as the 4- and 6- tap arrays respectively at the jammer's direction of -90°. The difference between the curves for the 2- and 3-tap arrays at the jammer's direction of 90° is because, from (4.49), the 2-tap array cannot have a perfect null at 90° while the 3-tap array can. The superiority of the even-tap array is obvious from these observations.

To study the variation of performance with tap spacing, fig. 4.10 shows graphs of JG against jammer's direction for a 4-tap array with 40% bandwidth at tap spacings of $1/4f_0$, $1/5f_0$, $1/6f_0$

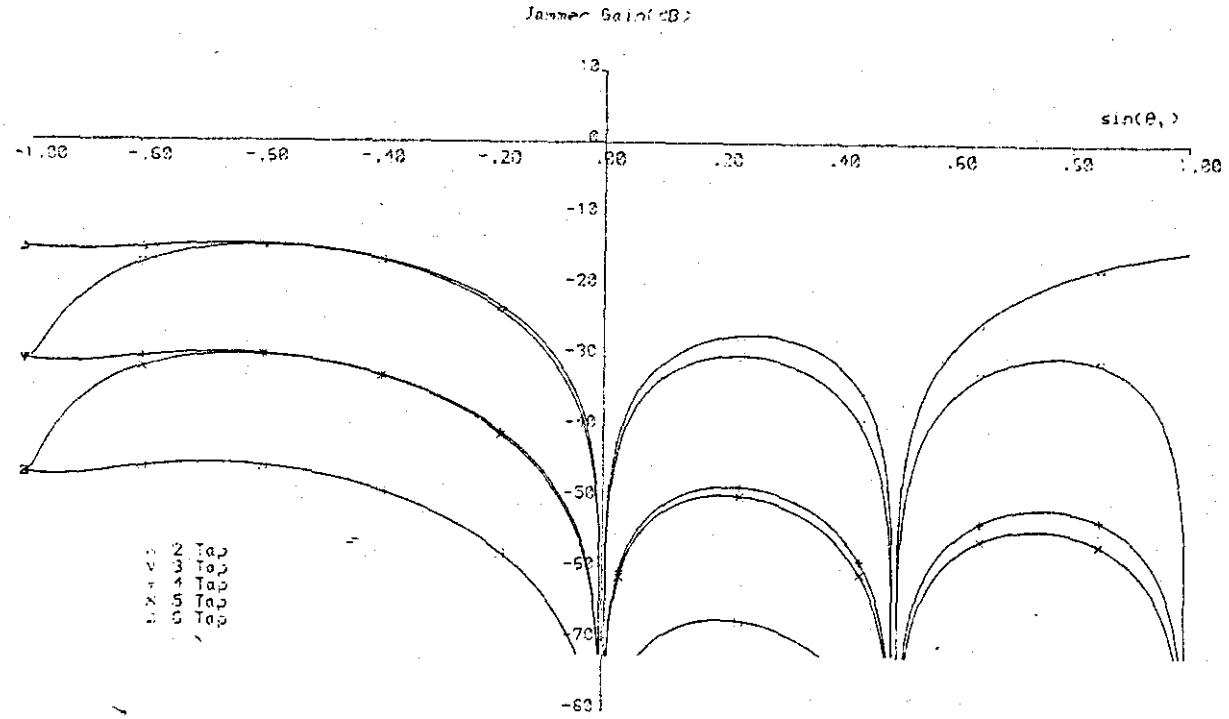

Fig.4.9 Graphs of JG against jammer's direction with numbers of taps equal to 2-6 for a 2-element, $1/4f_0$ tap spacing array at 20% bandwidth.

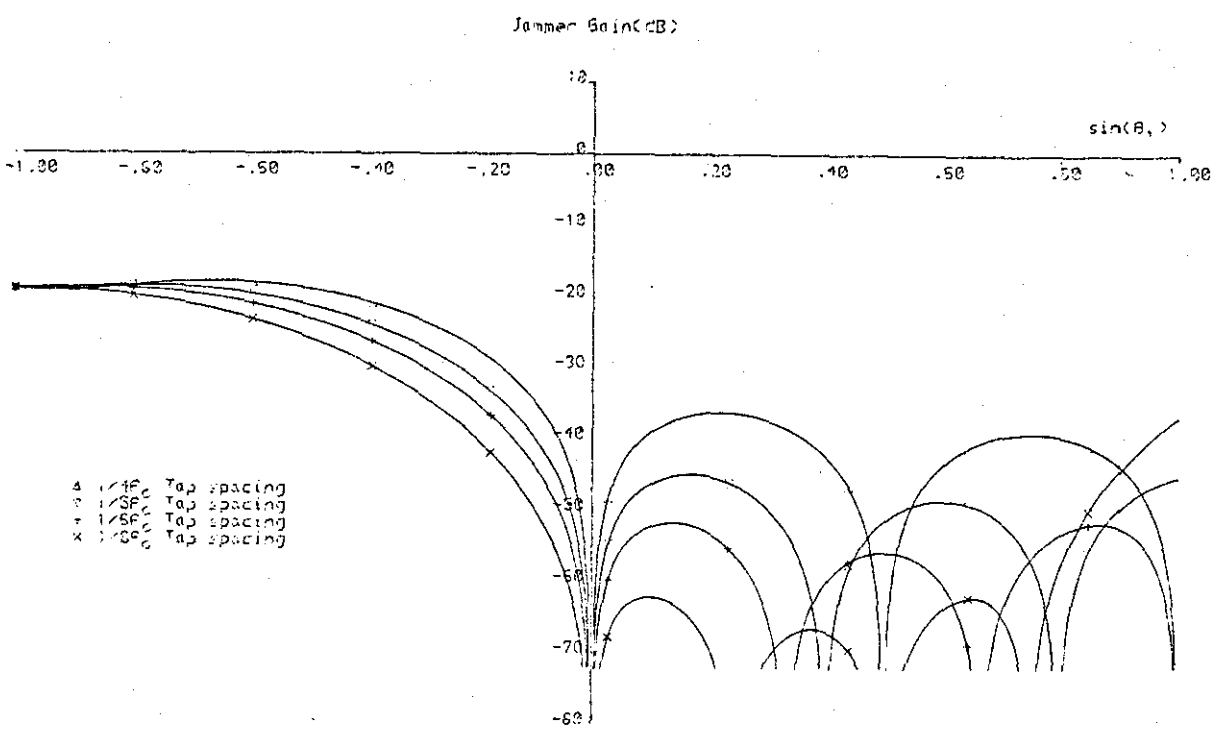

Fig.4.10 Graphs of JG against jammer's direction at tap spacings of $1/4f_0$, $1/5f_0$, $1/6f_0$ and $1/8f_0$ for a 2-element, 4-tap array with 40% bandwidth.

and $1/8f_0$. Again, the curves have the same general characteristics as discussed. Furthermore, for positive jammer's direction, the performance can be seen to be better if the tap spacing is roughly $1/6f_0$ or when the total length of the delay line is about $1/2f_0$ so that from (4.49), the 4 perfect nulling directions are approximately uniformly distributed between 0 and 1 in the $\sin\theta$ domain. For larger tap spacing, one or more of the perfect nulling directions are outside the range of physical significance, that is, corresponding to $\sin\theta$ greater than 1, and thus the performance is worse. However, if the tap spacing is reduced so that the perfect nulling directions move towards the broadside direction, the performance near broadside will be enhanced at the expense of perfo-rmance deterioration at jammer's direction near to 90°. In constrast, when the jammer's direction is negative, decreasing tap spacing always leads to better performance, although the improvement is negligible for jammer's direction near to -90° when the performance is the worse. In particular, the maximum values of the curves differ by less than 1 or 2 dB.

Last but not least, table 4.1a summarizes the worst performance of the 2-element array when the jammer's spectrum is flat. Specifically, tabulated as a function of bandwidth and number of taps, the JGs shown are the maximum values over the domain of jammer's direction. Note that these values are obtained for the maximum envisaged tap spacing of $1/4f_0$ since from the observations in the last paragraphs, they are only 1 or 2 dB above the values should smaller tap spacing be used. Also, the table is concerned with only even-tap array because, from fig.4.9 and other simulation results, the values shown will roughly equal those even if the number of taps is increased by one. With these considerations,

the results in table 4.1a are easily seen to lead to the important generalization

maximum value of JG for the 2-element, J-tap array with tap spacing τ and bandwidth B when the jammer's spectrum is flat (4.50)

$$= 1.6(0.8B)^{2\lfloor J/2 \rfloor}.$$

Bandwidth(%)	Number of taps 2	4	6	8
5	-26	-53	-81	
10	-20	-41	-63	
20	-14	-29	-45	-60
40	-8	-18	-27	-37

Table 4.1a 2-element array

Bandwidth(%)	Number of taps 2	4	6	8
5	-23	-47		
10	-17	-35	-54	
20	-11	-24	-37	-50
40	-5	-12	-20	-28

Table 4.1b 3-element array

Bandwidth(%)	Number of taps 2	4	6	8
5	-19	-44		
10	-14	-32	-51	
20	-8	-20	-33	-57
40	-3	-10	-17	-24

Table 4.1c 4-element array

Bandwidth(%)	Number of taps 2	4	6	8
5	-18	-40		
10	-12	-29	-52	
20	-7	-19	-32	-55
40	-2	-11	-17	-25

Table 4.1d 5-element array

Table 4.1 Maximum values of JG when all the jammers' spectrums are flat. These values are obtained at the maximum envisaged tap spacing of $1/4f_0$, but are only a few dB above the values for smaller tap spacing. Furthermore, although only even-tap array is concerned, the values shown are roughly those should the number of taps be increased by one.

4.4 Three-Element Array

Having investigated quantitatively in more detail the performance of the 2-element array using simulation results, similar study on the 3-element array will now be carried out in this sec-

tion.

For the 3-element array, C can easily be seen from fig.4.1 and the definition of (4.45) to have, in addition to the normal maximum value of 2J, the possible values of

$$C = J + u,\ u=1,\cdots,J-1,\ uc\tau \leq d, \tag{4.51}$$

when the jammer which gives rise to C arrives from the direction

$$\theta = -\sin^{-1}\left(\frac{uc\tau}{d}\right). \tag{4.52}$$

Thus, since the only non-trivial values for N are 1 and 2, (4.46) can be written as

$$JG = \begin{cases} f(J,\tau,\theta_1)B^{2J}, & N=1,\ 2J \leq C \\ f(J,\tau,\theta_1)B^{2LC/2J}, & N=1,\ 2J > C \\ f(J,\tau,\frac{s_1}{s_2},\theta_1,\theta_2)B^{2LJ/2J}, & N=2 \end{cases} \tag{4.53}$$

With objectives similar to the investigation of the last section, some typical simulation results on the 3-element array will now be presented and discussed.

The variation of array performance with jammer power ratio can be investigated with reference to table 4.2. This shows the JG as a function of jammers' directions and jammer power ratio for a 4-tap array array with 20% bandwidth and $1/4f_0$ tap spacing. The four entries, reading downwards, in each "direction cell" defined by the jammers' directions correspond to jammer power ratios of 0, 5, 10 and 15dB, s_1 being the stronger jammer. Entries with "XX" represent program failure due to negative computed JG values, that is, situations where all the jammers are roughly perfectly nulled. Obviously, when the stronger jammer's direction is positive, increasing the jammer power ratio usually leads to slightly better performance. This is in accordance with the deduction in section

$\sin(\theta_2)$	$\sin(\theta_1)$									
	-1.0	-.8	-.6	-.4	-.2	.0	.2	.4	.6	.8	1.0
-1.0	-46	-26	-21	-24	-25	-27	-26	-29	-31	-32	-30
	-46	-26	-24	-24	-27	-30	-30	-32	-34	-33	-31
	-46	-29	-25	-24	-26	-35	-33	-36	-37	-35	-33
	-46	-31	-25	-25	-29	-39	-35	-39	-40	-37	-37
-.8	-26	-65	-29	-29	-29	-27	-27	-26	-29	-30	-31
	-29	-65	-27	-27	-31	-30	-30	-30	-30	-30	-31
	-30	-65	-26	-27	-32	-35	-34	-33	-31	-30	-33
	-32	-65	-29	-27	-33	-39	-39	-35	-32	-32	-36
-.6	-24	-29	-70	-30	-29	-28	-29	-29	-29	-30	-30
	-24	-31	-69	-30	-32	-31	-32	-30	-29	-29	-30
	-25	-34	-69	-30	-34	-36	-35	-31	-29	-30	-31
	-26	-37	-70	-31	-36	-40	-38	-32	-30	-31	-32
-.4	-24	-29	-30	-79	-32	-34	-35	-33	-31	-31	-32
	-23	-31	-30	-78	-35	-37	-36	-33	-31	-32	-32
	-24	-33	-30	-77	-37	-41	-38	-33	-32	-32	-32
	-24	-35	-31	-78	-38	-46	-38	-33	-32	-32	-33
-.2	-25	-29	-29	-32	-95	-46	-43	-38	-37	-37	-38
	-24	-28	-28	-31	-95	-49	-43	-38	-38	-37	-38
	-24	-28	-27	-31	-94	-54	-43	-39	-38	-37	-38
	-24	-29	-28	-31	-95	-59	-43	-39	-39	-37	-38
.0	-27	-27	-28	-34	-46	-118	-55	-56	-54	-49	XX
	-26	-26	-26	-32	-44	-115	-53	-54	-52	-47	-128
	-25	-25	-26	-31	-44	XX	-52	-53	-51	-46	-126
	-25	-25	-26	-31	-44	XX	-52	-53	-51	-46	-122
.2	-28	-27	-29	-35	-43	-55	XX	-43	-47	-56	-46
	-26	-25	-27	-33	-43	-58	XX	-44	-48	-56	-44
	-26	-25	-27	-33	-43	-82	-134	-45	-49	-56	-43
	-26	-25	-27	-33	-43	-67	-130	-47	-50	-57	-44
.4	-29	-26	-29	-33	-38	-56	-43	-122	-72	-50	-49
	-28	-26	-28	-33	-38	-59	-43	-122	-72	-51	-47
	-27	-26	-28	-33	-38	-63	-43	-123	-73	-51	-47
	-28	-26	-28	-33	-38	-68	-44	-122	-76	-52	-48
.6	-31	-29	-29	-31	-37	-54	-47	-72	-122	-47	-45
	-30	-28	-29	-31	-37	-57	-46	-72	-122	-49	-45
	-30	-28	-29	-31	-37	-61	-46	-73	-129	-50	-45
	-31	-28	-29	-32	-37	-66	-46	-75	-124	-53	-46
.8	-32	-30	-30	-31	-37	-49	-56	-50	-47	-125	-35
	-32	-30	-30	-31	-38	-52	-56	-49	-47	-126	-35
	-34	-30	-30	-31	-38	-56	-56	-49	-48	-132	-36
	-37	-31	-30	-31	-38	-61	-56	-50	-50	-127	-39
1.0	-30	-31	-30	-32	-38	XX	-46	-49	-45	-35	XX
	-31	-31	-30	-32	-39	-122	-49	-50	-46	-35	XX
	-33	-33	-30	-32	-39	-123	-53	-52	-46	-36	XX
	-36	-36	-30	-32	-40	-126	-57	-53	-47	-38	-121

note: XX denotes program failure.

Table 4.2 Variation of JG against jammers' directions at various jammer power ratios when two jammers are present. The array has 3 elements, 4 taps, $1/4f_0$ tap spacing and 20% bandwidth. Reading downwards, the four entries in each direction cell correspond to jammer power ratios of 0, 5, 10 and 15dB, with s_1 as the stronger jammer.

3.3 that the performance is better if the jammer's direction is positive. On the other hand, virtually no change in performance from increase in jammer power ratio can be seen when the stronger jammer's direction is negative. These observations have also been obtained from other simulation results. Since worse performance is of more interest, all the simulation results to be presented in this section will be for the case of equal jammer powers.

As an example to verify the $B^{2LJ/2J}$ dependence in (4.53) when two jammers are present, table 4.3 shows the variation of JG with jammers' directions and bandwidth for a 2-tap array with $1/4f_0$ tap spacing. The entries in each direction cell now correspond to bandwidths of 5, 10, 20 and 40%. The B^2 dependence can be seen from the 6dB difference between adjacent entries in all the non-diagonal cells. The corresponding 1-jammer example is shown in fig.4.11 using the same array. Except at the jammer's direction of -30°, the curves can be seen to be separated by 12dB. Furthermore, comparing with fig.4.7 shows that the 3-element 2-tap array has very similar performance to the 2-element 4-tap array when the jammer's direction is negative. At the jammer's direction of -30°, however, the curves become discontinuous and peak. In fact, only 6dB difference can be found between adjacent curves and the JG actually equals that of the 2-element 2-tap array. These observations clearly verify the bandwidth power dependence in (4.53) for the 1-jammer situation, the dominating nature of this dependence as well as the possible inefficiency of the tapped delay line structure of fig.4.1 when the number of jammers is much less than the number of elements. Together with other simulation results, the bandwidth power dependence, at various tap spacing and number of taps, has been proved to about 40% bandwidth when one or two

$\sin(\theta_2)$ \ $\sin(\theta_1)$	-1.0	-.8	-.6	-.4	-.2	.0	.2	.4	.6	.8	1.0
-1.0	-54	-31	-25	-23	-23	-23	-24	-25	-26	-32	-54
	-42	-25	-19	-17	-17	-17	-18	-19	-22	-26	-42
	-30	-19	-13	-11	-11	-11	-12	-13	-16	-20	-30
	-16	-13	-8	-5	-6	-6	-6	-8	-11	-14	-18
-.8	-31	-54	-28	-25	-25	-24	-23	-24	-25	-27	-31
	-25	-42	-22	-20	-19	-18	-17	-18	-19	-21	-25
	-19	-30	-15	-14	-14	-12	-11	-12	-13	-15	-19
	-13	-18	-10	-8	-8	-6	-6	-7	-8	-9	-13
-.6	-25	-28	-55	-26	-26	-25	-25	-26	-25	-25	-25
	-19	-22	-43	-20	-20	-19	-19	-20	-19	-19	-19
	-13	-16	-31	-14	-14	-13	-13	-14	-13	-13	-13
	-8	-10	-20	-9	-8	-7	-7	-8	-8	-7	-8
-.4	-23	-26	-26	-62	-29	-29	-30	-29	-26	-24	-23
	-17	-20	-20	-50	-23	-23	-24	-23	-20	-18	-17
	-11	-14	-14	-38	-17	-17	-18	-17	-14	-12	-11
	-5	-8	-9	-26	-11	-12	-13	-11	-8	-7	-5
-.2	-23	-25	-26	-29	-77	-41	-39	-32	-30	-26	-23
	-17	-19	-20	-23	-65	-35	-33	-26	-24	-20	-17
	-11	-14	-14	-17	-53	-29	-27	-20	-18	-14	-11
	-6	-8	-8	-11	-41	-23	-21	-15	-12	-8	-6
.0	-23	-21	-25	-29	-41	XX	-46	-44	-39	-27	-23
	-17	-18	-19	-23	-35	-127	-40	-38	-33	-21	-17
	-11	-12	-13	-17	-29	XX	-34	-32	-27	-15	-11
	-6	-6	-7	-12	-23	XX	-28	-26	-21	-10	-6
.2	-24	-23	-25	-30	-39	-46	-101	-31	-29	-25	-24
	-18	-17	-19	-24	-33	-40	-89	-25	-23	-19	-18
	-12	-11	-13	-18	-27	-34	-77	-20	-17	-14	-12
	-6	-6	-7	-13	-21	-28	-65	-15	-12	-8	-6
.4	-25	-24	-26	-29	-32	-44	-31	-90	-26	-26	-25
	-19	-18	-20	-23	-26	-38	-25	-78	-21	-20	-19
	-13	-12	-14	-17	-20	-32	-20	-66	-16	-14	-13
	-8	-7	-8	-11	-15	-26	-15	-54	-12	-9	-8
.6	-28	-25	-25	-26	-30	-39	-29	-26	-77	-29	-28
	-22	-19	-19	-20	-24	-33	-23	-21	-65	-23	-22
	-16	-13	-13	-14	-18	-27	-17	-16	-53	-16	-16
	-11	-8	-8	-8	-12	-21	-12	-12	-41	-15	-11
.8	-32	-27	-25	-24	-26	-27	-25	-26	-29	-51	-32
	-26	-21	-19	-18	-20	-21	-19	-20	-23	-49	-26
	-20	-15	-13	-12	-14	-15	-14	-14	-18	-37	-20
	-14	-9	-7	-7	-8	-10	-8	-9	-15	-25	-14
1.0	-54	-31	-25	-23	-23	-23	-24	-25	-26	-32	-54
	-42	-25	-19	-17	-17	-17	-18	-19	-22	-26	-42
	-30	-19	-13	-11	-11	-11	-12	-13	-16	-20	-30
	-16	-13	-8	-5	-6	-6	-6	-8	-11	-14	-18

note: XX denotes program failure.

Table 4.3 Variation of JG against jammers' directions at various bandwidths when two jammers are present. The array has 3 elements, 2 taps and $1/4f_0$ tap spacing while the jammers have equal powers.

Reading downwards, the four entries in each direction cell correspond to bandwidths of 5, 10, 20 and 40%.

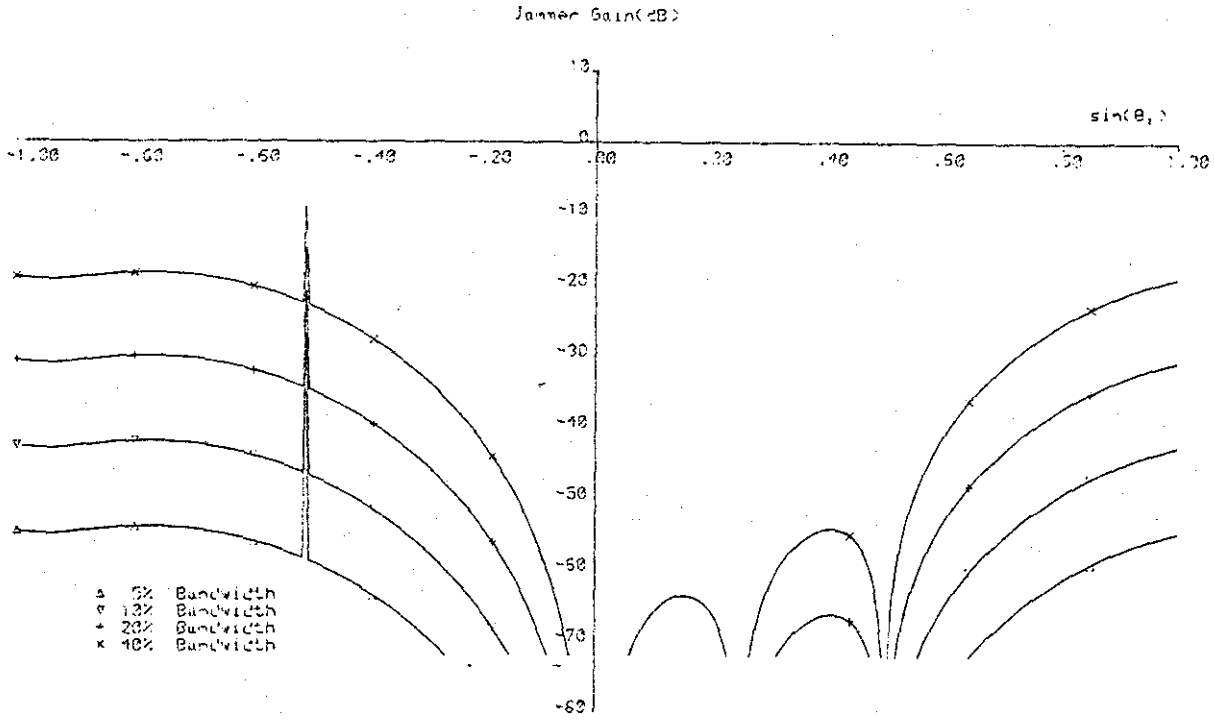

Fig.4.11 Graphs of JG against jammer's direction at bandwidths of 5, 10, 20 and 40% for a 3-element, 2-tap array with $1/4f_0$ tap spacing when only one jammer is present.

jammers with equal powers are present. For jammer power ratios of 10 and 20dB in the 2-jammer situation, however, the bandwidth power dependence is valid to only about 30 and 15% bandwidths respectively. For larger bandwidth, increase in bandwidth, as for the 2-element array, causes less performance deterioration than that predicted by (4.53).

With similar format to tables 4.2 and 4.3, table 4.4 shows the typical variation of performance against number of taps when two jammers are present. The numbers of taps for the four entries in each direction cell are 2, 3, 4 and 6, whereas the bandwidth and tap spacing used are 20% and $1/4f_0$ respectively. Neglecting the diagonal direction cells, the 2-tap array has very uniform performance with respect to the jammers' directions. The performance of the 3-tap array is very similar to the 2-tap one, apart from having much better performance when both the jammers' direc-

$\sin(\theta_2)$ \ $\sin(\theta_1)$	-1.0	-.8	-.6	-.4	-.2	.0	.2	.4	.6	.8	1.0
-1.0	-30	-19	-13	-11	-11	-11	-12	-13	-16	-20	-30
	-46	-20	-13	-11	-14	-27	-17	-16	-18	-23	-30
	-46	-28	-24	-24	-25	-27	-28	-29	-31	-32	-30
	-62	-40	-37	-37	-40	-43	-44	-45	-47	-47	-46
-.8	-19	-30	-16	-14	-14	-12	-11	-12	-13	-15	-19
	-20	-46	-18	-14	-15	-15	-13	-13	-14	-15	-22
	-28	-65	-29	-29	-29	-27	-27	-28	-29	-30	-31
	-40	-73	-41	-44	-45	-43	-42	-43	-44	-45	-46
-.6	-13	-16	-31	-14	-14	-13	-13	-14	-13	-13	-13
	-13	-18	-51	-19	-15	-14	-14	-14	-13	-14	-17
	-24	-29	-70	-30	-29	-28	-29	-29	-29	-30	-30
	-37	-41	-70	-46	-45	-44	-45	-45	-45	-45	-45
-.4	-11	-14	-14	-38	-17	-17	-18	-17	-14	-12	-11
	-11	-14	-19	-61	-22	-20	-20	-17	-15	-14	-17
	-24	-29	-30	-79	-32	-34	-35	-33	-31	-31	-32
	-37	-44	-46	XX	-48	-50	-51	-49	-48	-48	-48
-.2	-11	-14	-14	-17	-53	-29	-27	-20	-18	-14	-11
	-14	-15	-15	-22	-79	-32	-27	-22	-20	-19	-22
	-25	-29	-29	-32	-95	-46	-43	-38	-37	-37	-38
	-40	-45	-45	-48	XX	-63	-59	-55	-55	-55	-56
.0	-11	-12	-13	-17	-29	XX	-34	-32	-27	-15	-11
	-27	-15	-14	-20	-32	-115	-39	-38	-35	-27	XX
	-27	-27	-28	-34	-46	-118	-55	-56	-54	-49	XX
	-43	-43	-44	-50	-63	XX	-74	-75	-75	-71	-126
.2	-12	-11	-13	-18	-27	-34	-77	-20	-17	-14	-12
	-17	-13	-14	-20	-27	-39	-113	-32	-32	-56	-21
	-28	-27	-29	-35	-43	-55	XX	-43	-47	-56	-46
	-44	-42	-45	-51	-59	-74	XX	-62	-67	-71	-66
.4	-13	-12	-14	-17	-20	-32	-20	-66	-16	-14	-13
	-16	-13	-14	-17	-22	-38	-32	-113	-71	-27	-17
	-29	-28	-29	-33	-38	-56	-43	-122	-72	-50	-49
	-45	-43	-45	-49	-55	-75	-62	XX	-87	-76	-72
.6	-16	-13	-13	-14	-18	-27	-17	-16	-53	-18	-16
	-18	-14	-13	-15	-20	-35	-32	-71	-102	-26	-17
	-31	-29	-29	-31	-37	-54	-47	-72	-122	-47	-45
	-47	-44	-45	-46	-55	-75	-67	-87	-117	-70	-72
.8	-20	-15	-13	-12	-14	-15	-14	-14	-18	-37	-20
	-23	-15	-14	-14	-19	-27	-56	-27	-26	-81	-22
	-32	-30	-30	-31	-37	-49	-56	-50	-47	-125	-35
	-47	-45	-45	-48	-55	-71	-71	-76	-70	-119	-68
1.0	-30	-19	-13	-11	-11	-11	-12	-13	-16	-20	-30
	-30	-22	-17	-17	-22	XX	-21	-17	-17	-22	XX
	-30	-31	-30	-32	-38	XX	-46	-49	-45	-35	XX
	-46	-46	-45	-48	-56	-126	-66	-72	-72	-68	-125

note: XX denotes program failure.

Table 4.4 Variation of JG against jammers' directions at various numbers of taps when two jammers are present. The array has 3 elements, 20% bandwidth and $1/4f_0$ tap spacing while the jammers have equal powers. Reading downwards, the four entries in each direction cell correspond to numbers of taps of 2, 3, 4 and 6.

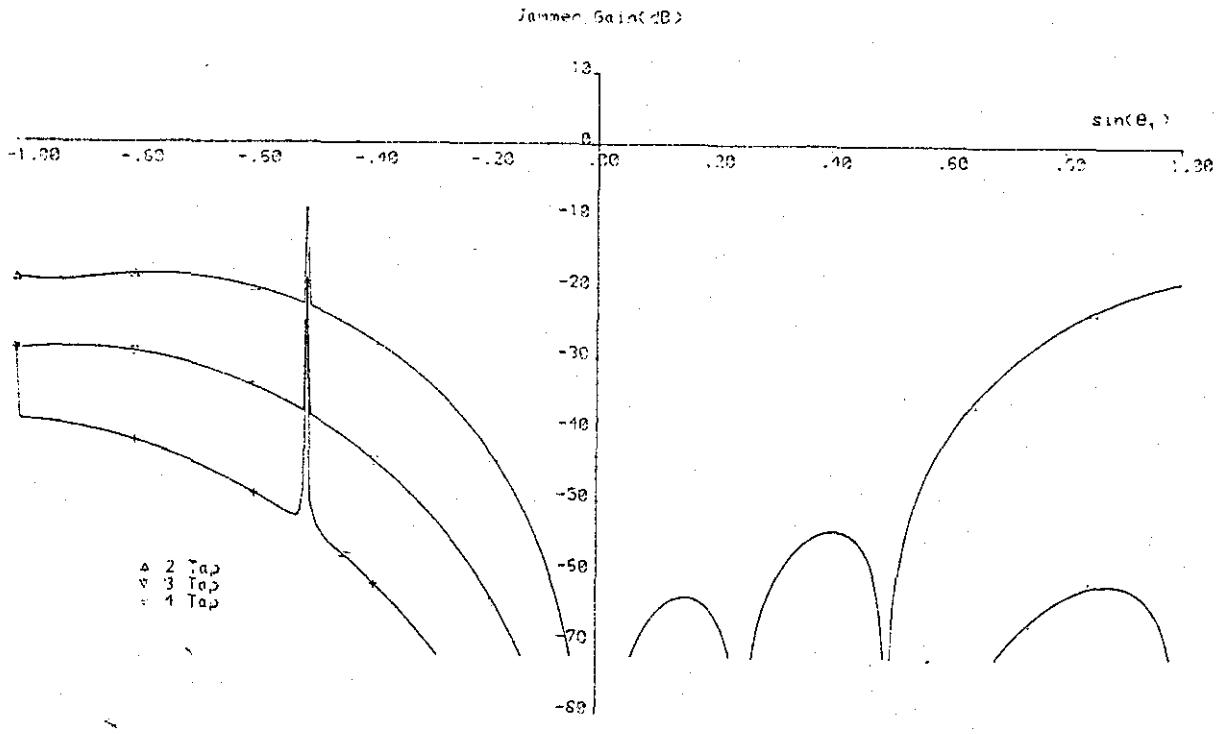

Fig.4.12 Graphs of JG against jammer's direction with numbers of taps of 2, 3 and 4 for a 3-element, $1/4f_0$ tap spacing array at 40% bandwidth when only one jammer is present.

tions are positive. As the number of taps increases, the performance becomes more nonuniform with the jammers' directions and much better performance results when all the jammers' directions are positive. Comparing the performance of the 2-, 3- and 4-tap arrays shows the inefficiency of the 3- or odd-tap array in general when all the spatial degrees of freedom are utilized. Fig.4.12 shows the typical variation of performance with number of taps when one jammer is present. 2-, 3- and 4-tap arrays with 40% bandwidth and $1/4f_0$ tap spacing are used. Apart from the points of discontinuity, the curves are roughly equally spaced and thus, increasing the number of taps always leads to significant performance improvement. The curve for the 4-tap array shows two points of discontinuity at the jammers' directions of -30° and -90°, in agreement with (4.51) -(4.53). However, the 3-tap array curve has only one point of di-

scontinuity at -30°, although according to (4.51)-(4.53), there should be another point of discontinuity at -90°. The missing of this point of discontinuity corresponds to the special situation mentioned in section 4.2 where, with V given by (4.39) and 2V greater than C, the 2NV equations of (4.37) are still consistent and so no significant performance deterioration results. At the jammer's direction of -30°, both the 3- and 4-tap arrays have the same performance and from (4.51) and (4.52), give rise to equal $\lfloor C/2 \rfloor$ of 2. Clearly, the dominating nature of the bandwidth power dependence is again illustrated.

In similar format to tables 4.2-4.4, table 4.5 shows the typical effects of varying tap spacing when two jammers are present. The four entries in each direction cell now correspond to tap spacings of $1/4f_0$, $1/5f_0$, $1/6f_0$ and $1/10f_0$ for a 4-tap array with 20% bandwidth. Clearly, in the region where one or both of the jammers' directions are negative, the performance improves only slightly when the tap spacing is decreased. In particular, the maximum values of JG for the four sets of results do not differ by more than 3dB. When both the jammers' directions are positive, however, decreasing tap spacing can lead to improvement or deterioration in performance depending on the jammers' directions. Thus, if one of the jammers is near to broadside and the other arrives from a positive direction, decreasing tap spacing always gives rise to better performance, whereas if both the jammers' directions are positive and far from broadside, decreasing tap spacing usually results in performance deterioration. On the whole, the best average performance is for tap spacing of around $1/6f_0$, that is, when the total length of the delay line is roughly $1/2f_0$. These observations are obviously similar to those in

$\sin(\theta_2)$	$\sin(\theta_1)$										
	-1.0	-.8	-.6	-.4	-.2	.0	.2	.4	.6	.8	1.0
-1.0	-46	-28	-24	-24	-25	-27	-28	-29	-31	-32	-30
	-62	-28	-25	-26	-27	-28	-28	-29	-30	-31	-30
	-46	-29	-27	-27	-28	-27	-28	-29	-30	-30	-30
	-64	-31	-30	-29	-28	-27	-28	-29	-30	-30	-30
-.8	-28	-55	-29	-29	-29	-27	-27	-28	-29	-30	-31
	-28	-46	-32	-31	-29	-27	-28	-28	-29	-30	-30
	-29	-64	-35	-31	-28	-28	-28	-29	-30	-30	-30
	-31	-61	-35	-30	-29	-30	-31	-31	-32	-32	-31
-.6	-24	-29	-70	-30	-29	-28	-29	-29	-29	-30	-30
	-25	-32	-67	-32	-30	-30	-31	-31	-31	-31	-31
	-27	-35	XX	-32	-31	-31	-32	-32	-32	-33	-32
	-30	-35	-61	-32	-33	-35	-36	-36	-35	-36	-34
-.4	-24	-29	-30	-79	-32	-34	-35	-33	-31	-31	-32
	-26	-31	-32	-35	-34	-37	-37	-35	-35	-35	-35
	-27	-31	-32	-66	-36	-39	-39	-37	-37	-37	-37
	-29	-30	-32	-69	-39	-45	-44	-43	-43	-42	-38
-.2	-25	-29	-29	-32	-95	-46	-43	-38	-37	-37	-38
	-27	-29	-30	-34	-95	-51	-45	-42	-42	-43	-45
	-28	-28	-31	-36	-90	-54	-48	-46	-46	-48	-47
	-28	-29	-33	-39	-60	-62	-55	-55	-55	-50	-41
.0	-27	-27	-28	-34	-46	-118	-55	-56	-54	-49	XX
	-28	-27	-30	-37	-51	XX	-64	XX	-59	XX	-54
	-27	-28	-31	-39	-54	XX	-72	-73	-70	-62	-123
	-27	-30	-35	-45	-62	XX	XX	XX	-127	-53	-40
.2	-28	-27	-29	-35	-43	-55	XX	-43	-47	-56	-46
	-28	-28	-31	-37	-45	-64	XX	-53	-66	-55	-51
	-28	-28	-32	-39	-48	-72	XX	-66	-67	-59	-47
	-28	-31	-36	-44	-55	XX	-119	XX	-55	-43	-35
.4	-29	-28	-29	-33	-38	-56	-43	-122	-72	-50	-49
	-29	-28	-31	-35	-42	XX	-53	XX	-55	XX	-44
	-29	-29	-32	-37	-46	-73	-66	XX	-66	-47	-37
	-29	-31	-36	-43	-55	XX	XX	-125	-44	-36	-31
.6	-31	-29	-29	-31	-37	-54	-47	-72	-122	-47	-45
	-30	-29	-31	-35	-42	-59	-66	-55	-130	-44	-35
	-30	-30	-32	-37	-46	-72	-67	-56	XX	-38	-32
	-30	-32	-36	-43	-55	-127	-55	-44	XX	-33	-30
.8	-32	-30	-30	-31	-37	-49	-56	-50	-47	-125	-35
	-31	-30	-31	-35	-43	XX	-55	XX	-44	XX	-32
	-30	-30	-33	-37	-48	-62	-59	-47	-38	-112	-31
	-30	-32	-36	-42	-50	-53	-43	-36	-33	-97	-31
1.0	-30	-31	-30	-32	-38	XX	-46	-49	-45	-35	XX
	-30	-30	-31	-35	-45	-54	-51	-44	-35	-32	-109
	-30	-30	-32	-37	-47	-123	-47	-37	-32	-31	-118
	-30	-31	-34	-38	-41	-48	-35	-31	-30	-31	-93

note: XX denotes program failure.

Table 4.5 Variation of JG against jammers' directions at various tap spacings when two jammers are present. The array has 3 elements, 4 taps and 20% bandwidth while the jammers have equal powers. Reading downwards, the four entries in each direction cell correspond to tap spacings of $1/4f_0$, $1/5f_0$, $1/6f_0$ and $1/10f_0$.

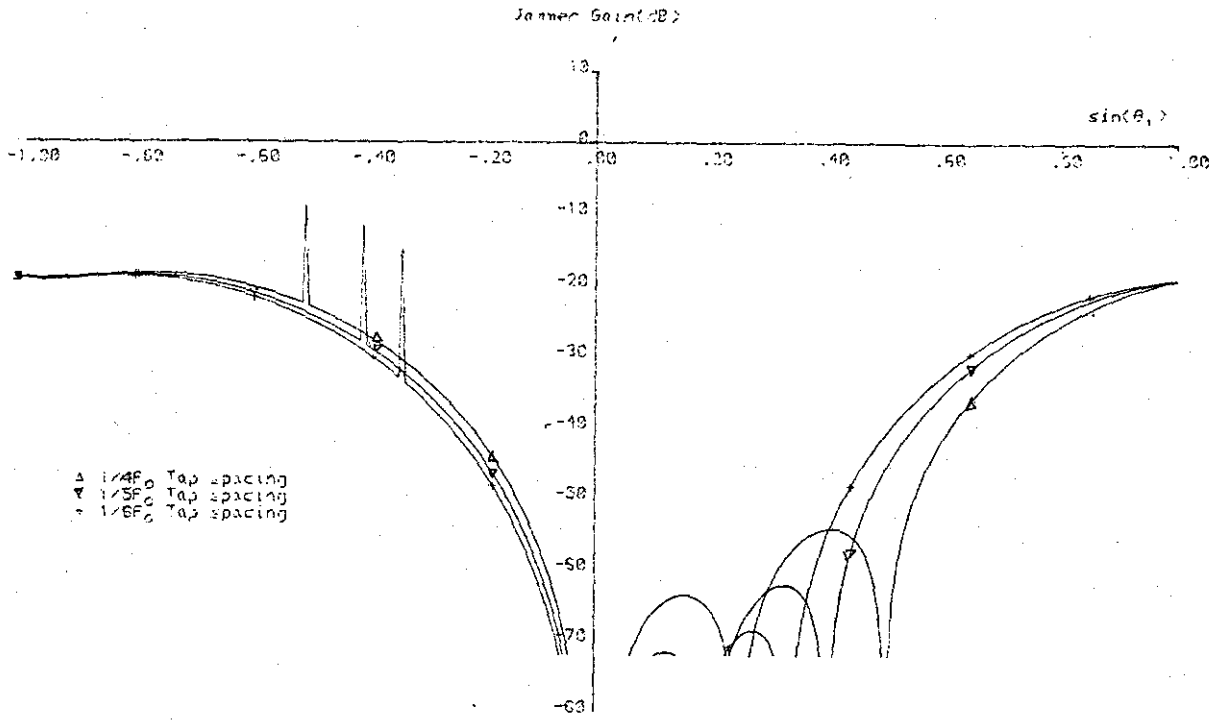

Fig.4.13 Graphs of JG against jammer's direction at tap spacings of $1/4f_0$, $1/5f_0$ and $1/6f_0$ for a 3-element, 2-tap array with 40% bandwidth when only one jammer is present.

the last section for the 2-element array. Fig.4.13 shows the typical effects of varying tap spacing when one jammer is present. A 2-tap, 40% bandwidth array is used at tap spacings of $1/4f_0$, $1/5f_0$ and $1/6f_0$. Clearly, as the tap spacing decreases, the performance for negative jammer's direction improves, but at the expense of performance deterioration for positive jammer's direction. Furthermore, in accordance with (4.51)-(4.53), the point of discontinuity shifts towards the broadside direction, resulting in better performance at this point. Obviously, if the performance is limited by points of discontinuity, significant improvement in performance can be obtained by decreasing tap spacing.

Last but not least, table 4.1b, as table 4.1a, summarizes the worst performance of the 3-element array when all the jammers' spectrums are flat. Note that, as can be expected from the results presented in this section, the worst performance tabulated is

always associated with 2-jammer environments so that the spatial degrees of freedom are fully utilized. Also, as with the 2-element array, only even-tap array is concerned because, from table 4.4 and other simulation results, the values shown are roughly equal to those should the number of taps be increased by one. Furthermore, the values shown are for the maximum envisaged tap spacing of $1/4f_0$, since from the last paragraph, they are only a few dB above the values for smaller tap spacing. With these considerations, the results of table 4.1b can easily be seen to give rise to the generalization

maximum value of JG for the 3-element, J-tap array with tap spacing τ and bandwidth B when all the jammers' spectrums are flat (4.54)

$$\approx 1.3(1.3B)^{2\lfloor J/2 \rfloor}.$$

4.5 Multi-Element Array

All the deductions in the last two sections regarding the 2- and 3-element arrays have been based on studying a large number of examples encompassing virtually all the possible situations. This is of course not practical for large number of elements because of the increase in the number of parameters requiring investigation and furthermore, the computer CPU time for calculating the JG is roughly proportional to the cube of the number of weights. Thus, for number of elements greater than 3, the performance charcteristics were studied in only some believe-to-be typical situations. These simulation examples will not be presented since they give rise to similar deductions and characteristics about the array performance as discussed in the last two sections. Specifically, all these simulation examples illustrate the following observations and deductions:

(a) In situations where the number of extra spatial degrees of freedom is relatively large, there exists a few environments, corresponding to points of discontinuity mentioned in the last section, associated with $2\lfloor(M-1)J/2NJ\rfloor C$ in (4.46) in which the performance is much worse than the normal performance when $2\lfloor(M-1)J/2NJ\rfloor C$. In these few environments, the tapped delay line structure concerned is relatively inefficient, in terms of the number of weights used, to reject the jammers.

(b) Worse performance is associated with environments where the spatial degrees of freedom are fully or nearly fully utilized so that the index of the dominating factor in (4.46) has the minimum value of $2\lfloor J/2 \rfloor$.

(c) Worse performance is associated with environments where the jammers are widely separated and at least some arrive from negative directions.

(d) Better average performance results when the jammers have widely different powers, although the performance in worse environments is virtually independent of the jammer power ratios.

(e) Odd-tap array is inefficient in worse situations. Particularly, in the worst situations, the JG remains roughly the same even though the number of taps of an even-tap array is increased by one.

(f) The array has best average performance if the total length of the delay line is about $1/2f_0$. In contrast, the performance in worse environments improves, though by only a few dB, as the tap spacing decreases.

(g) The bandwidth power dependence in (4.46) is valid to about 40% bandwidth in worse environments. In general, however, the domain of validity decreases as the jammer power ratios, the

number of taps, the number of extra spatial degrees of freedom and the number of elements increase. For bandwidth above the domain of validity, better performance than predicted by (4.46) usually results.

(h) As tables 4.1a and b, tables 4.1c and d summarize the worst performance of the 4- and 5-element arrays respectively. Due to the increasing number of parameters and computer CPU time mentioned, the latter two tables were obtained more crudely than the former two which are based on examining virtually every possible environment. Specifically, deductions (b)-(f) above have been used to reduce the domain of maximization for obtaining the worst performance. Thus, in accordance with (b) and (d), the jammer power ratios have been taken to be equal, with the number of jammers equal to the number of spatial degrees of freedom. Also, from (e) and (f), only even-tap array has been considered and the maximum envisaged tap spacing of $1/4f_0$ used, since the results obtained are still applicable, with perhaps a few dB above the actual values, should the number of taps be increased by one or the tap spacing be decreased. Then, by examining the JG calculated at the griding points of the "grid" of jammers' directions in the region of worse performance suggested by (c), tables 4.1c and d were obtained. Clearly, corresponding values in the two tables differ by no more than a few dB and thus, similar to those in tables 4.1a and b, lead to the generalization

maximum value of JG for the 4- and 5-element arrays with bandwidth B, tap spacing τ and J taps when all the jammers' spectrum are flat (4.55)

$$= 4(1.3B)^{2\lfloor J/2 \rfloor}.$$

The worst performance for arrays with more than 5 elements has

also been studied briefly from a few simulation examples. It has been found that the worst performance obtained is roughly the same as that in tables 4.1c and d. Therefore, it will be postulated that table 4.1c, d or (4.55) describes the worst performance of arrays with more than 3 elements.

Evidently, deductions (a)-(g) above have been worded such that all the important observations and deductions in the last two sections are also implied. Therefore, summarizing the quantitative investigation when all the jammers' spectrums are flat, (a)-(g) above are the general deductions regarding the performance while table 4.1 or the generalizations of (4.50), (4.54) and (4.55) gives the worst performance. Lastly, it is obvious that all these deductions as well as the more specific comments in the last two sections are in agreement with the theoretical derivations and deductions of section 4.2.

4.6 Other Jammers' Spectrums

The array performance has been studied quantitatively in the last three sections by assuming that all the jammers have flat spectrums. In this section, the situations when this is not so will be briefly examined by using some typical simulation results.

With the theoretical derivations in section 4.2 being independent of the jammers' spectrums, it may be expected that the deductions from the last three sections are also applicable even when the spectrums are not all flat. In similar manner as the last three sections, the variation of JG with the various parameters was studied in some believe-to-be typical and illustrative situations where, instead of flat spectrums, some jammers have some of the spectrums of fig.4.14. A few situations where the spectrums assume other shapes were also investigated. Generally,

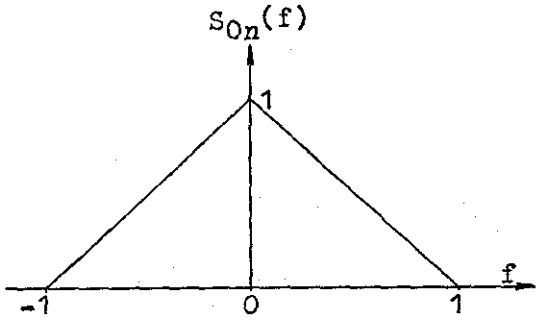

Fig.4.14a "Triangular" spectrum

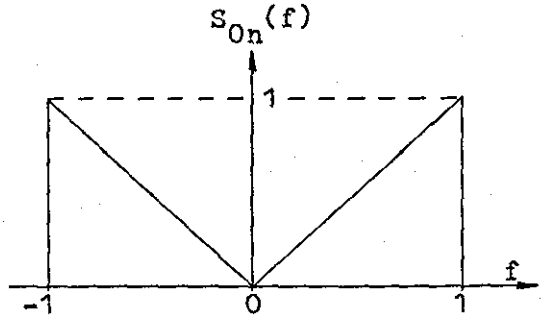

Fig.4.14b "Inverted-triangular" spectrum

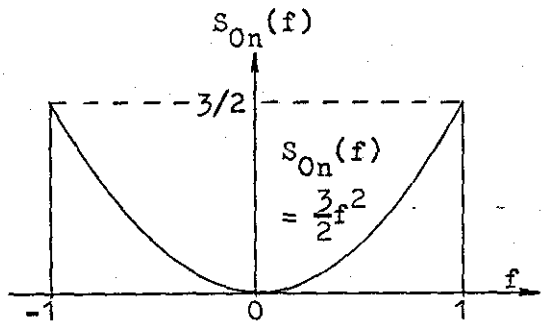

Fig.4.14c "Square-law" spectrum

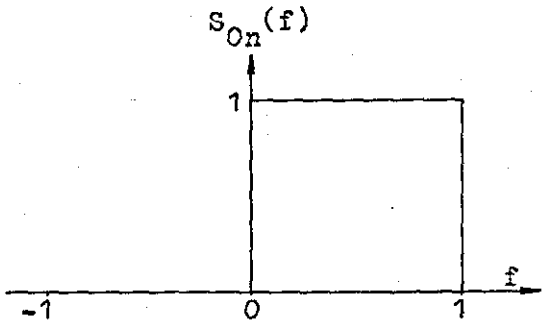

Fig.4.14d "Half-flat" spectrum

Fig.4.14 The other most studied spectrums.

the results obtained agree with the theoretical derivations of section 4.2 as well as the deductions of the last three sections. This being the case, most of the results obtained will not be presented and discussed. Instead, for illustrating purpose, a few examples which demonstrate the important bandwidth power dependence in (4.46) and compares the typical characteristics of having different spectrums will be discussed.

Figs.4.15 and 4.16 show the same set of curves as fig.4.6 but with the jammer having triangular and half-flat spectrums respectively. Obviously, comparing the three figures indicates that although the spectrums are very different, the bandwidth power dependence in (4.46) is still valid to about 40% bandwidth. Specifically, all the comments regarding fig.4.6 in section 4.3 are also applicable to figs.4.15 and 4.16, except that the decrease in JG at

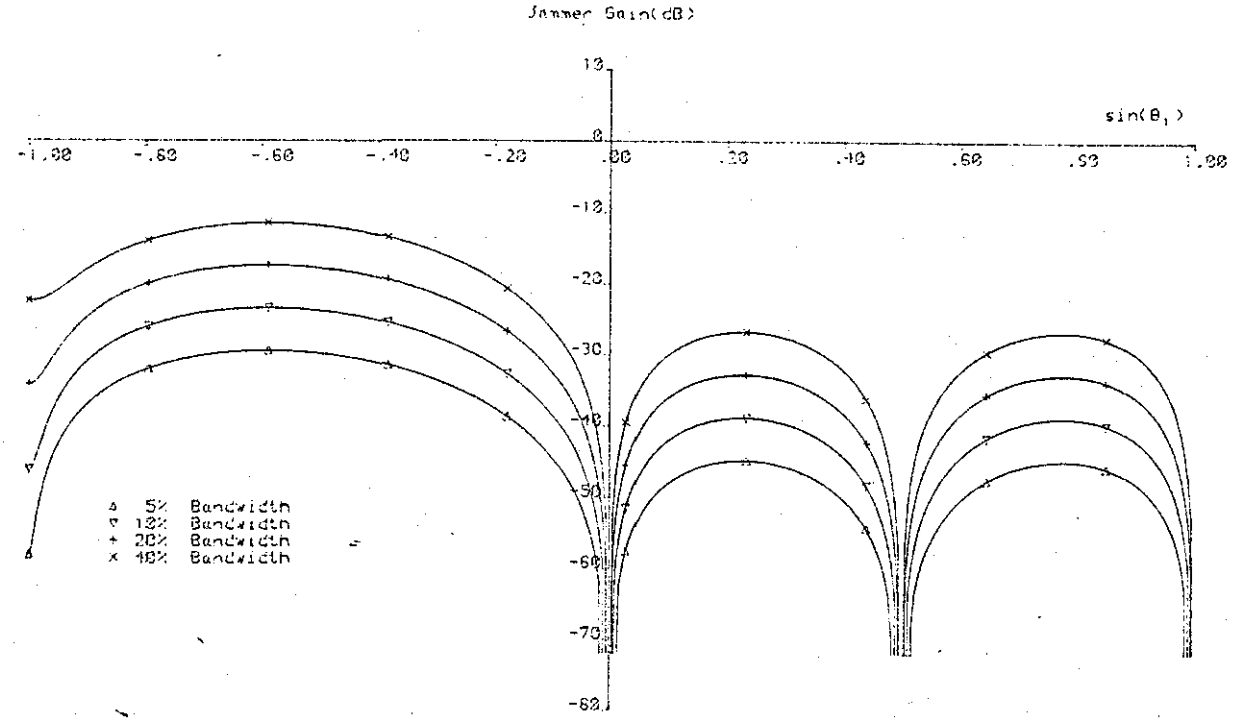

Fig.4.15 Graphs of JG against jammer's direction at bandwidths of 5, 10, 20 and 40% obtained for the situations of fig.4.6 but with the jammer having triangular spectrum.

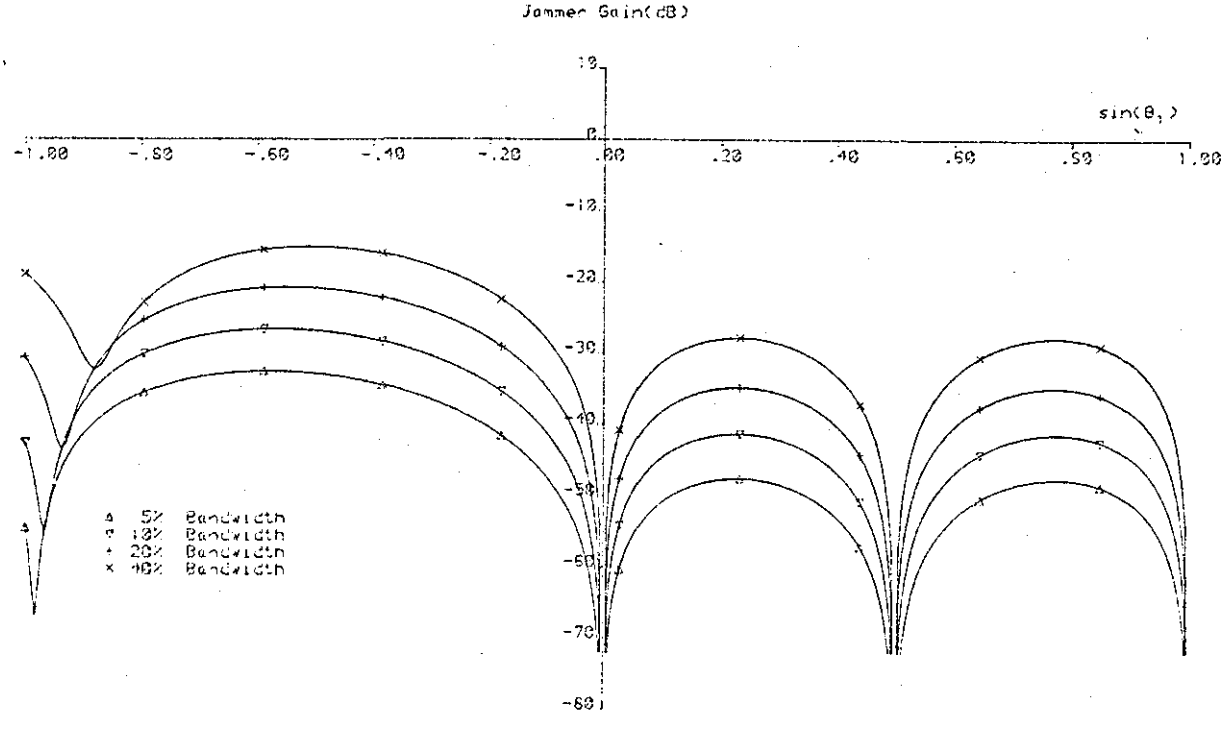

Fig.4.16 Graphs of JG against jammer's direction at bandwidths of 5, 10, 20 and 40% obtained for the situations of fig.4.6 but with the jammer having half-flat spectrum.

the jammer's direction of -90° in figs. 4.6 and 4.15 has shifted slightly, in proportional to bandwidth, to the left in fig.4.16. This is because, with a half-flat spectrum, the jammer's power density spectrum will be flat across the whole band should the array operate at the frequency of $f_0(1+B/4)$ over an absolute bandwidth of $f_0B/2$. Thus, effectively, the array element spacing d is decreased by a factor of $(1+B/4)$. Since the JG depends on $d\sin\theta_1$ instead of $\sin\theta_1$ so that as d increases, $\sin\theta_1$ has to be decreased to keep $d\sin\theta_1$ constant, the shifting mentioned results. Corresponding to table 4.3, table 4.6 shows the results obtained when s_1 and s_2 have triangular and half-flat spectrums respectively. Obviously, adjacent entries in the diagonal and non-diagonal cells differ by 12 and 6dB respectively, verifying again the bandwidth power dependence in (4.46) to about 40% bandwidth.

To compare the typical characteristics of various jammers' spectrums, fig.4.17 shows graphs of JG against jammer's direction for a 2-element, 2-tap, 20% bandwidth, $1/4f_0$ tap spacing array with the jammer having flat and the four spectrums of fig.4.14. Clearly, with approximately constant spacings between curves, the variation of JG with jammer's direction is quite independent of the jammer's spectrum. Furthermore, as the jammer concentrates its power from the centre to the edges of the band, that is, as the jammer's spectrum becomes more peaky at the band edges rather than at the band centre, the performance deteriorates, though by only a few dB. In particular, the performance for inverted-triangular and square-law spectrums is worse than that for flat spectrum. Table 4.7 shows the variation of JG against jammers' directions for a 3-element, 2-tap, $1/4f_0$ tap spacing, 10% bandwidth array when two jammers having equal powers are present. The spectrum

$\sin(\theta_2)$	$\sin(\theta_1)$										
	-1.0	-.8	-.6	-.4	-.2	.0	.2	.4	.5	.8	1.0
-1.0	-57	-34	-29	-27	-28	-29	-29	-31	-34	-38	-57
	-45	-28	-23	-21	-22	-23	-24	-26	-25	-32	-45
	-33	-21	-16	-15	-16	-17	-18	-20	-24	-28	-33
	-21	-14	-10	-9	-9	-11	-12	-16	-23	-24	-21
-.8	-35	-56	-31	-30	-31	-30	-29	-30	-30	-31	-35
	-30	-44	-25	-24	-25	-24	-23	-24	-24	-26	-30
	-25	-32	-19	-17	-19	-18	-18	-18	-19	-20	-25
	-21	-21	-13	-11	-13	-13	-12	-13	-14	-15	-21
-.6	-29	-34	-59	-31	-31	-31	-31	-31	-30	-29	-29
	-23	-28	-46	-25	-25	-25	-25	-25	-24	-23	-23
	-18	-23	-34	-19	-19	-19	-19	-19	-18	-17	-18
	-13	-16	-22	-12	-14	-13	-13	-13	-12	-12	-13
-.4	-27	-31	-31	-68	-34	-35	-36	-33	-30	-29	-27
	-21	-25	-25	-53	-28	-29	-30	-27	-24	-23	-21
	-15	-20	-19	-41	-22	-23	-24	-21	-18	-17	-15
	-10	-14	-13	-29	-15	-16	-17	-15	-12	-11	-10
-.2	-26	-29	-29	-32	-62	-46	-43	-36	-34	-30	-26
	-20	-23	-23	-26	-65	-40	-37	-30	-28	-24	-20
	-15	-17	-17	-20	-55	-34	-31	-24	-22	-18	-15
	-9	-12	-12	-14	-43	-27	-25	-18	-15	-12	-9
.0	-26	-27	-28	-32	-44	XX	-49	-47	-42	-30	-26
	-20	-21	-22	-26	-36	XX	-43	-41	-36	-24	-20
	-14	-15	-16	-20	-32	XX	-37	-35	-30	-18	-14
	-9	-9	-10	-14	-26	-135	-31	-29	-24	-12	-9
.2	-27	-26	-28	-34	-43	-52	XX	-35	-33	-29	-27
	-21	-20	-22	-26	-37	-45	-94	-29	-27	-23	-21
	-15	-14	-16	-22	-31	-39	-80	-22	-20	-17	-15
	-9	-8	-10	-16	-25	-32	-57	-15	-13	-10	-9
.4	-28	-27	-29	-33	-37	-50	-36	XX	-30	-29	-28
	-22	-21	-23	-27	-31	-44	-30	-81	-24	-23	-22
	-15	-15	-17	-21	-25	-37	-24	-68	-17	-17	-16
	-10	-10	-12	-15	-19	-30	-19	-56	-11	-11	-10
.6	-31	-29	-30	-30	-34	-45	-33	-31	-85	-32	-31
	-25	-23	-24	-24	-28	-38	-28	-26	-67	-26	-25
	-19	-17	-18	-18	-22	-32	-22	-21	-55	-20	-19
	-14	-12	-12	-12	-16	-25	-16	-16	-43	-16	-14
.8	-36	-31	-29	-29	-31	-33	-31	-31	-35	-63	-36
	-30	-26	-23	-22	-25	-27	-25	-25	-30	-51	-30
	-25	-20	-17	-16	-19	-21	-19	-20	-25	-39	-25
	-21	-15	-11	-10	-12	-14	-13	-15	-20	-27	-21
1.0	-57	-35	-29	-27	-28	-29	-29	-31	-34	-36	-57
	-45	-29	-23	-21	-22	-23	-24	-25	-27	-30	-45
	-33	-24	-17	-15	-16	-17	-18	-20	-21	-23	-33
	-21	-18	-11	-9	-10	-12	-12	-14	-14	-15	-21

note: XX denotes program failure.

Table 4.6 Variation of JG against jammers' directions at bandwidths of 5, 10, 20 and 40% obtained for the situations of table 4.3 but with s_1 and s_2 having triangular and half-flat spectrums respectively.

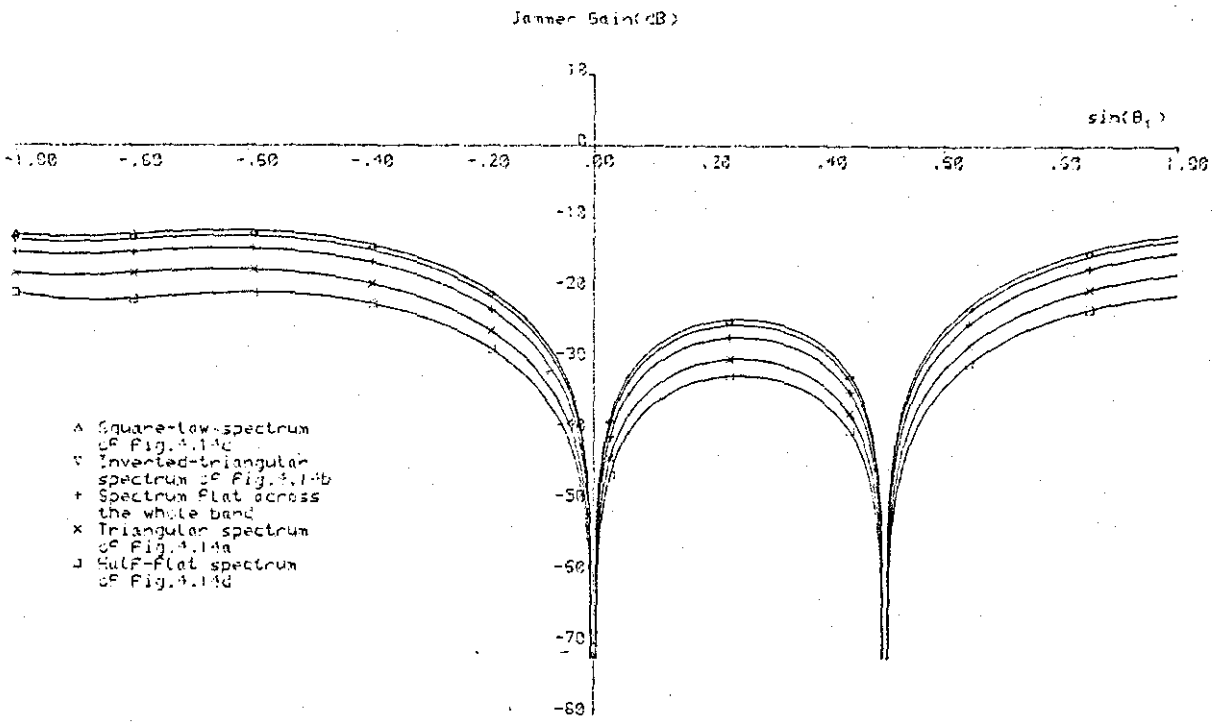

Fig.4.17 Graphs of JG against jammer's direction with the jammer having square-law, inverted-triangular, flat, triangular and half-flat spectrums for a 2-element, 2-tap, $1/4f_0$ tap spacing array at 20% bandwidth.

for s_1 is flat, while the four entries in each direction cell are associated with s_2 having flat and the spectrums of figs.4.14a-c. Again, like fig.4.17, the performance can be seen to deteriorate, though by only a few dB, as s_2 concentrates its power from the centre to the edges of the band. Fig.4.18 shows the same set of curves as fig.4.17, but with the 2-element array having 4 taps and 40% bandwidth instead. Again, the variation of JG with jammer's direction can be seen to be roughly independent of the jammer's spectrum. Comparing with fig.4.17, the difference between the curve associated with half-flat spectrum and the other curves is increased. With the array having more taps, this results essentially from the bandwidth power dependence in (4.46) as the actual bandwidth of half-flat spectrum is halved that of the other spectrums. Apart from this, note that with more taps, the performance

$\sin(\theta_2)$ \ $\sin(\theta_1)$	-1.0	-.8	-.6	-.4	-.2	.0	.2	.4	.6	.8	1.0
-1.0	-42	-23	-17	-15	-15	-15	-15	-17	-19	-24	-42
	-42	-24	-18	-16	-16	-16	-16	-17	-20	-25	-42
	-42	-25	-19	-17	-17	-17	-18	-19	-22	-26	-42
	-43	-26	-20	-18	-19	-20	-20	-22	-25	-28	-43
-.8	-23	-41	-22	-19	-17	-15	-15	-15	-17	-19	-23
	-24	-41	-22	-20	-18	-16	-15	-16	-18	-20	-24
	-25	-42	-22	-20	-19	-18	-17	-18	-19	-21	-25
	-26	-43	-22	-21	-22	-21	-20	-21	-21	-22	-26
-.6	-17	-20	-43	-19	-18	-16	-16	-17	-18	-18	-17
	-18	-21	-43	-19	-18	-17	-17	-18	-18	-18	-18
	-19	-22	-43	-20	-20	-19	-19	-20	-19	-19	-19
	-20	-25	-44	-22	-22	-22	-22	-22	-20	-20	-20
-.4	-16	-18	-19	-50	-21	-21	-22	-21	-19	-17	-16
	-16	-19	-19	-50	-21	-21	-23	-22	-19	-17	-16
	-17	-20	-20	-50	-23	-23	-24	-23	-20	-18	-17
	-18	-22	-22	-51	-25	-26	-27	-24	-21	-20	-18
-.2	-17	-19	-20	-22	-65	-32	-31	-25	-22	-19	-17
	-17	-19	-20	-23	-65	-33	-32	-26	-23	-19	-17
	-17	-19	-20	-23	-65	-35	-33	-26	-24	-20	-17
	-17	-20	-20	-23	-66	-36	-34	-28	-25	-21	-17
.0	-17	-18	-19	-23	-35	XX	-40	-30	-33	-21	-17
	-17	-18	-19	-23	-35	-111	-40	-36	-33	-21	-17
	-17	-18	-19	-23	-35	-127	-40	-38	-33	-21	-17
	-17	-18	-19	-23	-35	XX	-40	-38	-33	-21	-17
.2	-17	-17	-19	-24	-31	-37	XX	-24	-22	-19	-17
	-17	-17	-19	-24	-32	-38	-88	-24	-22	-19	-17
	-18	-17	-19	-24	-33	-40	-89	-25	-23	-19	-18
	-18	-17	-19	-25	-34	-43	-92	-27	-24	-20	-18
.4	-19	-18	-19	-21	-25	-36	-24	-79	-19	-19	-19
	-19	-18	-19	-22	-25	-35	-25	-77	-20	-19	-19
	-19	-18	-20	-23	-26	-38	-25	-78	-21	-20	-19
	-19	-18	-20	-24	-28	-41	-26	-79	-22	-20	-19
.6	-22	-18	-18	-19	-22	-30	-22	-19	-64	-23	-22
	-22	-19	-18	-19	-23	-31	-22	-20	-64	-23	-22
	-22	-19	-19	-20	-24	-33	-23	-21	-65	-23	-22
	-22	-20	-20	-21	-25	-36	-24	-22	-66	-24	-22
.8	-25	-19	-17	-17	-18	-19	-17	-18	-21	-48	-25
	-25	-20	-18	-18	-19	-20	-18	-18	-22	-49	-25
	-26	-21	-19	-18	-20	-21	-19	-20	-23	-49	-26
	-27	-22	-20	-20	-22	-24	-22	-22	-26	-50	-27
1.0	-42	-23	-17	-15	-15	-15	-15	-17	-19	-24	-42
	-42	-24	-18	-16	-16	-16	-16	-17	-20	-25	-42
	-42	-25	-19	-17	-17	-17	-18	-19	-22	-26	-42
	-43	-26	-20	-18	-19	-20	-20	-22	-25	-28	-43

note: XX denotes program failure.

Table 4.7 Variation of JG against jammers' directions for various jammers' spectrums when two jammers are present. The array has 3 elements, 2 taps, $1/4f_0$ tap spacing and 10% bandwidth while the jammers have equal powers. The spectrum for s_1 is flat, while reading downwards, the four entries in each direction cell correspond to s_2 having square-law, inverted-triangular, flat and triangular spectrums.

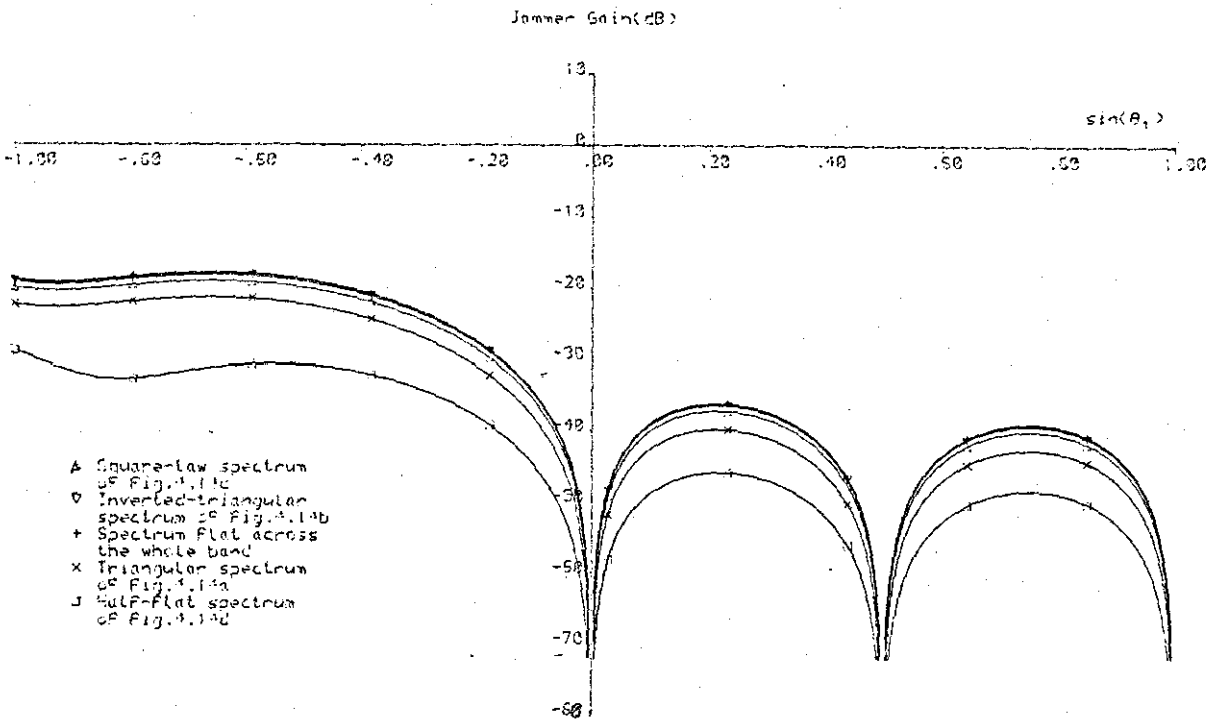

Fig.4.18 Graphs of JG against jammer's direction for various jammers' spectrums obtained in the situations of fig.4.17 but with the array having 4 taps and 40% bandwidth.

variation resulting from having different spectrums is decreased. Furthermore, unlike the 2-tap array, the performance improves as the spectrum becomes more peaky at either the band edges or the centre of the band. In particular, amongst all the spectrums, flat spectra is now associated with roughly the worst performance. All these observations and deductions are also generally confirmed by other simulation results. Therefore, within a few dB above the actual values when the number of taps is small, the results of table 4.1 or the generalization of (4.50), (4.54) and (4.55), obtained when all the jammers' spectrums are flat, can be taken as giving the MJG defined in (4.2). Thus, combining (4.50), (4.54) and (4.55) leads to

$$MJG \approx b_1(b_2B)^{2LJ/2J} \qquad (4.56a)$$

where

$$b_1 = \begin{cases} 1.6, & M=2 \\ 1.3, & M=3 \\ 4, & M\geq 3 \end{cases} \qquad (4.56b)$$

and

$$b_2 = \begin{cases} 0.8, & M=2 \\ 1.3, & M\geq 2 \end{cases}. \qquad (4.56c)$$

Evidently, this has the form of (4.42) derived theoretically in section 4.2.

Summarizing, it has been found that in general, the array performance is fairly insensitive to the jammers' spectrums and that worst performance is associated with all the jammers' spectrums being roughly flat. In addition to the theoretical derivations of section 4.2, the deductions of the last sections are therefore still applicable even when the jammers' spectrums are not all flat. In particular, based on the generalization of (4.50), (4,54) and (4.55) obtained from the results of table 4.1, the MJG of (4.56) was derived.

4.7 Applications of results

Having studied the array performance in terms of the JG in the last five sections, this section will discuss the various practical applications mentioned in section 4.1 by using the results obtained and requiring that the performance be satisfactory under all the environments to be envisaged. First, however, the relationship between JG and ONR, briefly discussed in section 4.1, need and will be discussed in more detail.

As discussed in section 4.1, the array performance is most suitably measured by the ONR and the JG is used for this purpose because it is independent of receiver noise power and closely related to the ONR. Fig.4.19a shows the usual typical variation of

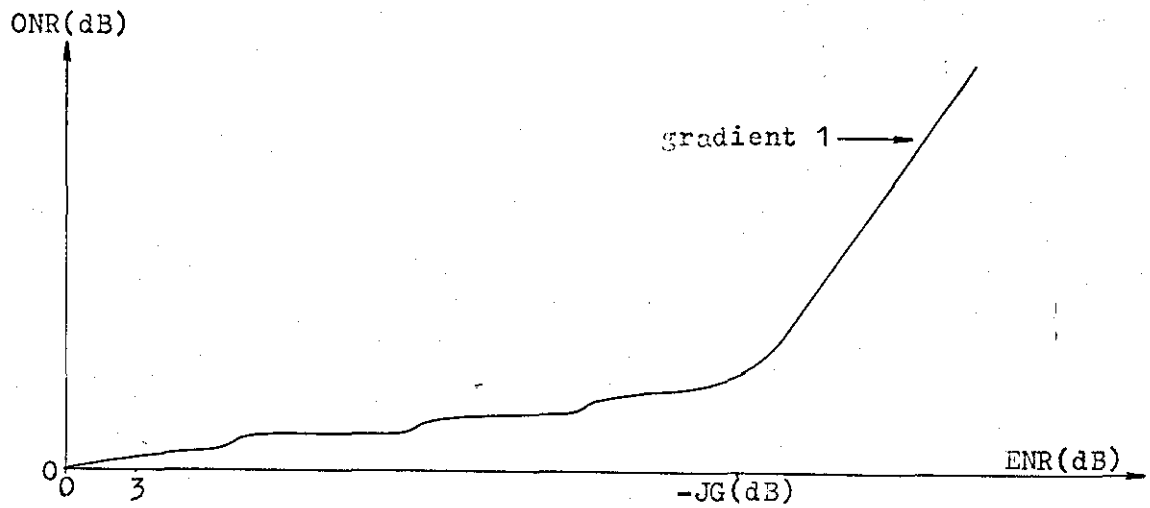

Fig.4.19a Usual typical variation of ONR with ENR

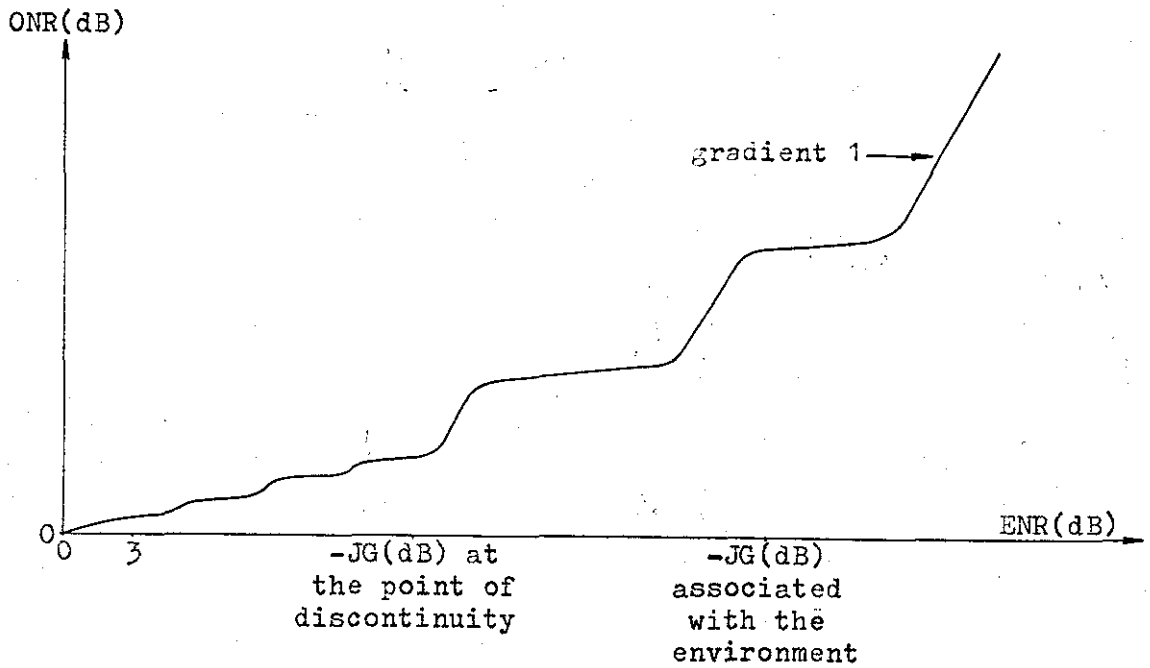

Fig.4.19b Variation of ONR with ENR when the environment is closed to one of the relatively few associated with points of discontinuity

Fig.4.19 Variation of ONR with ENR showing the relationship with JG.

ONR with element to receiver noise power ratio (ENR) and illustrates the relationship between ONR, ENR and JG. For very small ENR roughly between 0 and 3dB, the total jammer power is less than receiver noise power. Thus, in this trivial region, the optimal weights will be predominantly determined by receiver noise and the ONR roughly equal to 0dB. In particular, for ENR of 0dB, implying

that no jammer is present, the optimal weights will be equal to 0 and the ONR equal to 0dB. As the ENR increases, the jammers will become dominant. The optimal weights will then be determined principally by the necessity to reject the jammers and secondarily by the presence of receiver noise. As indicated in fig.4.19a for ENR roughly between 3dB and -JG in dB, the power inversion array is able to devote part or all of its degrees of freedom to reject the jammers without the output power component due to receiver noise being excessive. Therefore, in this region, the optimal output power and so ONR are due mostly to receiver noise and increase in small steps as shown, each step being due to the switching of degrees of freedom originally "tied" up with receiver noise towards rejecting the jammers. In other words, as the ENR increases so that the component of ONR due to the jammers increases and tends to be significant, the array will direct more degrees of freedom to further reject the jammers. As a result, although the jammers are further rejected, the number of degrees of freedom tied up with receiver noise is decreased and so the ONR, due mostly to receiver noise in this region, increases slightly in a step-like manner as the degrees of freedom are switched over. Of course, if the degrees of freedom can easily be switched over, that is, with the ONR component due to receiver noise increased only very slightly, or if the switching over takes place gradually, the step increases may not be observable and the curve appears to be smoother. Eventually, if the ENR is increased so that it becomes greater than -JG in dB (which gives the jamming rejection capability of the array), the jammers cannot be rejected to below receiver noise power even when all the degrees of freedom are employed for their rejection. Hence, the array will use all its degrees of freedom to re-

ject the jammers but even so, the rejection is not satisfactory and the optimal output power will still be mostly due to the jammers, resulting in the curve of fig.4.19a to increase drastically with gradient 1. Clearly, the performance can and will be considered as inadequate if the ENR is greater than -JG in dB. The above discussion has been found from simulation results to be applicable in all situations except when the external environment is closed to the relatively few where $2L(M-1)J/2NJ\lambda C$ in (4.46) and associated with points of discontinuity discussed in section 4.4. From the discussion in previous sections, a point of discontinuity is due to the inability of the array to direct more than a certain maximum number of degrees of freedom towards rejecting one of the jammers and results from the coinciding of some of the tapping points of the equivalent filter of the jammer concerned. Of course, in the neighbourhood of the point of discontinuity, these coinciding tapping points will become separated, though only slightly. Thus, although the JG in the neighbourhood of the point of discontinuity is much smaller than that at the point of discontinuity, it is obtained with the array using also some of the "would-be-inapplicable" degrees of freedom to reject the jammer concerned and so associated with the weights having large magnitudes. The typical variation of ONR with ENR in these situations is therefore that shown in fig.4.19b. For ENR less than the value of -JG in dB at the point of discontinuity, the jammers can still be well rejected by using the degrees of freedom that are still applicable at the point of discontinuity and hence, with the same behaviour as in fig.4.19a, the ONR increases only slightly with ENR. However, for larger ENR, some of the would-be-inapplicable degrees of freedom are also needed to reject the jammer giving rise to the point

of discontinuity and this leads to the optimal weights having large magnitudes and so significant increase in the ONR component due to receiver noise and thus ONR itself. Hence, as the ENR increases, the ONR increases significantly in large steps as shown. The reason for the step increase is the same as that discussed for fig. 4.19a. One difference, however, is that in the usual situations of fig.4.19a, the switching of degrees of freedom to further reject the jammers usually occurs when the ONR component due to the jammers is still much smaller than that due to receiver noise. Because of the heavy penalty of switching the would-be-inapplicable degrees of freedom, this is not so here. Eventually, if the ENR is increased above the point where even with all the degrees of freedom used for rejecting the jammers, the optimal output power is still dominated by the jammers, the curve of fig.4.19b, like that of fig.4.19a, will increase with gradient 1. Since the ONR has increased significantly, the ENR at which this takes place is considerably greater than -JG in dB. Obviously, in the few situations of fig.4.19b, the performance can and will be considered as inadequate if the ENR is greater than the value of -JG in dB at the point of discontinuity. The JG associated with the situation, however, does not have much physical significance. Therefore, although the array has zero probability to be in environments corresponding to points of discontinuity, the JG for these environments is not trivial because of the effect of receiver noise. Evidently, the above discussion regarding the relationship of ONR, ENR and JG justifies the use of JG instead of ONR as the performance measure.

Fig.4.20 shows some typical simulation results investigated to verify the discussion of the last paragraph. Fig.4.20a shows graphs of ONR against ENR for a 3-element, 2-tap, $1/4f_0$ tap spaci-

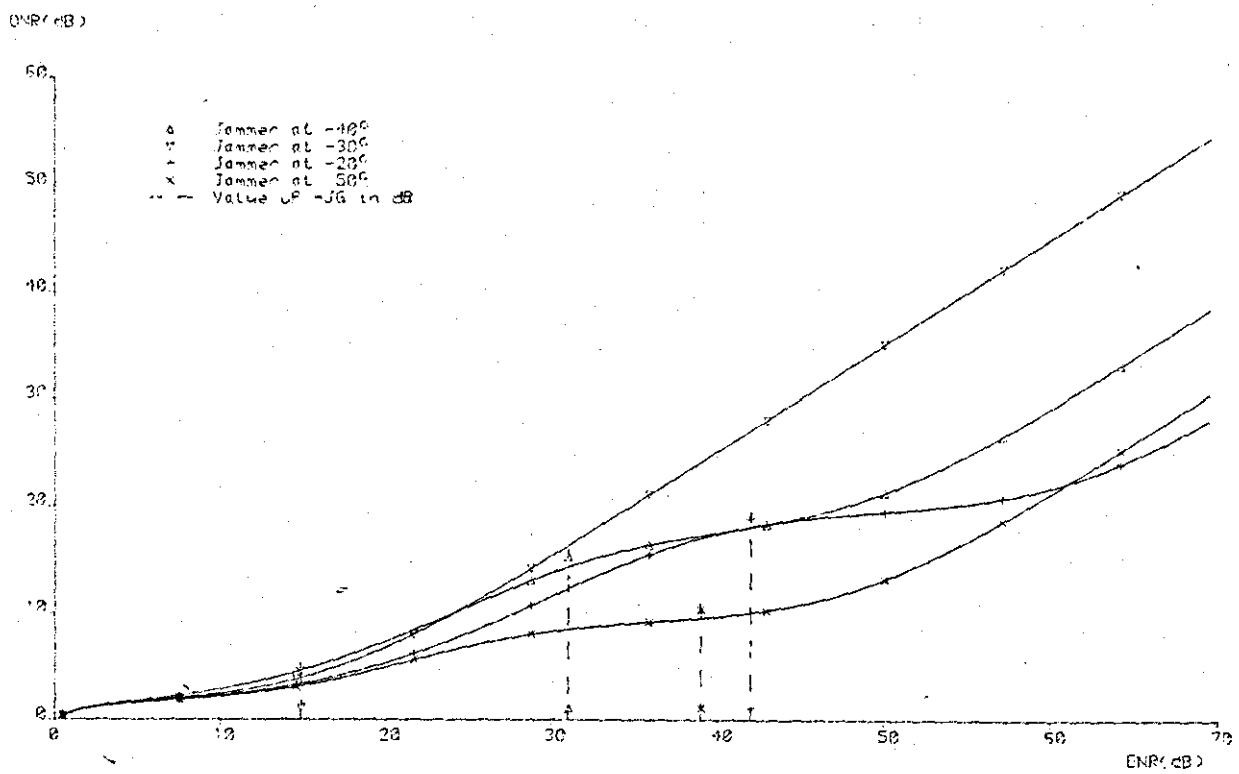

Fig.4.20a Variation of ONR with ENR at the jammers' directions of -40°, -30°, -20° and 50°, the jammer's direction of -30° being a point of discontinuity

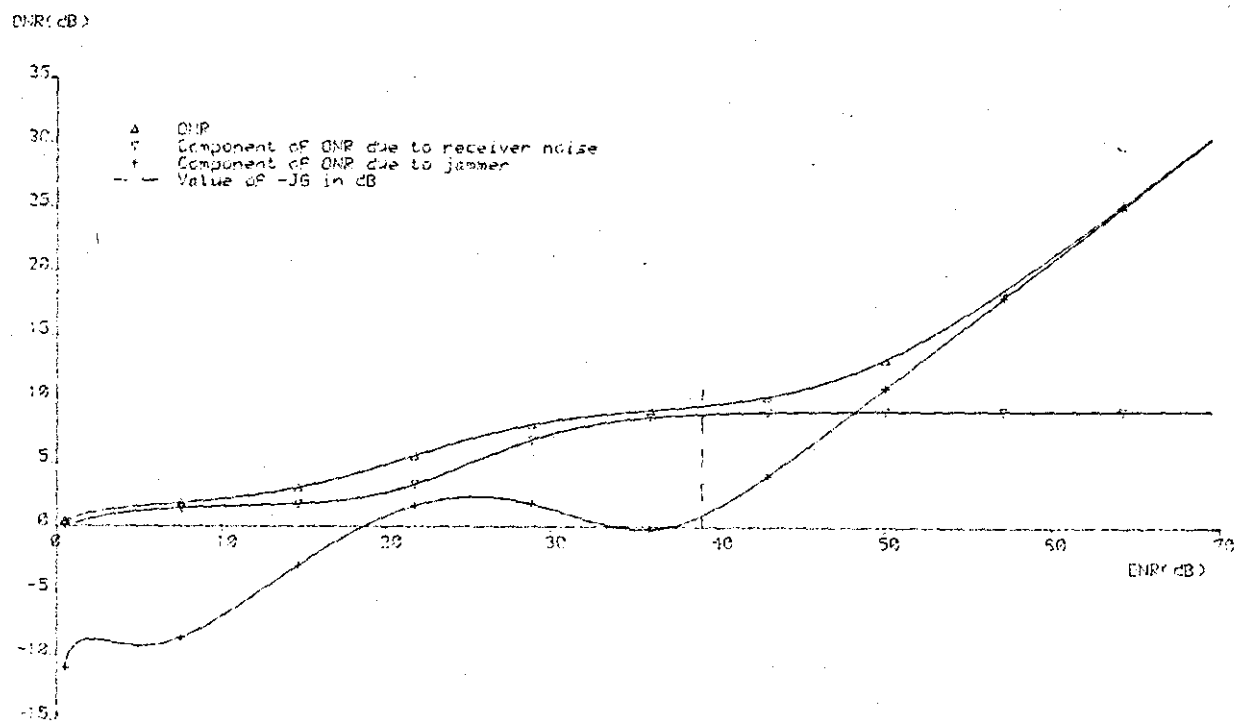

Fig.4.20b Variation of ONR and its components with ENR at the jammer's direction of 50°, far from the point of discontinuity

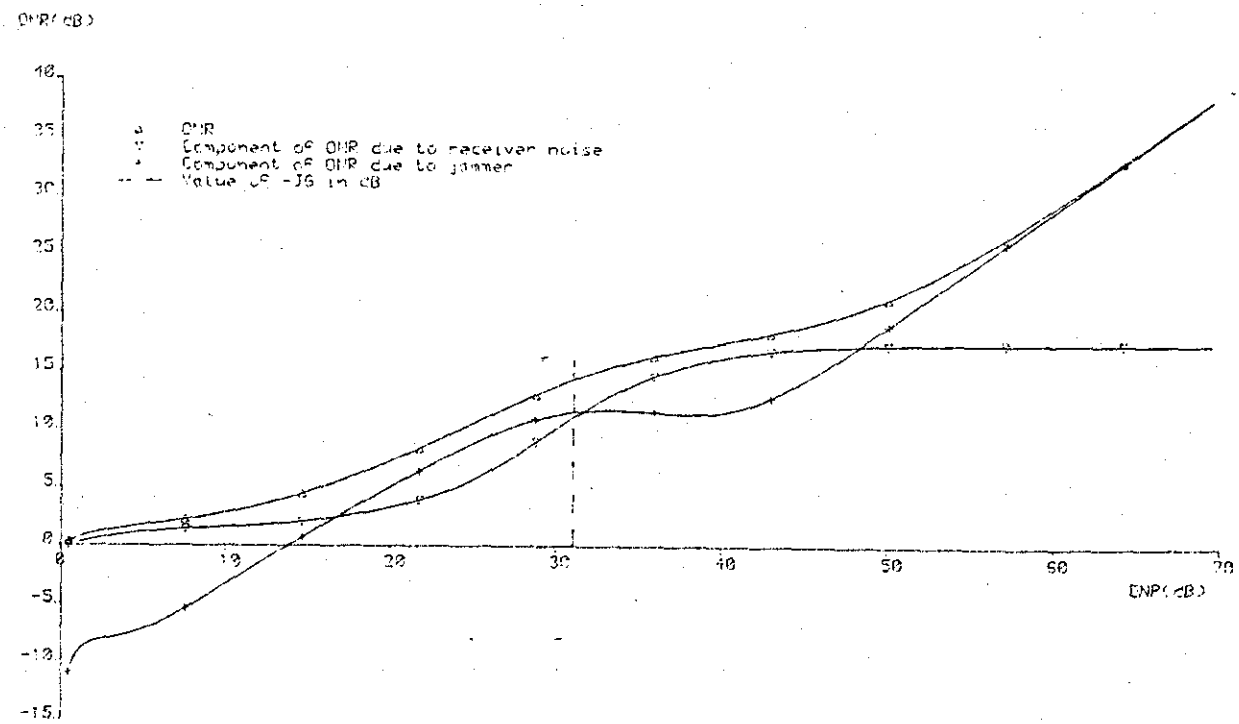

Fig.4.20c Variation of ONR and its components with ENR at the jammer's direction of -40°, closed to the point of discontinuity

Fig.4.20 Variation of ONR and its components with ENR at various jammers' directions for a 3-element, 2-tap, $1/4f_0$ tap spacing array with 20% bandwidth when one jammer with flat spectrum is present.

ng array with 20% bandwidth at the jammers' directions of -40°, -30°, -20° and 50° when one jammer having flat spectrum is present. Fig.4.20b shows the same graph at the jammer's direction of 50° and also its components due to the jammer and receiver noise, while fig.4.20c shows those at the jammer's direction of -40°. Also drawn on the figures are broken lines giving the values of -JG in dB in each environment. Note that the graph of JG against jammer's direction in fig.4.11 for this situation has a maximum at the jammer's direction of -30°, the only point of discontinuity. Clearly, the curves in fig.4.20 at this jammer's direction and at the jammer's direction of 50°, far from the point of discontinuity, have characteristics as discussed for fig.4.19a, whereas those at the jammers' directions of -20° and -40°, closed to the point of disc-

ontinuity, agree with the discussion regarding fig.4.19b. Specifically, for the former two jammers' directions, the ONR increases drastically and the performance becomes inadequate if the ENR is greater than roughly -JG in dB. Furthermore, for the jammer's direction of 50°, the ONR is principally due to receiver noise when as depicted by the two troughs in the curve due to the jammer in fig.4.20b, the degrees of freedom are switched towards rejecting the jammer. On the other hand, for the latter two jammers' directions, drastic increase in ONR and performance inadequacy occur for ENR greater than roughly the value of -JG in dB at the point of discontinuity. Moreover, the curves in fig.4.20c have the same characteristics as that of fig.4.20b, except that the switching over of the would-be-inapplicable degrees of freedom now takes place when the ONR is due principally to the jammer.

From the discussion of the above two paragraphs, it is evident that if the array is to have adequate performance in all environments with ENR less than a designed maximum ENR (MENR), the ME NR should not be greater than the value of -MJG in dB:

$$\text{MJG} \angle \frac{1}{\text{MENR}}. \tag{4.57}$$

Using (4.56a), the minimum number of taps required for a particular bandwidth and MENR is then

$$J \simeq -2\left\lfloor \frac{\log(b_1 \text{MENR})}{2\log(b_2 B)} \right\rfloor \tag{4.58}$$

where b_1 and b_2 are given in (4.56b,c). Fig.4.21 shows the variation of the number of taps required with bandwidth at 20 and 40dB MENR. (4.56b,c) and (4.58) are used with the operation $\lfloor \cdot \rfloor$ neglected for convenience. As can be derived from (4.58), the number of taps required can be seen to increase fairly linearly with MENR in dB and bandwidth.

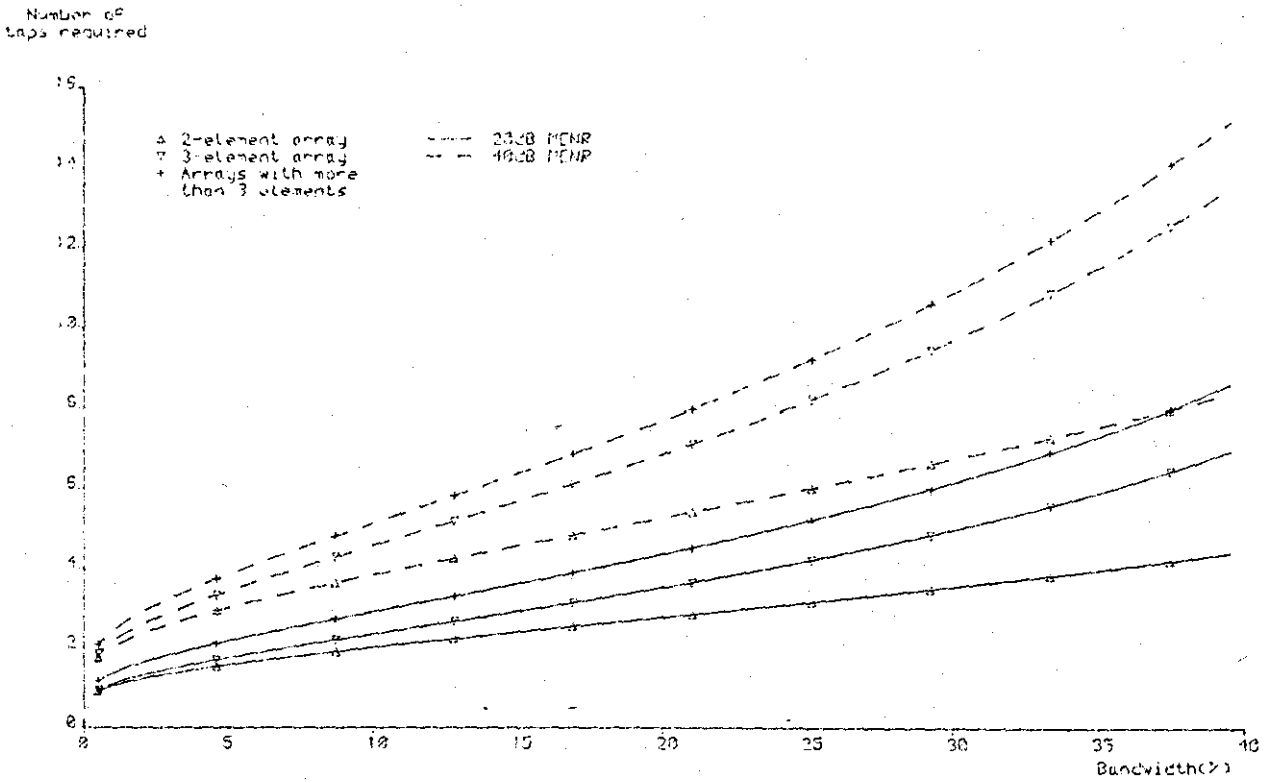

Fig.4.21 Graphs of number of taps required against bandwidth at 20 and 40dB MENR, obtained using (4.56b,c) and (4.58) with the operation $\lfloor \cdot \rfloor$ neglected.

Using again (4.56a) and the principle expressed by (4.57), the maximum bandwidth for adequate performance of arrays using 2-tap delay lines or with negligible difference, quadrature weighting is

$$B \approx \frac{1}{b_2(b_1 MENR)^{1/2}}. \qquad (4.59)$$

Therefore, if the alternative broadband processing method discussed in section 4.1 is to be employed, the number of narrowband processors required is

$$\frac{J_N}{2} \approx \lfloor 1 - B b_2 (b_1 MENR)^{1/2} \rfloor \qquad (4.60)$$

where J_N is obviously the number of weights per element for this processing method. Note that strictly, in deriving (4.60) from (4.59), it has been assumed implicitly that the array element power as seen by each narrowband processor is the same. This is obv-

iously the case when, for example, all the jammers have flat spectrums. In cases when this is not so and (4.60) is used, some of the narrowband processors may be "overloaded" while some may be " underloaded". However, even in the extreme case where all the jammers' powers are concentrated into just one processor with the other processors seeing no jammer, the final ONR is easily deduced to be not very different from that should all the jammers have flat spectrums. Hence, (4.60) can and will be taken as applicable generally. From (4.58) and (4.60), the relative advantage of using tapped delay line and the alternative broadband processings, in terms of the number of weights required, is obviously reflected in the ratio

$$\frac{J_N}{J} \approx \frac{-Bb_2(b_1 MENR)^{1/2}}{\lfloor \log(b_1 MENR)/2\log(b_2 B) \rfloor}. \qquad (4.61)$$

Again, neglecting the operation $\lfloor \cdot \rfloor$ and using (4.56b,c), fig.4.22 shows the variation of this ratio with bandwidth at 20 and 40dB MENR. Note that from (4.61), the ratio J_N/J can easily be seen to be roughly independent of b_2 while proportional to the square root of b_1, accounting, with (4.56b,c), for the large difference between the curve corresponding to more than 3 elements and the other two curves at the same MENR. Clearly, the array using the alternative broadband processing becomes more inefficient relatively as the MENR and for bandwidth less than about 20%, the bandwidth increase. For larger bandwidth, increase in bandwidth does not lead to much change in the relative efficiency. As an example, for bandwidth and MENR greater than about 20% and 20dB respectively, the array with tapped delay line processing uses at most half the number of weights as that when the alternative broadband processing is employed.

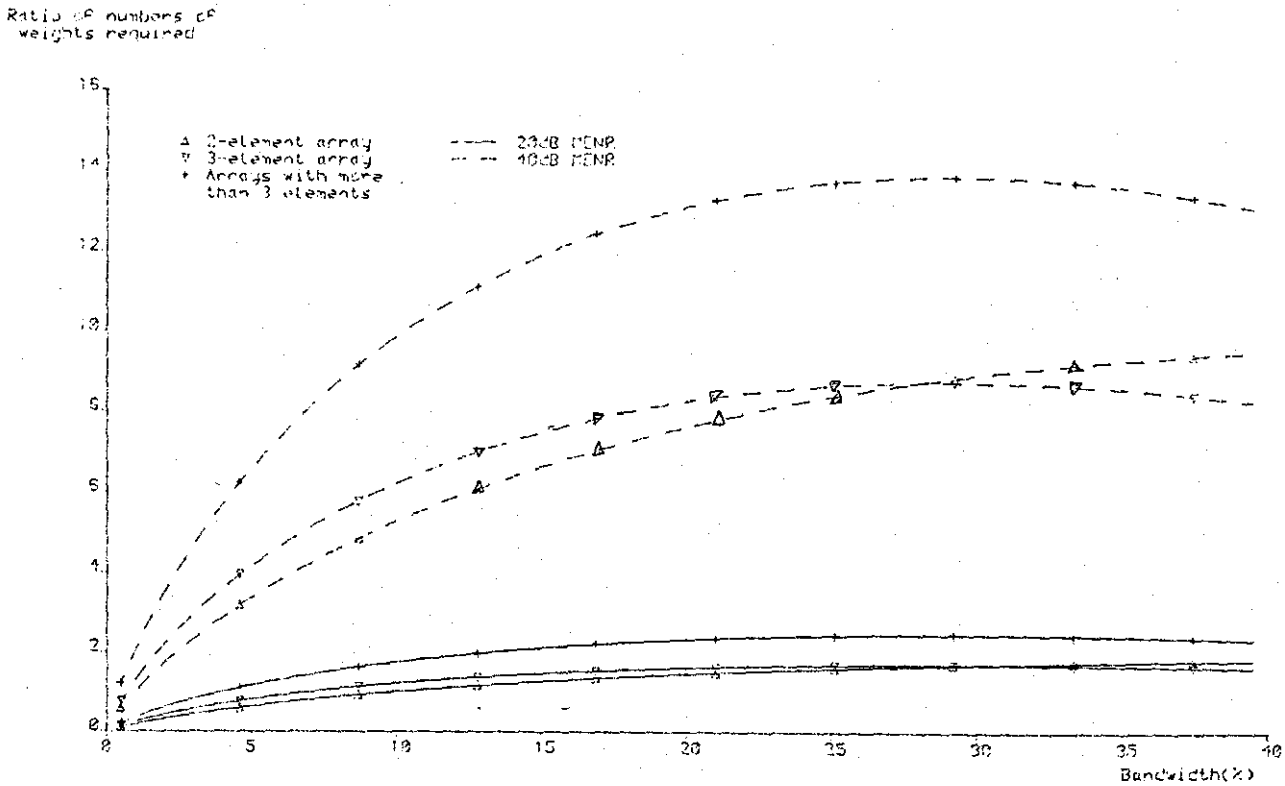

Fig.4.22 Variation, with bandwidth at 20 and 40dB MENR, of ratio of the number of weights required with the alternative broadband processing to that with tapped delay line processing. The curves are obtained using (4.56b,c) and (4.61) with the operation $\lfloor \cdot \rfloor$ neglected.

Summarizing, this section has discussed in more detail the relationship between ONR, ENR and JG. From the discussion, the array performance was deduced to be adequate in general unless the ENR is greater than roughly -JG in dB. However, when the environment is closed to one giving rise to a point of discontinuity, the performance becomes inadequate if the ENR increases above roughly the value of -JG in dB at the point of discontinuity. Thus, by using (4.56), the number of taps required such that the performance is adequate under all environments with ENR less than the designed MENR value was derived to be given by (4.58) or graphically, fig.4.21. Similarly, the number of narrowband processors required with the alternative broadband processing was derived to be given by (4.60). Comparison of the alternative broadband and tapped delay line processings in terms of the number of variable weights

required is therefore given by (4.61) or graphically, fig.4.22. Incidentally, although the tap spacing for the latter processing was not discussed in this section, the best tap spacing, from the discussion in previous sections, is obviously such that the entire length of the delay line is about $1/2f_0$ to give the best average performance.

4.8 Frequency Distortion introduced by rejecting the Jammers

The previous sections have investigated the performance of the array using the measure JG which only gives information averaged over the entire band. The investigation is useful for the various practical applications discussed in the last section. However, with the direction of the desired signal being unknown a priori to any reasonable degree of accuracy in many communication purposes involving the power inversion array, it is also of interest to determine the amount of frequency distortion at various directions due to employing the optimal weights to reject the jammers. Note that frequency distortion as used here refers to any departure from the ideal frequency response of which the amplitude and phase responses are independent of and proportional to frequency respectively, that is, that associated with a pure time delay. The purpose of this section is therefore to briefly and qualitatively investigate, using some typical simulation results obtained, the variation of array response, as a function of frequency and direction, with the various parameters when the optimal weights are employed. Because of the inefficiency of odd-tap array discussed, the discussion in this section will be limited to the even-tap array.

Firstly, for general discussion, fig.4.23 shows the amplitu-

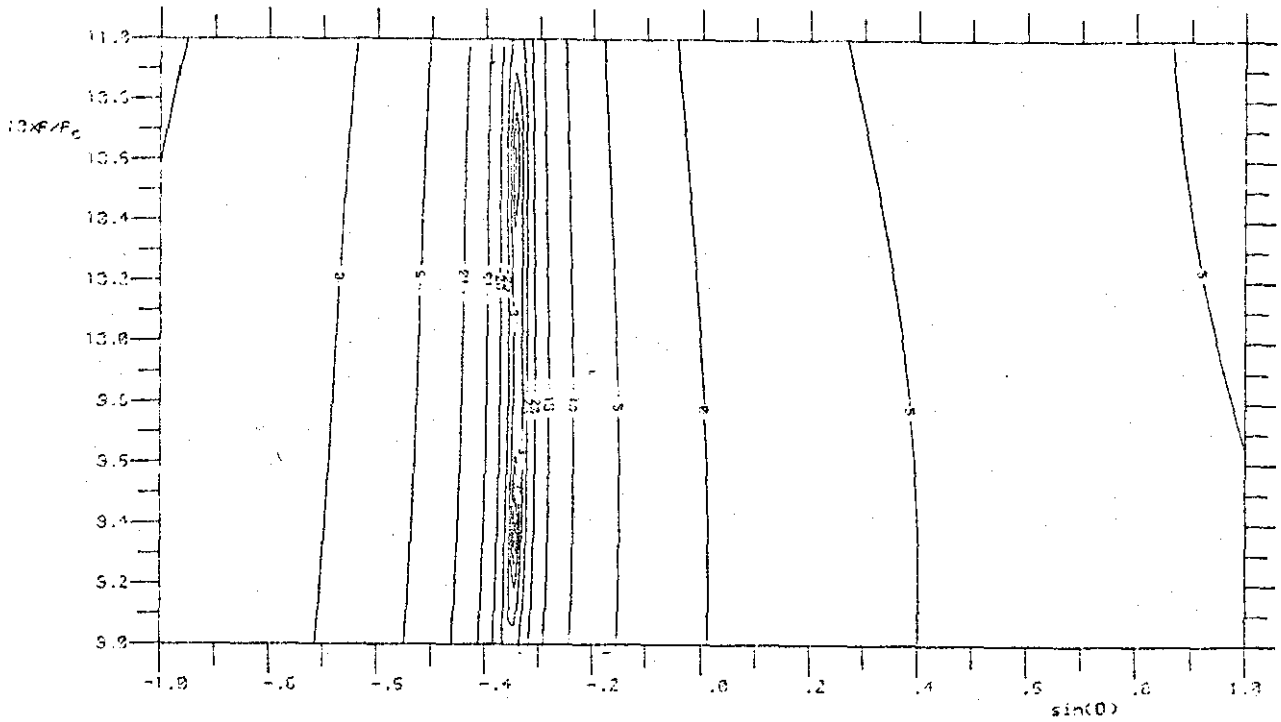

Fig.4.23a Amplitude response in dB

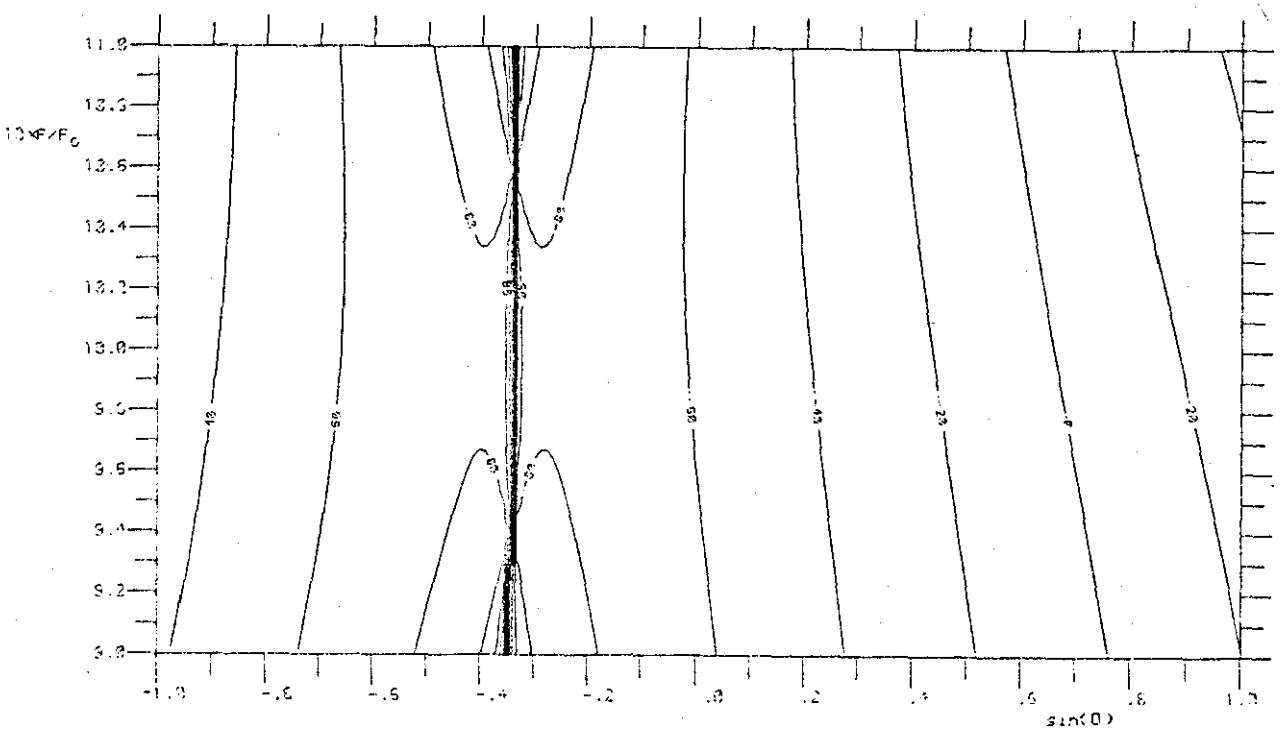

Fig.4.23b Phase response in degree

Fig.4.23 Array response against frequency and direction for a 2-element, 4-tap, $1/4f_0$ tap spacing, 20% bandwidth array with 30dB ENR. The jammer arrives from -20° and has flat spectrum.

de and phase responses plotted as contour maps against frequency and direction when one jammer with flat spectrum arrives from -20°. A 2-element, 4-tap array with 20% bandwidth and $1/4f_0$ tap spacing is used, while the ENR is 30dB, roughly equal to the value of -MJG in dB given by (4.56). Adjacent contours in the amplitude and and phase response maps are separated by 5dB and 20° respectively. The phase response is calculated treating the first array element as the phase centre. Note that the contours in both response maps become more congested as the frequency increases. This is because as the frequency increases, the array element spacing, as a fraction of wavelength, increases. As expected, two nulls can be seen steered towards the jammer in the amplitude response map. Furthermore, the spatial extent of "near-jammer amplitude distortion", as determined by the spatial extent of these nulls, is very small. Apart from this distortion, the amplitude response, though varying quite widely with direction, is fairly uniform with frequency. By comparing the phase response shown with the proportionality relationship between ideal phase response and frequency, it is obvious that the jammer has introduced a "background phase distortion" of the order of 20° at almost every direction. Moreover, depicted as a series of nearly overlapping contours, there is 180° phase shift across the jammer's direction. Corresponding to the spatial extent over which this 180° phase jump takes place, the spatial extent of "near-jammer phase distortion" is very small and roughly equals that of the near-jammer amplitude distortion.

Secondly, fig.4.24 shows the array response when the jammer arrives from -60°, all the other parameters being the same as that of fig.4.23. By comparison, the relative positions of the amplit-

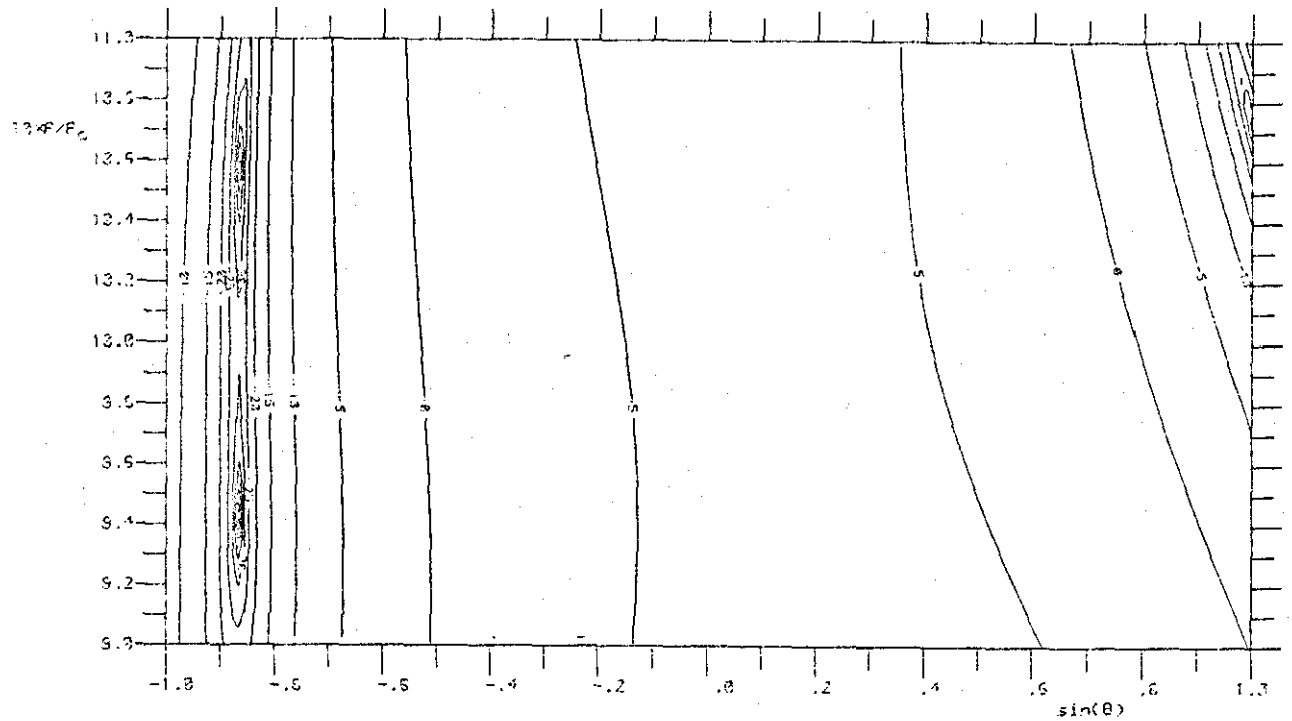

Fig.4.24a Amplitude response in dB

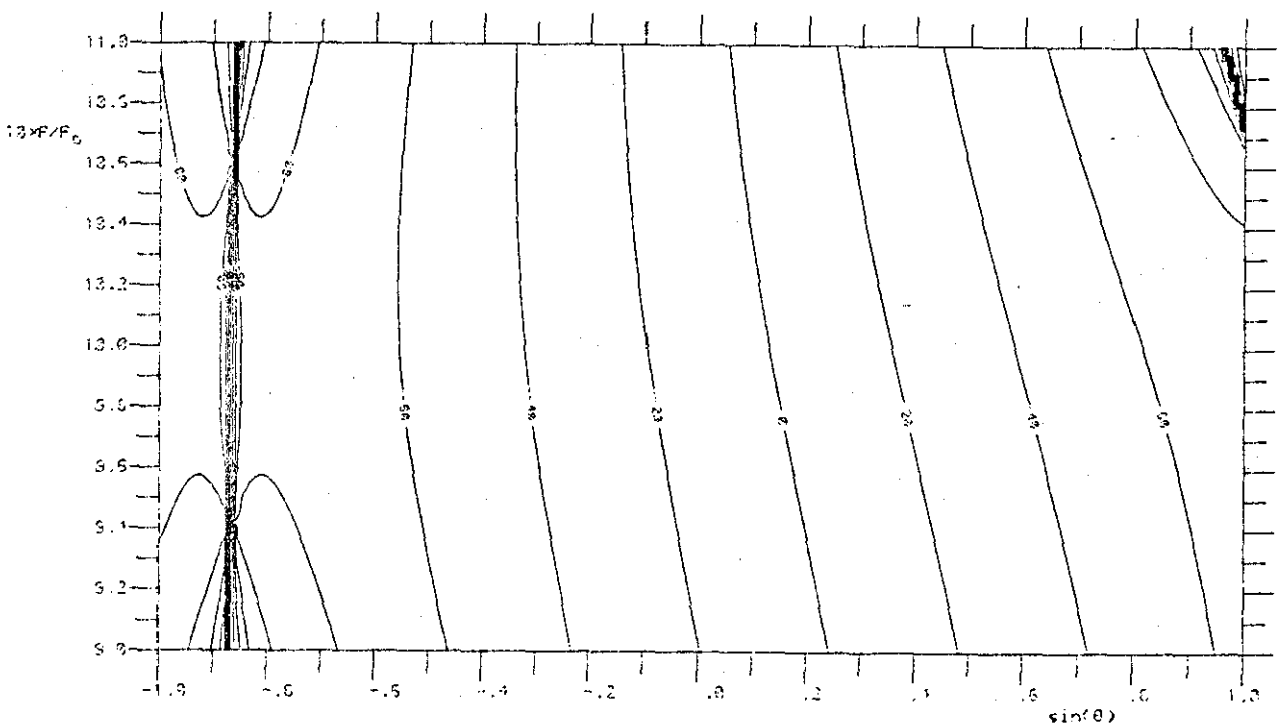

Fig.4.24b Phase response in degree

Fig.4.24 Array response against frequency and direction for the situation of fig.4.23, except with the jammer arriving from -60° instead.

ude and phase contours with respect to the jammer's direction in fig.4.24 are very similar to those in fig.4.23. In particular, the near-jammer distortions in the sinθ domain are quite independent of the jammer's direction, implying that, in terms of θ, these distortions will become more extended as the jammer approaches the endfire directions. Due to the effect of grating lobes, distortion in frequency response can be seen at directions near to 90° in fig. 4.24. The "grating amplitude distortion" depends on the amplitude response, particularly its slope, around the high frequency region near the opposite endfire direction. The "grating phase distortion", whose spatial extent is less than that of the corresponding amplitude distortion, also depends on the phase response over the same region. Thus, these distortions also become more serious and extended as the jammer approaches the endfire directions. Obviously, unless the array element spacing is reduced by a fraction of about B so that effectively, the region corresponding to sinθ greater than 1-B or less than -1+B in the figure do not have any physical significance and thus, these distortions are eliminated, the reception capability of the array near the endfire directions may be considerably impaired.

Thirdly, fig.4.25 shows the array response maps obtained when the ENR is decreased to 15dB, all the other parameters being the same as that of fig.4.24. The apparent multi-null feature in the high frequency grating response of fig.4.25a is due to the algorithm and tne finite size of the matrix used for the contouring subroutine in the computer program. Comparing fig.4.25 with 4.24 indicates that except for the shifting of the two nulls towards the band edges and the smearing out of the nearly overlapping phase contours between the two nulls, changing the ENR has no effect on

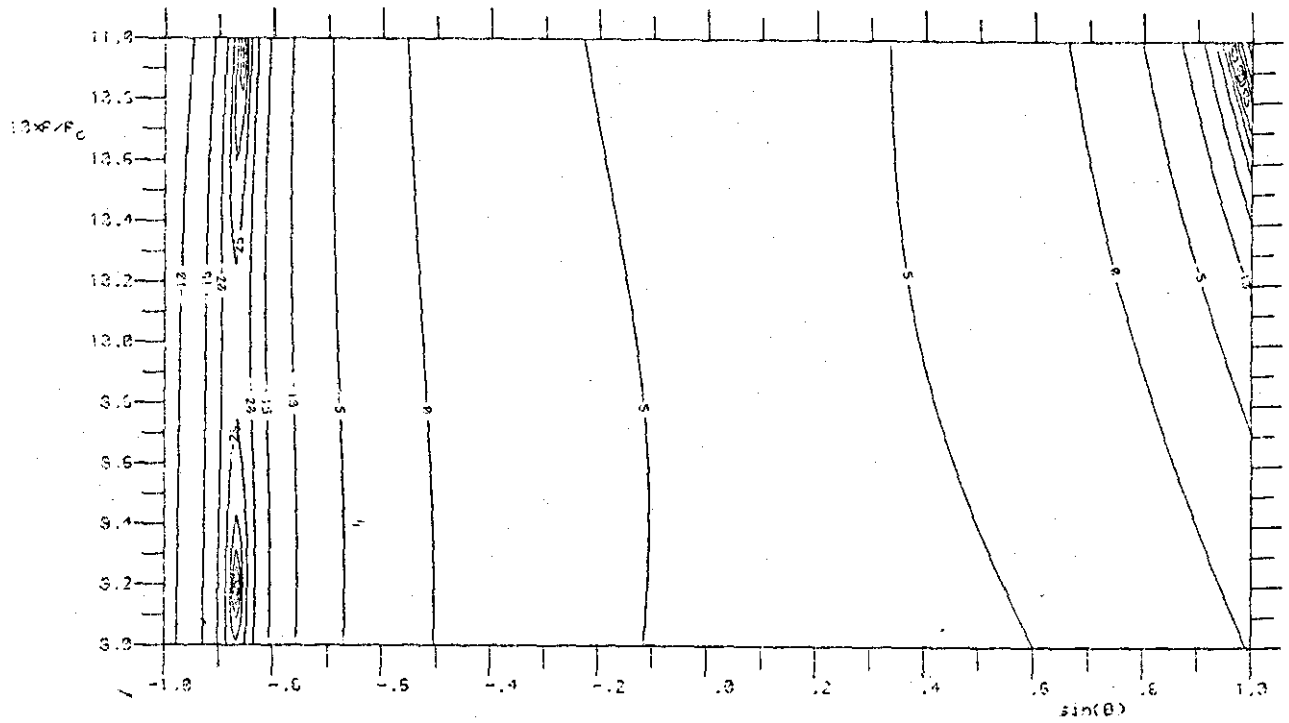

Fig.4.25a Amplitude response in dB

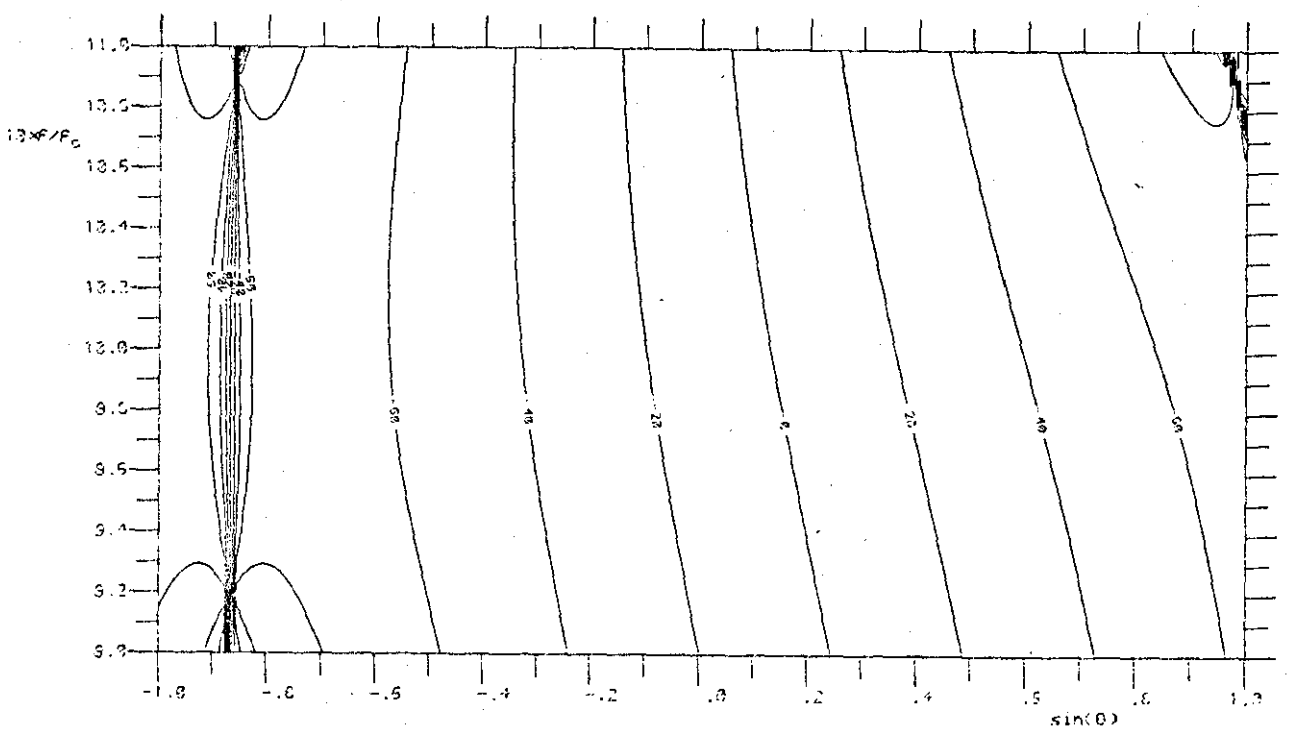

Fig.4.25b Phase response in degree

Fig.4.25 Array response against frequency and direction for the situation of fig.4.24, except that the ENR is decreased to 15dB.

the array response. The two effects observed are obviously because the presence of receiver noise alone would drive all the weights to zero, resulting in an omni frequency-directional response.

Fourthly, fig.4.26 shows the array response for the situation of fig.4.24, except that the bandwidth is decreased to 10%. Note that the contours are drawn only within the frequency band of interest. As expected, similar but much better array response can be seen as the bandwidth is decreased. Though not quite clear from the response maps, the two nulls of fig.4.26 have actually moved slightly towards the band edges and their extent in the spatial domain decreased, when compared with those of fig.4.24. Moreover, the background phase distortion has decreased by about a half to very roughly 10°. Furthermore, there is only a very small grating amplitude distortion while the grating phase distortion has virtually vanished. Nevertheless, note that it is still necessary to decrease the array element spacing by about a fraction of B to ensure that there is no grating amplitude distortion at the endfire directions.

Fifthly, fig.4.27 shows the array response when the number of taps is increased to 6, all the other parameters being the same as that of fig.4.24. As expected, three nulls can be vaguely seen in the amplitude response map. Apart from a decrease in the extent of the nulls and the region for the 180° phase jump in the spatial domain, the contours of fig.4.27 are roughly identical to those of fig.4.24 and so changing the number of taps does not have any significant effect on the variation of array response. This is generally the case except when the number of taps is decreased to 2. Fig.4.28 shows the array response for a 3-element, 2-tap, $1/4f_0$ tap spacing array with 20% bandwidth. Only one jammer arriving from

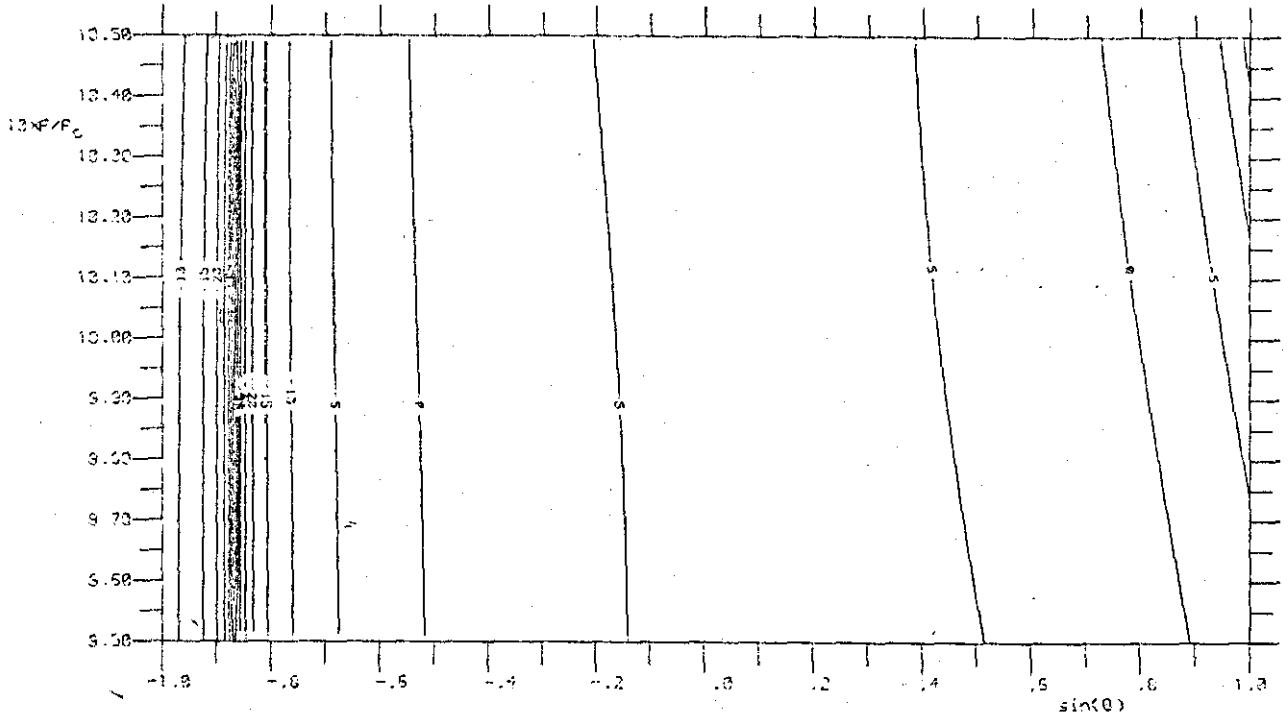

Fig.4.26a Amplitude response in dB

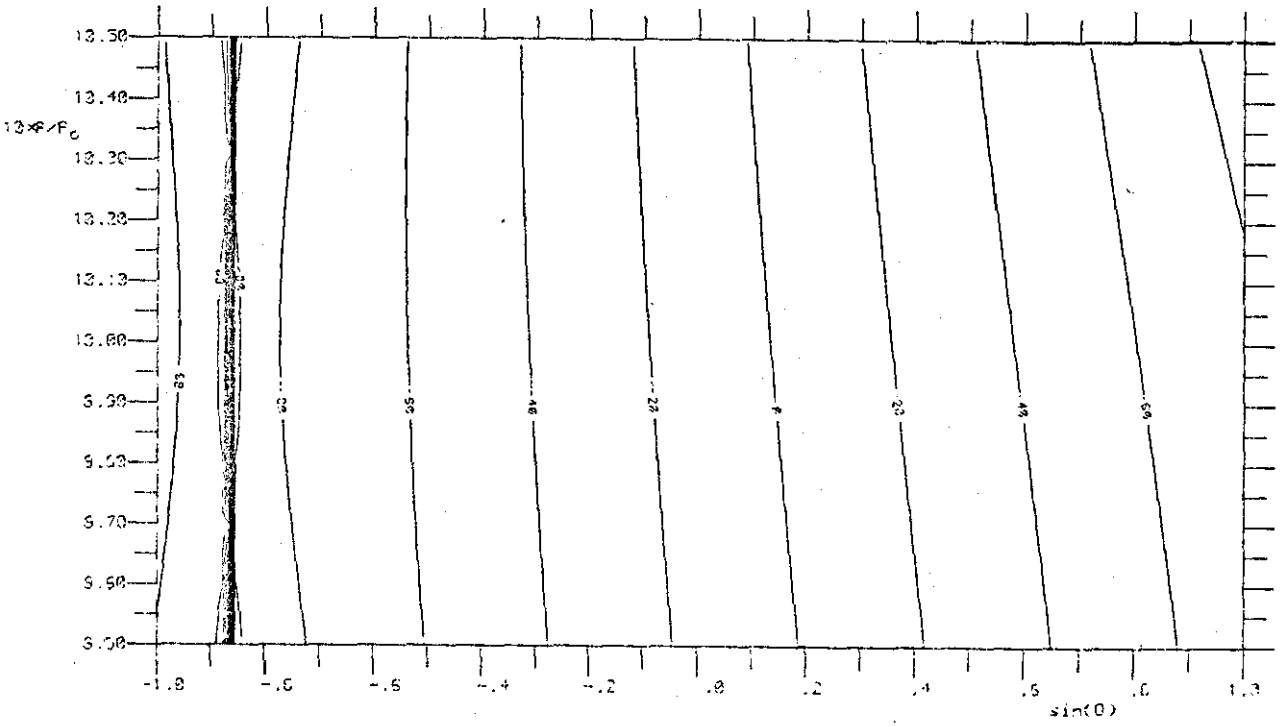

Fig.4.26b Phase response in degree

Fig.4.26 Array response against frequency and direction for the situation of fig.4.24, except that the bandwidth is decreased to 10%.

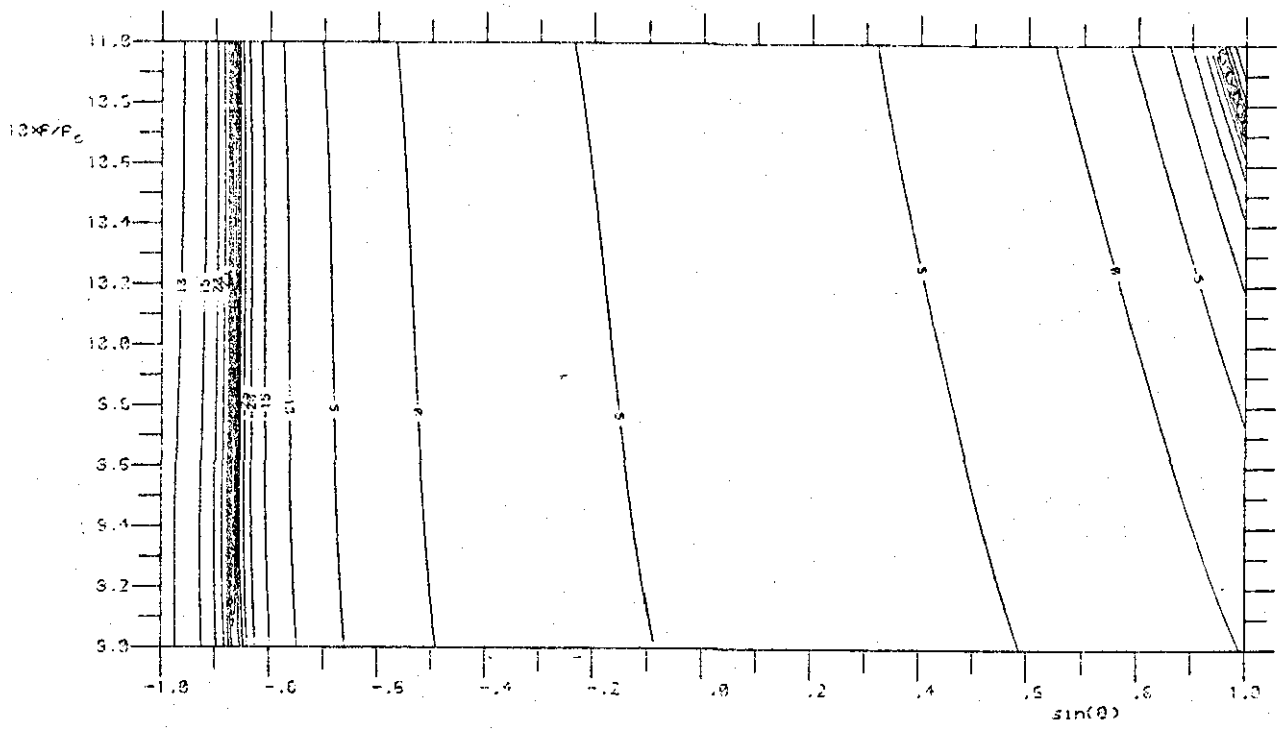

Fig.4.27a Amplitude response in dB

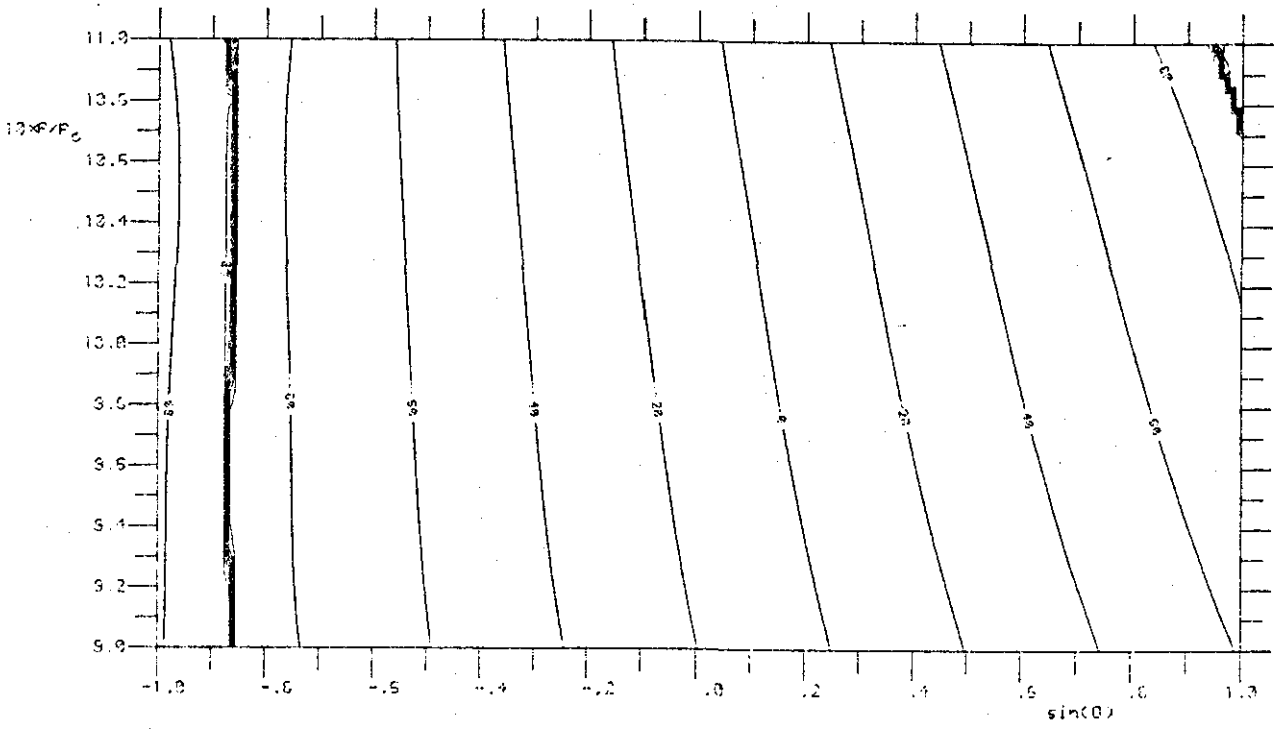

Fig.4.27b Phase response in degree

Fig.4.27 Array response against frequency and direction for the situation of fig.4.24, except that the number of taps is increased to 6.

50° and having flat spectrum is present. The ENR is 10dB, roughly equal to the value of -MJG in dB as given by (4.56). Clearly, with only one null steered towards the jammer, the contours near to the jammer's direction have become skewed and so the near-jammer distortions increased. On the other hand, the background phase distortion has reduced significantly and the grating distortions are virtually non-existent. Other simulation results also give the same observations but not surprisingly, also indicate the proportionality of the spatial extent of near-jammer distortions of the 2-tap array with bandwidth. Evidently, even though the jamming rejection capability obtained is satisfactory, the 2-tap array may not be suitable for use in large bandwidth applications because of the large spatial extent of near-jammer distortions.

Sixthly, the effect of varying tap spacing has also been studied. Since virtually no change in array response is observed, the results will not be presented.

Seventhly, fig.4.29 shows the array response for a 3-element, 4-tap, $1/4f_0$ tap spacing, 20% bandwidth array in a 2-jammer environment. The two jammers have equal powers, flat spectrums and arrive from -20° and -60°. The ENR is 25dB, roughly equal to the value of -MJG in dB as given by (4.56). Obviously, the contours have the same characteristics as in the 2-element situations treated. Specifically, because the jammers have equal powers, two nulls can be seen steered towards each jammer. Furthermore, although the phase contours are more closely spaced, they are more vertical and give rise to roughly the same background phase distortion as for the 2-element, 20% bandwidth situations discussed. Fig.4.30 shows the array response obtained for the situation of fig.4.29 when only the jammer at -60° is present. Again, two nulls are ste-

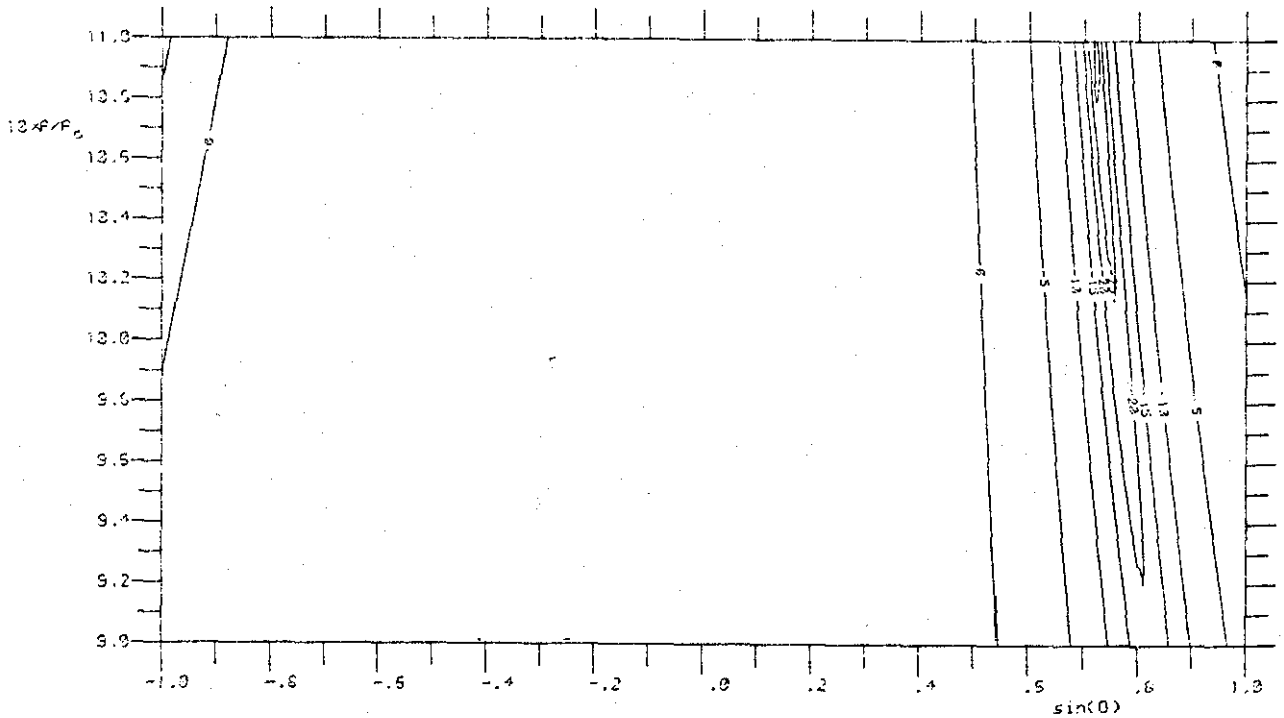

Fig.4.28a Amplitude response in dB

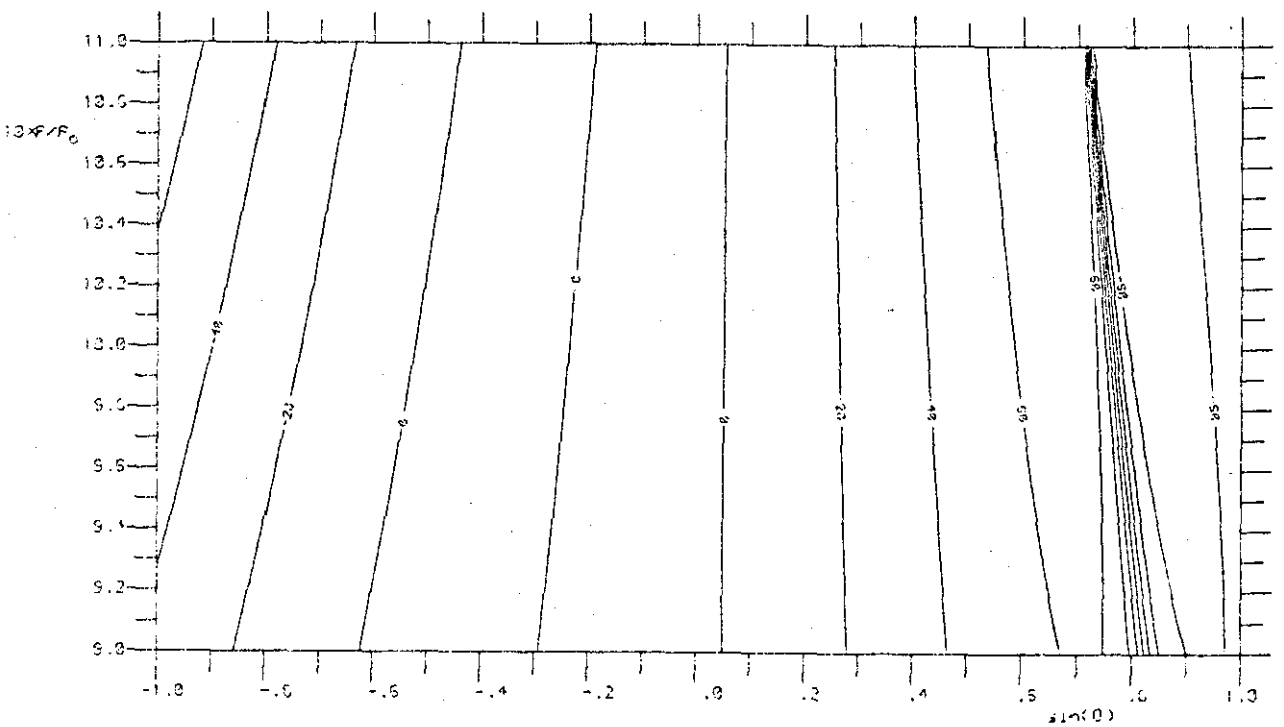

Fig.4.28b Phase response in degree

Fig.4.28 Array response against frequency and direction for a 2-tap array with 3 elements, $1/4f_0$ tap spacing and 20% bandwidth. Only one jammer arriving from 50° and having flat spectrum is present. The ENR is 10dB.

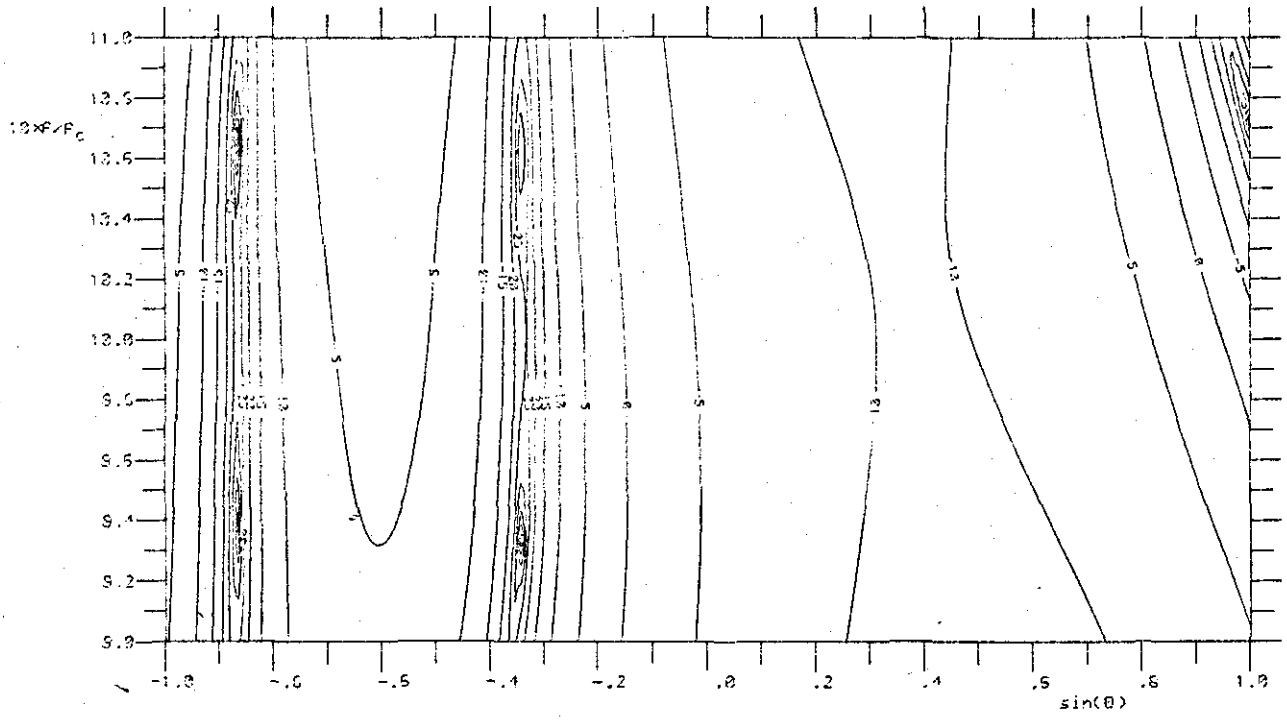

Fig.4.29a Amplitude response in dB

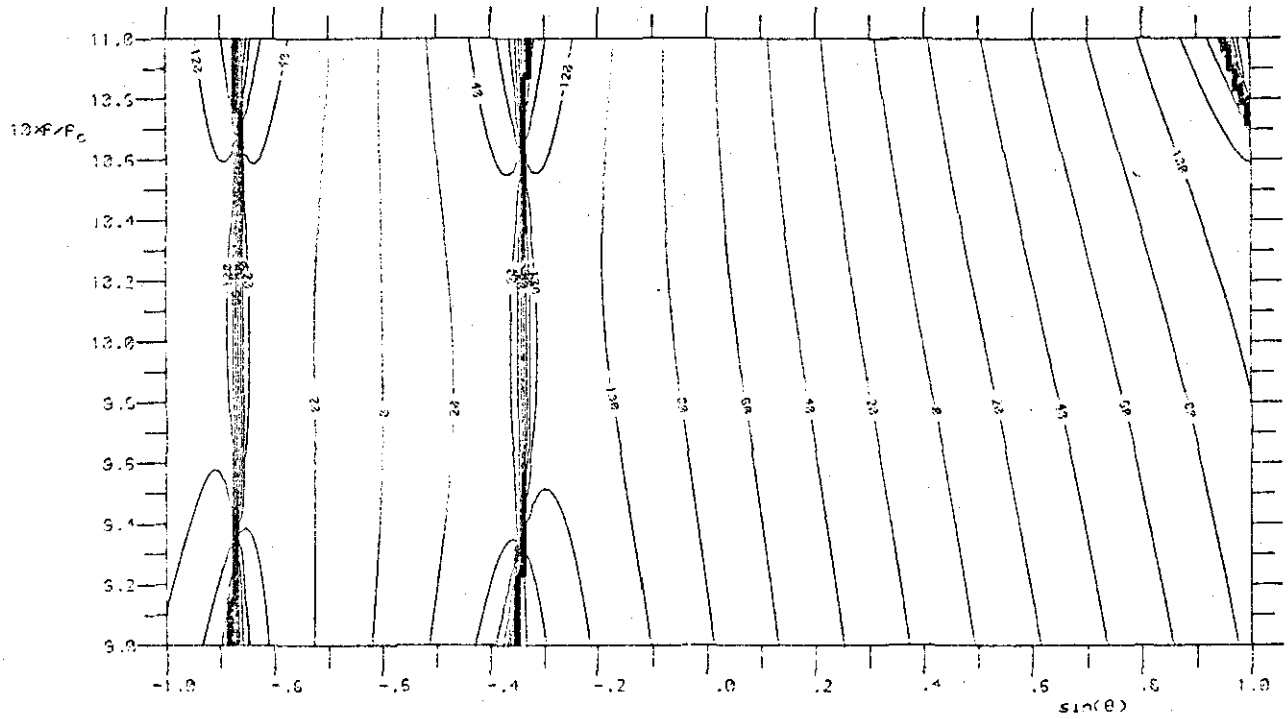

Fig.4.29b Phase response in degree

Fig.4.29 Array response against frequency and direction for a 3-element, 4-tap, $1/4f_0$ tap spacing, 20% bandwidth array in a 2-jammer environment. Both jammers have equal powers, flat spectrums and arrive from -20° and -60°. The ENR is 25dB.

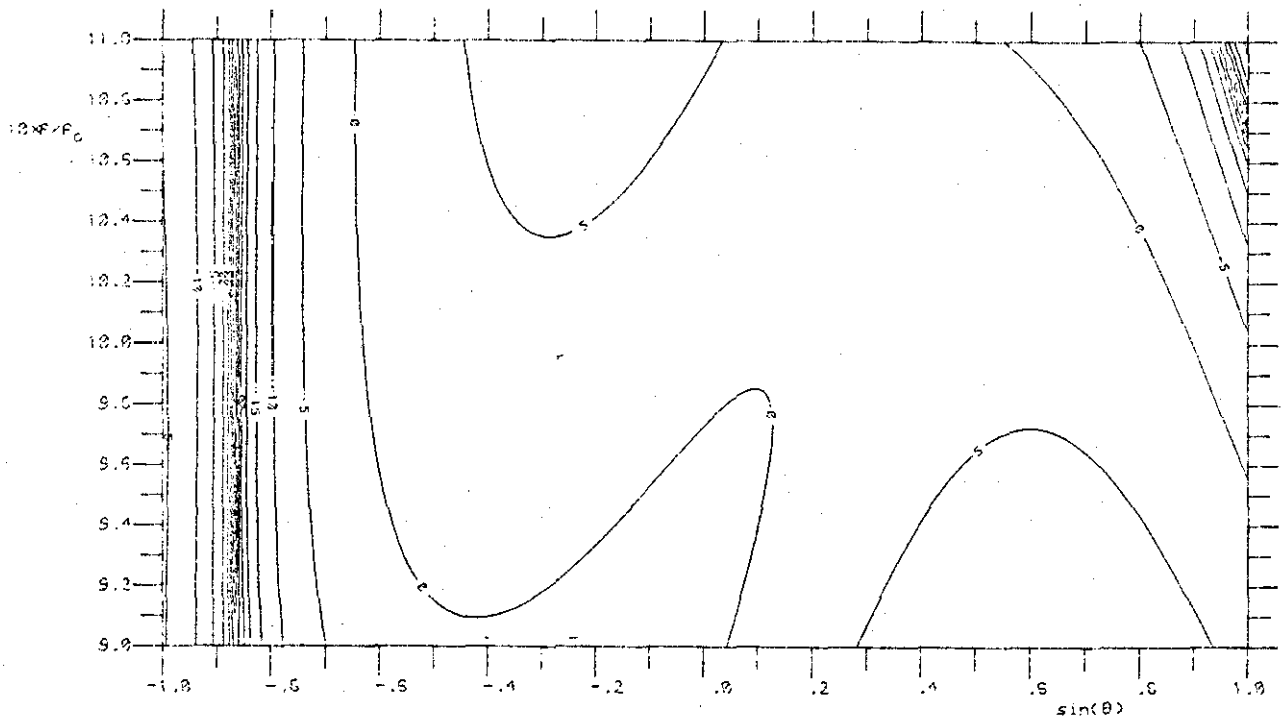

Fig.4.30a Amplitude response in dB

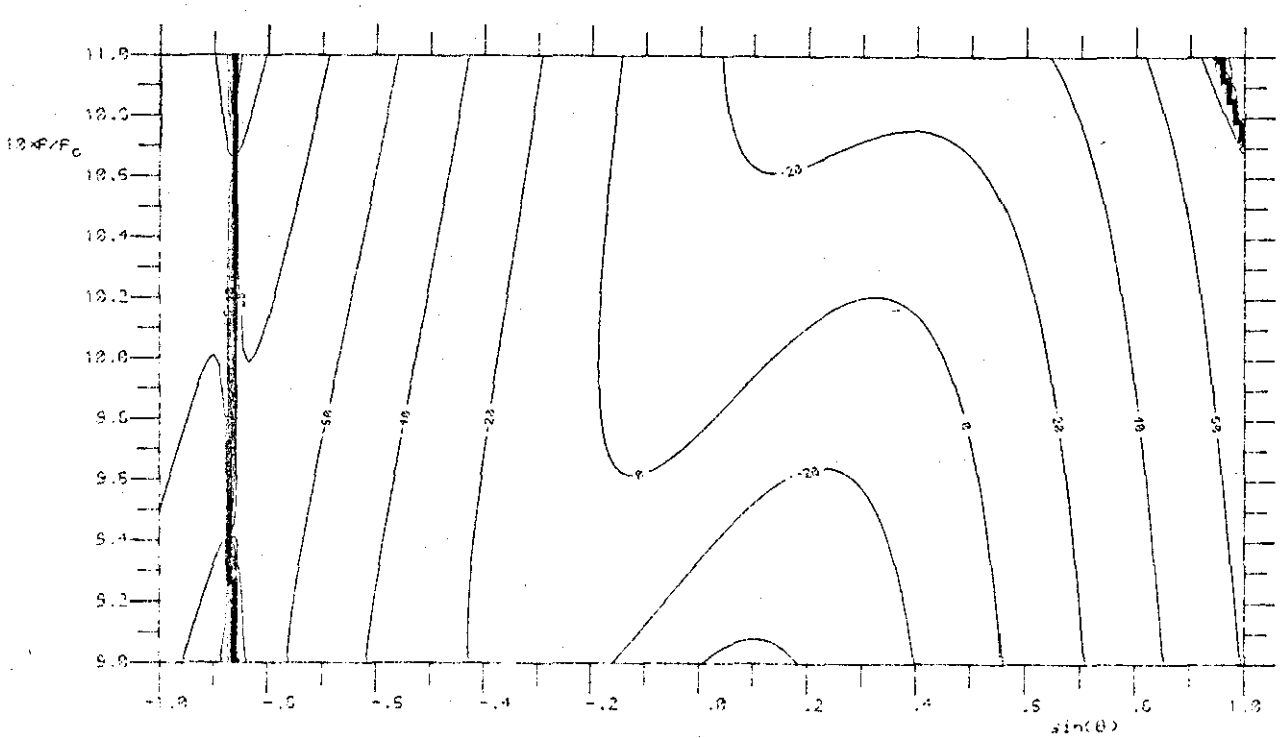

Fig.4.30b Phase response in degree

Fig.4.30 Array response against frequency and direction for the situation of fig.4.29 when only the jammer at -60^{0} is present.

ered towards the jammer. Moreover, although the contours are slightly different from those of fig.4.29, they lead to roughly the same amount of distortions. In general, the various distortions are fairly independent of the numbers of elements and jammers.

Eighthy, fig.4.31 shows the array response for the situation of fig.4.29, except that the jammer at -60° has inverted-triangular spectrum instead. Clearly, since this jammer concentrates more power from the the centre towards the edges of the band, the two nulls steered towards this jammer have moved slightly towards the edges of the band. Apart from this difference, however, the contours are roughly the same as those of fig.4.29, indicating that generally, the various distortions are fairly insensitive to the jammers' speetrums. Similarly, the variation of jammers' relative powers and directions have been studied. Again, no significant change in the various distortions is observed and the results will not be presented.

So far, the discussion and results presented have been for situations to be anticipated where the ENR is less than or roughly equal to the designed MENR. Clearly, from the results obtained, the number of nulls steered towards each jammer in these normal situations does not exceed $J/2$. To complete the discussion in this section, some situations where the ENR is greater than the MENR and some jammers "absorb" more nulls will be studied. Figs.4.32 and 4.33 show the array responses for the situation of fig.4.28, except that the ENR is increased to 30 and 40dB respectively, as compared to the MENR (equal to -MJG in dB) of about 10dB. Note that from the variation of ONR with ENR given in fig.4.20b for this environment, the performance in terms of jamming rejection is still

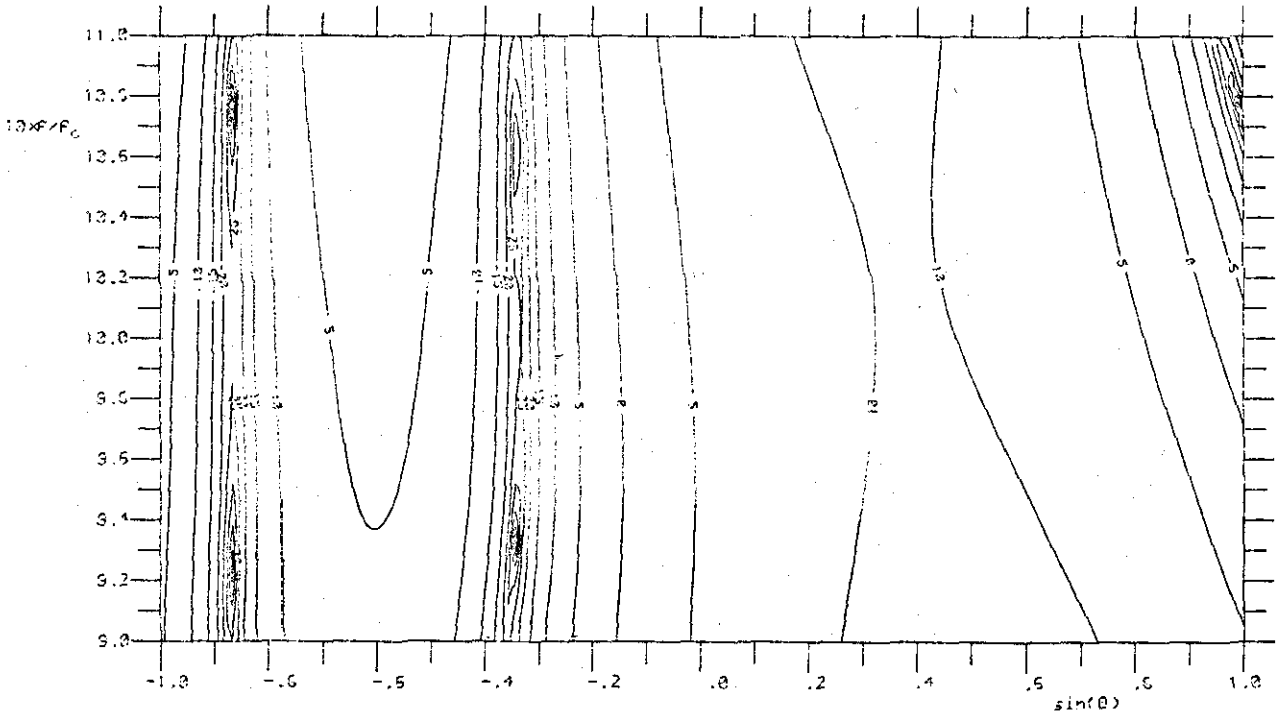

Fig.4.31a Amplitude response in dB

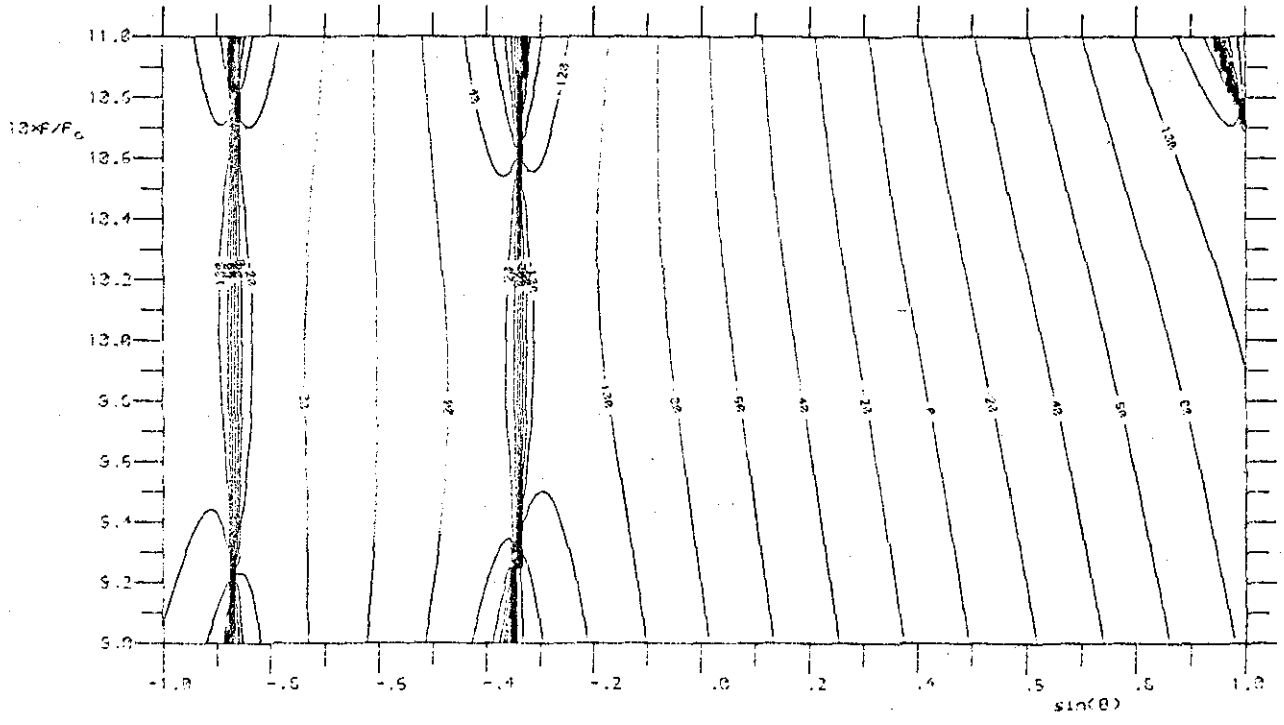

Fig.4.31b Phase response in degree

Fig.4.31 Array response against frequency and direction for the situation of fig.4.29, except that the jammer at -60° now has inverted-triangular spectrum.

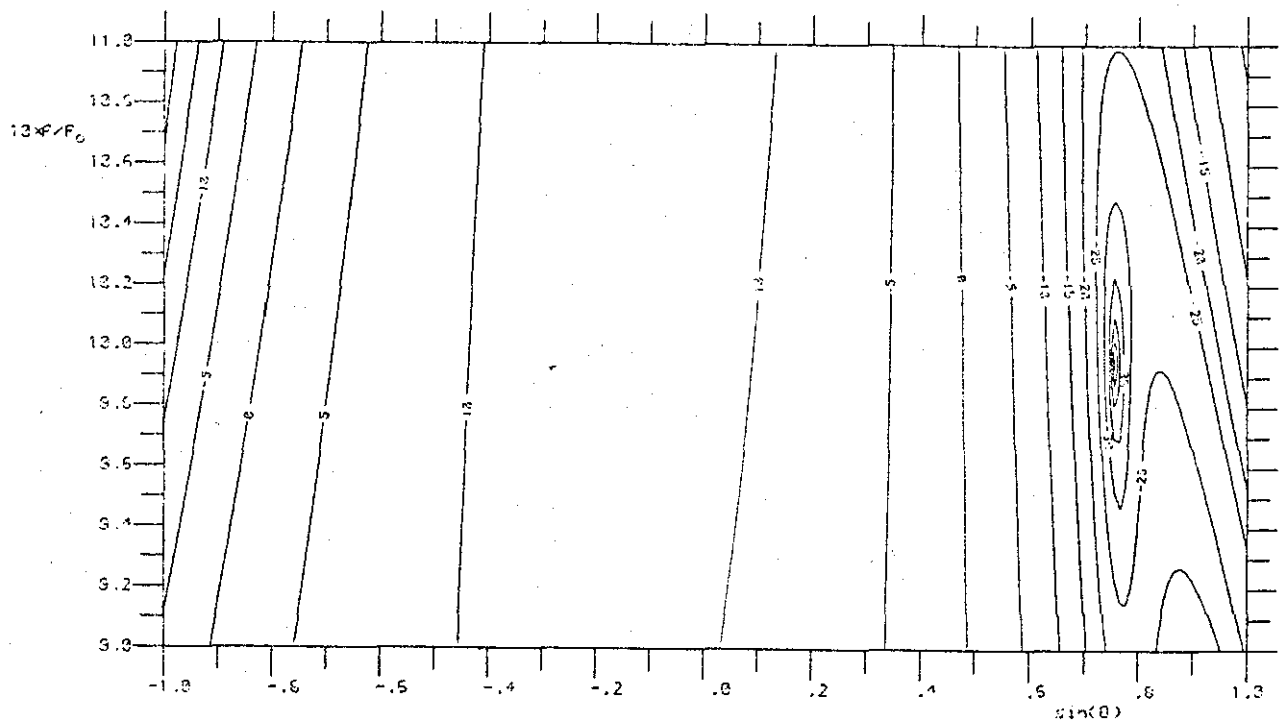

Fig.4.32a Amplitude response in dB

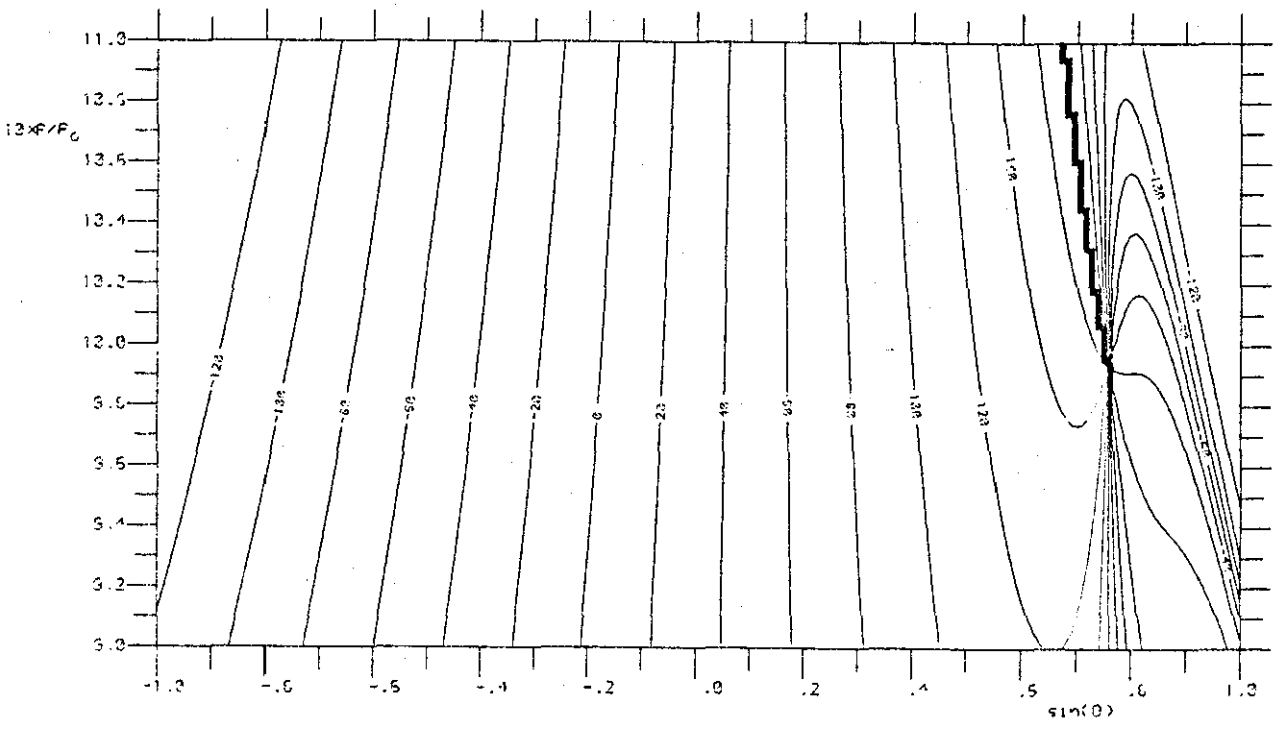

Fig.4.32b Phase response in degree

Fig.4.32 Array response against frequency and direction for the situation of fig.4.28, except that the ENR is increased to 30dB.

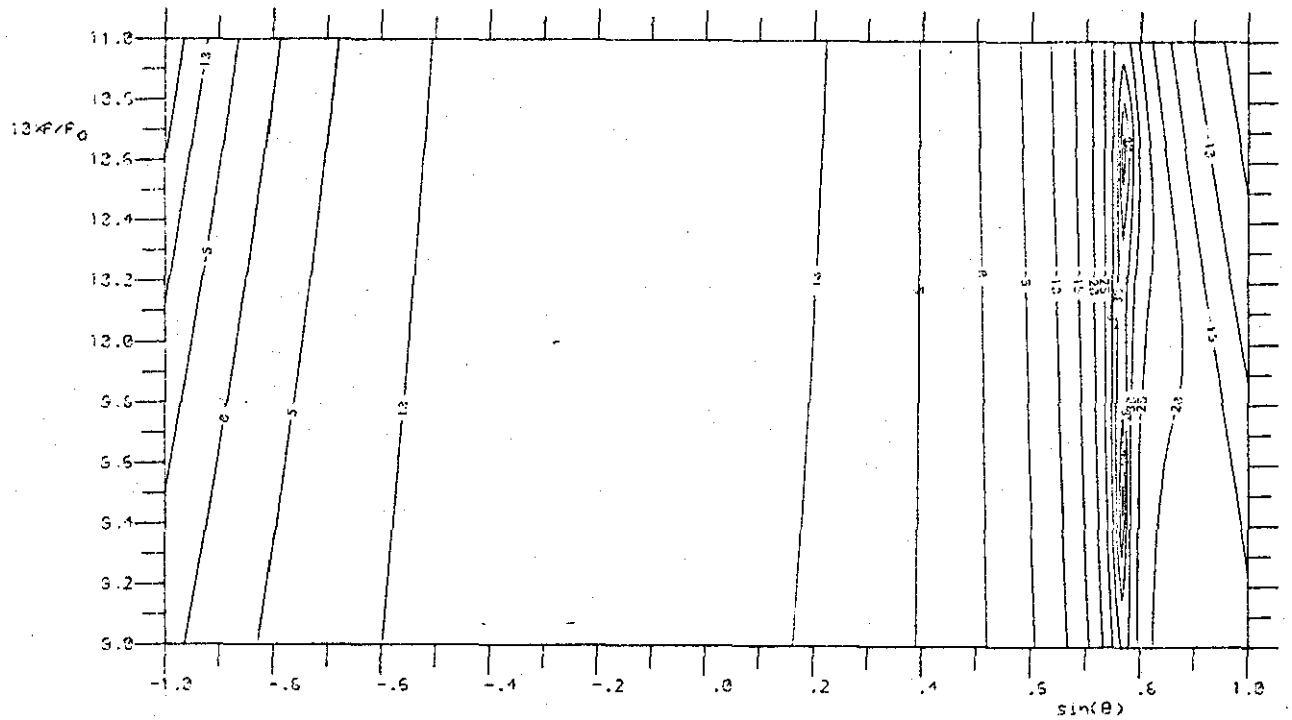

Fig.4.33a Amplitude response in dB

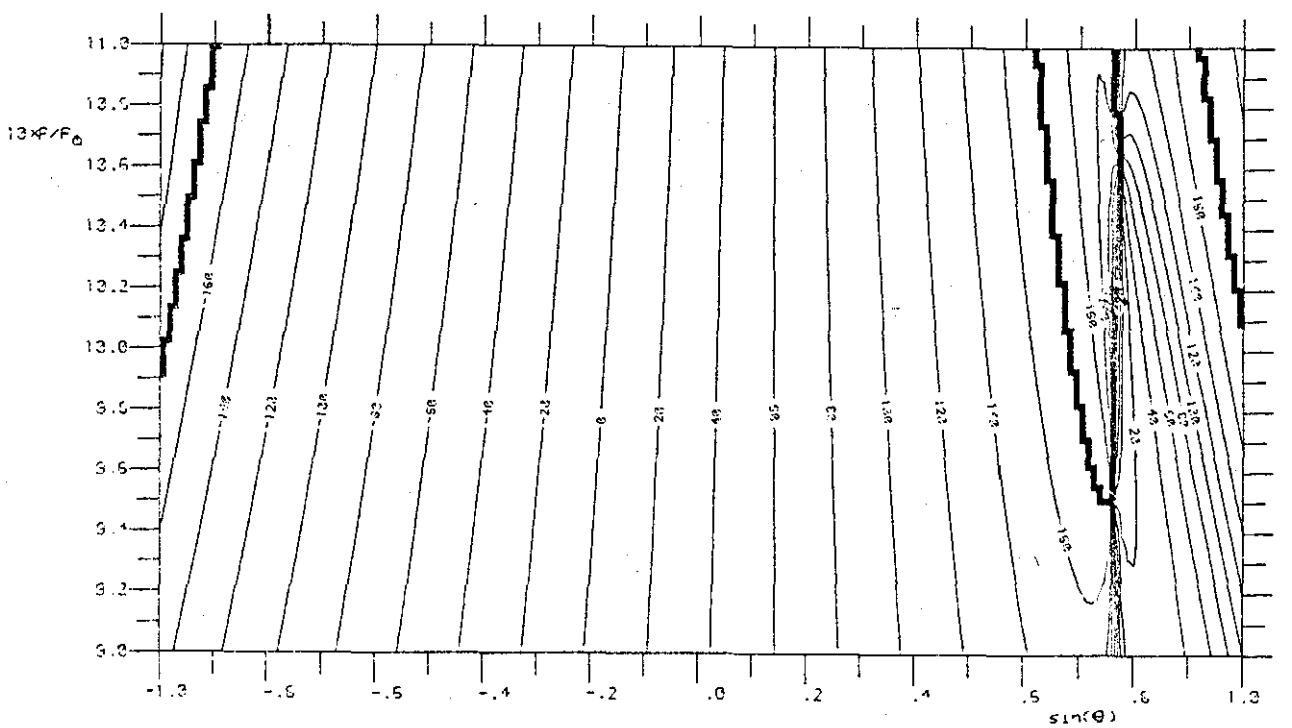

Fig.4.33b Phase response in degree

Fig.4.33 Array response against frequency and direction for the situation of fig.4.28, except that the ENR is increased to 40dB.

adequate for the increased ENRs. Clearly, as the ENR increases to 30dB, the null which was originally at the upper band edge of fig. 4.28 has shifted to the centre of the band in fig.4.32. Furthermore, the behaviour of the contours near to the null in fig.4.32 indicates that, as may also be expected from the ONR against ENR graph of fig.4.20b, an additional null is about to move into the array frequency band and steer towards the jammer. The formation of this new null obviously leads to the increase of all, especially near-jammer, distortions. As may be expected from fig.4.20b again and demonstrated in fig.4.33, the additional null has formed towards the jammer at the ENR of 40dB. Clearly, although the various distortions are still more severe than that of fig.4.28, they are less severe than that of fig.4.32, because the additional null has been formed. Note that the apparent solid zig-zag phase contours, which should be smooth curves, in figs.4.32b and 4.33b are due to the failure of the contouring subroutine mentioned earlier. Finally, with all these observations also confirmed by other simulation results, it is evident that even though the jamming rejection capability may still be adequate in situations where the ENR exceeds the MENR, the various, especially near-jammer, distortions due to the formation of extra, in addition to the usual J/2 per jammer, nulls necessary to reject some of the jammers may be very severe.

Summarizing, this section has briefly and qualitatively investigated, using simulation results, the frequency distortion introduced by rejecting the jammers. In situations expected to be anticipated where the ENR is less than the MENR, two significant distortions are generally observed. The first is the background phase distortion which, in degree, is of the order of percentage bandwidth across the entire band at almost every direction. The

second is the grating amplitude distortion which can seriously impair the reception capability near endfire directions unless the element spacing is reduced to about (1-B) of half a wavelength at the centre frequency. These distortions obviously become more serious as the bandwidth increases and are roughly independent of the other parameters. One exception, however, is with the 2-tap array for which these distortions are less severe whereas the near-jammer distortions can be very serious should they be employed in large bandwidth applications. In situations not envisaged where the ENR is greater than the MENR, the various, especially near-jammer, distortions due to the formation of extra, in addition to the usual J/2 per jammer, nulls to reject some of the jammers may be very severe even though the performance in terms of jamming rejection is still adequate.

4.9 Conclusion

The jamming rejection capability, as given by the Jammer Gain of (4.1), of the broadband tapped delay line power inversion array has been investigated as a function of the various parameters in this chapter. Theoretically, the JG was derived to be proportional to the 2Vth power of bandwidth for small bandwidth. V is normally equal to the largest integer not greater than the number of even degrees of freedom available per jammer, though it may take smaller value if the number of elements is large compared with the number of jammers and there are jammers arriving from certain directions relating to the number of taps, tap and element spacings. These special situations do not arise when the tapped delay line structure is modified, for example, by using tapped delay lines with unequal tap spacings. Though not discussed, such modifications are essential for better performance in these situations. Since the

minimum value for V, corresponding to all the spatial degrees of freedom being fully utilized, are (number of taps)/2 and (number of taps - 1)/2 for even- and odd-tap arrays respectively, the odd-tap array is relatively inefficient in such situations of worse performance. Using computer simulation, the JG bandwidth power law is proved for bandwidth up to tens of percents, hence verifying the theoretical deductions made. Additionally, it has been found that the optimal tap spacing for best average performance is such that the length of the delay line roughly equals half a wavelength delay at the centre frequency. Furthermore, the Maximum Jammer Gain, giving the worst performance, was found to be given by (4.56). For adequate performance in all environments with element to receiver noise power ratio below a certain designed MENR value, this equation was used to determine the number of taps required ((4.58) and fig.4.21) for a specific bandwidth as well as to assess, in terms of the number of weights required, the relative advantage ((4.61) and fig.4.22) of employing tapped delay line processing as compared with employing the alternative broadband processing method which uses several narrowband array processors in parallel. The use of tapped delay line processing was found to be more efficient for large bandwidth and MENR. The frequency distortion introduced at various directions due to rejecting the jammers was then studied qualitatively by examining simulation results. In situations expected to be anticipated where the ENR is less than the designed M ENR value, two significant distortions are generally observed. The first is the background phase distortion which, in degree, is of the order of percentage bandwidth across the entire band at almost every direction. The second is the grating amplitude distortion which can seriously impair the reception capability near end-

fire directions unless the element spacing is reduced to about (1 - bandwidth) of half a wavelength at the centre frequency. These distortions become more serious as the bandwidth increases and are roughly independent of the other parameters. One exception, however, is with the 2-tap array for which these distortions are less severe though the near-jammer distortions can be very serious should they be employed in large bandwidth applications. In situations not envisaged where the ENR is greater than the MENR, the various, especially near-jammer, distortions due to the formation of extra nulls to reject the jammers may be very severe even though the performance in terms of jamming rejection is still adequate.

CHAPTER 5 THE CONVERGENCE BEHAVIOUR OF THE BROADBAND FROST TAPPED DELAY LINE POWER INVERSION ARRAY AND SIMPLE PREPROCESSOR FOR FASTER CONVERGENCE

5.1 Introduction

The last chapter has discussed the jamming rejection capability of the broadband tapped delay line[15] power inversion[28,29] array. Briefly, the use of tapped delay line processing on the array has been found to be more efficient, in terms of the number of weights required, than employing the alternative broadband processing using several narrowband array processors in parallel, especially if the bandwidth and the designed maximum element to receiver noise power ratio (MENR) are large. However, it is evident that in adaptive array processing, apart from the best performance obtainable as measured by the jamming rejection capability, the convergence behaviour of the array towards the optimal performance is also of much interest. The convergence behaviour depends, of course, on the particular algorithm employed.

In this chapter, the convergence behaviour of the tapped delay line power inversion array employing the well known stochastic gradient descent algorithm will be investigated in stationary environments both theoretically for small bandwidth and using simulation results. For convenience, since using this algorithm on the array concerned corresponds to a special case in Frost's formulation[23], the resulting adaptive array will be referred to as the Frost system. Comparison of convergence behaviour with that obtained from using the same algorithm on the power inversion array employing the alternative broadband processing, to be referred to as the alternative system for convenience, will also be given in terms of the lower bound on the convergence time constants. Cons-

equently and most importantly, a simple transformation preprocessor, independent of the external noise environment, for use with tapped delay line processing will be derived and shown, theoretically and using simulation results, to improve the convergence behaviour of the Frost system considerably in broadband jamming situations. Note that although only the stochastic gradient descent algorithm is used, the deductions in this chapter will mostly be based on analyzing the eigenvalues of the covariance matrix. The deductions and derivations are therefore easily extended to many other, especially closed-loop, algorithms as well as to other similar tapped delay line signal processing systems.

This chapter is organized as follows. Section 5.2 gives a preliminary discussion of the convergence behaviour, the various assumptions made and the alternative system. As in the last chapter, by expanding the autocorrelation functions of all the power density spectrums in power series of bandwidth, section 5.3 decomposes the covariance matrix into forms suitable for subsequent analysis. Using these decompositions, the eigenvalues and eigenvectors of the covariance matrix are analyzed theoretically for small bandwidth in section 5.4. The eigenvalues, which are the parameters of most importance as they determine the time constants of the Frost system, are then studied by using simulation results in section 5.5 to verify the theoretical deductions and to provide more insight. Also investigated briefly in section 5.5, from simulation results, are the eigenvector power components which are defined in section 5.2 and are the other parameters of importance in determining the convergence behaviour of the Frost system. From the theoretical analysis of section 5.3, the preprocessor mentioned is derived and its effects on convergence behaviour analyzed for small

bandwidth theoretically in section 5.6. The eigenvalues and eigenvector power components resulting from using the preprocessor are then studied by using simulation results in section 5.7 to verify the theoretical deductions and to gain more insight. Comparisons with the alternative system are given in sections 5.4 and 5.6. Conclusions are drawn in section 5.8.

5.2 Preliminary Discussion

Before the more detailed analysis and discussion of later sections, this section will first formulate the convergence behaviour of the Frost system as well as discuss the alternative system. In the process, the main assumptions, notations and terminologies used will be introduced.

5.2.1 Frost system

Firstly, the convergence behaviour of the Frost system will be formulated in this subsection. The broadband tapped delay line power inversion array of interest is that shown in fig.4.1 and discussed in the last chapter. However, because of the inefficiency of odd-tap array in situations of worse performance as discussed in the last chapter, this chapter will be concerned with only the even-tap array.

The basic principle and formulation of the stochastic gradient descent algorithm has been discussed in section 3.2 for the narrowband power inversion array in discrete time and using complex notation. Furthermore, section 3.3 has derived the characteristics of the narrowband array in stationary environments using this formulation. The derivations in these two sections are of course directly applicable to the Frost system of interest here. Nevertheless, for completeness, the essense of the analysis will now be

applied to the Frost system, leading to a formulation of its convergence behaviour.

Defining the weight and input vectors as

$$W(k) = [w_1(k)\ w_2(k)\ \cdots\ w_{(M-1)J}(k)]^T \tag{5.1}$$

and

$$X(k) = [x_1(k)\ x_2(k)\ \cdots\ x_{(M-1)J}(k)]^T \tag{5.2}$$

respectively, where k specifies the kth sampling instant and T denotes transpose, the updating of the weights in the Frost system due to the stochastic gradient descent algorithm to minimize output power can be described, corresponding to (3.9), by

$$W(k+1) = W(k) - \alpha y(k)X(k) \tag{5.3}$$

where α is the feedback factor of the algorithm and y(k), given by

$$y(k) = x_0(k) + W(k)^T X(k), \tag{5.4}$$

is the array output. With the same analysis as in sections 3.2 and 3.3, the average convergence behaviour of the weight vector in stationary environments is, corresponding to (3.27), then described by

$$\overline{W(k)} = W_{opt} + (I - \alpha R)^k [W(0) - W_{opt}] \tag{5.5}$$

where the overbar denotes ensemble average, W_{opt}, given by

$$W_{opt} = -R^{-1}R_0, \tag{5.6}$$

is the optimal weight vector to which the average weight vector eventually converges and the covariance matrix and vector, R and R_0 respectively, are given by

$$R = \overline{X(k)X(k)^T} \tag{5.7}$$

and

$$R_0 = \overline{x_0(k)X(k)}. \tag{5.8}$$

Using the polar decomposition

$$R = \sum_{m=1}^{(M-1)J} h_m H_m H_m^T \tag{5.9}$$

where h_m, $m=1,\cdots,(M-1)J$, is the mth largest eigenvalue with H_m as the corresponding normalized eigenvector, the convergence behaviour of the ensemble average weight vector as given by (5.5) becomes

$$\overline{W(k)} = W_{opt} + \sum_{m=1}^{(M-1)J} (1 - \alpha h_m)^k e_m H_m \tag{5.10}$$

where

$$e_m = H_m^T[W(0) - W_{opt}] \tag{5.11}$$

is the component of the initial weight vector lag, $W(0)-W_{opt}$, in the direction of H_m.

As discussed in sections 3.2 and 3.3, the ensemble average output power s(k), given by $\overline{y(k)^2}$ here, consists of two components: $s_y(k)$, referred to as the output power, due to the average behaviour of the weights plus $s_{wt}(k)$, referred to as the weight variance noise, due to the variances of the weights about the average values. Mathematically, the output power in this chapter is

$$s_y(k) = s_x + 2R_0^T\overline{W(k)} + \overline{W(k)}^T R \overline{W(k)} \tag{5.12}$$

where s_x is the element power, while the weight variance noise is

$$s_{wt}(k) = \overline{[W(k) - \overline{W(k)}]^T R [W(k) - \overline{W(k)}]}. \tag{5.13}$$

Using (5.6), (5.9) and (5.10), the output power converges according to

$$s_y(k) = s_{opt} + \sum_{m=1}^{(M-1)J} h_m e_m^2 (1 - \alpha h_m)^{2k} \tag{5.14}$$

where

$$s_{opt} = s_x - W_{opt}^T R W_{opt} \qquad (5.15)$$

is the optimal or minimum possible output power to which the output power eventually converges. As mentioned in sections 3.2 and 3.3, the convergence behaviour of the weight variance noise is difficult to analyze but fortunately, since the output power is much greater than the weight variance noise during the transient convergence period, it is not of importance. Specifically, the convergence behaviour of the average output power will be roughly given by (5.14) for the output power with the feedback factor being determined by the desired relative amount of weight variance noise in the steady state as measured by the misadjustment defined by (3.41). Using the same analysis as in sections 3.2 and 3.3, the misadjustment for the Frost system is also roughly equal, for small misadjustment, to

$$M_{wt} \approx \frac{\alpha tr R}{2}. \qquad (5.16)$$

The above two paragraphs have formulated the convergence behaviour of the Frost system in terms of the average weight vector and output power. Specifically, as can be seen from (5.10), the former converges as a sum of exponentially decaying component vectors, the mth vector being initially equal to $e_m H_m$ and converging with a time constant of $-1/\ln(1-\alpha h_m)$ sampling period. Note that for convenience, e_m will be referred to as the mth eigenvector component. More importantly, from (5.14), the output power or roughly, the average output power converges also as a sum of exponentially decaying components, the mth component being initially equal to $h_m e_m^2$, to be referred to as the mth eigenvector power component for convenience, and converging with a time constant τ_m, half that of the corresponding average weight vector component, of

$$\tau_m \approx \frac{-1}{2\ln(1 - \alpha h_m)} \text{ sampling period.} \qquad (5.17)$$

Since the misadjustment and so, from (5.16), αtrR and αh_m will be small, the mth time constant is, using (5.16),

$$\tau_m \approx \frac{trR}{4M_{wt} h_m} \text{ sampling period.} \qquad (5.18)$$

Evidently, since the time constants for the convergence of the weight vector and output power are determined by the eigenvalues, the eigenvalues are the parameters of most importance and will be most thoroughly studied. Note that unless stated otherwise, time constants will henceforth be used to mean those for the convergence of the output power. The next parameters of importance are obviously the eigenvector power components as they also determine the convergence of the output power. However, contrary to the eigenvalues, they depend on the eigenvector components which depend on the initial weight vector and thus are not so "unique". Furthermore, even if similar theoretical analysis for examining the eigenvalues are applied to analyze the eigenvector components, as in [82], no simple and general deductions can be reached. For these reasons, the eigenvector power components will only be briefly investigated in this chapter by using simulation results which show that these can in fact have quite complex behaviour. Since the detailed convergence behaviour of the weight vector is of relatively little interest, the parameters of least interest are the eigenvectors. However, because of their close link with the eigenvalues, they will also be briefly discussed in the theoretical analysis, but will not be examined from simulation results.

Since the eigenvector power components are proportional to the eigenvalues, it is obvious that long time constants are usually

associated with small eigenvector power components. Thus, though some time constants are very long, their associated eigenvector power components may be so small that even if these components do not converge, the increase in output power is negligible. Clearly, in evaluating the convergence behaviour, the time constants and eigenvalues corresponding to insignificant eigenvector power components should not be considered. In this chapter, the level of significance for the eigenvector power components will, for convenience, be taken as the optimal output power. Furthermore, the term "effective time constants" will be used to refer to those with significant eigenvector power components, while the term "final effective time constant" will be used to mean the longest effective time constant. Evidently, as the effective time constants determine the effective convergence rate of the system, they, especially the final effective one, are of most importance. As will be illustrated in some simulation examples later, it is not surprising that in situations of severe broadband jamming where all the degrees of freedom have to be employed to reject the jammers, the smallest eigenvalues usually determine the final effective time constant. Finally, note that also for convenience, the initial weights are taken to be zero for calculating the eigenvector power components of the power inversion array in this chapter.

5.2.2 Alternative system

Having formulated the convergence behaviour of the Frost system, that for the alternative system will now be discussed. As mentioned in sections 4.1 and 4.7, with the alternative broadband processing, each of the element inputs is first bandpass filtered into $J_N/2$ narrowband components. All the element inputs in one

frequency bin are then processed by one narrowband array processor using quadrature weights or with negligible difference, 2-tap delay lines at $1/4f_0$ tap spacing. J_N is therefore the number of weights required per element when the alternative broadband processing is employed. Finally, the outputs from the narrowband processors are combined to give the array output. Note that in practical applications, the outputs from the narrowband processors are most probably not combined but used directly for signal extraction. However, for the purpose of comparing convergence behaviour, the combining of the outputs will be assumed in this chapter so that the array inputs and output in the alternative system are equivalent to those in the Frost system.

For the purpose of comparison, each narrowband processor in the alternative system is taken as employing the stochastic gradient descent algorithm for weight updating. Clearly, the convergence behaviour of the system is a linear combination of that for the narrowband array processors implied in the discussion of the last subsection. Denoting the feedback factor and covariance matrix associated with the mth of the $J_N/2$ narrowband processors by a_m and R_m respectively, the total misadjustment of the system is, using (5.16),

$$M_{wt} \simeq \sum_{m=1}^{J_N/2} \frac{a_m \mathrm{tr} R_m}{2} \qquad (5.19)$$

where, for convenience, the narrowband processors will be taken as using 2-tap delay lines so that R_m is real and has dimension $2(M-1) \cdot 2(M-1)$. Obviously, with receiver noise of s_0 per element, the smallest possible eigenvalue associated with each narrowband covariance matrix is $2s_0/J_N$, the receiver noise per element seen by

each processor. Therefore, the set of time constants, $\{\tau_N\}$, for the convergence of the output power in the alternative system is bounded, using (5.17), by

$$\{\tau_N\} \leq \max_m \left\{ \frac{-1}{2\ln(1 - 2a_m s_0/J_N)} \right\} \text{ sampling period} \qquad (5.20)$$

where $\max_z\{f(z)\}$ denotes the maximum value of the function $f(z)$ with respect to z. Evidently, for a certain designed misadjustment of (5.19), this bound is minimized if and only if all the feedback factors are equal to say, a. (5.19) is then given by

$$M_{wt} \approx \frac{a}{2} \sum_{m=1}^{J_N/2} \text{tr}R_m = a(M-1)s_x \qquad (5.21)$$

and because the misadjustment, and so as_x and as_0, will be small, (5.20) becomes

$$\{\tau_N\} \leq B_N \qquad (5.22)$$

where

$$B_N \approx \frac{ENR(M-1)J_N}{4M_{wt}} \text{ sampling period} \qquad (5.23)$$

and ENR is the element to receiver noise power ratio. Of course, using the same feedback factor for all the processors does not imply best convergence behaviour in all situations. For instance, if all the jammers are narrowband, faster convergence can result when all the feedback factors corresponding to processors with only receiver noise are zero so that the feedback factors associated with the other processors can be increased, keeping the misadjustment constant. However, in situations where the smallest eigenvalues with significant eigenvector power components in the narrowband processors are roughly equal, using the same feedback factor clearly leads to the minimum final effective time constant and for

simplicity, will be taken to be so in this chapter. Note that since the external environment is not known a priori or measured in any detail, the feedback factor have to be chosen from some ad hoc principles in any case. Finally, it is obvious that the bound B_N is loosely approached when with respect to some of the narrowband processors, some jammers are close together or have very different powers so that the smallest eigenvalues with significant eigenvector power components are not very much greater than that due to only receiver noise.

Summarizing, this section has formulated the convergence behaviour of the Frost system in terms of the eigenvalues, eigenvectors, eigenvector and eigenvector power components. Particularly, the output power converges as a sum of exponentially decaying components, with initial magnitudes given by the eigenvector power components and convergence time constants by and inversely proportional to the eigenvalues. Being a linear combination of that for several 2-tap narrowband Frost systems at different frequency bins, the convergence behaviour of the alternative system has also been discussed, leading to the lower bound of (5.23) for the convergence time constants of the system.

5.3 Decomposition of the Covariance Matrix

From the discussion of the last section, the convergence behaviour of the Frost system can be obtained by investigating the eigenvalues, eigenvectors and eigenvector power components. However, before studying the eigenvalues and eigenvectors theoretically in the next section, this section will first decompose the covariance matrix into forms suitable for subsequent analysis. As in the last chapter, the derivations will be based on expressing the aut-

ocorrelation functions of all the power density spectrums in power series of bandwidth.

In subsection 4.2.1, the autocorrelation function for the power density spectrum of the nth of the N jammers has been derived as a power series given by (4.6) and (4.7). The derivation is of course also applicable to the receiver noise power density spectrum. Therefore, for consistency in notation, the index n in these two equations for the autocorrelation functions will range from 0 to N in this chapter, with n=0 being associated with receiver noise and n=1,··,N with the nth jammer:

$$R_n(t) = s_n \sum_{p=0}^{\infty} M_{pn} \frac{(\pi B f_0 t)^p}{p!} \cos(2\pi f_0 t + \frac{\pi p}{2}), \quad n=0,\cdot\cdot,N, \tag{5.24}$$

where

$$M_{pn} = \int_{-1}^{1} S_{0n}(f) f^p df, \quad p=0,\cdot\cdot,\infty, \tag{5.25}$$

and $S_{0n}(f)$ is the spectrum giving the shape of the corresponding power density spectrum.

The derivation of (5.24) clearly indicates that the covariance matrix can also be expressed as a power series of bandwidth:

$$R = \sum_{p=0}^{\infty} \sum_{n=0}^{N} R_{pn} B^p \tag{5.26}$$

where R_{pn} is due to the autocorrelation function $R_n(t)$ and associated with the pth power of bandwidth. Having derived R_{pn} as a function of the various parameters by using (5.24), appendix 5.9.1 shows, after some further manipulation, that the (M-1)J·(M-1)J covariance matrix can be expressed as

$$R = \sum_{g,h=0}^{J/2-1} B^{g+h} U_g R^0_{gh} U_h^T \tag{5.27}$$

where R_{gh}^{0}, g,h=0,··,J/2-1, of dimension 2(M-1)·2(M-1), and U_g, of demension (M-1)J·2(M-1), are given as follows. Defining the matrix $\hat{P}_g$, of demension J·2, as

$$\hat{P}_g = \begin{bmatrix} (f_0\tau)^g\cos(2\pi f_0\tau + \frac{g\pi}{2}) & -(f_0\tau)^g\sin(2\pi f_0\tau + \frac{g\pi}{2}) \\ (2f_0\tau)^g\cos(4\pi f_0\tau + \frac{g\pi}{2}) & -(2f_0\tau)^g\sin(4\pi f_0\tau + \frac{g\pi}{2}) \\ \vdots & \vdots \\ (Jf_0\tau)^g\cos(2J\pi f_0\tau + \frac{g\pi}{2}) & -(Jf_0\tau)^g\sin(2J\pi f_0\tau + \frac{g\pi}{2}) \end{bmatrix}, \quad (5.28)$$

J/2 mutually orthogonal matrices, of deminsions J·2 and which together span the whole J dimensional vector space, can be obtained by using the Gram-Schmidt orthogonalization process:

$$\hat{U}_g = \begin{cases} \hat{P}_0, & g=0 \\ \prod_{h=1}^{g} [I - \hat{U}_{h-1}(\hat{U}_{h-1}^T\hat{U}_{h-1})^{-1}\hat{U}_{h-1}^T]\hat{P}_g, & g=1,\cdot\cdot,\frac{J}{2}-1 \end{cases} \quad (5.29)$$

Note that in this chapter, the vector space or subspace spanned by a matrix refers to that spanned by the columns of the matrix. Furthermore, as used above, two matrices will be referred to as mutually orthogonal if the subspace of one is orthogonal to that of the other matrix. With (5.28) and (5.29) giving $\hat{U}_g$, U_g is

$$U_g = \begin{bmatrix} \hat{U}_g & & 0 \\ & \hat{U}_g & \\ & & \ddots \\ 0 & & \hat{U}_g \end{bmatrix}, \quad g=0,\cdot\cdot,\frac{J}{2}-1. \quad (5.30)$$

Clearly, U_0, U_1, ·· and $U_{J/2-1}$ are mutually orthogonal and depend only on the tap spacing and number of taps. On the other hand, defining Q_n as

$$Q_n = \begin{cases} I, & n=0 \\ \begin{bmatrix} \cos\Phi_n & -\sin\Phi_n \\ \sin\Phi_n & \cos\Phi_n \\ \cos 2\Phi_n & -\sin 2\Phi_n \\ \sin 2\Phi_n & \cos 2\Phi_n \\ \vdots & \vdots \\ \cos(M-1)\Phi_n & -\sin(M-1)\Phi_n \\ \sin(M-1)\Phi_n & \cos(M-1)\Phi_n \end{bmatrix}, & n=1,\cdots,N \end{cases} \tag{5.31}$$

where

$$\Phi_n = \frac{2\pi f_0 d \sin\theta_n}{c} \tag{5.32}$$

and c is the wave velocity, R^0_{gh} is given, after neglecting all higher order terms proportional to the first or higher powers of bandwidth, by

$$R^0_{gh} = \sum_{n=0}^{N} s_n M^0_{ghn} Q_n Q_n^T \tag{5.33}$$

where as (4.17) of chapter 4, M^0_{ghn} is

$$M^0_{ghn} = \frac{\pi^{g+h}}{g!h!} M_{g+h\ n} = \frac{\pi^{g+h}}{g!h!} \int_{-1}^{1} S_{0n}(f) f^{g+h} df. \tag{5.34}$$

Obviously, in contrast to U_g, R^0_{gh} as given depends on the environment and is independent of the array parameters of bandwidth, tap spacing and number of taps. Specifically, it is symmetrical and is the covariance matrix for an ideal narrowband array in the same environment except with the power s_n multiplied by the factor M^0_{ghn}. As used in this chapter, an ideal narrowband array means a 2-tap, $1/4f_0$ tap spacing array with zero bandwidth. Also shown in appendix 5.9.1, R^0_{gh} satisfies, exactly,

$$R^0_{gh} = R^{0\ T}_{hg}. \tag{5.35}$$

As described above, (5.27) is interesting because the covariance matrix has been separated essentially into two parts - that

due to the environment and the array. To decompose the covariance matrix into a more useful form, note that (5.27) can be written in matrix form as

$$R = \begin{bmatrix} U_0^T \\ BU_1^T \\ \vdots \\ B^{J/2-1}U_{J/2-1}^T \end{bmatrix}^T \begin{bmatrix} R_{00}^0 & R_{01}^0 & \cdots & R_{0\,J/2-1}^0 \\ R_{10}^0 & R_{11}^0 & & \\ \vdots & & & \\ R_{J/2-1\,0}^0 & & & \end{bmatrix} \begin{bmatrix} U_0^T \\ BU_1^T \\ \vdots \\ B^{J/2-1}U_{J/2-1}^T \end{bmatrix}. \quad (5.36)$$

From (5.35), the second matrix factor is obviously symmetrical. Furthermore, since the covariance matrix is positive definite and so has full rank even when only receiver noise is present, this matrix factor also has full rank and thus, with similar arguments leading to (4.30) in subsection 4.2.2, can be decomposed as

$$\begin{bmatrix} R_{00}^0 & R_{01}^0 & \cdots & R_{0\,J/2-1}^0 \\ R_{10}^0 & R_{11}^0 & & \\ \vdots & & & \\ R_{J/2-1\,0}^0 & & & \end{bmatrix} = \begin{bmatrix} R_{00}^0 \\ R_{10}^0 \\ \vdots \\ R_{J/2-1\,0}^0 \end{bmatrix} (R_{00}^0)^{-1} \begin{bmatrix} R_{00}^0 \\ R_{10}^0 \\ \vdots \\ R_{J/2-1\,0}^0 \end{bmatrix}^T \quad (5.37)$$

$$+ \begin{bmatrix} 0 \\ R_{11}^1 \\ R_{21}^1 \\ \vdots \\ R_{J/2-1\,1}^1 \end{bmatrix} (R_{11}^1)^{-1} \begin{bmatrix} 0 \\ R_{11}^1 \\ R_{21}^1 \\ \vdots \\ R_{J/2-1\,1}^1 \end{bmatrix}^T + \cdots$$

$$+ \begin{bmatrix} 0 \\ 0 \\ \vdots \\ 0 \\ R_{J/2-1\,J/2-1}^{J/2-1} \end{bmatrix} (R_{J/2-1\,J/2-1}^{J/2-1})^{-1} \begin{bmatrix} 0 \\ 0 \\ \vdots \\ 0 \\ R_{J/2-1\,J/2-1}^{J/2-1} \end{bmatrix}^T$$

where

$$R_{gh}^p = R_{gh}^{p-1} - R_{g\,p-1}^{p-1}(R_{p-1\,p-1}^{p-1})^{-1}R_{h\,p-1}^{p-1\,T}, \quad p=1,\cdots,\frac{J}{2}-1, \quad (5.38)$$

$$g,h=p,\cdots,\frac{J}{2}-1.$$

Note that the full rank of the l.h.s. of (5.37) is essential to guarantee that R^p_{pp}, p=1,··,J/2-1, has full rank and so an inverse. Substituting (5.37) into (5.36) then gives, finally,

$$R = \sum_{p=0}^{J/2-1} B^{2p} V_p (R^p_{pp})^{-1} V_p^T \tag{5.39}$$

where

$$V_p = \sum_{g=p}^{J/2-1} B^{g-p} U_g R^p_{gp}. \tag{5.40}$$

The significance of the decomposition, expressed by (5.39) and (5.40), of the covariance matrix in terms of eigenvalues and eigenvectors will be discussed in the next section.

Summarizing, by using the power series in bandwidth of the autocorrelation functions of (5.24), the covariance matrix has been formulated in the form of (5.26) in appendix 5.9.1. The formulation leads to the elegant expression of (5.27) which is then decomposed to give (5.39).

5.4 Eigenvalues and Eigenvectors from Theoretical Analysis

Having decomposed the covariance matrix into elegant forms in the last section, this section will investigate theoretically for small bandwidth the implication of the decomposition on the eigenvalues and eigenvectors. In the process, the lower bound on the convergence time constants of the Frost system will be obtained and compared with (5.21) of the alternative system. Note that since the eigenvectors are not of much importance, the analysis will be baised towards the eigenvalues. In particular, only the eigenvalues will be addressed in the important theroems to be derived.

5.4.1 General structure

Firstly, this subsection will discuss the general structure

of the eigenvalues and eigenvectors. The decomposition expressed by (5.39) is elegant and interesting because the covariance matrix is decomposed as a sum of J/2 matrices, each having rank 2(M-1) equal to the dimension of R_{pp}^{p}, p=0,··,J/2-1, and with the covariance matrix being positive definite, being positive semi-definite. Furthermore, from (5.40) with U_0, U_1, ·· and $U_{J/2-1}$ being mutually orthogonal, the matrix product $V_p{}^T V_q$, p≠q, p,q=0,··,J/2-1, is proportional to at least B even though the multiplying matrices are proportional to only B^0. Therefore, for small bandwidth, V_0, V_1, ·· and $V_{J/2-1}$ will also become mutually orthogonal. Evidently, for the purpose of determining the eigenvalues and eigenvectors in a first order approximation, terms proportional to the first and higher powers of bandwidth in (5.40) for V_p can be neglected so that (5.39) becomes

$$R \approx \sum_{p=0}^{J/2-1} B^{2p} U_p R_{pp}^{p} U_p{}^T. \tag{5.41}$$

With R_{pp}^{p}, given in terms of (5.33) and (5.38), being roughly independent of bandwidth, the general structure of the eigenvalues implied by this equation can then be summarized by

The eigenvalues of the covariance matrix can be divided into J/2 sets. The 2(M-1) eigenvalues in the ith set are given by the nonzero eigenvalues of $B^{2(i-1)} U_{i-1} R_{i-1}^{i-1} {}_{i-1} U_{i-1}{}^T$ and are thus proportional to $B^{2(i-1)}$. (5.42a)

The associated eigenvectors in the ith set are obviously given by the corresponding eigenvectors of $U_{i-1} R_{i-1}^{i-1} {}_{i-1} U_{i-1}{}^T$ and thus together span the same subspace as that spanned by U_{i-1}. Since the spectrum $S_{On}(f)$, n=0,··,N, is normalized to have area 1 and so M_{00n}^{0}, given by (5.34), equals 1, (5.42a) can be supplemented by

The first set of eigenvalues, as determined by U_0 $(\sum_{n=0}^{N} s_n Q_n Q_n^T) U_0^T$, is independent of the jammers' spectrums and is the same as that should all the noise processes be ideally narrowband, that is, have zero bandwidth. (5.42b)

This is clearly also true for the first set of eigenvectors.

5.4.2 At $1/4f_0$ tap spacing

Having deduced the general structure of the eigenvalues and eigenvectors, this subsection will discuss in more detail the case when the tap spacing is $1/4f_0$. This tap spacing is of most interest because, as may be expected intuitively and demonstrated later, it is associated with the spread of eigenvalues being a minimum and so better convergence behaviour of the Frost system. Furthermore, the preprocessor to be discussed in section 5.6 is particularly simple and easy to implement at this tap spacing.

Before applying the particular condition of $1/4f_0$ tap spacing, however, the eigenvalues and eigenvectors of R_{gh}^p, p=0,··,J/2-1, g,h=p,··,J/2-1, will first be discussed. As mentioned in section 5.3, R_{gh}^0 has the form of the covariance matrix for an ideal narrowband array. Thus, as shown in appendix 5.9.2, it is not surprising that the polar decomposition of R_{gh}^p, given by (5.33) and (5.38), can in general be expressed as

$$R_{gh}^p \simeq s_0 M_{gh0}^p E E^T + \sum_{n=1}^{N} c_{ghn}^p C_{ghn}^p C_{ghn}^{pT} \qquad (5.43)$$

which also has the same form as that for the covariance matrix of an ideal narrowband array. Specifically, there are N+1 distinct eigenvalues, c_{gh1}^p, c_{gh2}^p, ··, c_{ghN}^p and $s_0 M_{gh0}^p$, whose associated eigenvectors are given by the columns of C_{gh1}^p, C_{gh2}^p, ··, C_{ghN}^p and E respectively. The first N eigenvalues, each having multiplicity

2, are due to the jammers and reciever noise. Their associated eigenvectors together span the same subspace as that spanned together by Q_1, Q_2, $\cdot\cdot$ and Q_N. The last eigenvalue, due only to receiver noise, has 2(M-N-1) associated eigenvectors which, spanning the complimentary subspace, are independent of p, g and h. Note that M^0_{ghO} is given by (5.34), while as (4.31), M^p_{ghO}, p=1,$\cdot\cdot$,J/2-1, is obtained from M^0_{ghO} by

$$M^p_{ghO} = M^{p-1}_{ghO} - \frac{M^{p-1}_{g\ p-1\ 0} M^{p-1}_{h\ p-1\ 0}}{M^{p-1}_{p-1\ p-1\ 0}}, \quad g,h=p,\cdot\cdot,\frac{J}{2}-1. \tag{5.44}$$

Consider now the relationship between the eigenvalues and eigenvectors of R^p_{pp}, p=0,$\cdot\cdot$,J/2-1, with those of $U_p R^p_{pp} U_p^T$. Clearly, there is no simple relationship unless, with u_p^2 representing a positive scalar constant,

$$U_p^T U_p = u_p^2 I \tag{5.45}$$

so that when z is an eigenvalue of R^p_{pp} with Z as the associated normalized eigenvector, $U_p Z/u_p$ will be a normalized eigenvector of $U_p R^p_{pp} U_p^T$ corresponding to an eigenvalue $u_p^2 z$. Therefore, if (5.45) is valid, the polar decomposition of the covariance matrix can be written, from (5.41) and (5.43), as

$$R \propto \sum_{p=0}^{J/2-1} [s_0 u_p^2 B^{2p} M^p_{ppO} (\frac{U_p E}{u_p})(\frac{U_p E}{u_p})^T + \sum_{n=1}^{N} u_p^2 B^{2p} c^p_{ppn} (\frac{U_p C^p_{ppn}}{u_p})(\frac{U_p C^p_{ppn}}{u_p})^T] \tag{5.46}$$

where the columns of the matrices within the curved brackets give the normalized eigenvectors. As may be expected intuitively, it will be demonstrated later in subsection 5.4.4 that over the tap spacing of interest, (5.45) and so (5.46) are valid at only $1/4f_0$

tap spacing. Thus, the structure of the eigenvalues can be summarized, in addition to (5.42), by

At $1/4f_0$ tap spacing. each set of eigenvalues has structure very similar to that for an ideal narrowband array. Specifically, there are N+1 distinct eigenvalues in the ith set. The largest N distinct eigenvalues, each of multiplicity 2, are due to the jammers and receiver noise. The smallest eigenvalue, of value $s_0 M_{i-1}^{i-1}{}_{i-1\ i-1}\ {}^0u_{i-1}\ {}^2{}_B{}^{2(i-1)}$, has multiplicity 2(M-N-1) and is due to only receiver noise. (5.47a)

Note that the smallest distinct eigenvalue is due to only receiver noise because the presence of the jammers can only lead to the eigenvalues having larger values. As can be seen from (5.46), the eigenvectors in the ith set also have structure very similar to that for an ideal narrowband array. As (5.42a), (5.47a) can be supplemented, from (5.42b) and (5.45), by

At $1/4f_0$ tap spacing, the first set of eigenvalues are given by that of $\sum_{n=0}^{N} s_n Q_n Q_n^T$, the covariance matrix for an ideal narrowband array in the same environment, multiplied by u_0^2. (5.47b)

Obviously, pre-multiplying the eigenvectors of $\sum_{n=0}^{N} s_n Q_n Q_n^T$ by U_0/u_0 also gives the corresponding eigenvectors in the first set.

5.4.3 When all the jammers' spectrums are flat and the tap spacing is $1/4f_0$

As discussed in section 4.3, the case when the jammers have flat spectrums is physically of most significance and interest and will now be treated. When all the jammers have the same spectrum as receiver noise, R_{gh}^0, g,h=0,··,J/2-1, becomes, from (5.33),

$$R_{gh}^0 = M_{ghO}^0 \sum_{n=0}^{N} s_n Q_n Q_n^T. \tag{5.48}$$

Substituting into (5.38), R^1_{gh}, g,h=1,··,J/2-1, is thus

$$R^1_{gh} = (M^0_{ghO} - \frac{M^0_{gOO}M^0_{hOO}}{M^0_{OOO}}) \sum_{n=0}^{N} s_n Q_n Q_n^T = M^1_{ghO} \sum_{n=0}^{N} s_n Q_n Q_n^T \qquad (5.49)$$

where M^1_{ghO} can be obtained from (5.44). Substituting into (5.38) again and so on therefore yields

$$R^p_{gh} = M^p_{ghO} \sum_{n=0}^{N} s_n Q_n Q_n^T, \quad p=0,\cdot\cdot,\frac{J}{2}-1, \quad g,h=p,\cdot\cdot,\frac{J}{2}-1, \qquad (5.50)$$

where M^p_{ghO} is given by (5.34) and (5.44). (5.41) then becomes

$$R = \sum_{p=0}^{J/2-1} M^p_{ppO} B^{2p} U_p \Big(\sum_{n=0}^{N} s_n Q_n Q_n^T \Big) U_p^T. \qquad (5.51)$$

Again, except (5.42), no simple deduction can be made regarding the eigenvalues and eigenvectors of the covariance matrix from this equation unless the tap spacing is $1/4f_0$ and (5.45) is valid so that (5.47) can be further supplemented by

If, in addition to $1/4f_0$ tap spacing, all the jammers also have flat spectrums, the similarity in structure between the ith set of eigenvalues and that for an ideal narrowband array is even more prominent. Specifically, the ith set of eigenvalues is equal to that of $\sum_{n=0}^{N} s_n Q_n Q_n^T$, the covariance matrix for an ideal narrowband array in the same environment, multiplied by $u_{i-1}{}^2 M^{i-1}_{i-1\ i-1\ O} B^{2(i-1)}$. (5.52)

Clearly, pre-multiplying the eigenvectors of $\sum_{n=0}^{N} s_n Q_n Q_n^T$ by U_{i-1}/u_{i-1} also gives the corresponding eigenvectors in the ith set.

5.4.4 When only receiver noise is present

Having discussed the eigenvalues and eigenvectors of the covariance matrix in general and in the specific situations of most interest, the case when only receiver noise is present will now be considered. This trivial case is of importance because it leads

to the derivation of the lower bound on the convergence time constants of the Frost system. Comparison with the corresponding bound of (5.23) for the alternative system can then be made.

With only receiver noise present, (5.51) becomes

$$R \simeq \sum_{p=0}^{J/2-1} s_0 M_{pp0} B^{2p} U_p U_p^T. \tag{5.53}$$

Note that the nonzero eigenvalues of $U_p U_p^T$, $p=0,\cdots,J/2-1$, are equal to those of $U_p^T U_p$ which, from (5.30), is

$$U_p^T U_p = \begin{bmatrix} \hat{U}_p^T \hat{U}_p & & & 0 \\ & \hat{U}_p^T \hat{U}_p & & \\ & & \ddots & \\ 0 & & & \hat{U}_p^T \hat{U}_p \end{bmatrix}. \tag{5.54}$$

Clearly, with (5.28) and (5.29) giving $\hat{U}_p$, $U_p^T U_p$ has only two distinct eigenvalues equal to that of the 2·2 matrix $\hat{U}_p^T \hat{U}_p$. Thus, from (5.53), it can be deduced that

When only receiver noise is present, there are only two distinct eigenvalues in the ith set of eigenvalues. They equal $s_0 u_{1\ i-1} M_{i-1\ i-1\ 0}^{i-1} B^{2(i-1)}$ and $s_0 u_{2\ i-1} M_{i-1\ i-1\ 0}^{i-1} B^{2(i-1)}$ where u_{1p} and u_{2p} are the large and small eigenvalues of $\hat{U}_p^T \hat{U}_p$ respectively. (5.55)

Obviously, since the presence of the jammers can only lead to larger eigenvalues, the eigenvalues in the ith set cannot be smaller than $s_0 u_{2\ i-1} M_{i-1\ i-1\ 0}^{i-1} B^{2(i-1)}$. Therefore, the set of convergence time constants, $\{\tau_F\}$, for the Frost system is bound, using (5.18), by

$$\{\tau_F\} \leq B_F \tag{5.56}$$

where

$$B_F \simeq \frac{\mathrm{tr}R}{4 s_0 u_{2\ J/2-1} M_{wt} B^{J-2} M_{J/2-1\ J/2-1\ 0}^{J/2-1}}$$

$$= \frac{ENR(M-1)J}{4u_{2\,J/2-1}M_{wt}B^{J-2}M^{J/2-1}_{J/2-1\,J/2-1\,0}} \text{ sampling period.} \qquad (5.57)$$

From (5.42) and the polar decomposition of (5.43), it is obvious that only two degrees of freedom in each set of eigenvalues can be associated with the rejection of the same jammer. Clearly, unless at least one of the jammers is so broadband that J degrees of freedom, the maximum designed for each jammer, are required for its rejection and thus at least one eigenvalue in each, including the last, set has significant eigenvector power component, the bound B_F will not be approached by the final effective time constant. Of course, even if the jamming is broadband, the smallest eigenvalue in the last set with significant eigenvector power component may still be considerably larger than the smallest possible eigenvalue and the bound still not closely approached. These arguments illustrate that the bound B_F is only very loosely approached in a few broadband jamming situations.

Fig.5.1 shows graphs of $u_{1p}M^p_{ppO}$ and $u_{2p}M^p_{ppO}$ against tap spacing for arrays with 2-8 taps. Evidently, at $1/4f_0$ tap spacing, the separation between the curves is at a minimum. This of course indicates that the spread of eigenvalues at this tap spacing is also at a minimum as mentioned in subsection 5.4.2. Also, note that only at this tap spacing, $u_{1p}M^p_{ppO}$ is equal to $u_{2p}M^p_{ppO}$. This implies that the 2·2 matrix $\hat{U}_p{}^T\hat{U}_p$ has only one distinct eigenvalue and hence equal to $u_{1p}I$ or $u_{2p}I$, indicating that at only $1/4f_0$ tap spacing with $u_p{}^2$ given by u_{1p} or u_{2p}, (5.45) is valid as mentioned in subsection 5.4.2. Obviously, the curves associated with $u_{2\,J/2-1}M^{J/2-1}_{J/2-1\,J/2-1\,0}$, on which the bound B_F depends, are the most important and can be seen to decrease with increasing slope as the tap spacing deviates from $1/4f_0$.

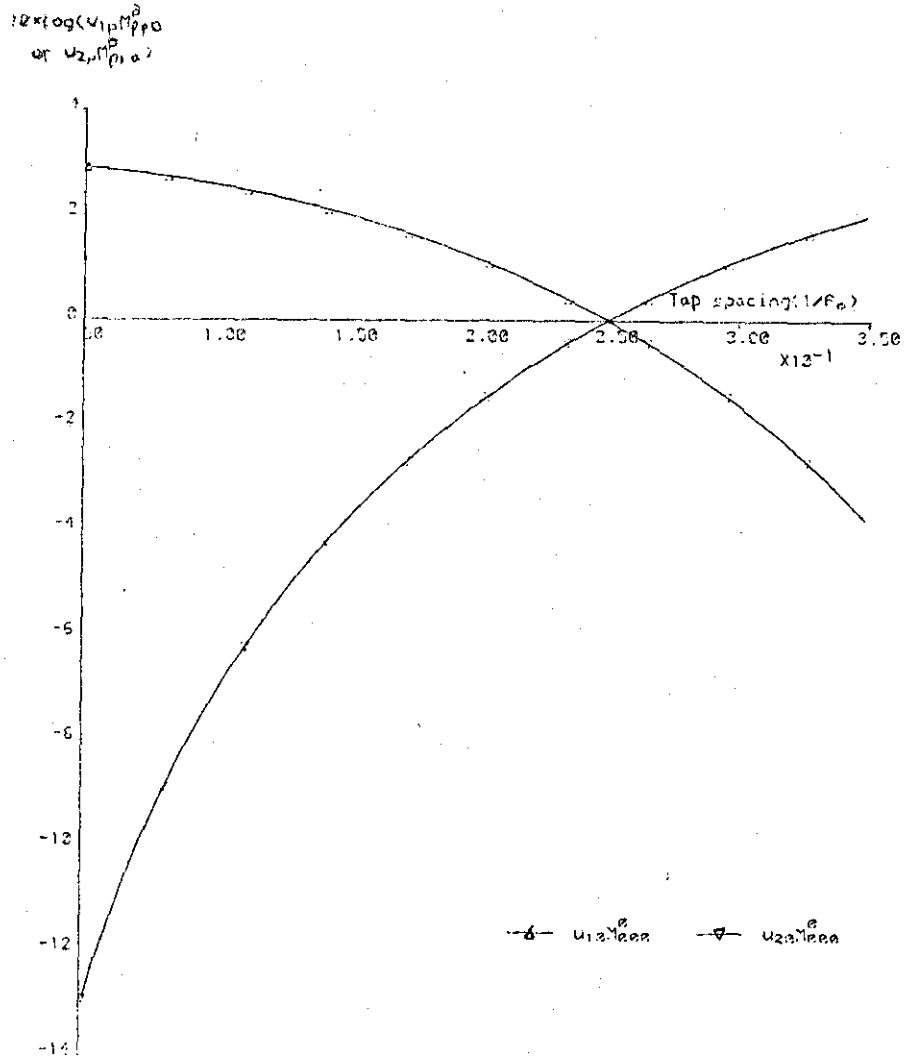

Fig.5.1a 2 taps

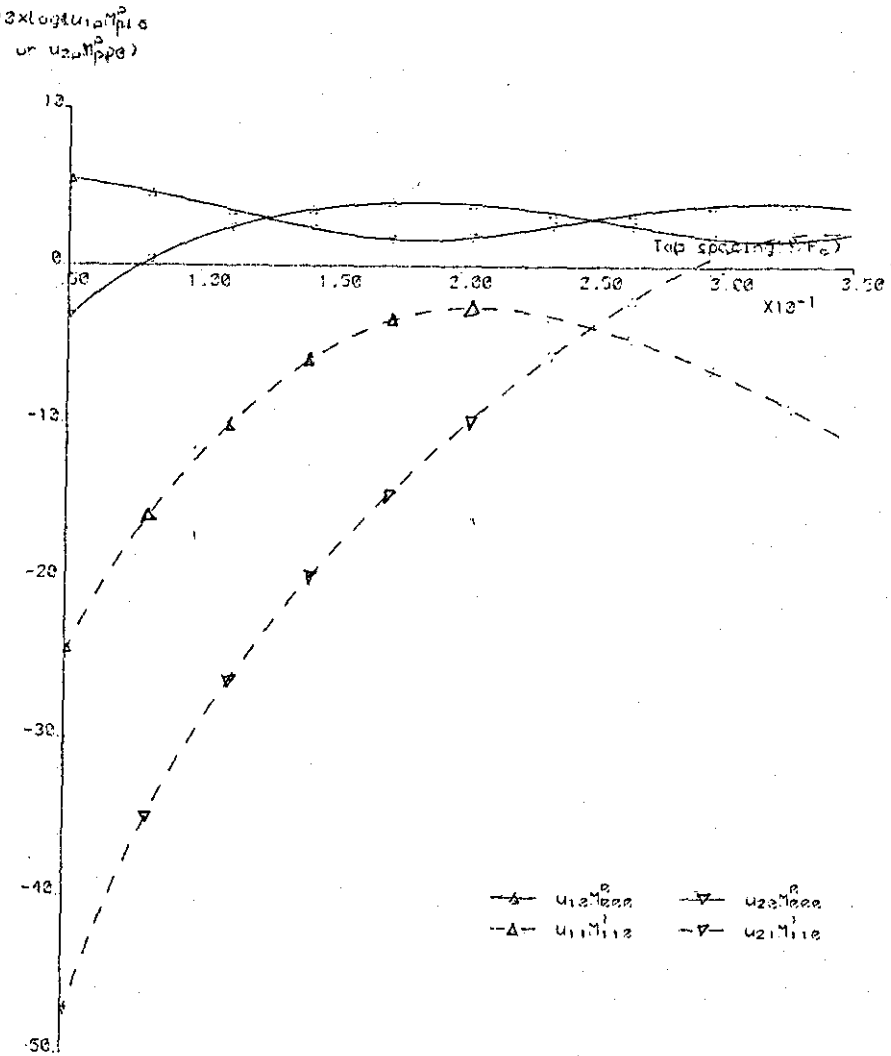

Fig.5.1b 4 taps

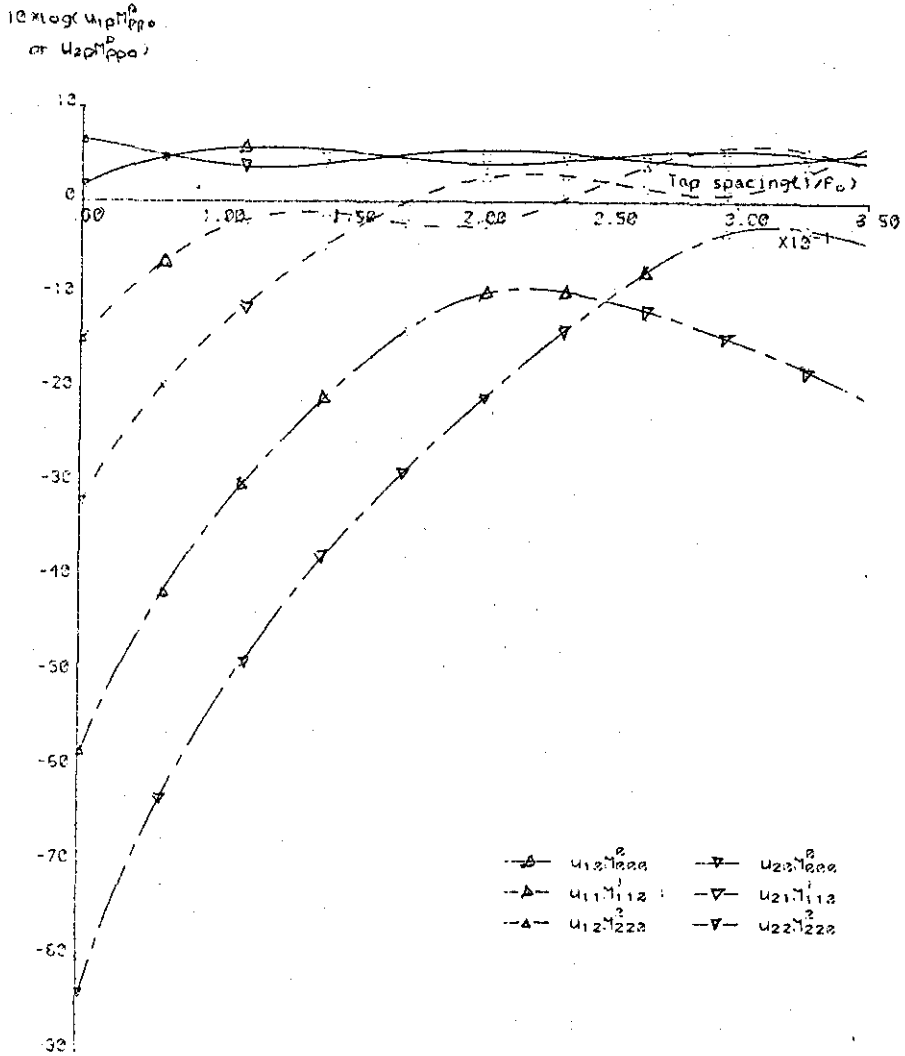

Fig.5.1c 6 taps

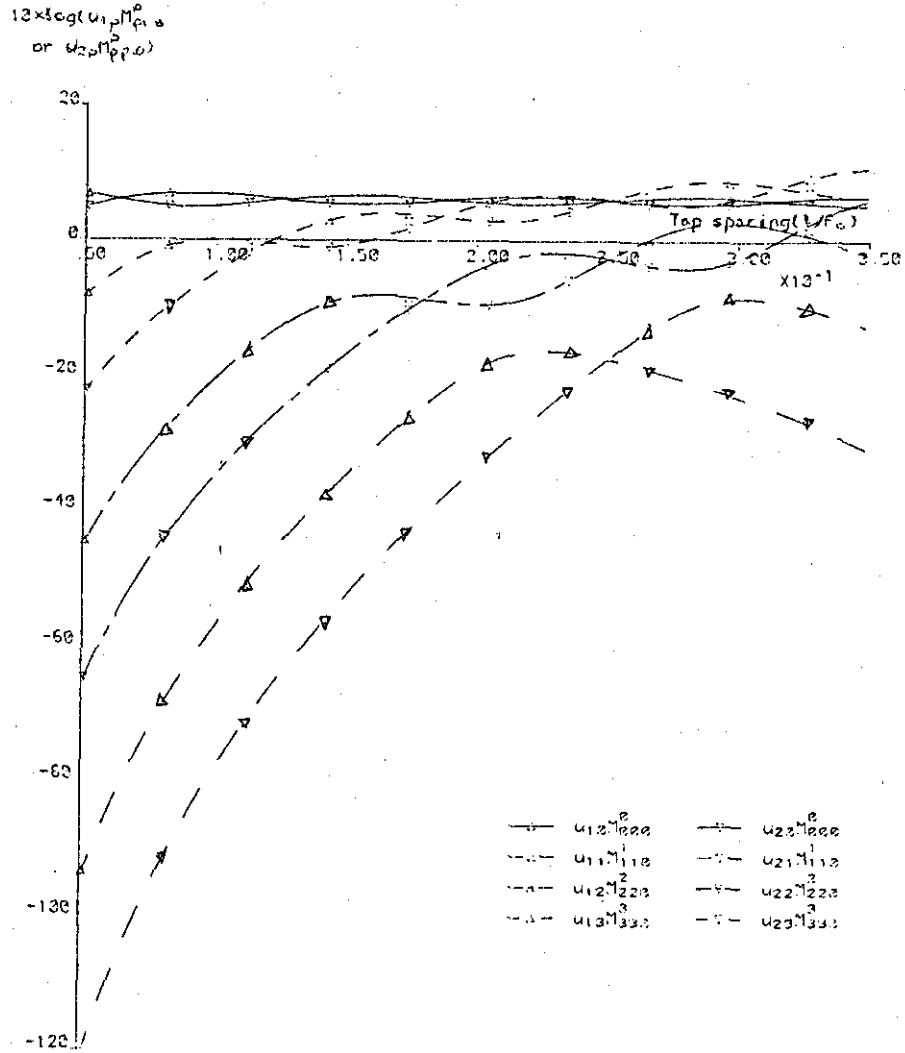

Fig.5.1d 8 taps

Fig.5.1 Grpahs of $u_{1p}M^{p}_{ppO}$ and $u_{2p}M^{p}_{ppO}$, p=0,··,J/2-1, against tap spacing for arrays with 2-8 taps. With (5.55), $u_{1p}M^{p}_{ppO}$ and $u_{2p}M^{p}_{ppO}$ give the eigenvalues of the covariance matrix should only receiver noise be present.

From (5.23) and (5.57), the ratio B_F/B_N is

$$\frac{B_F}{B_N} \approx \frac{J}{J_N B^{J-2} u_{2\ J/2-1} M^{J/2-1}_{J/2-1\ J/2-1\ 0}} \tag{5.58}$$

and can be used as a crude measure for comparing the convergence behaviour of the Frost and alternative system. Although B_F and B_N are lower bounds for the convergence time constants in the two systems and as discussed previously, are only loosely approached by the final effective time constants in a few situations, their ratio has greater physical significance. Consider the most interesting case when the tap spacing is $1/4f_o$ and all the jammers have flat spectrums. Obviously, all the narrowband processors in the alternative system will see the same set of eigenvalues which, from (5.52), is also the same, apart from a scaling factor, as the ith set of eigenvalues in the Frost system. Since the bounds B_F and B_N are obtained from the smallest eigenvalues due to only receiver noise, the ratio B_F/B_N gives the ratio of any time constant due to the last set of eigenvalues in the Frost system to that due to the corresponding eigenvalue in the alternative system. Therefore, if the jamming is so broadband that at least one eigenvalue in each set in the Frost system has significant eigenvector power component, the ratio B_F/B_N will give the ratio of the final effective time constants of the two systems, when the eigenvalues determining these time constants also correspond with each other. Of course, even when the tap spacing is changed, this will still be true if the eigenvalue determining the final effective time constant in the Frost system changes in the same manner as $u_{2\ J/2-1} M^{J/2-1}_{J/2-1\ J/2-1\ 0}$ changes. There are evidently many other situations, for example, when all the jammers are narrowband so that only the first set of eigenvalues in the Frost system has significant eigenvector power

components, in which the ratio B_F/B_N has no physical significance. However, in situations of broadband jamming where at least one eigenvalue in the last set in the Frost system has significant eigenvector power component, it has been found from simulation results (some to be presented in the next section) that, in general, the ratio B_F/B_N can usually be used to give an order of magnitude for the ratio of the final effective time constants. This is not surprising because as implied in earlier discussion, the ratio in these situations is mainly due to the separation between the last set of eigenvalues in the Frost system and the sets of eigenvalues seen by the narrowband processors in the alternative system. Having discussed the physical significance of the ratio B_F/B_N which illustrates its suitability for very roughly comparing the convergence behaviour of the two systems, fig.5.2 shows graphs of this ratio against bandwidth for the designed MENR of 20 and 40dB at $1/4f_0$ tap spacing. The number of taps for the Frost system and the number of narrowband processors for the alternative system are obtained from (4.56b,c), (4.58) and (4.60) with the operation $\lfloor\cdot\rfloor$ neglected for convenience. Furthermore, interpolation has been used to determine $u_{2\ J/2-1}{}^{M^{J/2-1}_{J/2-1}}{}_{J/2-1\ 0}$ when J/2 so obtained is not an integer. From the figure, the ratio B_F/B_N increases drastically with MENR and for bandwidth greater than about 5%, increases roughly exponentially with bandwidth. As can be deduced from (5.58) and fig.5.1, the ratio has even larger values at tap spacing other than $1/4f_0$. The slow convergence of the Frost relative to the alternative system is clearly illustrated by the figure. For example, for MENR and bandwidth greater than 20dB and 20% respectively, the final effective time constant of the Frost system can be 10 times or more larger than that of the alternative system.

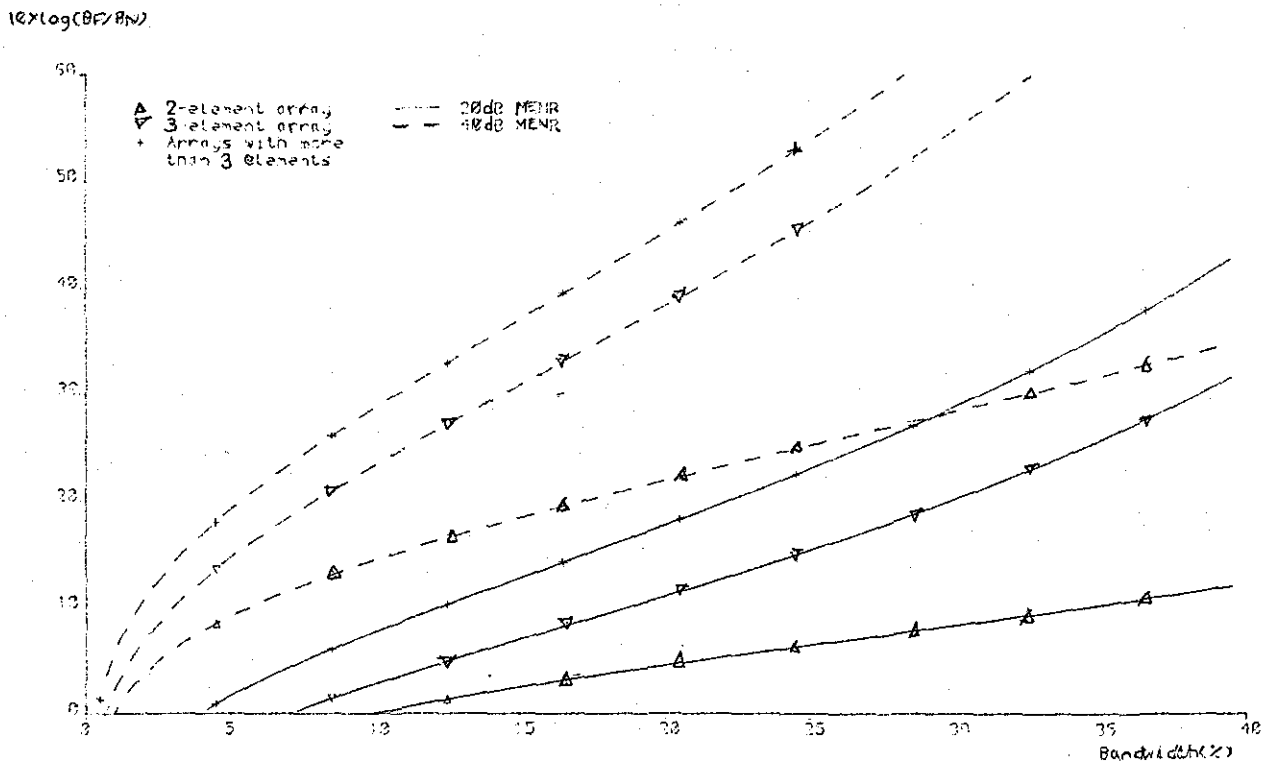

Fig.5.2 Graphs of B_F/B_N against bandwidth for 20 and 40dB MENR at $1/4f_0$ tap spacing. B_F and B_N are the lower bounds for the convergence time constants in the Frost and alternative system respectively. Very roughly, their ratio gives the ratio of the final effective time constants of the two systems in broadband jamming environments.

Summarizing, this section has studied the structure of the eigenvalues and eigenvectors of the covariance matrix theoretically for small bandwidth. Using the elegant (5.39) for the covariance matrix, the elegant structure of the eigenvectors and, summarized by (5.42), (5.47) and (5.52), the eigenvalues is obtained. Briefly, the (M-1)J eigenvalues can be divided equally into J/2 sets, those in the ith set being proportional to the 2(i-1)th power of bandwidth. Moreover, if the tap spacing is $1/4f_0$, corresponding to the spread of eigenvalues being a minimum, each set of eigenvalues and eigenvectors is very similar to that for an ideal narrowband array. The similarity is even more pronounced if, in addition, all the jammers have flat spectrums. Finally, by studying the situation when only receiver noise is present, the lower bound of

(5.57) for the convergence time constants is obtained. The ratio of this bound to the corresponding bound of (5.23) for the alternative system gives very roughly the ratio of the final effective time constants of the two systems in broadband jamming environments where at least one eigenvalue in the last set of eigenvalues in the Frost system has significant eigenvector power component. This ratio shows that the Frost system can be considerably slower than the alternative system.

5.5 Eigenvalues and Eigenvector Power Components from Simulation Results

The convergence behaviour of the output power of the Frost system has been formulated in terms of the eigenvalues and eigenvector power components in subsection 5.2.1. The structure of the eigenvalues and eigenvectors has been investigated in the last section theoretically for small bandwidth. To study the convergence behaviour in more detail, this section will investigate the eigenvalues and eigenvector power components by using some typical simulation results so as to verify the important theoretical deductions and obtain more insight.

Fig.5.3a shows graphs of eigenvalues and optimal output power against bandwidth for a 3-element, 4-tap, $1/4f_0$ tap spacing array with -20dB receiver noise. Two jammers both of powers -3dB with flat spectrums arrive from -20° and -60°. Note that the bandwidth axis is log-scaled. Clearly, there are 2 sets of 4 eigenvalue curves with 0 and 20dB per decade gradients, indicating that in agreement with (5.42), there are 2 sets of 4 eigenvalues proportional to B^0 and B^2 respectively. Furthermore, the structure of the eigenvalues is also in agreement with (5.47) and (5.52) which are also

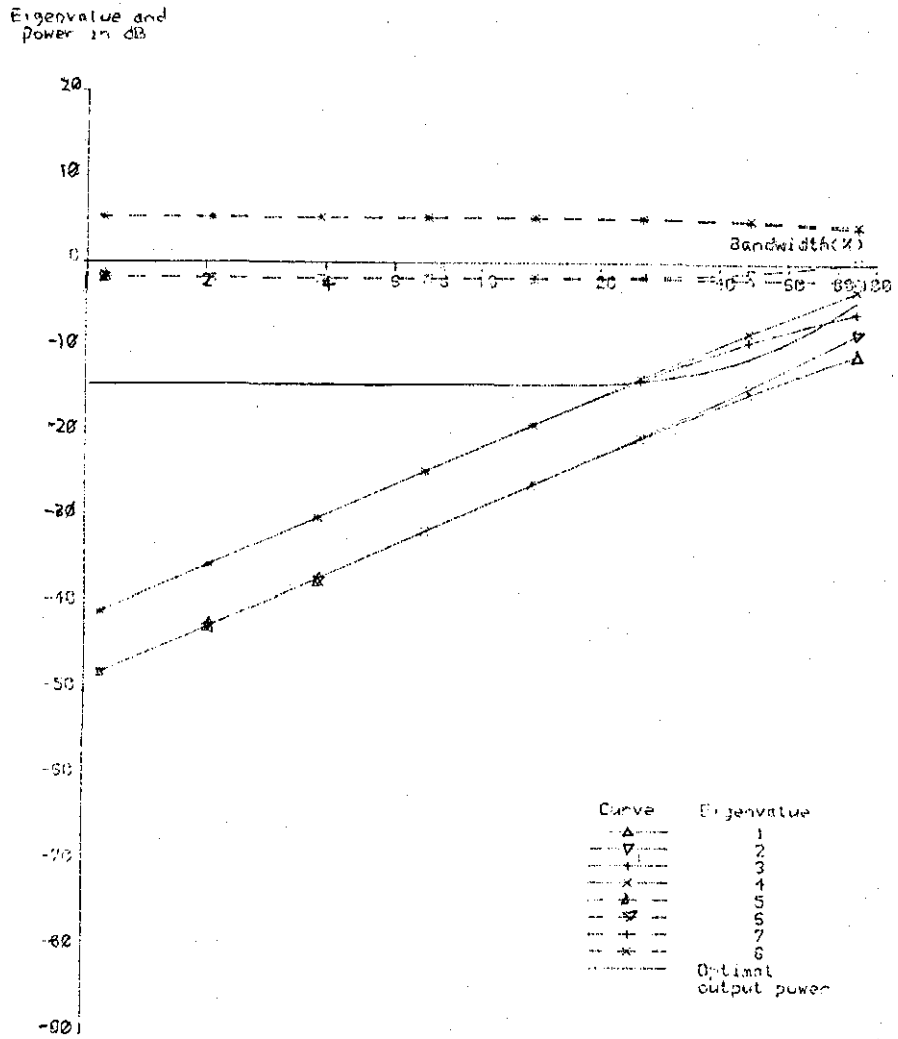

Fig.5.3a Eigenvalues and optimal output power

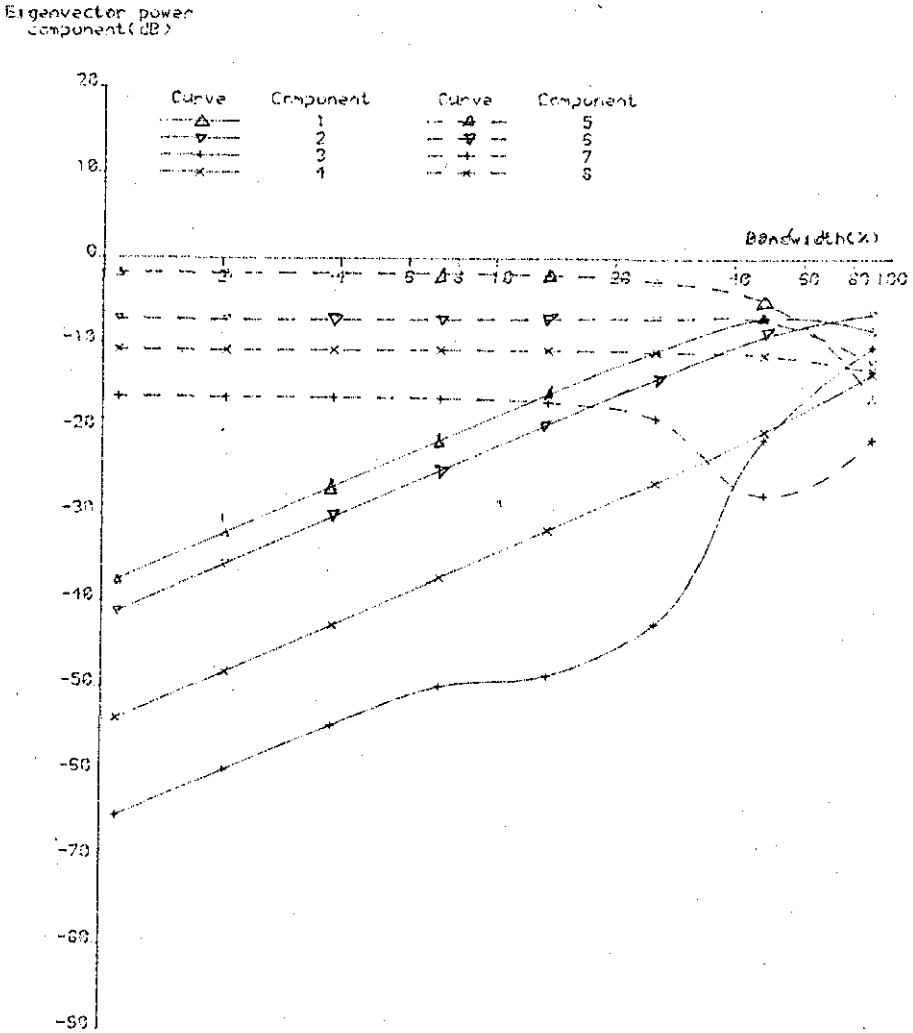

Fig.5.3b Eigenvector power components

Fig.5.3 *Graphs of eigenvalues, eigenvector power components and optimal output power against bandwidth for a 3-element, 4-tap, $1/4f_0$ tap spacing array. The receiver noise is -20dB and two jammers, both of power -3 dB and having flat spectrums, arrive from -20° and -60°.*

applicable in this situation. In particular, corresponding eigenvalues in the two sets can be calculated, using (5.52) with $u_0{}^2M^0_{000}$ and $u_1{}^2M^1_{110}$ given by the graphs of fig.5.1b at $1/4f_0$ tap spacing, to differ by 26dB at 10% bandwidth. This agrees with that obtained from the figure to within 1dB. Fig.5.3b shows graphs of eigenvector power components in this situation. Comparing with fig.5.3a shows that, for bandwidth less than about 10%, corresponding curves in the two figures have the same gradient. This indicates that, for small bandwidth, all the eigenvector components are independent of bandwidth. For larger bandwidth, the eigenvector power components can be seen to have more complex behaviour. From fig.5.3a, the performance of the array to reject the jammers obviously starts to deteriorate as the optimal output power begins to increase drastically at about 30% bandwidth, in agreement with the value calculated from (4.56b,c) and (4.58) for a MENR of 20dB. For bandwidth below this value but above about 20%, eigenvector power component 1 in fig.5.3b can be seen to be greater than and hence significant compared with the optimal output power of about -15dB. For bandwidth within this region when, obviously, the jamming is broadband and all the degrees of freedom are directed towards rejecting the jammers, the final effective time constant is therefore determined by eigenvalue 1, one of the smallest eigenvalues, and using (5.18) and fig.5.3a, is roughly 3000 sampling period at 25% bandwidth and 10% misadjustment. From (4.56b,c) and (4.60), 3 narrowband processors are needed in the alternative system at 25% bandwidth and 20dB MENR. With all the jammers having flat spectrums in this environment, the eigenvalues seen by the narrowband processors are clearly the same, apart from a scaling factor, as the eigenvalues

in the first set and all have significant eigenvector power components. The ratio of the trace of the covariance matrix to the smallest eigenvalue in each processor is thus about 10 (twice the largest divided by the smallest eigenvalue in the first set). Therefore, using (5.18) with the misadjustment for each processor being 10/3% so that the total misadjustment is equal to that of the corresponding Frost system, the final effective time constant of the alternative system is roughly 75 sampling period. The Frost system is hence effectively about 40 times slower than the alternative system in the environment considered. The significance of the ratio B_F/B_N, from (5.58) and fig.5.1b, of about 30 is thus illustrated, although the bound B_F can be calculated from (5.57) and fig.5.1b to be about 80000 sampling period, 30 times greater than the corresponding final effective time constant. Of course, for bandwidth smaller than about 10%, only the first set of eigenvalues will have significant eigenvector power components and two degrees of freedom per jammer are sufficient to well reject the jammers. Clearly, in such effectively narrowband situations, B_F and B_F/B_N will be too large and do not have much physical significance as the effective time constants of the two systems will not be very different.

Fig.5.4 shows the results obtained when the tap spacing is changed to $1/6f_0$, all the other parameters being the same as that of fig.5.3. Obviously, the theoretical eigenvalue structure of (5.42) can be seen to be still valid, although the more simpler structure of (5.47) and (5.52) are now inapplicable. Comparing fig.5.4a with 5.3a indicates the theoretical deduction that as the tap spacing deviates from $1/4f_0$, the spread of eigenvalues increases. Comparing fig.5.4b with 5.3b shows that the eigenvector pow-

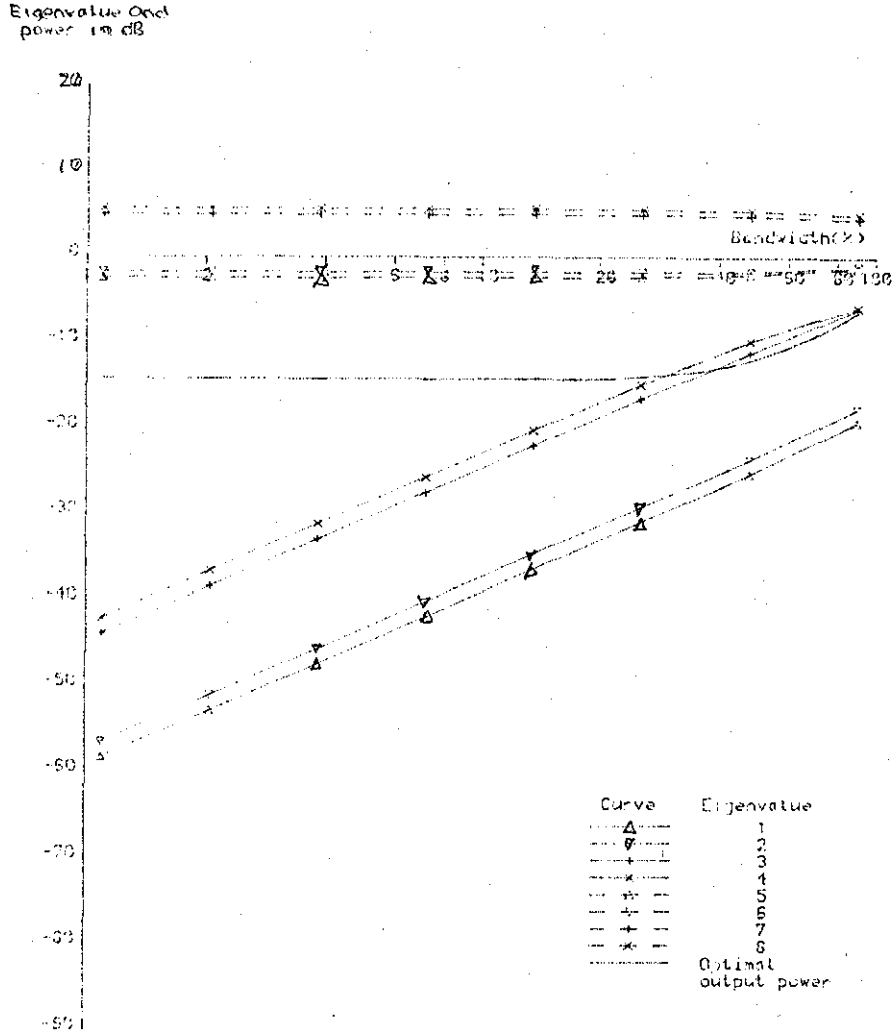

Fig.5.4a Eigenvalues and optimal output power

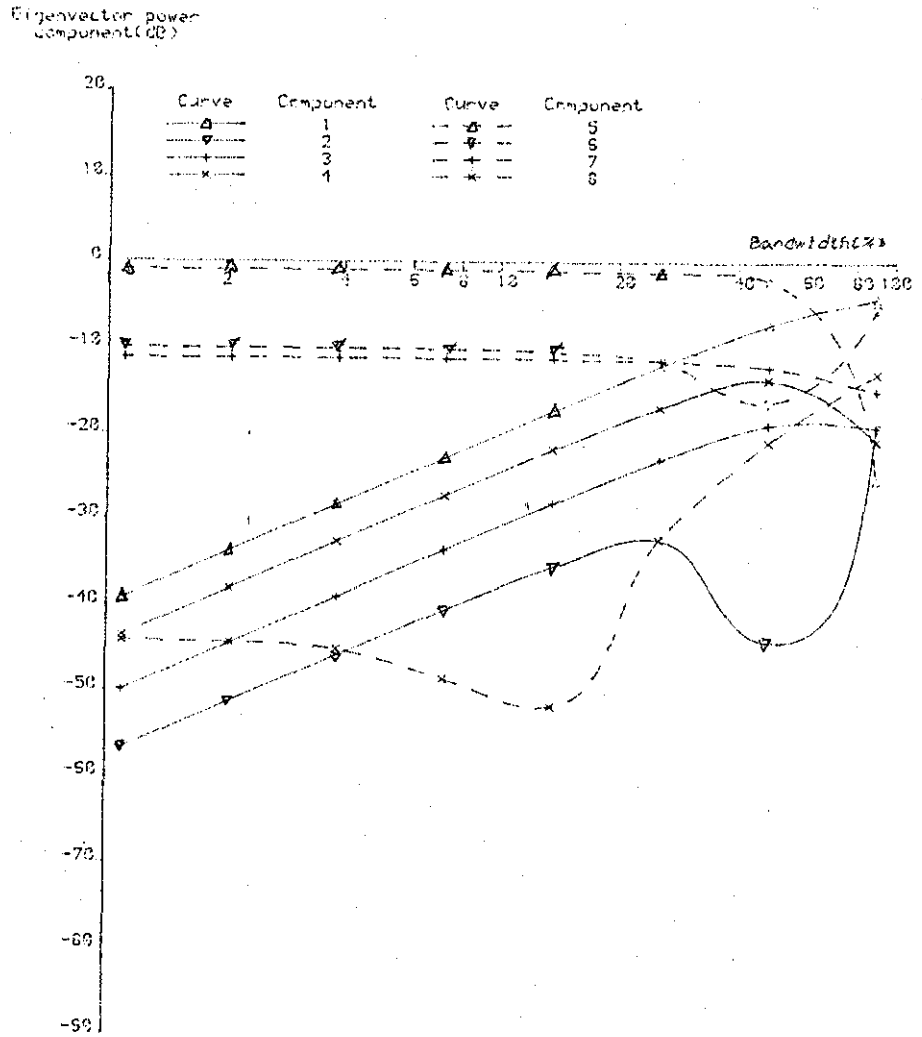

Fig.5.4b Eigenvector power components

Fig.5.4 Graphs of eigenvalues, eigenvector power components and optimal output power against bandwidth for the situation of fig.5.3 except with the tap spacing being changed to $1/6f_0$ instead.

er component curves have more complex behaviour, although for small bandwidth, they still have the same gradient as the corresponding eigenvalue curves. Indicating again that the eigenvector components are independent of bandwidth, this has been found from other simulation results to be the case whenever there is no extra spatial degree of freedom and all the jammers' spectrum have even symmetry. Since the eigenvector power component 1 and optimal output power curves of fig.5.4 are roughly equal to those of fig.5.3, the final effective time constant will still be determined by the smallest eigenvalue, eigenvalue 1, for bandwidth between 20 and 30% when the jamming is broadband and all the degrees of freedom have to be employed to reject the jammers. With eigenvalue 1 about 10 dB below that of fig.5.3a, the final effective time constant is thus roughly 30000 sampling period, 10 times more than the corresponding value calculated at $1/4f_0$ tap spacing, at 25% bandwidth and 10% misadjustment. Therefore, effectively, the Frost system is now about 400 times slower than the alternative system. From (5.57), (5.58) and fig.5.1b again, the ratio B_F/B_N is about 300, even though the bound B_F is roughly 1000000 sampling period, 30 times greater than the final effective time constant. Moreover, for bandwidth less than about 10%, the effective time constants will be due to the first set of eigenvalues and so will not be very different from those of the alternative system. Evidently, the same deductions as in the last example can be reached.

Fig.5.5 shows the same set of graphs as fig.5.3 when the external environment consists of only one jammer of power 0dB at -20° and having inverted-triangular spectrum, all the other parameters being the same as that of fig.5.3. For bandwidth below about 10%, the eigenvalue curves can again be seen to agree with the theoret-

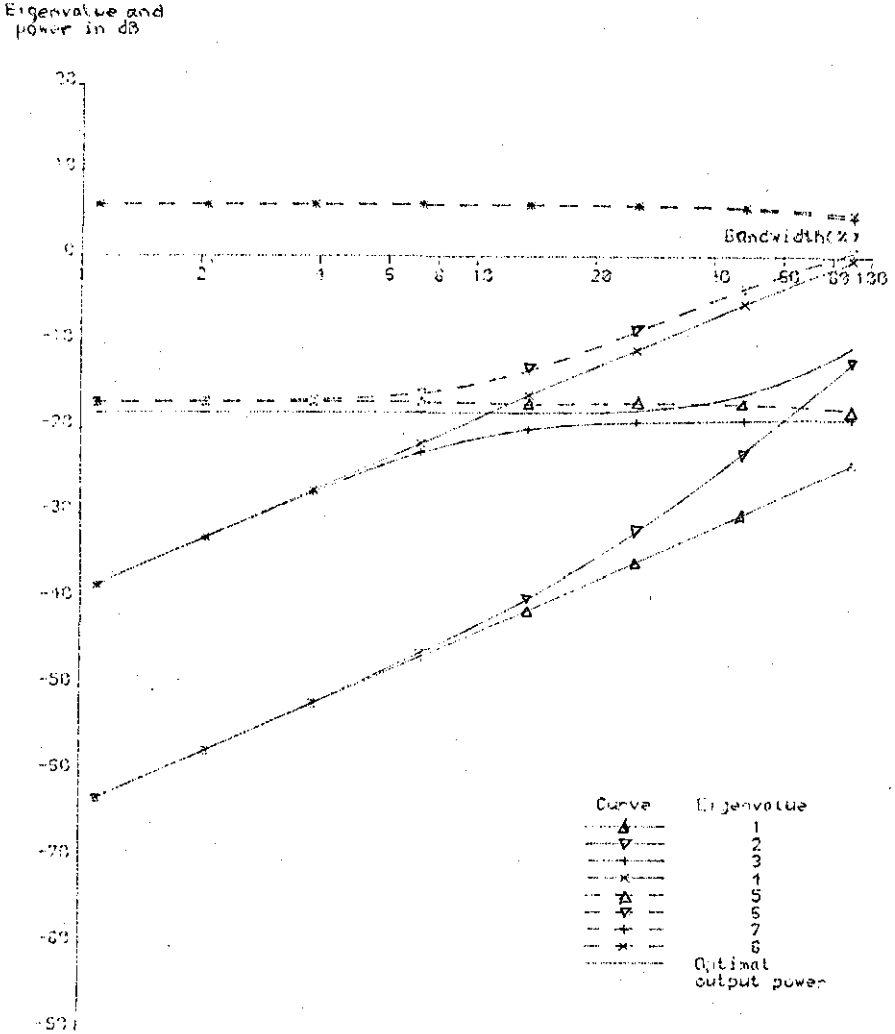

Fig.5.5a Eigenvalues and optimal output power

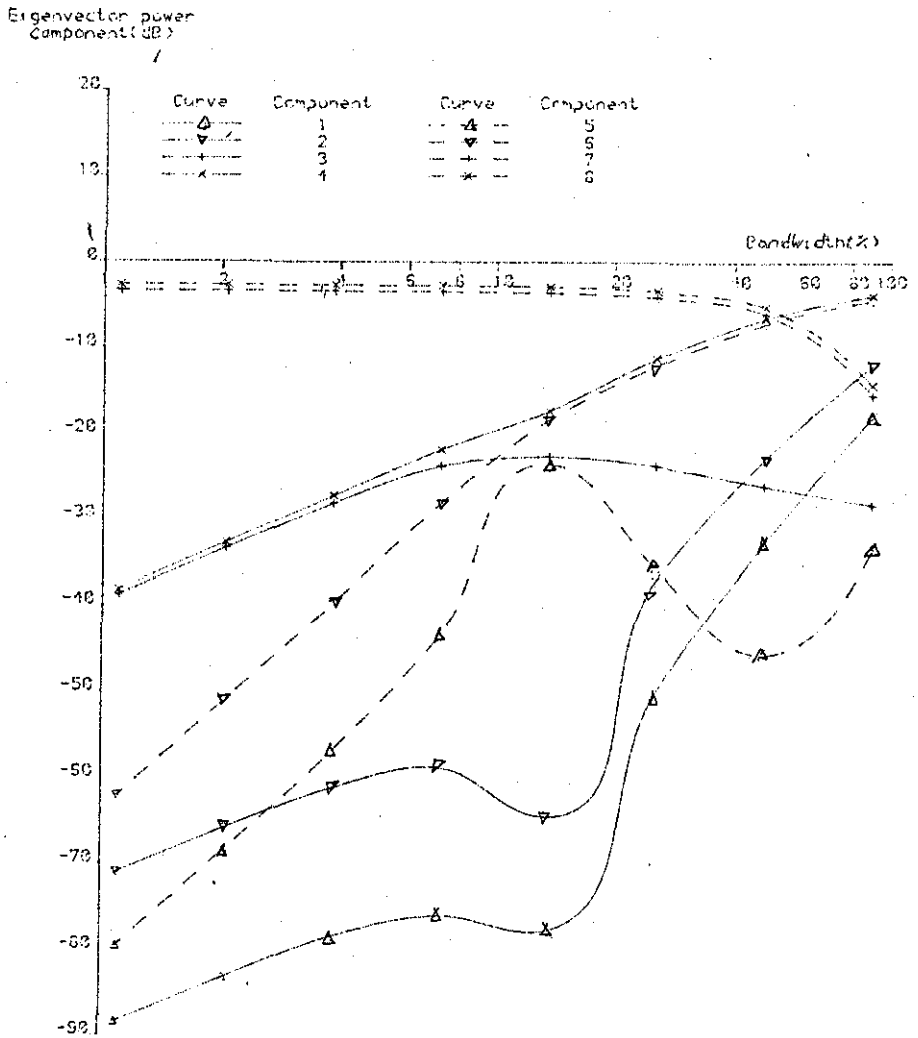

Fig.5.5b Eigenvector power components

Fig.5.5 Graphs of eigenvalues, eigenvector power components and optimal output power against bandwidth for the situation of fig.5.3 except that the external environment now consists of only one jammer of power 0dB with inverted-triangular spectrum arriving from -20°.

ical description of (5.42) and (5.47), with eigenvalues 1, 2, 5 and 6 being due to only receiver noise and the other eigenvalues due to the jammer and receiver noise. However, as the bandwidth increases and eigenvalue curves 3 and 4 are about to meet with curves 5 and 6, the "roles" of eigenvalues 3 and 6 start to change over. Eventually, the former, becoming proportional to B^2, is one of the first set of eigenvalues and is due to only receiver noise, while the latter, becoming proportional to B^2, is one of the second set of eigenvalues and is due to the jammer and receiver noise. Moreover, the gradient of eigenvalue curve 1 begins to increase to 40dB per decade eventually. Overall, the net effect is that one of the smallest eigenvalues proportional to B^2 has become proportional to B^4. Generally, it can be proved [82] that for large bandwidth, some small eigenvalues proportional to large even powers of bandwidth may become increasing faster with still larger even powers of bandwidth. Comparing fig.5.5a with 5.3a and 5.4a, the more complex behaviour of the eigenvalues can be seen to be due to the wide range of eigenvalues within each set of eigenvalues, relative to the separation between adjacent sets of eigenvalues. Clearly, this will be the case if say, the jammers have very different powers, some of the jammers are closed together or the spatial degrees of freedom are not fully utilized. Regarding fig.5.5b, the eigenvector power components obviously have much more complex behaviour than that of figs.5.3b and 5.4b. For small bandwidth, components 5, 6 and 7, 8 can be seen to be proportional to B^4 and B^0 respectively, while the other components are proportional to B^2. From the small bandwidth behaviour of the eigenvalues, this implies that all the eigenvector components are proportional to at least B^0. Generally, this can be proved [82] to be so for a 4-tap

array if all the jammers' spectrums have even symmetry. By examining the curves in fig.5.5 and using similar arguments as in the last two examples, the same deductions discussed regarding B_F, B_F/B_N and the effective time constants can once more be obtained for this example. In general, when the jamming is broadband so that at least one eigenvalue in the last set has significant eigenvector power component, the ratio B_F/B_N has been found to be relevant for comparing the convergence behaviour of the two systems. Specifically, in most of such situations, the ratio gives at least an order of magnitude for the ratio of the final effective time constants, even though B_F and actually, B_N may only be very loosely approached. However, in the other extreme when the jamming is effectively narrowband so that only the first set of eigenvalues has significant eigenvector power components, B_F/B_N and B_F will certainly be too large and have no physical relevance as the effective time constants of the two systems will not be very different. Of course, if the number of taps and thus number of sets of eigenvalues is large, there exist other intermediate cases as well.

Fig.5.6 shows graphs of eigenvalues against bandwidth for the situation of fig.5.5 except with the jammer having half-flat spectrum instead. For bandwidth smaller than about 20%, the theoretical description of (5.42) and (5.47) is again verified. In particular, the eigenvalues in the first set or due to only receiver noise are the same as those in fig.5.5a. However, because of the decrease of the actual bandwidth of the jammer with a half-flat spectrum, the other eigenvalues have become smaller. As may be expected, this effect is also generally observed when the jammers' spectrums become more peaky at the centre of the band. In all other aspects, the behaviour of the eigenvalues is the same as that

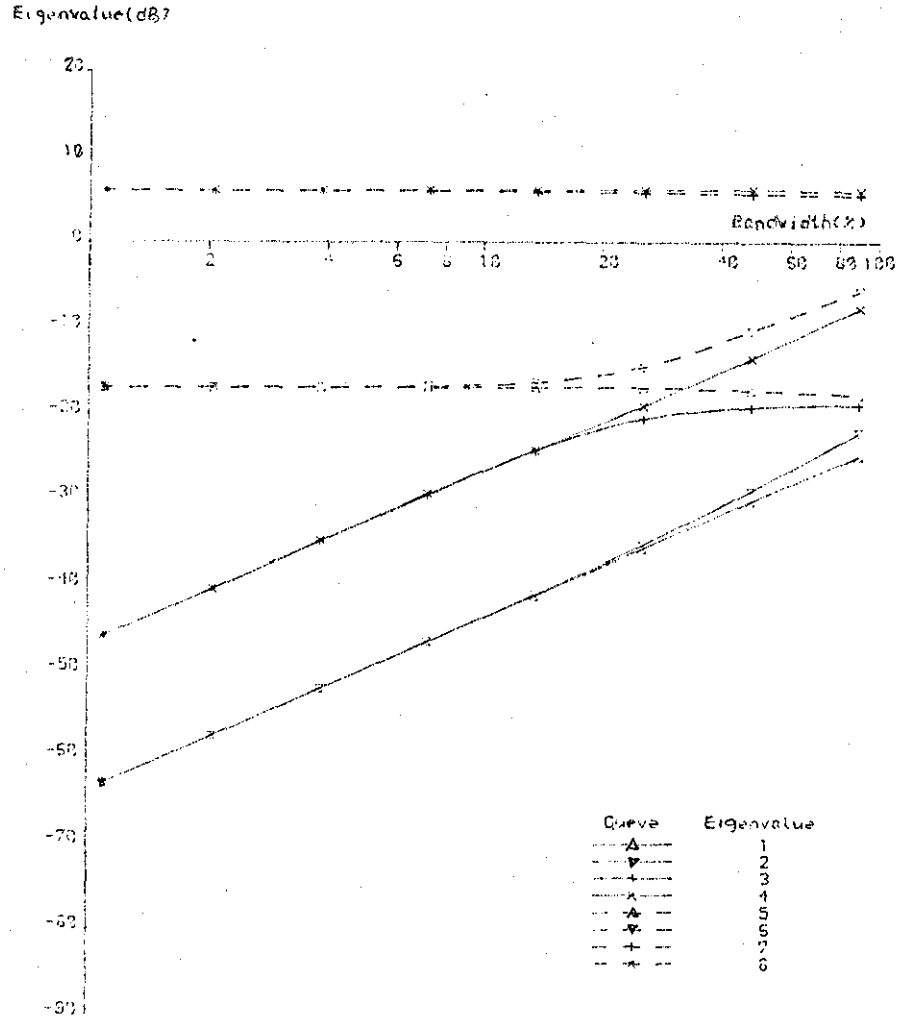

Fig.5.6 Graphs of eigenvalues against bandwidth for the situation of fig.5.5 except with the spectrum having half-flat spectrum instead.

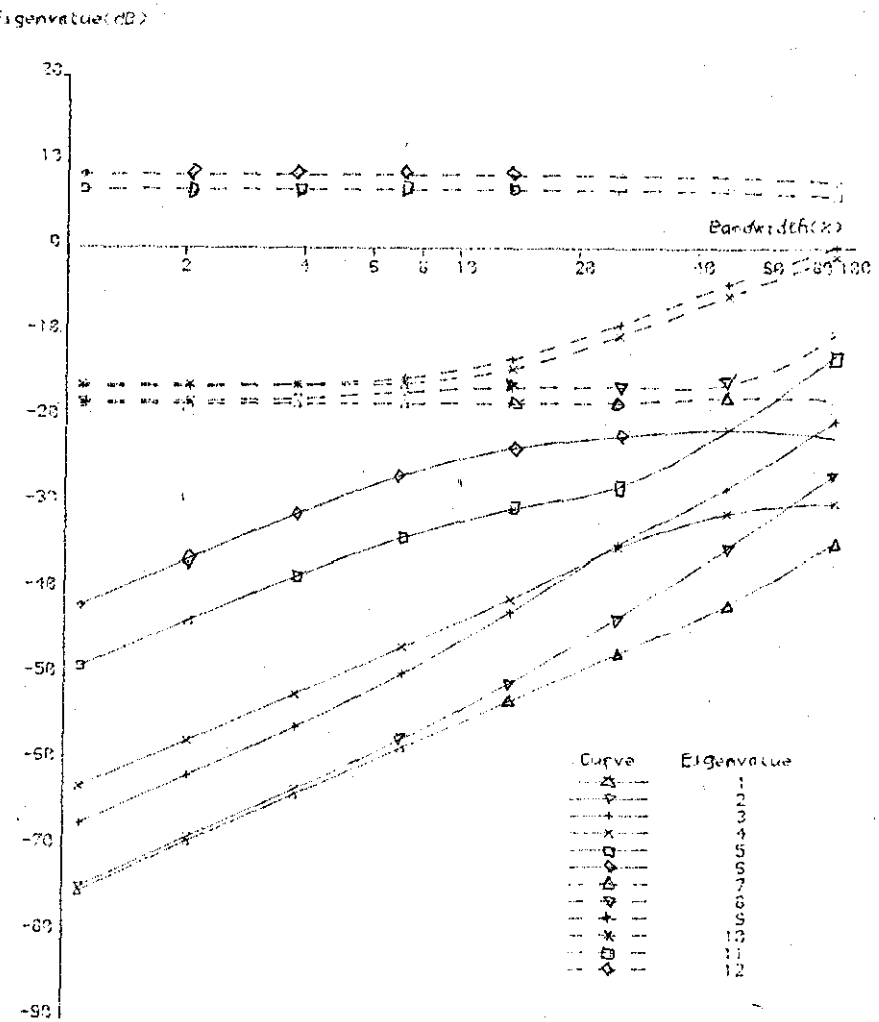

Fig.5.7 Graphs of eigenvalues against bandwidth for a 4-element, 4-tap, $1/6f_0$ tap spacing array with -20 dB receiver noise. Only one jammer of power 0dB and having triangular spectrum arrives from -60°.

of fig.5.5a.

Finally, fig.5.7 shows graphs of eigenvalues against bandwidth for a more complex 4-element, 4-tap, $1/6f_0$ tap spacing array with -20dB receiver noise. Only one jammer of power 0dB and having triangular spectrum is present at -60°. Again, for small bandwidth, the behaviour of the eigenvalues as described by (5.42) can be seen. Also, as fig.5.4a, the spreading out of the eigenvalues at tap spacing other than $1/4f_0$ can be observed. In particular, although the number of spatial degrees of freedom is more than the number of jammers, it is obvious from the structure of the eigenvalues that no eigenvalue due to only receiver noise exists. Evidently, at $1/4f_0$ tap spacing, the eigenvalues have the minimum spread and with (5.47) and possibly, (5.52) applicable, the simplest structure. Though more complex, the behaviour of the eigenvalues at large bandwidth is essentially the same as that discussed for fig.5.5a.

Summarizing, this section has investigated the eigenvalues and eigenvector power components using some typical simulation results obtained. The important theoretical deductions of the last section have been verified. Specifically, the structure of the eigenvalues as described by (5.42), (5.47) and (5.52) is valid to bandwidths of tens of percents depending on the environment. Also, the eigenvalues have minimum spread and so the Frost system has best convergence behaviour at $1/4f_0$ tap spacing. Most importantly, the relevance of the ratio B_F/B_N for very roughly comparing the final effective time constants of the Frost and alternative system in broadband jamming environments is illustrated. Regarding the eigenvector power components, the results show that they can have quite complex behaviour, even for small bandwidth.

5.6 Theoretical Derivation and Consequences of the Preprocessor

Because of the elegance of (5.27) for the covariance matrix derived in appendix 5.9.1 and discussed in section 5.3, it is possible to construct a matrix preprocessor which, being independent of the external environment, transforms the inputs so that they become partially "block" decorrelated. Therefore, if the stochastic gradient descent algorithm is applied to these transformed inputs instead, resulting in what will be referred to as the "preprocessed Frost system", much better convergence behaviour will be obtained. This section is concerned with the theoretical derivation and consequences of the preprocessor. In the process, the lower bound for the convergence time constants of the preprocessed Frost system will be derived and compared with that of the alternative system. Note that the derivation of the preprocessor will be general, although the analysis of its consequences will be based on the assumption of small bandwidth.

5.6.1 Derivation of the preprocessor

Firstly, the preprocessor will be derived in this subsection. As its name implies, the preprocessor derives a transformed set of inputs from linear combinations of the original inputs. Of course, for the power inversion array of fig.4.1, only the inputs from element 2 to M are of concern to the preprocessor as only these are weighted. Therefore, denoting $\tilde{x}_m(k)$, $m=1,\cdots,(M-1)J$, as the mth transformed input, the transformed input vector, defined as

$$\tilde{X}(k) = [\tilde{x}_1(k)\ \tilde{x}_2(k)\ \cdots\ \tilde{x}_{(M-1)J}(k)]^T, \tag{5.59}$$

is obtained from the input vector by

$$\tilde{X}(k) = L^T X(k) \tag{5.60}$$

where L is a $(M-1)J \cdot (M-1)J$ matrix representing the transformation preprocessing. For convenience, the term preprocessor will also be used to refer to the matrix L. Obviously, the array output is given by

$$y(k) = x_0(k) + W(k)^T \tilde{X}(k) \tag{5.61}$$

should the preprocessor be used. Thus, with stochastic gradient descent algorithm used for updating the weights to minimize output power, the preprocessed Frost system will have similar characteristics and behaviour as for the Frost system. In particular, the discussion in subsection 5.2.1 for the Frost system will also be valid for the preprocessed Frost system if the covariance matrix and vector are replaced by the transformed covariance matrix and vector, defined as

$$\tilde{R} = \overline{\tilde{X}(k)\tilde{X}(k)^T} \tag{5.62}$$

and

$$\tilde{R}_0 = \overline{x_0(k)\tilde{X}(k)} \tag{5.63}$$

respectively. Furthermore, the discussion of the last chapter does not depend on whe ther the preprocessor is employed or not. Note that by substituting (5.60), the transformed covariance matrix and vector are related to the covariance matrix and vector by

$$\tilde{R} = L^T R L \tag{5.64}$$

and

$$\tilde{R}_0 = L^T R_0. \tag{5.65}$$

As discussed in previous sections, the eigenvalues of the covariance matrix determines the convergence time constants of the Frost system and are therefore of particular importance. This is

of course also true for the preprocessed Frost system. Obviously, from (5.64), the eigenvalues of the transformed covariance matrix will be different from those of the covariance matrix. It is thus of great interest to see if by choosing the preprocessor suitably, the spread of eigenvalues can be substantially reduced, resulting in the preprocessed Frost system having much better convergence behaviour. In the following discussion, it is convenient to view the preprocessor as consisting of three component preprocessors in series:

$$L = FGD \tag{5.66}$$

where F, G and D represent and will be referred to as the first, second and third component preprocessors respectively.

Substituting (5.66) into (5.64), the transformed covariance matrix is

$$\tilde{R} = D^T G^T F^T R F G D. \tag{5.67}$$

Consider now the purpose of the first component preprocessor F. Partitioning F, which has dimension $(M-1)J \cdot (M-1)J$, as

$$F = [F_0 \; F_1 \; \cdots \; F_{J/2-1}] \tag{5.68}$$

where F_g, $g=0,\cdots,J/2-1$, has dimension $(M-1)J \cdot 2(M-1)$, the transformed covariance matrix of (5.67) is, after substituting (5.36) which is equivalent to (5.27),

$$\tilde{R} = D^T G^T \begin{bmatrix} F_0^T \\ F_1^T \\ \vdots \\ F_{J/2-1}^T \end{bmatrix} \begin{bmatrix} U_0^T & & & \\ & BU_1^T & & \\ & & \ddots & \\ & & & B^{J/2-1}U_{J/2-1}^T \end{bmatrix}^T \begin{bmatrix} R_{00}^0 & R_{10}^0 & \cdots & R_{J/2-1}^0 \; 0 \\ R_{10}^0 & R_{11}^0 & & \\ \vdots & & & \\ R_{0\,J/2-1}^0 & & & \end{bmatrix} \tag{5.69}$$

$$\cdot \begin{bmatrix} U_0^T & & \\ & BU_1^T & \\ & & \ddots \\ & & B^{J/2-1}U_{J/2-1}^T \end{bmatrix} \begin{bmatrix} F_0^T & & \\ & F_1^T & \\ & & \ddots \\ & & F_{J/2-1}^T \end{bmatrix}^T GD.$$

Since, as discussed in section 5.3, U_g depends only on the number of taps and tap spacing whereas for small bandwidth, R^0_{gh}, h=0,$\cdots$, J/2-1, is independent of these two array parameters, it is obvious that if the first component preprocessor is such that

$$F_g^T U_h = k_{gh} I \tag{5.70}$$

where k_{gh} is the Kronecker delta, then the transformed covariance matrix will be rendered, for small bandwidth at least, independent of tap spacing and apart from the dimension of the matrix, number of taps. Specifically, (5.69) can easily be seen, from (5.70), to become

$$\tilde{R} = G^T D^T \begin{bmatrix} I & & & 0 \\ & BI & & \\ & & \ddots & \\ 0 & & & B^{J/2-1}I \end{bmatrix} \begin{bmatrix} R^0_{00} & R^0_{01} & \cdots & R^0_{0\,J/2-1} \\ R^0_{10} & R^0_{11} & & \\ \vdots & & & \\ R^0_{J/2-1\,0} & & & \end{bmatrix} \tag{5.71}$$

$$\cdot \begin{bmatrix} I & & & 0 \\ & BI & & \\ & & \ddots & \\ 0 & & & B^{J/2-1}I \end{bmatrix} GD.$$

Note that as given in terms of (5.68) and (5.70), the first component preprocessor clearly depends only on the number of taps and tap spacing.

From the transformed covariance matrix of (5.71), the choice for the second component preprocessor is obvious. Thus, with G given by

$$G = \begin{bmatrix} I & & 0 \\ & B^{-1}I & \\ & \ddots & \\ 0 & & B^{-J/2+1}I \end{bmatrix} \tag{5.72}$$

which depends only on the bandwidth, (5.71) becomes

$$\tilde{R} = D^T \begin{bmatrix} R^0_{00} & R^0_{01} & \cdots & R^0_{0\,J/2-1} \\ R^0_{10} & R^0_{11} & & \\ \vdots & & & \\ R^0_{J/2-1\,0} & & & \end{bmatrix} D. \tag{5.73}$$

Clearly, with (5.33) and (5.34) giving R^0_{gh}, the transformed covariance matrix and so its eigenvalues and eigenvectors, due to the second component preprocessor, has also become independent of bandwidth, at least for small bandwidth.

Although the spread of eigenvalues have been reduced significantly by the component preprocessors discussed, there will still be considerably spread in eigenvalues due to the second factor of (5.73). The purpose of the third component preprocessor D is therefore to further reduce this spread of eigenvalues. To determine D, consider substituting the polar decomposition of (5.43) for R^0_{gh} in (5.73) so that the transformed covariance matrix becomes, for small bandwidth,

$$\tilde{R} \simeq \varepsilon_0 D^T \begin{bmatrix} M^0_{000}EE^T & M^0_{010}EE^T & \cdots & M^0_{0\,J/2-1\,0}EE^T \\ M^0_{100}EE^T & M^0_{110}EE^T & & \\ \vdots & & & \\ M^0_{J/2-1\,00}EE^T & & & \end{bmatrix} D + \sum_{n=1}^{N} D^T \tag{5.74}$$

$$\cdot \begin{bmatrix} c^0_{00n}c^0_{00n}c^0_{00n}{}^T & c^0_{01n}c^0_{01n}c^0_{01n}{}^T & \cdots & c^0_{0\,J/2-1\,n}c^0_{0\,J/2-1\,n}c^0_{0\,J/2-1\,n}{}^T \\ c^0_{10n}c^0_{10n}c^0_{10n}{}^T & c^0_{11n}c^0_{11n}c^0_{11n}{}^T & & \\ \vdots & & & \\ c^0_{J/2-1\,0n}c^0_{J/2-1\,on}c^0_{J/2-1\,on}{}^T & & & \end{bmatrix} D.$$

Note that as discussed in subsection 5.4.2, C^0_{gh1}, C^0_{gh2}, $\cdots$ and C^0_{ghN} together span the same subspace as that spanned together by Q_1, Q_2, $\cdots$ and Q_N and are mutually orthogonal to E. Thus, if D has the form

$$D = \begin{bmatrix} d_{00}I & d_{01}I & \cdots & d_{0\ J/2-1}I \\ d_{10}I & d_{11}I & & \\ \vdots & & & \\ d_{J/2-1\ 0}I & & & \end{bmatrix} = \hat{D} \times I \tag{5.75}$$

where $\times$ denotes Kronecker product and $\hat{D}$ is a $J/2 \cdot J/2$ matrix with d_{gh} as the $(g+1,h+1)$ element, the first term of (5.74) will remain mutually orthogonal to the other terms and define $(M-N-1)J$ eigenvalues due to only receiver noise, while the other terms will give rise to NJ eigenvalues due to the jammers and receiver noise. Defining M_0 as

$$M_0 = \begin{bmatrix} M^0_{000} & M^0_{010} & \cdots & M^0_{0\ J/2-1\ 0} \\ M^0_{100} & M^0_{110} & & \\ \vdots & & & \\ M^0_{J/2-1\ 00} & & & \end{bmatrix}, \tag{5.76}$$

using (5.75) and the easily verified mathematical theorem

$$(A_1 \times A_2)(A_3 \times A_4) = (A_1 A_3) \times (A_2 A_4) \tag{5.77}$$

for compatible Kronecker products, the first term of (5.74) can be expressed as

$$s_0 D^T \begin{bmatrix} M^0_{000}EE^T & M^0_{010}EE^T & \cdots & M^0_{0\ J/2-1\ 0}EE^T \\ M^0_{100}EE^T & M^0_{110}EE^T & & \\ \vdots & & & \\ M^0_{J/2-1\ 00}EE^T & & & \end{bmatrix} D \tag{5.78}$$

$$= s_0(\hat{D}^T \times I)(M_0 \times EE^T)(\hat{D} \times I) = s_0(\hat{D}^T M_0 \hat{D}) \times EE^T.$$

With the 2(M-N-1) columns of E being normalized eigenvectors of R_{gh}^{0} associated with only receiver noise, it is obvious that if the third preprocessor is chosen such that

$$\hat{D}^T M_0 \hat{D} = I, \tag{5.79}$$

then all the eigenvalues of the transformed covariance matrix due to only receiver noise will be equal to simply s_0. This is possible because, with receiver noise having flat spectrum, M_0 is a constant matrix and is given, from (5.34) and (5.76), by

$$M_0 = \begin{bmatrix} \frac{\pi^0}{0!} & & 0 \\ & \frac{\pi^1}{1!} & \\ & & \ddots \\ 0 & & \frac{\pi^{J/2-1}}{(J/2-1)!} \end{bmatrix} \begin{bmatrix} 1 & 0 & \frac{1}{3} & 0 & \cdots \\ 0 & \frac{1}{3} & 0 & \cdots & \\ \frac{1}{3} & 0 & \cdots & & \\ 0 & \cdots & & & \end{bmatrix} \begin{bmatrix} \frac{\pi^0}{0!} & & 0 \\ & \frac{\pi^1}{1!} & \\ & & \ddots \\ 0 & & \frac{\pi^{J/2-1}}{(J/2-1)!} \end{bmatrix}. \tag{5.80}$$

Note that since M_0 is symmetrical, $\hat{D}$ will not be uniquely determined by (5.79). Specifically, there are only $(1+J/2)J/4$ independent equations for the $J^2/4$ elements of $\hat{D}$. Therefore, for simplicity, $\hat{D}$ will be further constrained to be an upper triangular matrix in this chapter so that it is uniquely specified. Except the number of taps which determines the dimension of M_0, it is evident that the third component preprocessor, based on receiver noise having flat spectrum, is independent of all other parameters.

To see in more detail the structure of the preprocessing, note that with U_g having the form of (5.30), the $(M-1)J \cdot 2(M-1)$ matrix F_g, given by (5.70), also has the form

$$F_g = \begin{bmatrix} \hat{F}_g & & 0 \\ & \hat{F}_g & \\ & & \ddots \\ 0 & & \hat{F}_g \end{bmatrix} \tag{5.81}$$

where $\hat{F}_g$ has dimension J·2 and is related to $\hat{U}_g$ by

$$\hat{F}_g^T \hat{U}_h = k_{gh} I. \tag{5.82}$$

Therefore, summarizing, the preprocessor L is, from the various equations,

$$L = \left[\begin{array}{c|c|c|c} \begin{matrix}\hat{F}_0 & 0 \\ & \hat{F}_0 \\ 0 & \ddots \end{matrix} & \begin{matrix}\hat{F}_1 & 0 \\ & \hat{F}_1 \\ 0 & \ddots \end{matrix} & \cdots & \begin{matrix}\hat{F}_{J/2-1} & 0 \\ & \hat{F}_{J/2-1} \\ 0 & \ddots \end{matrix} \end{array}\right] \cdot \left[\begin{matrix} I & & & 0 \\ & B^{-1}I & & \\ & & \ddots & \\ 0 & & & B^{-J/2+1}I \end{matrix}\right] \left[\begin{matrix} d_{00}I & d_{01}I & \cdots & d_{0\,J/2-1}I \\ & d_{11}I & & d_{1\,J/2-1}I \\ & 0 & \ddots & \vdots \\ & & & d_{J/2-1\,J/2-1}I \end{matrix}\right] \tag{5.83}$$

where $\hat{F}_g$ is specified in terms of (5.82) with (5.28) and (5.29) giving $\hat{U}_g$, while d_{gh}, h=g,··,J/2-1, is given in terms of (5.79) with (5.80) giving M_0. The preprocessor obviously does not require any measurement regarding the environment and depends only on the number of taps, tap spacing and bandwidth. Furthermore, from the numbering of the inputs in fig.4.1, the defining equation of (5.60) for the preprocessor and the structure of the matrices in (5.83), the (M-1)J dimension preprocessing L on the inputs from elements 2, 3, ·· and M is composed of M-1 identical preprocessings, each transforming the J inputs behind only one of these elements. Specifically, the preprocessing for the inputs behind element m+1, m=1, ··,M-1, is given by

$$\begin{bmatrix} \tilde{x}_{2m-1}(k) \\ \tilde{x}_{2m}(k) \\ \tilde{x}_{2(M-1)+2m-1}(k) \\ \tilde{x}_{2(M-1)+2m}(k) \\ \vdots \\ \tilde{x}_{2(M-1)(J/2-1)+2m-1}(k) \\ \tilde{x}_{2(M-1)(J/2-1)+2m}(k) \end{bmatrix} = \hat{L}^T \begin{bmatrix} x_{(m-1)J+1}(k) \\ x_{(m-1)J+2}(k) \\ \vdots \\ x_{mJ}(k) \end{bmatrix} \tag{5.84}$$

where $\hat{L}$, being independent of m, is

$$\hat{L} = \hat{F}\left(\begin{bmatrix} 1 & & & 0 \\ & B^{-1} & & \\ & & \ddots & \\ 0 & & & B^{-J/2+1} \end{bmatrix} \times \begin{bmatrix} 1 & 0 \\ 0 & 1 \end{bmatrix}\right) \tag{5.85}$$

$$\cdot \left(\begin{bmatrix} d_{00} & d_{01} & \cdots & d_{0\,J/2-1} \\ & d_{11} & & d_{1\,J/2-1} \\ & & \ddots & \vdots \\ 0 & & & d_{J/2-1\,J/2-1} \end{bmatrix} \times \begin{bmatrix} 1 & 0 \\ 0 & 1 \end{bmatrix}\right)$$

and

$$\hat{F} = [\hat{F}_0 \; \hat{F}_1 \cdots \hat{F}_{J/2-1}]. \tag{5.86}$$

Note that in (5.84), the numbering of the transformed inputs is different from that of the original inputs. Using (5.79) and (5.80), the upper triangular matrix in the last factor of (5.85), $\hat{D}$, is tabulated in table 5.1 for arrays with 2-8 taps. Similarly, using (5.28), (5.29), (5.82) and (5.86), $\hat{F}$ is tabulated in table 5.2 at $1/4f_0$ tap spacing for arrays with 2-8 taps. Evidently, the preprocessing shown can easily be implemented at this tap spacing. At other tap spacing, the preprocessing expressed by $\hat{F}$ is more complex and not so elegant.

Finally, it should be noted that there are a few arbitrary elements in the above derivation of the preprocessor. Specifically, although the forms of the first and second component preprocessors

Number of taps	$\hat{D}$
2	$\begin{bmatrix} 0!/\pi^0 \end{bmatrix}\begin{bmatrix} 1 \end{bmatrix}$
4	$\begin{bmatrix} 0!/\pi^0 & 0 \\ 0 & 1!/\pi^1 \end{bmatrix}\begin{bmatrix} 1 & 0 \\ 0 & 3^{1/2} \end{bmatrix}$
6	$\begin{bmatrix} 0!/\pi^0 & 0 & 0 \\ 0 & 1!/\pi^1 & 0 \\ 0 & 0 & 2!/\pi^2 \end{bmatrix}\begin{bmatrix} 1 & 0 & -5^{1/2}/2 \\ 0 & 3^{1/2} & 0 \\ 0 & 0 & 5^{1/2}3/2 \end{bmatrix}$
8	$\begin{bmatrix} 0!/\pi^0 & 0 & 0 & 0 \\ 0 & 1!/\pi^1 & 0 & 0 \\ 0 & 0 & 2!/\pi^2 & 0 \\ 0 & 0 & 0 & 3!/\pi^3 \end{bmatrix}\begin{bmatrix} 1 & 0 & -5^{1/2}/2 & 0 \\ 0 & 3^{1/2} & 0 & 7^{1/2}3/2 \\ 0 & 0 & 5^{1/2}3/2 & 0 \\ 0 & 0 & 0 & 7^{1/2}5/2 \end{bmatrix}$

Table 5.1 Tabulation of $\hat{D}$ with number of taps equal to 2, 4, 6 and 8. $\hat{D}$ is upper triangular and specifies the third component preprocessor, $\hat{D}xI$, for equalizing, for small bandwidth, the eigenvalues of the transformed covariance matrix due to only receiver noise.

Number of taps	$\hat{F}$
2	$\begin{bmatrix} 0 & -1 \\ -1 & 0 \end{bmatrix}$
4	$\begin{bmatrix} 0 & -1/2 & 2 & 0 \\ -1/2 & 0 & 0 & -2 \\ 0 & 1/2 & 2 & 0 \\ 1/2 & 0 & 0 & -2 \end{bmatrix}$
6	$\begin{bmatrix} 0 & -1/3 & 1 & 0 & 0 & 2 \\ -1/3 & 0 & 0 & -1 & 2 & 0 \\ 0 & 1/3 & 0 & 0 & 0 & 4 \\ 1/3 & 0 & 0 & 0 & 4 & 0 \\ 0 & -1/3 & -1 & 0 & 0 & 2 \\ -1/3 & 0 & 0 & 1 & 2 & 0 \end{bmatrix}$
8	$\begin{bmatrix} 0 & -1/4 & 3/5 & 0 & 0 & 1 & -4/3 & 0 \\ -1/4 & 0 & 0 & -3/5 & 1 & 0 & 0 & 4/3 \\ 0 & 1/4 & -1/5 & 0 & 0 & 1 & -4 & 0 \\ 1/4 & 0 & 0 & 1/5 & 1 & 0 & 0 & 4 \\ 0 & -1/4 & -1/5 & 0 & 0 & -1 & -4 & 0 \\ -1/4 & 0 & 0 & 1/5 & -1 & 0 & 0 & 4 \\ 0 & 1/4 & 3/5 & 0 & 0 & -1 & -4/3 & 0 \\ 1/4 & 0 & 0 & -3/5 & -1 & 0 & 0 & 4/3 \end{bmatrix}$

Table 5.2 Tabulation of $\hat{F}$ with number of taps equal to 2, 4, 6 and 8 at $1/4f_0$ tap spacing. $\hat{F}$ specifies the first component preprocessor which renders, for small bandwidth, the transformed covariance matrix to be independent of tap spacing and apart from the dimension of the matrix, also the number of taps.

for rendering the eigenvalues to be roughly independent of bandwidth, tap spacing and apart from the dimension of the matrices concerned, the number of taps are quite obvious, the choosing of the third component preprocessor is in certain sense similar to the choosing of the feedback factors for the narrowband processors in the alternative system and hence is not so obvious. Thus, instead of choosing the feedback factors so as to equalize the eigenvalues due to only receiver noise, the smallest eigenvalues possible, it may also be of interest to normalize, as for an ideal narrowband array, the feedback factors with respect to the element powers seen by the narrowband processors in the alternative system. Similarly, for the preprocessed Frost system, the third component preprocessor may be chosen to equalize the powers of the transformed inputs instead of equalizing the eigenvalues due to only receiver noise. Obviously, the third component preprocessor will then become a diagonal matrix and together with the second component preprocessor, can be implemented simply by employing AGC circuits. For simplicity, these alternatives will not be investigated.

5.6.2 Theoretical analysis on the consequences of the preprocessor

Having derived the preprocessor in the last subsection, this subsection will analyze in more detail, theoretically for small bandwidth, the consequences of the preprocessor. With the same reason as investigating the Frost system, the analysis will be concerned principally with the eigenvalues, though the eigenvectors will also be briefly discussed.

Firstly, with D given by (5.75) and as described in appendix 5.9.2, C^{0}_{ghn}, n=1,··,N, g,h=0,··,J/2-1, having the form of (5A.31), the matrix sum under the summation of n in (5.74) clearly has the

form of (5A.36), except that the dimension should now be (M-1)J· (M-1)J. Thus, the eigenvalues due to this matrix sum will be in equal pairs. From also the discussion in the last subsection regarding the third component preprocessor D, the general structure of the eigenvalues of the transformed covariance matrix can then be summarized, for small bandwidth, by

The transformed covariance matrix has in general NJ/2+1 distinct eigenvalues. The largest NJ/2, each of multiplicity 2, are due to the jammers and receiver noise. The smallest eigenvalue, of multiplicity (M-N-1)J, is equal to s_0 and is due to only receiver noise. (5.87)

Note that again, the smallest eigenvalue is due to only receiver noise as the presence of the jammers cannot lead to smaller eigenvalues. Regarding the structure of the eigenvectors, it is obvious that the eigenvectors associated with the jammers and receiver noise together span the same subspace as that spanned together by $I \times Q_1$, $I \times Q_2$, ·· and $I \times Q_N$, while those associated with only receiver noise are given by the columns of IxE and together span the complimentary subspace.

Consider now the interesting and significant case when all the jammers have flat spectrums. With R^0_{gh}, D and M_0 given by (5.48), (5.75) and (5.76) respectively, the transformed covariance matrix of (5.73) becomes, for small bandwidth,

$$\tilde{R} \simeq (\hat{D}^T \times I)(M_0 \times \sum_{n=0}^{N} s_n Q_n Q_n^T)(\hat{D} \times I). \tag{5.88}$$

Using (5.79) and the mathematical theorem of (5.77), this yields

$$\tilde{R} \simeq (\hat{D}^T M_0 \hat{D}) \times \sum_{n=0}^{N} s_n Q_n Q_n^T = I \times \sum_{n=0}^{N} s_n Q_n Q_n^T. \tag{5.89}$$

The structure of the eigenvalues of the transformed covariance matrix can then be summarized in addition to (5.87) by

If all the jammers have flat spectrums, each eigenvalue for an ideal narrowband array in the same environment becomes an eigenvalue, with multiplicity J/2, of the transformed covariance matrix. (5.90)

Clearly, the J/2 associated eigenvectors are given by the columns of the Kronecker product of I and the corresponding eigenvector of the ideal narrowband array. Evidently, in this situation, the preprocessor is the best in the sense that the "temporal" spread of eigenvalues has been reduced to zero and thus the spread of eigenvalues is due only to the spatial and power distributions of the jammers, at least for small bandwidth. Furthermore, from (5.89), the transformed covariance matrix is now reduced by the preprocessor to a block diagonal form, illustrating that the transformed inputs have become block decorrelated. Specifically, if the (M-1)J transformed inputs are divided into J/2 groups with the ith group consisting of the 2(M-1)(i-1)+1th to the 2(M-1)ith transformed inputs, then each group of transformed inputs will be uncorrelated with the other groups of transformed inputs and give rise to the same covariance matrix as that for an ideal narrowband array in the same environment. (Note that even if not all the jammers' spectrums is flat, each group of transformed inputs will, from (5.73) and (5.75), still give rise to the same covariance matrix as that for an ideal narrowband array, but not in the same environment.) The block decorrelation is of course of importance in applications when, say, the hardware for updating the weights is limited so that the weights are updated in a time-multiplexed sequence. Thus, for example, it will be practical and more efficient to first update the weights associated with only the first group of transformed inputs until convergence is nearly achieved. If the output power reduction is not adequate, updating can then be carried out for

the weights associated with only the second group of transformed inputs until, again, convergence is nearly reached. Updating can then be applied to the next group of weights if the output power reduction is still not satisfactory and so on until eventually, the output power is small enough. All later updating of weights to keep track of the changing environment can then be limited to only the weights which have been updated, that is, which give rise to significant output power reduction. In this way, the weights that give practically no decrease in output power will not be updated, hence improving the overall convergence behaviour. Of course, as the bandwidth increases or the jammers' spectrums deviate from flat ones, the block decorrelation introduced by the preprocessor will become less and less perfect. Nevertheless, the scheme described is obviously still useful even though the transformed inputs may only be partially block decorrelated. For simplicity, this scheme and similar ones will not be studied in this chapter. Note that because of the partial block decorrelation, the tapped delay line processing has become essentially several narrowband processings in parallel. The difference with the alternative broadband processing is obviously that while this is based on the use of preprocessing on tapped delay lines, the alternative broadband processing is based on using bandpass filters. Of course, the preprocessor can be viewed as performing filtering operations.

When all the jammers have flat spectrums, the trace of the transformed covariance matrix, from (5.89), is

$$\mathrm{tr}\tilde{R} \approx (M-1)J \sum_{n=0}^{N} s_n . \tag{5.91}$$

Since, from (5.87), the smallest eigenvalue is equal to s_0, the set of time constants, $\{\tau_p\}$, for the preprocessed Frost system is

thus bounded, using (5.18), by

$$\{\tau_P\} \leq B_P \tag{5.92}$$

where

$$B_P \approx \frac{ENR(M-1)J}{4M_{wt}} \text{ sampling period} \tag{5.93}$$

With the structure of the eigenvalues as described by (5.90), this bound is obviously also loosely approached in situations where the bound B_N of (5.23) for the alternative system is loosely approached. Moreover, from (5.23) and (5.93), the ratio of the bounds is

$$\frac{B_P}{B_N} \approx \frac{J}{J_N} \tag{5.94}$$

and gives the ratio of any time constant in the preprocessed Frost system to that due to the corresponding eigenvalue in the alternative system. In particular, this gives the ratio of the effective time constants and as the ratio B_F/B_N, can be used as a crude measure for comparing the convergence behaviour of the two systems. From (5.94), the ratio B_P/B_N is equal to the ratio of the number of weights required in using tapped delay line processing to that should the alternative broadband processing be used. The reciprocal of the latter ratio is plotted against bandwidth in fig.4.22 at 20 and 40dB MENR, using (4.56b,c) and (4.61) with the operation $\lfloor\cdot\rfloor$ neglected for convenience. Obviously, with the preprocessor, the slow convergence behaviour of the Frost system, relative to the alternative system, has been improved to slightly better than the latter system. Furthermore, contrary to the Frost system, the preprocessed Frost system has even better convergence behaviour relative to the alternative system when the MENR and for bandwidth less than about 20%, the bandwidth increase.

The comparison of the preprocessed Frost and alternative

system in the last paragraph has been based on all the jammers having flat spectrums. As may be expected intuitively, it has been found from simulation results that the eigenvalues are fairly insensitive to variation in the jammers' spectrums, unless the changes are so drastic as to result in say, effectively narrowband jamming. Therefore, the comparison discussed will still roughly hold in most cases. Specifically, the effective time constants of the preprocessed Frost system will not be very different from, perhaps slightly shorter than, those of the alternative system and the ratio B_P/B_N is relevant for roughly comparing the final effective time constants of the two systems. Mathematically, by using (5.33) and (5.73), the trace of the transformed covariance matrix is shown in appendix 5.9.3 to be bounded by

$$\mathrm{tr}\tilde{R} \approx \frac{(M-1)J^2}{2} \sum_{n=0}^{N} s_n \qquad (5.95)$$

with equality when there is no receiver noise and all the jammers have spectrums consisting of only delta functions at either band edges. Substituting into (5.18) with the smallest eigenvalue, due to only receiver noise, being s_0, the bound B_P now becomes

$$B_P \approx \frac{ENR(M-1)J^2}{8M_{wt}} \text{ sampling period} \qquad (5.96)$$

which is not very different from (5.93). Evidently, this gives one indication for the general validity of the comparison discussed and that the preprocessor works in all situations.

Summarizing, from the elegant (5.27) for the covariance matrix, a transformation preprocessor has been derived and for small bandwidth, analyzed theoretically in this section. As discussed, the (M-1)J dimension preprocessing consists of M-1 identical prep-

rocessings, the mth preprocessing transforming only the J inputs behind the m+1th element. The preprocessor depends only on the tap spacing, bandwidth and number of taps and is particular simple at $1/4f_0$ tap spacing. With the preprocessor, the covariance matrix is rendered independent of bandwidth, tap spacing and apart from its dimension, the number of taps. The eigenvalues then have the elegant structure of (5.87) and (5.90). Furthermore, the inputs after preprocessing can now be divided into J/2 groups, the 2(M-1) transformed inputs in each group being partially decorrelated with the other groups of transformed inputs and having the same covariance matrix as that for an ideal narrowband array. The decorrelation is perfect when all the jammers have flat spectrums. Briefly, the preprocessor, which can be considered as equivalent to the set of bandpass filters in the alternative broadband processing method, has reduced the temporal spread of eigenvalues to virtual nonexistence. The effective time constants of the preprocessed Frost system are thus, in general, not very different from, perhaps slightly shorter than, those of the alternative system and the ratio of (5.94) can be used roughly for comparing the final effective time constants of the two systems.

5.7 Eigenvalues and Eigenvector Power Components after Preprocessing from Simulation Results

Having theoretically derived and discussed the preprocessor, this section will, in the same way as section 5.5, study the eigenvalues and eigenvector power components in the preprocessed Frost system so as to verify the important theoretical deductions as well as to provide more insight. Note that for the same reason as that when studying the Frost system, the eigenvector power components have not been investigated theoretically.

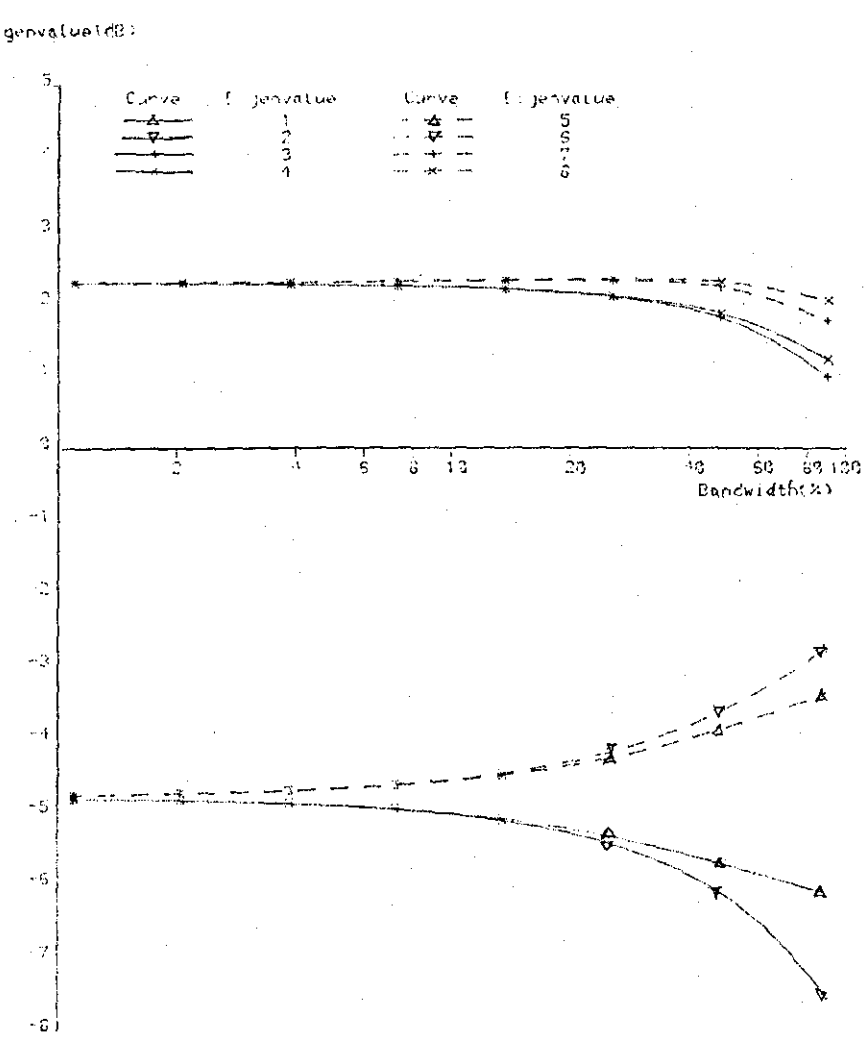

Fig.5.8a Eigenvalues

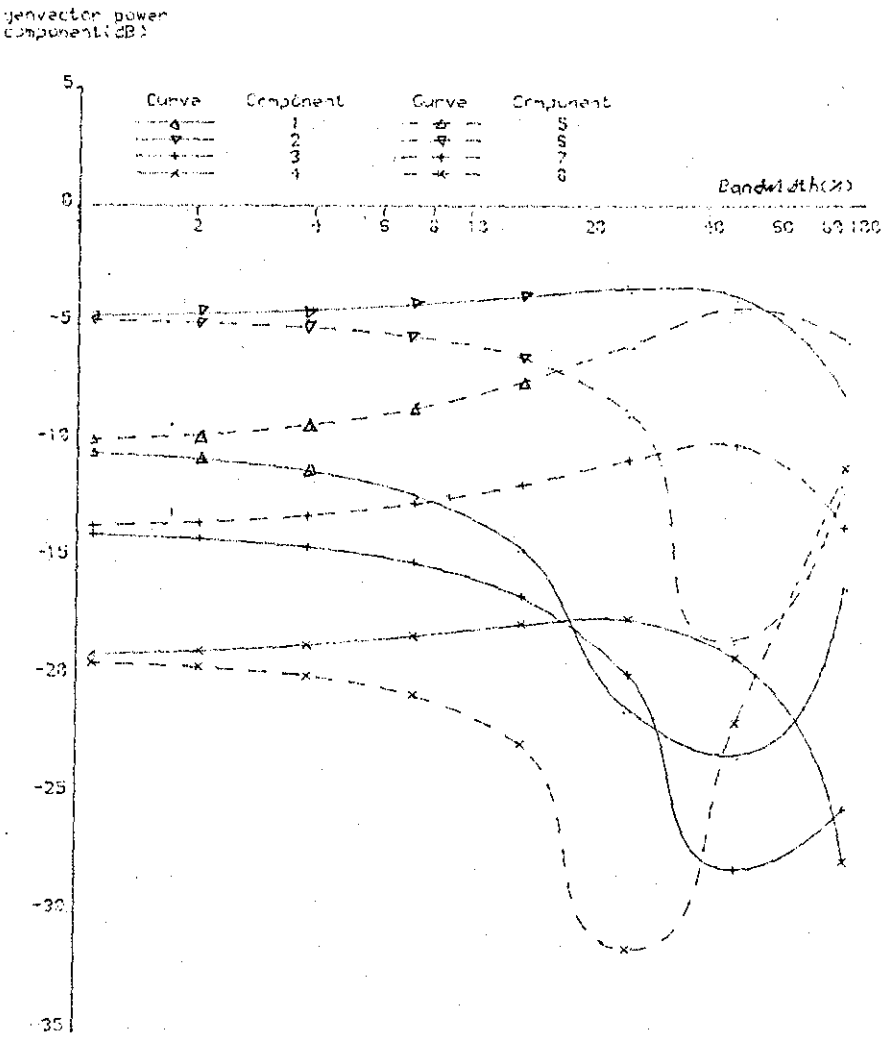

Fig.5.8b Eigenvector power components

Fig.5.8 Graphs of eigenvalues and eigenvector power components against bandwidth for the situation of fig.5.3 when preprocessing is employed.

Fig.5.8 shows graphs of eigenvalues and eigenvector power components against bandwidth for the situation of fig.5.3 when preprocessing is employed. For small bandwidth, the behaviour of the eigenvalues obviously agrees with the theoretical deductions of (5.87) and (5.90). In particular, the two groups of eigenvalues in fig.5.8a are separated by 7dB, roughly equal to the difference between the pairs of eigenvalues in either set of eigenvalues in fig.5.3a. From fig.5.8b, the eigenvector power components are proportional to B^0 for small bandwidth. Again, this indicates that the eigenvector components are proportional to B^0 which, as with the Frost system, has been found to be the case whenever all the spatial degrees of freedom are used to reject jammers whose spectrums have even symmetry. For larger bandwidth, the eigenvector power components have more complex behaviour. From fig.5.8, the final effective time constant can be seen to be always determined by the smallest eigenvalue which, having significant eigenvector power component relative to the optimal output power of about -15 dB in fig.5.3a, varies only slightly even at large bandwidth. Using (5.18) with the ratio of the trace of the transformed covariance matrix to the smallest eigenvalue being about 13dB (separation between the two groups of eigenvalues 7dB + number of large eigenvalues 6dB), this is roughly 50 sampling period at 10% misadjustment regardless of the bandwidth. Comparing with that for the alternative system of about 75 sampling period calculated earlier at 25% bandwidth, the preprocessed Frost system is now marginally faster by about 1.5 times, in agreement with the theoretical ratio B_P/B_N, from (5.94) and the alternative system needing 3 narrowband processors at 25% bandwidth, of 1.5. The improvement by the preprocessor on the convergence behaviour of the Frost system for ban-

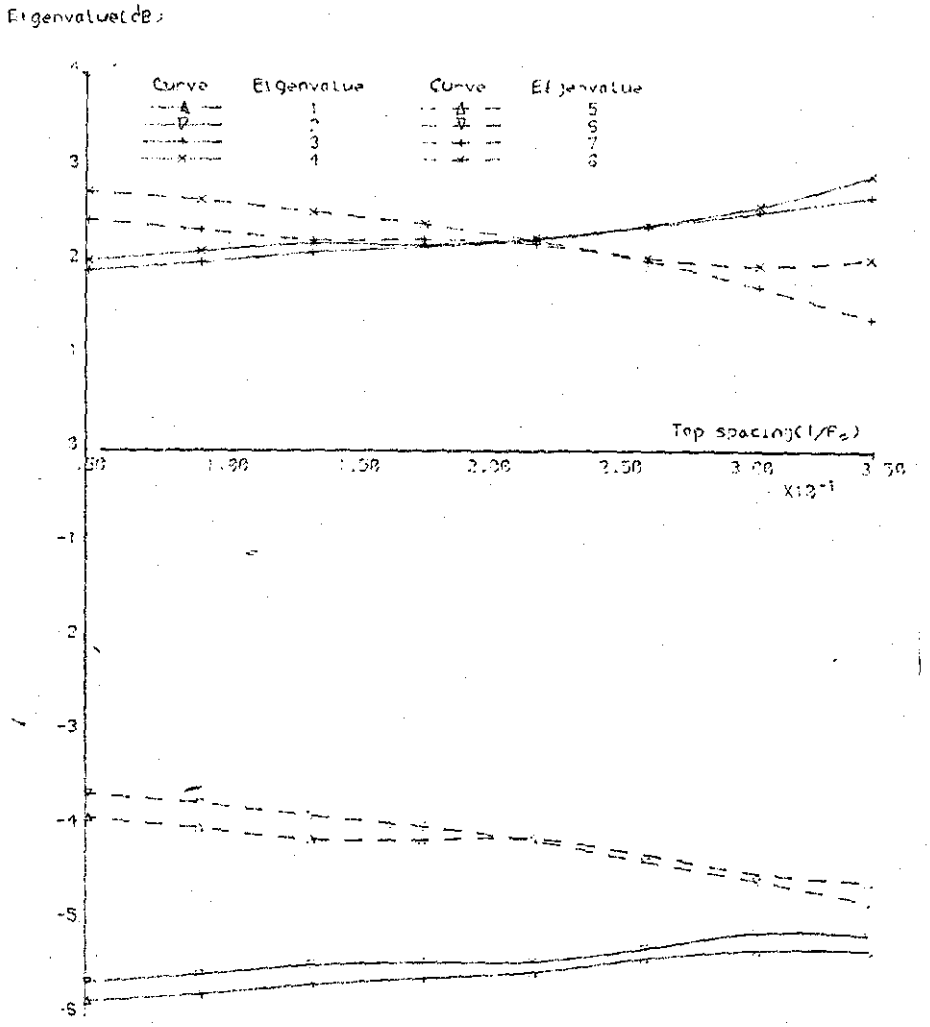

Fig.5.9 Graphs of eigenvalues against tap spacing for the situation of fig.5.8 at 25% bandwidth.

dwidth between 20 and 30% when the jamming is broadband and the smallest eigenvalue determines the final effective time constant is obvious.

Fig.5.9 shows graphs of eigenvalues against tap spacing for the situation of fig.5.8 at 25% bandwidth. Evidently, due to the preprocessor, the eigenvalues and so the effective time constants have become roughly independent of tap spacing. In particular, the spreading of the eigenvalues leading to deterioration in the convergence behaviour of the Frost system as the tap spacing deviates from $1/4f_0$ now does not exist. The preprocessed Frost system is as fast at any other tap spacing.

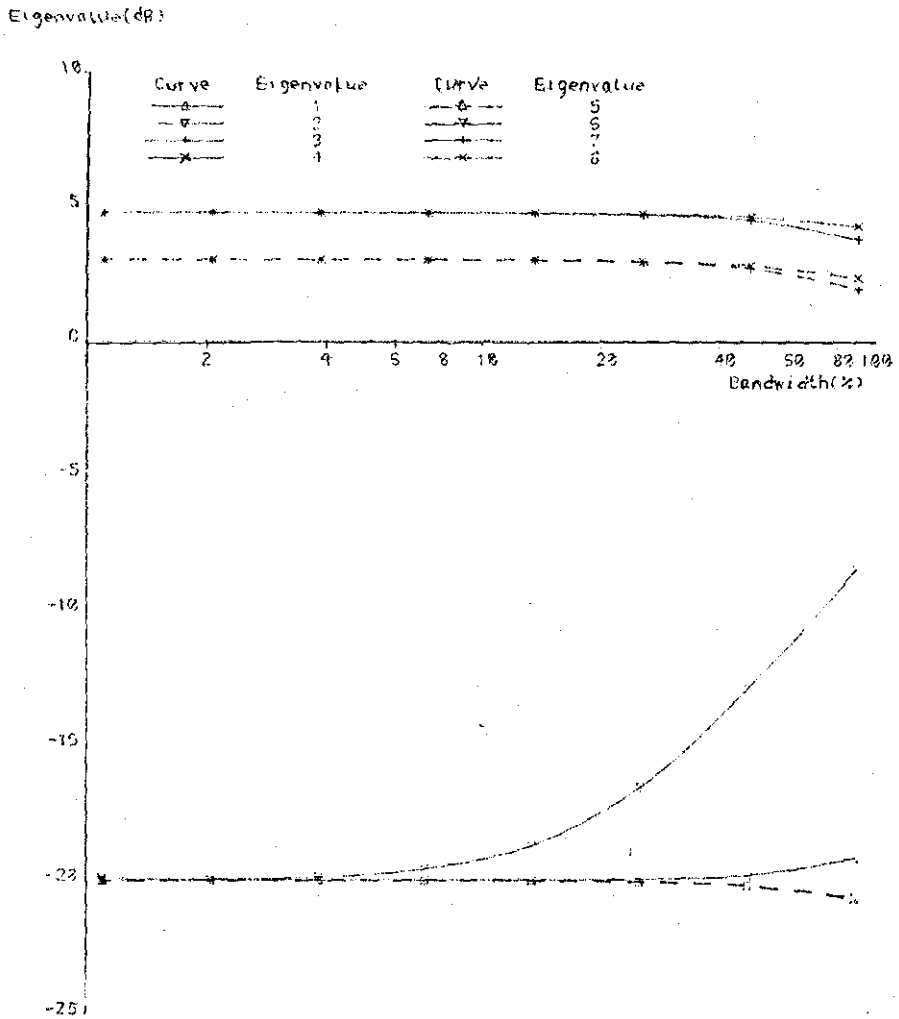

Fig.5.10a Eigenvalues

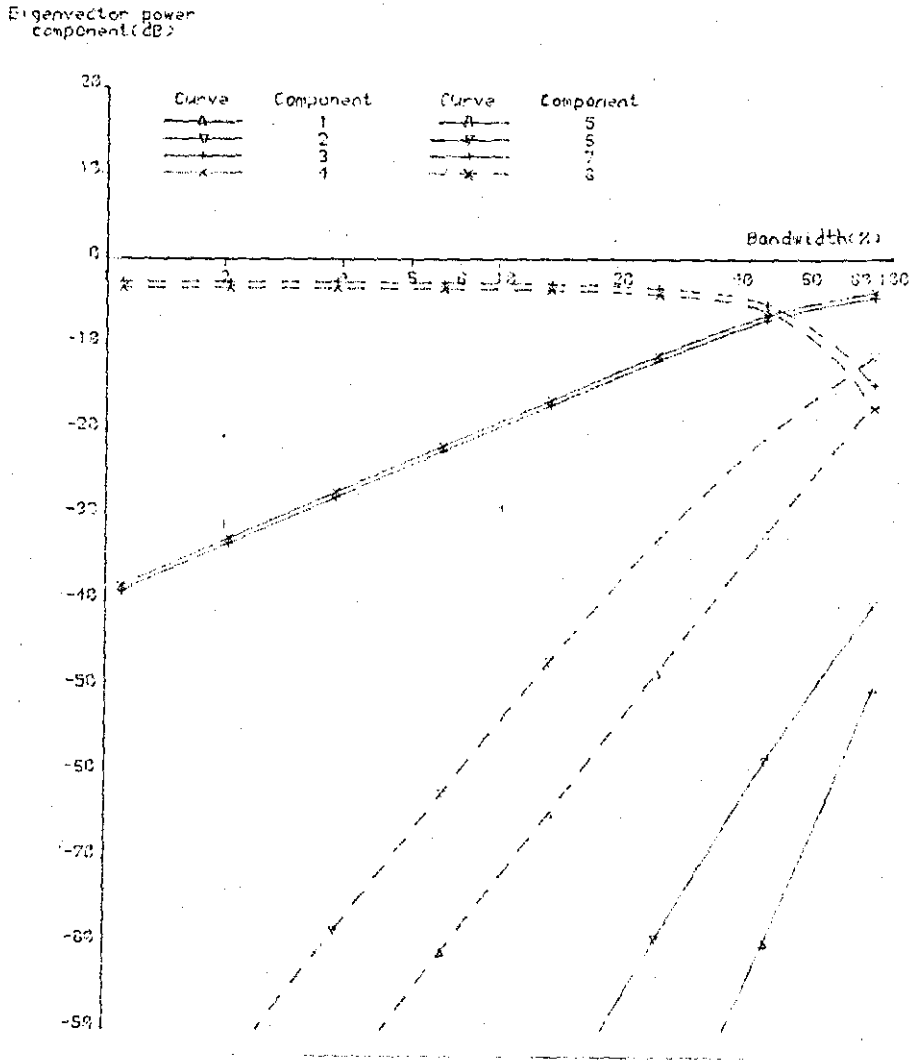

Fig.5.10b Eigenvector power components

Fig.5.10 Graphs of eigenvalues and eigenvector power components against bandwidth for the situation of fig.5.5 when preprocessing is employed.

Fig.5.10 shows graphs of eigenvalues and eigenvector power components against bandwidth for the situation of fig.5.5 when preprocessing is employed. For small bandwidth, the behaviour of the eigenvalues obviously agrees with the theoretical description of (5.87), although with the jammer having inverted-triangular spectrum, the theoretical deduction of (5.90) is now not valid. As the bandwidth increases, eigenvalue 2 can be seen to start to increase and become proportional to B^2 eventually. Of course, this results from the increase in the gradient of eigenvalue curve 2 in fig.5.5a from 20 to 40dB per decade. Generally, from also other simulation results, it has been found that if the spread of eigenvalues is large as when the jammers have very different powers, are closed together or the spatial degrees of freedom are not fully utilized, some of the small eigenvalues may increase and become proportional to some even powers of bandwidth as the bandwidth increases. From fig.5.10b, eigenvector power components 1, 2 and 5, 6 can be seen to be roughly proportional to B^6 and B^8 respectively. From also the optimal output power curve in fig.5.5a, these components, which are associated with eigenvalues due to only receiver noise, are obviously insignificant except at bandwidth so large that the performance of the array to reject the jammer has deteriorated. On the other hand, eigenvector power components 7, 8 and 3, 4 are roughly proportional to B^0 and B^2 respectively and are due to the jammer and receiver noise. Components 7, 8 are obviously always significant, while components 3, 4 are only significant for bandwidth greater than about 10%. These observations are fairly general and are also obtained from other simulation results. Specifically, in situations to be expected when the ENR is less than the designed MENR, the eigenvector power components ass-

ociated with eigenvalues due to only receiver noise are usually proportional to large even powers of bandwidth and insignificant, while the other components due to the jammers and receiver noise are proportional to small even powers of bandwidth and can be significant. Using arguments and calculations similar to that with fig.5.8, the effective time constants in this situation can also be verified to be roughly the same as those for the alternative system. Illustrating again the relevance of the ratio B_P/B_N, this has been found to be so in most of the situations studied. There are only a few situations where the final effective time constants of the two systems differ by more than say, a factor of 10. In any case, the time constants in the preprocessed Frost system will be less than the bound of (5.96), at least for small bandwidth.

Finally, fig.5.11 shows graphs of eigenvalues against bandwidth for the situation of fig.5.10 except that the jammer has triangular spectrum instead. Obviously, the eigenvalues in the two figures are roughly identical except that due to the jammer's spectrum becoming peaky towards the centre of the band, eigenvalues 3 and 4, due to the jammer and receiver noise, are now smaller. As may be expected, this phenomenon is also generally observed.

Summarizing, the eigenvalues and eigenvector power components after preprocessing have been investigated by using simulation results in this section. The important theoretical deductions of the last section have been verified. Specifically, the structure of the eigenvalues as given by (5.87) and (5.90) is valid to bandwidth of tens of percents depending on the environment. Furthermore, the effective time constants of the preprocessed Frost and alternative system are not very different and the relevance of the ratio B_P/B_N of (5.94) for roughly comparing the final effective

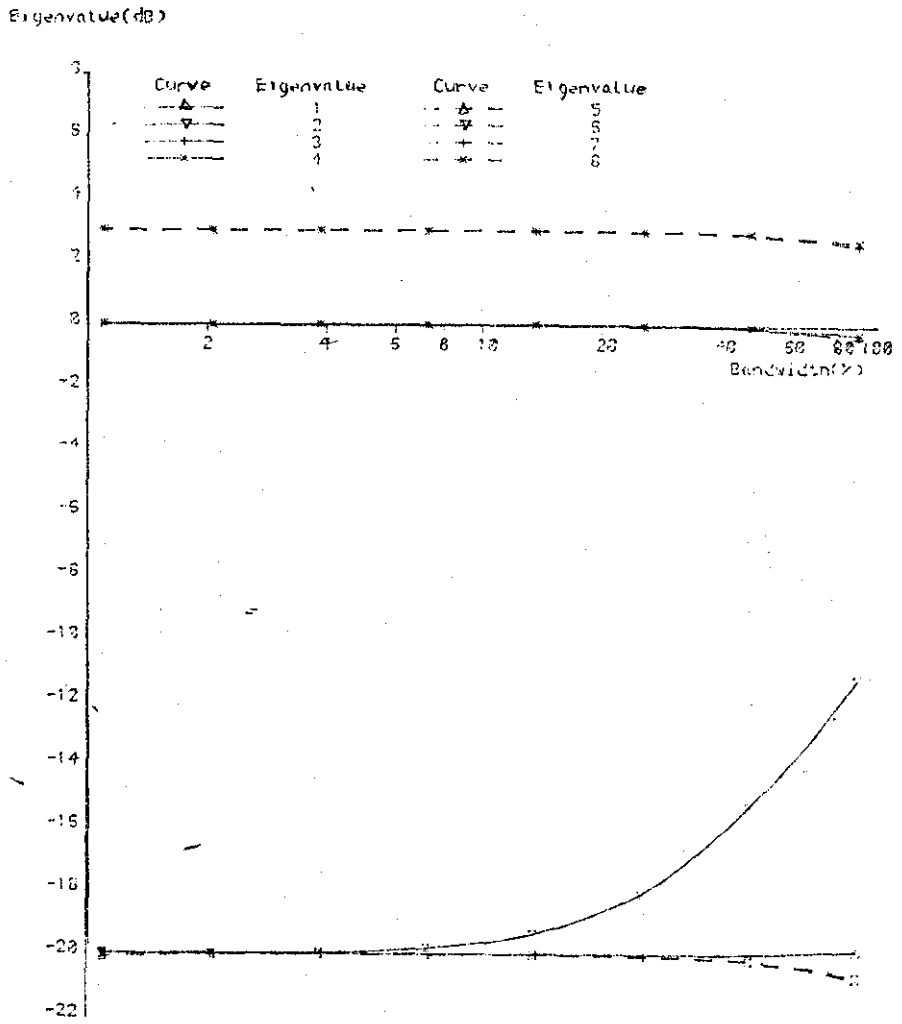

Fig.5.11 Graphs of eigenvalues against bandwidth for the situation of fig.5.10 except with the jammer having triangular spectrum instead.

time constants of the two systems is illustrated. The results also show that the eigenvector power components usually have more complex behaviour than the eigenvalues and moreover, those associated with eigenvalues due to only receiver noise are insignificant when the ENR is below the designed MENR.

5.8 Conclusion

The convergence behaviour of the broadband tapped delay line Frost system has been formulated in this chapter. Particularly, the output power converges as a sum of exponentially decaying components with time constants inversely proportional to the eigenva-

lues of the covariance matrix. By expressing the autocorrelation functions of the jammers and receiver noise in power series of bandwidth, the covariance matrix was manipulated into an elegant form, (5.27). With the assumption of small bandwidth, the elegant structure of the eigenvalues, as described by (5.42), (5.47) and (5.52), was then derived. Briefly, the eigenvalues can be divided into (number of taps)/2 sets. The eigenvalues in the ith set are proportional to the 2(i-1)th power of bandwidth and should the tap spacing be equal to a quarter wavelength delay at the centre frequency, have the same structure as that for an ideal narrowband array. The lower bound of (5.57) for the convergence time constants was then derived and compared with (5.23) for the alternative broadband system using several narrowband processors. This shows that the Frost system can be considerably slower than the alternative system in broadband jamming environments, although the two systems have roughly the same effective time constants if the jamming is effectively narrowband. For example, the final effective time constants can differ by a factor of 10 at 20% bandwidth and 20dB element to receiver noise power ratio and increases as the two parameters increase and also as the tap spacing deviates from a quarter wavelength delay at the centre frequency. From the elegant (5.27) for the covariance matrix, a transformation preprocessor was derived. The preprocessor depends only on the number of taps, tap spacing and bandwidth and is particular simple at the tap spacing just mentioned. Assuming small bandwidth, the array inputs after preprocessing was found to be partially block decorrelated and give rise to eigenvalue structure as described by (5.87) and (5.90). Briefly, the eigenvalues are now independent of tap spacing and bandwidth and have spread due effectively to only the power

and spatial distributions of the jammers. Thus, the preprocessor is essentially equivalent to the set of bandpass filters used in the alternative system. With the preprocessor, the Frost system was then deduced to have effective time constants not very different from, perhaps slightly shorter than, that of the alternative system in all environments. Generally verifying all these important deductions to bandwidth of tens of percents, simulation results have also been examined to provide more insight.

5.9 Appendix

5.9.1 Formulation of the covariance matrix in the form of (5.26) and derivation of (5.27)

With reference to (5.26), consider now R_{pn}, $p=0,\cdot\cdot,\infty$, $n=1,\cdot\cdot,N$, due to the nth jammer and associated with the pth power of bandwidth. Partitioning R_{pn} as

$$R_{pn} = \begin{bmatrix} A_{11} & A_{12} & \cdots & A_{1\,M-1} \\ A_{21} & A_{22} & & \\ \vdots & & & \\ A_{M-1\,1} & & & \end{bmatrix}, \qquad (5A.1)$$

A_{st}, $s,t=1,\cdot\cdot,M-1$, of dimension $J\cdot J$, is obviously the component covariance matrix giving the covariances concerned between the inputs behind the s+1th element with those behind the t+1th element. Hence, defining

$$d_n = \frac{d\sin\theta_n}{c} \qquad (5A.2)$$

$$= \text{difference in time of arrival between adjacent element inputs due to the nth jammer}$$

and using (5.24), the (u,v) element of A_{st} is

$$[A_{st}]_{uv} = \frac{s_n M_{pn} \pi^p}{p!} f_0^p [(u\tau + sd_n) - (v\tau + td_n)]^p \qquad (5A.3)$$

$$\cdot \cos\{2\pi f_0[(u\tau + sd_n) - (v\tau + td_n)] + \frac{\pi p}{2}\}.$$

Using the binomial expansion, the factor $f_0^{\,p}[(u\tau+sd_n)-(v\tau+td_n)]^p$ can be expressed as

$$\begin{aligned} & f_0^{\,p}[(u\tau + sd_n) - (v\tau + td_n)]^p \\ &= \sum_{q=0}^{p} \binom{p}{q} [f_0(u\tau + sd_n)]^{p-q} [f_0(v\tau + td_n)]^q \cos\pi q \\ &= \sum_{q=0}^{p} \sum_{g=0}^{p-q} \sum_{h=0}^{q} \binom{p}{q}\binom{p-q}{g}\binom{q}{h} (f_0 sd_n)^{p-q-g} (f_0 td_n)^{q-h} \\ &\quad \cdot (f_0 u\tau)^g (f_0 v\tau)^h \cos\pi q. \end{aligned} \tag{5A.4}$$

Substituting into (5A.3) then gives

$$\begin{aligned} [A_{st}]_{uv} = \frac{s_n M_{pn} \pi^p}{p!} & \sum_{q=0}^{p} \sum_{g=0}^{p-q} \sum_{h=0}^{q} \binom{p}{q}\binom{p-q}{g}\binom{q}{h} (f_0 sd_n)^{p-q-g} \\ & \cdot (f_0 td_n)^{q-h} (f_0 u\tau)^g (f_0 v\tau)^h \\ & \cdot \cos\{2\pi f_0[(u-v)\tau + (s-t)d_n] + \frac{\pi}{2}(p-2q)\}. \end{aligned} \tag{5A.5}$$

Considering the definition of (5.28) for $\hat{P}_g$ being valid for g=0,$\cdots$, ∞ in this appendix, the last three factors together are obviously equal to the (u,v) element of

$$\begin{aligned} & \hat{P}_g \begin{bmatrix} \cos[2\pi f_0(s-t)d_n + \frac{\pi}{2}(p-2q-g+h)] & -\sin[2\pi f_0(s-t)d_n + \frac{\pi}{2}(p-2q-g+h)] \\ \sin[2\pi f_0(s-t)d_n + \frac{\pi}{2}(p-2q-g+h)] & \cos[2\pi f_0(s-t)d_n + \frac{\pi}{2}(p-2q-g+h)] \end{bmatrix} \hat{P}_h^{\,T} \\ & \quad = \hat{P}_g \hat{Q}_{p-q-g\ ns} \hat{Q}_{q-h\ nt}^{\ T} \hat{P}_h^{\,T} \end{aligned} \tag{5A.6}$$

where

$$\hat{Q}_{gns} = \begin{bmatrix} \cos(2s\pi f_0 d_n + \frac{\pi g}{2}) & -\sin(2s\pi f_0 d_n + \frac{\pi g}{2}) \\ \sin(2s\pi f_0 d_n + \frac{\pi g}{2}) & \cos(2s\pi f_0 d_n + \frac{\pi g}{2}) \end{bmatrix}. \tag{5A.7}$$

Clearly, from (5A.5) and (5A.6), A_{st} can be written in matrix form as

$$\begin{aligned} A_{st} = \frac{s_n M_{pn} \pi^p}{p!} & \sum_{q=0}^{p} \sum_{g=0}^{p-q} \sum_{h=0}^{q} \binom{p}{g}\binom{p-q}{g}\binom{q}{h} (f_0 sd_n)^{p-q-g} \\ & \cdot (f_0 td_n)^{q-h} \hat{P}_g \hat{Q}_{p-q-g\ ns} \hat{Q}_{q-h\ nt}^{\ T} \hat{P}_h^{\,T}. \end{aligned} \tag{5A.8}$$

Therefore, by defining

$$P_g = \begin{bmatrix} \hat{P}_g & & 0 \\ & \hat{P}_g & \\ & & \ddots \\ 0 & & \hat{P}_g \end{bmatrix} \qquad (5A.9)$$

and

$$Q_{gn} = \begin{bmatrix} (f_0 d_n)^g \hat{Q}_{gn1} \\ (2f_0 d_n)^g \hat{Q}_{gn2} \\ \vdots \\ [(M-1)f_0 d_n]^g \hat{Q}_{gn\ M-1} \end{bmatrix}, \qquad (5A.10)$$

R_{pn}, from (5A.1) and (5A.8), becomes

$$R_{pn} = \frac{s_n M_{pn} \pi^p}{p!} \sum_{q=0}^{p} \sum_{g=0}^{p-q} \sum_{h=0}^{q} \binom{p}{q} \binom{p-q}{g} \binom{q}{h} P_g Q_{p-q-g\ n} Q_{q-h\ n}^T P_h^T. \qquad (5A.11)$$

Consider now R_{p0}, due to receiver noise, in (5.26). Because receiver noise is independent between elements, R_{p0} clearly has the form

$$R_{p0} = \begin{bmatrix} A & & 0 \\ & A & \\ & & \ddots \\ 0 & & A \end{bmatrix} \qquad (5A.12)$$

where A, of dimension $J \cdot J$, is the component covariance matrix concerned due to receiver noise for inputs behind one of element 2 to M. The (u,v) element of A is obviously also given by (5A.5) with $s_n M_{pn}$ replaced by $s_0 M_{p0}$ and $f_0 s d_n$ equal to $f_0 t d_n$ equal to, say, 1 for convenience. Therefore, with the same manipulation leading to (5A.8) from (5A.5), A is given by

$$A = \frac{s_0 M_{p0} \pi^p}{p!} \sum_{q=0}^{p} \sum_{g=0}^{p-q} \sum_{h=0}^{q} \binom{p}{q} \binom{p-q}{g} \binom{q}{h} \hat{P}_g \hat{Q}_{p-q-g\ 0} \hat{Q}_{q-h\ 0}^T \hat{P}_h^T \qquad (5A.13)$$

where

$$\hat{Q}_{g0} = \begin{bmatrix} \cos\frac{\pi g}{2} & -\sin\frac{\pi g}{2} \\ \sin\frac{\pi g}{2} & \cos\frac{\pi g}{2} \end{bmatrix}. \qquad (5A.14)$$

Thus, with P_g given by (5A.9) and defining Q_{g0} as

$$Q_{g0} = \begin{bmatrix} \hat{Q}_{g0} & & 0 \\ & \hat{Q}_{g0} & \\ & & \ddots \\ 0 & & \hat{Q}_{g0} \end{bmatrix}, \qquad (5A.15)$$

R_{p0}, from (5A.12) and (5A.8), becomes

$$R_{p0} = \frac{s_n M_{p0} \pi^p}{p!} \sum_{q=0}^{p} \sum_{g=0}^{p-q} \sum_{h=0}^{q} \binom{p}{q}\binom{p-q}{g}\binom{q}{h} P_g Q_{p-q-g\ 0} Q_{q-h\ 0}{}^T P_h{}^T \qquad (5A.16)$$

which has the same form as (5A.11).

Substituting (5A.11) and (5A.16) into (5.26) then gives the covariance matrix as

$$R = \sum_{n=0}^{N} \sum_{p=0}^{\infty} \sum_{q=0}^{p} \sum_{g=0}^{p-q} \sum_{h=0}^{q} \frac{s_n M_{pn} (\pi B)^p}{p!} \binom{p}{q}\binom{p-q}{g}\binom{q}{h} \qquad (5A.17)$$
$$\cdot P_g Q_{p-q-g\ n} Q_{q-h\ n}{}^T P_h{}^T.$$

Applying the mathematical theorem (4.12), this becomes

$$R = \sum_{n=0}^{N} \sum_{p,q=0}^{\infty} \sum_{g=0}^{p} \sum_{h=0}^{q} \frac{s_n M_{p+q\ n} (\pi B)^{p+q}}{(p+q)!} \binom{p+q}{q}\binom{p}{g}\binom{q}{h} P_g Q_{p-g\ n} Q_{q-h\ n}{}^T P_h{}^T$$

$$= \sum_{n=0}^{N} \sum_{p,q,g,h=0}^{\infty} \frac{s_n M_{p+q+g+h\ n} (\pi B)^{p+q+g+h}}{(p+q+g+h)!} \binom{p+q+g+h}{q+h}\binom{p+g}{g}$$
$$\cdot \binom{q+h}{h} P_g Q_{pn} Q_{qn}{}^T P_h{}^T$$

$$= \sum_{g,h=0}^{\infty} B^{g+h} P_g \hat{R}_{gh} P_h{}^T \qquad (5A.18)$$

where

$$\hat{R}_{gh} = \sum_{p,q=0}^{\infty} B^{p+q} \binom{p+g}{g}\binom{q+h}{h} \sum_{n=0}^{N} s_n M^0_{p+g\ q+h}\ Q_{pn} Q_{qn}{}^T, \qquad (5A.19)$$
$$g,h=0,\cdots,\infty,$$

and

$$M^{O}_{ghn} = \frac{\pi^{g+h}}{g!h!} M_{g+h\ n} = \frac{\pi^{g+h}}{g!h!}\int_{-1}^{1} S_{On}(f) f^{g+h} df \qquad (5A.20)$$

after substituting (5.25). Clearly, $\hat{R}_{gh}$ is symmetrical and satisfies

$$\hat{R}_{gh} = \hat{R}_{hg}{}^{T}. \qquad (5A.21)$$

P_g, as given by (5.28) and (5A.9), obviously has dimension $(M-1)J \cdot 2(M-1)$ and with the Gram-Schmidt orthogonalization process, can be used to define a set of mutually orthogonal matrices:

$$U_g = \begin{cases} P_0, & g=0 \\ \prod_{h=1}^{g} [I - U_{h-1}(U_{h-1}{}^{T}U_{h-1})^{-1}U_{h-1}{}^{T}]P_g, & g=1,\cdot\cdot,\frac{J}{2}-1. \\ 0, & g=J,\cdot\cdot,\infty \end{cases} \qquad (5A.22)$$

Obviously, U_0, U_1, $\cdot\cdot$ and $U_{J/2-1}$ as defined here are the same as that given by (5.29) and (5.30) in section 5.3 and with each having full rank, have columns which together span the whole vector space. Hence, the definition, for notational convenience, of $U_{J/2}$, $U_{J/2+1}$, $\cdot\cdot$ being zero is necessary if U_0, U_1, $\cdot\cdot$ are to be mutually orthogonal. From (5A.22), P_g, $g=0,\cdot\cdot,\infty$, can be expressed as a linear combination of U_0, U_1, $\cdot\cdot$ and U_g:

$$P_g = \sum_{s=0}^{g} U_s G_{gs} \qquad (5A.23)$$

where

$$G_{gg} = I, \quad g=0,\cdot\cdot,\frac{J}{2}-1. \qquad (5A.24)$$

Therefore, substituting (5A.23), (5A.18) becomes

$$R = \sum_{g,h=0}^{\infty} \sum_{s=0}^{g} \sum_{t=0}^{h} B^{g+h} U_s G_{gs} \hat{R}_{gh} G_{ht}{}^{T} U_t{}^{T}. \qquad (5A.25)$$

Using the mathematical theorem (4.12) and then (5A.22), this gives rise to

$$R = \sum_{g,h=0}^{J/2-1} B^{g+h} U_g R^0_{gh} U_h^T \qquad (5A.26)$$

where

$$R^0_{gh} = \sum_{s,t=0}^{\infty} B^{s+t} G_{g+s}\, {}_g\hat{R}_{g+s\ h+t}\, G_{h+t}^T{}_h, \quad g,h=0,\cdot\cdot,\infty. \qquad (5A.27)$$

From (5A.21), R^0_{gh} clearly satisfies

$$R^0_{gh} = R^{0\,T}_{hg}. \qquad (5A.28)$$

Furthermore, from (5A.19) and (5A.24), (5A.27) becomes

$$R^0_{gh} \approx \frac{\pi^{g+h}}{g!h!} \sum_{n=0}^{N} s_n M_{g+h\ n} Q_{0n} Q_{0n}^T \qquad (5A.29)$$

should all higher order terms proportional to the first or higher powers of bandwidth be neglected. Evidently, (5A.26) and (5A.28) correspond to (5.27) and (5.35) respectively, whereas with the definition for Q_n, n=0,··,N, given by (5.31) and (5.32) being the same as that by (5A.2), (5A.7), (5A.10), (5A.14) and (5A.15) for Q_{0n}, (5A.29) corresponds to (5A.33).

5.9.2 The polar decomposition of R^p_{gh}

With Q_n, n=0,··,N, defined by (5.31), it is well known that the polar decomposition for R^0_{gh}, g,h=0,··,J/2-1, as given by (5.33), can be expressed in general as

$$R^0_{gh} \approx s_0 M^0_{gh0} EE^T + \sum_{n=1}^{N} c^0_{ghn} C^0_{ghn} C^{0\,T}_{ghn} \qquad (5A.30)$$

where the meaning of the various terms and factors are as described in subsection 5.4.2. In addition, however, C^0_{ghn}, n=1,··,N, has the form

$$C^0_{ghn} = \begin{bmatrix} a_1\cos b_1 & -a_1\sin b_1 \\ a_1\sin b_1 & a_1\cos b_1 \\ a_2\cos b_2 & -a_2\sin b_2 \\ a_2\sin b_2 & a_2\cos b_2 \\ \cdot & \cdot \\ \cdot & \cdot \\ a_{M-1}\cos b_{M-1} & -a_{M-1}\sin b_{M-1} \\ a_{M-1}\sin b_{M-1} & a_{M-1}\cos b_{M-1} \end{bmatrix} \qquad (5A.31)$$

which is very similar to that given by (5.31) for Q_n. From (5A.30), the polar decomposition for the inverse of R^0_{00} which, as discussed in section 5.3, has full rank is obviously

$$(R^0_{00})^{-1} \simeq \frac{EE^T}{s_0 M^0_{000}} + \sum_{n=1}^{N} \frac{C^0_{00n} C^{0\,T}_{00n}}{c^0_{00n}}. \qquad (5A.32)$$

By substituting (5A.30) and (5A.32), R^1_{gh}, g,h=1,··,J/2-1, as given by (5.38), is thus

$$\begin{aligned} R^1_{gh} \simeq\ & s_0 M^0_{gh0} EE^T + \sum_{n=1}^{N} c^0_{ghn} C^0_{ghn} C^{0\,T}_{ghn} \qquad (5A.33) \\ & - (s_0 M^0_{g00} EE^T + \sum_{n=1}^{N} c^0_{g0n} C^0_{g0n} C^{0\,T}_{g0n}) \\ & \cdot (\frac{EE^T}{s_0 M^0_{00n}} + \sum_{n=1}^{N} \frac{C^0_{00n} C^{0\,T}_{00n}}{c^0_{00n}})(s_0 M^0_{h00} EE^T + \sum_{n=1}^{N} c^0_{h0n} C^0_{h0n} C^{0\,T}_{h0n}). \end{aligned}$$

From the orthogonality of eigenvectors or more specifically, E being mutually orthogonal with C^0_{ghn}, g,h=0,··,J/2-1, this becomes

$$\begin{aligned} R^1_{gh} \simeq\ & s_0 M^0_{gh0} EE^T + [\sum_{n=1}^{N} c^0_{ghn} C^0_{ghn} C^{0\,T}_{ghn} - (\sum_{n=1}^{N} c^0_{g0n} C^0_{g0n} C^{0\,T}_{g0n}) \qquad (5A.34) \\ & \cdot (\sum_{n=1}^{N} \frac{C^0_{00n} C^{0\,T}_{00n}}{c^0_{00n}})(\sum_{n=1}^{N} c^0_{h0n} C^0_{h0n} C^{0\,T}_{h0n})], \quad g,h=1,\cdot\cdot,\frac{J}{2}-1, \end{aligned}$$

where

$$M^1_{gh0} = M^0_{gh0} - \frac{M^0_{g00} M^0_{h00}}{M^0_{000}}. \qquad (5A.35)$$

Clearly, with C^0_{00n} and C^0_{ghn} having the form of (5A.31), the square bracketed term is easily seen to have the form

$$\sum_{n=1}^{N} c^0_{ghn} c^0_{ghn} c^{0\ T}_{ghn} - \left(\sum_{n=1}^{N} c^0_{g0n} c^0_{g0n} c^{0\ T}_{g0n}\right) \qquad (5A.36)$$

$$\cdot \left(\sum_{n=1}^{N} \frac{C^0_{00n} C^0_{00n}}{c^0_{00n}}\right)\left(\sum_{n=1}^{N} c^0_{h0n} c^0_{h0n} c^{0\ T}_{h0n}\right) =$$

$$\begin{bmatrix}
a_{11} & 0 & a_{21}\cos b_{21} & a_{21}\sin b_{21} & a_{31}\cos b_{31} & a_{31}\sin b_{31} & \cdot & \cdot \\
0 & a_{11} & -a_{21}\sin b_{21} & a_{21}\cos b_{21} & -a_{31}\sin b_{31} & a_{31}\cos b_{31} & \cdot & \cdot \\
a_{21}\cos b_{21} & -a_{21}\sin b_{21} & a_{22} & 0 & a_{32}\cos b_{32} & a_{32}\sin b_{32} & \cdot & \cdot \\
a_{21}\sin b_{21} & a_{21}\cos b_{21} & 0 & a_{22} & -a_{32}\sin b_{32} & a_{32}\cos b_{32} & \cdot & \cdot \\
a_{31}\cos b_{31} & -a_{31}\sin b_{31} & a_{32}\cos b_{32} & -a_{32}\sin b_{32} & a_{33} & 0 & & \\
a_{31}\sin b_{31} & a_{31}\cos b_{31} & a_{32}\sin b_{32} & a_{32}\cos b_{32} & 0 & a_{33} & \cdot & \cdot \\
\cdot & \cdot & \cdot & \cdot & & & & \\
\cdot & \cdot & \cdot & \cdot & & & &
\end{bmatrix}.$$

Also, since C^0_{gh1}, C^0_{gh2}, $\cdot\cdot$ and C^0_{ghN} together span the same subspace as Q_1, Q_2, $\cdot\cdot$ and Q_N, so will the square bracketed term. Therefore, from (5A.34) and (5A.36), the polar decomposition for R^1_{gh} can be written as

$$R^1_{gh} = s_0 M^1_{gh0} E E^T + \sum_{n=1}^{N} c^1_{ghn} C^1_{ghn} C^{1\ T}_{ghn} \qquad (5A.37)$$

where c^1_{ghn} and C^1_{ghn} have meanings as described in subsection 5.4.2 and C^1_{ghn} also has the form of (5A.31). Evidently, the same arguments discussed can be used to find the polar decomposition of R^2_{gh}, g,h=2,$\cdot\cdot$,J/2-1, and so on, resulting in (5.43), (5.44) and the associated description in subsection 5.4.2.

5.9.3 <u>The upper bound on the trace of the transformed covariance matrix</u>

Using the mathematical theorem (3.14) and (5.77), the trace of the transformed covariance matrix can be obtained from (5.73) and (5.75) as

$$\mathrm{tr}\tilde{R} = \mathrm{tr}\left[(\hat{D}^T \times I)\begin{bmatrix} R^0_{00} & R^0_{01} & \cdots & R^0_{0\,J/2-1} \\ R^0_{10} & R^0_{11} & & \\ \vdots & & & \\ R^0_{J/2-1\,0} & & & \end{bmatrix}(\hat{D}\times I)\right]$$

$$= \mathrm{tr}\left[(\hat{D}\hat{D}^T \times I)\begin{bmatrix} R^0_{00} & R^0_{01} & \cdots & R^0_{0\,J/2-1} \\ R^0_{10} & R^0_{11} & & \\ \vdots & & & \\ R^0_{J/2-1\,0} & & & \end{bmatrix}\right]$$

$$= \sum_{g,h=0}^{J/2-1} [\hat{D}\hat{D}^T]_{g+1\ h+1}\, \mathrm{tr}R^0_{hg}. \qquad (5A.38)$$

From (5.79), $\hat{D}\hat{D}^T$ is easily seen to be given by

$$\hat{D}\hat{D}^T = M_0^{-1} \qquad (5A.39)$$

so that (5A.38) becomes

$$\mathrm{tr}\tilde{R} = \sum_{g,h=0}^{J/2-1} [M_0^{-1}]_{g+1\ h+1}\, \mathrm{tr}R^0_{hg}. \qquad (5A.40)$$

With M_0 given by (5.80), the (g+1,h+1) element of M_0^{-1} is obviously zero if g+h is odd. (5A.39) therefore becomes

$$\mathrm{tr}\tilde{R} = \sum_{g,h=0,\, g+h=\text{even}}^{J/2-1} [M_0^{-1}]_{g+1\ h+1}\, \mathrm{tr}R^0_{hg}. \qquad (5A.41)$$

From (5.34), M^0_{ghn}, n=0,··,N, g,h=0,··,J/2-1, is clearly greater than zero but less than or equal to 1 if g+h is even. Furthermore, M^0_{ghn} is equal to 1 if and only if the associated spectrum consists of only delta functions at either band edges. Evidently, $\mathrm{tr}R^0_{gh}$, from (5.33), is bounded, for small bandwidth and even g+h, by

$$0 \leq \mathrm{tr}R^0_{gh} \leq \frac{2(M-1)\pi^{g+h}}{g!h!} \sum_{n=0}^{N} s_n \qquad (5A.42)$$

where the upper bound is achieved if there is no receiver noise and all the jammers have spectrums given by delta functions at either band edges. Substituting (5A.42) into (5A.41), the trace

of the transformed covariance matrix is thus bounded by

$$\mathrm{tr}\tilde{R} \leq 2(M-1)\sum_{n=0}^{N} s_n\Big(\sum_{g,h=0,\,g+h=\text{even}}^{J/2-1} \frac{[M_0^{-1}]_{g+1\ h+1}\,\pi^{g+h}}{g!h!}\Big). \qquad (5A.43)$$

Using (5.80), the last bracketed factor has been found from computer simulation to be

$$\sum_{g,h=0,\,g+h=\text{even}}^{J/2-1} \frac{[M_0^{-1}]_{g+1\ h+1}\,\pi^{g+h}}{g!h!} = \frac{J^2}{4} \qquad (5A.44)$$

so that (5A.43) becomes (5.95) with equality under the condition stated.

REFERENCES

[1] B D STEINBERG, Principle of Aperture and Array System Design: including Random and Adaptive Arrays, Wiley 1976, ch.1-10.

[2] M T MA, Theory and Application of Antenna Arrays, Wiley 1974, ch.1-3.

[3] B D STEINBERG, Principle of Aperture and Array System Design: including Random and Adaptive Arrays, Wiley 1976, ch.11-14.

[4] R A MANZINGO and T W MILLER, Introduction to Adaptive Arrays, Wiley Interscience 1980.

[5] J E HUDSON, Adaptive Array Principles, Peter Peregrinus 1981.

[6] IEEE Trans. Antennas Propagat. (Special Issue on Adaptive Antennas), vol.AP-24, Sep.1976.

[7] W F GABRIEL, "Adaptive arrays - an introduction," Proc.IEEE, vol.64, pp.239-272, Feb.1976.

[8] A M VURAL, "An overview of adaptive array processing for sonar applications," IEEE EASCON Conv. Rec., pp.34A-34M, 1975.

[9] L C VAN ATTA, "Electromagnetic reflection," U.S.Patent 29080 02, 6 Oct.1959.

[10] IEEE Trans. Antennas Propagat. (Special Issue on Active and Adaptive Antennas), vol.AP-12, Mar.1964.

[11] D L MARGERUM, "Self-phased arrays," in Microwave Scanning Antennas, vol.3, R C Hansen, Ed. New York: Academic Press, 1966, ch.5.

[12] P W HOWELLS, "Intermediate frequency sidelobe canceller," U. S.Patent 3202990, 24 Aug.1965 (filed 4 May 1959).

[13] B WIDROW, "Adaptive filters," in Aspects of Network and System Theory, R E Kalman and N DeClaris, Eds. New York: Holt, Rinchart and Winston, 1971, ch.5.

[14] B WIDROW et al., "Adaptive noise cancelling: principles and applications," Proc.IEEE, vol.63, pp.1692-1716, Dec.1975.

[15] B WIDROW, P E MANTEY, L J GRIFFITHS and B B GOODE, "Adaptive antenna systems," Proc.IEEE, vol.55, pp.2143-2159, Dec.1967.

[16] R W LUCKY, "Automatic equalization for digital communication," Bell Syst. Tech. J., vol.44, pp.547-588, April 1965.

[17] F BRYN, "Optimum signal processing of three-dimensional arrays operating on Gaussian signals and noise," J. Acoust. Soc. Amer., vol.34, pp.289-297, March 1962.

[18] H MERMOZ, "Filtrage Adapte'et Utilization Optinale d'une Antenne," Proc. NATO Advanced Study Institute on Signal Processing, Grenoble, 1964.

[19] S W W SHOR, "Adaptive technique to discriminate against coherent noise in a narrowband system," J. Acoust. Soc. Amer., vol.39, pp.74-78, Jan.1966.

[20] J CAPON, R J GREENFIELD and R J KELLER, "Multidimensional maximum likelihood processing of a large aperture seismic array," Proc.IEEE, vol.55, pp.192-211, Feb.1967.

[21] R T LACOSS, "Adaptive combining of wideband array data for optimal reception," IEEE Trans. Goesci. Electron., vol.GE-6, pp.78-86, May 1968.

[22] L J GRIFFITHS, "A simple adaptive algorithm for real-time processing in antenna arrays," Proc.IEEE, vol.57, pp.1696-1704, Oct.1969.

[23] O L FROST, III, "An algorithm for linearly constrained adaptive array processing," Proc.IEEE, vol.60, pp.926-935, Aug.1972.

[24] C L ZAHM, "Effects of errors in the direction of incidence on the performance of an adaptive array," Proc. IEEE, vol.60, pp.1008-1009, Aug.1972.

[25] S P APPLEBAUM and D J CHAPMAN, "Adaptive arrays with main beam constraints," IEEE Trans. Antennas Propagat. vol.AP-24, pp.650-662, Sep.1976.

[26] K TAKAO, M FUJITA and T NISHI, "An adaptive antenna array under directional constraints," IEEE Trans. Antennas Propagat., vol.AP-24, pp.662-669, Sep.1976.

[27] J E HUDSON, "An adaptive array with tailored robustness," Proc. Institute of Acoustics Symposium on Adaptive Signal Processing, 14 June 1977, paper 3.1.

[28] C L ZAHM, "Application of adaptive arrays to surpress strong jammers in the presence of weak signals," IEEE Trans. Aerosp. Electron. Syst., vol.AES-9, pp.260-271, March 1973.

[29] R T COMPTON, Jr., "The power inversion array: concept and performance," IEEE Trans. Aerosp. Electron. Syst., vol.AES-15, pp.803-814, Nov.1979.

[30] S P APPLEBAUM, "Adaptive arrays," IEEE Trans. Antennas Propagat., vol.AP-24, pp.585-598, Sep.1976.

[31] L E BRENNAN and I S REED, "Theory of adaptive radar," IEEE Trans. Aerosp. Electron. Syst., vol.AES-9, pp.237-252, March 1973.

[32] L E BRENNAN, E L PUGH and I S REED, "Control-loop noise in adaptive array antennas," IEEE Trans. Aerosp. Electron. Syst., vol.AES-7, pp.254-262, March 1971.

[33] L E BRENNAN and I S REED, "Effect of envelope limiting in adaptive array control loops," IEEE Trans. Aerosp. Electron. Syst., vol.AES-7, pp.698-700, July 1971.

[34] R T COMPTON, Jr., "Improved feedback loop for adaptive arrays," IEEE Trans. Aerosp. Electron. Syst., vol.AES-16, pp.159-168, March 1980.

[35] W D WHITE, "Cascade preprocessors for adaptive antennas," IEEE Trans. Antennas Propagat., vol.AP-24, pp.670-684, Sep.1976.

[36] A CANTONI, "Application of orthogonal perturbation sequences to adaptive beamforming," IEEE Trans. Antennas Propagat., vol. AP-28, pp.191-202, March 1980.

[37] B WIDROW and J M MCCOOL, "Comparison of adaptive algorithms based on the methods of steepest descent and random search," IEEE Trans. Antennas Propagat., vol.AP-24, pp.615-637, Sep. 1976.

[38] S PRASAD, "Adaptive array processing of HF signals," First annual report on GCHQ contract F7A/156/75, Dept. Electronic Electrical Engineering, Loughborough University of Technology, U.K., Aug.1977.

[39] J E HUDSON, "A perturbation algorithm for adaptive antennas with a rapid analogue loop," Unpublished Report, Dept. Electronic Electrical Engineering, Loughborough University of Technology, U.K.

[40] I S REED, J D MALLETT and L E BRENNAN, "Rapid convergence rate in adaptive arrays," IEEE Trans. Aerosp. Electron. Syst., vol. AES-10, pp.853-863, Nov.1974.

[41] E B LUNDE, "The forgotten algorithm in adaptive beamformer," in Aspects of Signal Processing, part 2, G Tacconi, Ed. D. Reidel: Dordrecht - Holland, 1977, pp.411-421.

[42] J E HUDSON, "A Kalman-type algorithm for adaptive radar arrays and modelling of non-stationary weights," IEE Conference Publication no.180, pp.198-202, 1979.

[43] F F KRETSCHMER, Jr. and B L LEWIS, "A digital open-loop adaptive processor," IEEE Trans. Aerosp. Electron. Syst., vol.AES -14, pp.165-170, Jan.1978.

[44] J E HUDSON, "An adaptive antenna with computer assisted convergence," Proc. IEE Conf. Antennas Propagat., pp.46-50, London, Nov.1978.

[45] D J EDELBLUTE, J M FISH and G L KINNISON, "Criteria for optimal-signal-detection theory for arrays," J. Acoust. Soc. Amer., vol.41, pp.199-205, Jan.1967.

[46] L J GRIFFITHS, "A comparison of multidimensional Wiener and maximum-likelihood filters for antenna arrays," Proc.IEEE, vol.55, pp.2045-2047, Nov.1967.

[47] H S C WANG, "Interference rejection by amplitude shading of of sonar transducer arrays," J. Acoust. Soc. Amer., vol.61, pp.1251-1259, May 1977.

[48] C A BAIRD and G G RASSWEILER, "Adaptive sidelobe nulling using digitally controlled phase-shifters," IEEE Trans. Antennas Propagat., vol.AP-24, pp.638-649, Sep.1976.

[49] D J CHAPMAN, "Partial adaptivity for the large array," IEEE Trans. Antennas Propagat., vol.AP-24, pp.685-696, Sep.1976.

[50] D R MORGAN, "Patrially adaptive array techniques," IEEE Trans. Antennas Propagat., vol.AP-26, pp.823-833, Nov.1978.

[51] W D WHITE, "Adaptive cascade notwork for deep nulling," IEEE Trans. Antennas Propagat., vol.AP-26, pp.396-402, May 1978.

[52] C C KO, "Perturbation algorithms on the Davies beamformer," Proc. Institute of Acoustics Conf. Signal Processing in Underwater Acoustics, Loughborough University of Technology, U.K., 21-22 May 1980.

[53] T S DURRANI and N L M MURUKUTLA, "Multi-dimensional constrained lattice processor for passive arrays," Proc. NATO Advanced Study Institute on Signal Processing, Denmark, Aug.1980.

[54] R L REIGLER and R T COMPTON, Jr., "An adaptive array for interference rejection," Proc.IEEE, vol.61, pp.748-758, June 1973.

[55] D E SUSANS, "An adaptive receiving system for UHF television," BBC Engineering, pp.39-50, 1972.

[56] R T COMPTON, Jr., "An experimental four-element adaptive array," IEEE Trans. Antennas Propagat., vol.AP-24, pp.697-706, Sep.1976.

[57] R T COMPTON, Jr., "An adaptive array in a spread-spectrum communication system," Proc.IEEE, vol.66, pp.289-298, March 1978.

[58] R T COMPTON, Jr., "Multiplier offset voltage in adaptive arrays," IEEE Trans. Aerosp. Electron. Syst., vol.AES-12, pp.616-626, Sep.1976.

[59] D M DICARLO and R T COMPTON, Jr., "Reference loop phase shift in adaptive arrays," IEEE Trans. Aerosp. Electron. Syst., vol. AES-14, pp.599-607, July 1978.

[60] A D WHITE, "Artifical noise in adaptive arrays," IEEE Trans. Aerosp. Electron. Syst., vol.AES-14, pp.380-384, March 1978.

[61] A ISHIDE and R T COMPTON, Jr., "On grating nulls in adaptive array," IEEE Trans. Antennas Propagat., vol.AP-28, pp.467-475, July 1980.

[62] J D R KREMMER, "Adaptive antenna array processing: a study of weight error effects," IEE Conference Publication no.180, pp. 184-189, 1979.

[63] W E RODGERS and R T COMPTON, Jr., "Adaptive array bandwidth with tapped-delay-line processing," IEEE Trans. Aerosp. Electron. Syst., vol.AES-15, pp.363-373, May 1979.

[64] L J GRIFFITHS, "Time-domain adaptive beamforming of HF backscatter radar signals," in Aspects of Signal Processing, part 2, G Tacconi, ed. D. Reidel: Dordrecht - Holland, pp.443-453, 1977.

[65] C GIRAUDON, "Optimum antenna processing: a modular approach," in Aspects of Signal Processing, part 2, G Tacconi, ed. D. Reidel: Dordrecht - Holland, pp.401-410, 1977.

[66] W D WINDRAM, "Adaptive antennas for UHF broadcast reception," Proc. ERC Symposium on Adaptive Antenna Array Signal Processing, pp.30-35, May 1978.

[67] J E HUDSON, "The effect of signal and weight coefficient quantization in adaptive array processing," in Aspects of Signal Processing, part 2, G Tacconi, ed. D. Reidel: Dordrecht - Holland, pp.423-428, 1977.

[68] A M VURAL, "Effects of perturbations on the performance of optimum/adaptive arrays," IEEE Trans. Aerosp. Electron. Syst., vol.AES-15, pp.76-87, Jan.1979.

[69] H COX, "Sensitivity consideration in adaptive beamforming," Proc. NATO Advanced Study Institute on Signal Processing, Loughborough, 1972.

[70] R T COMPTON, Jr., "Pointing accuracy and dynamic range in a steered beam adaptive array," IEEE Trans. Aerosp. Electron. Syst., vol.AES-16, pp.280-287, May 1980.

[71] R NITZBERG, "Computational precision requirements for optimal weights in adaptive processing," IEEE Trans. Aerosp. Electron. Syst., vol.AES-16, pp.418-425, July 1980.

[72] D M BOROSON, "Sample size considerations for adaptive arrays," IEEE Trans. Aerosp. Electro. Syst., vol.AES-16, pp.446-451, July 1980.

[73] J T MAYHAN, "Some techniques for evaluating the bandwidth characteristics of adaptive nulling systems," IEEE Trans. Antennas Propagat., vol.AP-27, pp.363-373, May 1979.

[74] R A DOCTOR, W K MASENTEN and J F KINDEL, "Trends in adaptive antenna circuit design," Proc. ELECTRO 79, pp.1-9, New York.

[75] W K MASENTEN, "Adaptive signal processing," IEE Conference Publication no.180, pp.168-177, 1979.

[76] R T COMPTON, Jr., R J HUFF, W G SWARNER and A A KSIENSKI, " Adaptive arrays for communication systems: an overview of research at the Ohio State University," IEEE Trans. Antennas Propagat., vol.AP-24, pp.599-607, Sep.1976.

[77] B WIDROW, J MCCOOL, M G LARIMORE and C R JOHNSON, Jr., "Stationary and nonstationary learning characteristics of the LMS adaptive filters," in Aspects of Signal Processing, part 1, G Tacconi, Ed. D. Reidel: Dordrecht - Holland, pp.355-393, 1977.

[78] C C KO, "Power inversion array in a rotating source environment," IEEE Trans. Aerosp. Electron. Syst., vol.AES-16, pp.755 -762, Nov.1980.

[79] N R GOODMAN, "Statistical analysis based on a certain multivariate complex Gaussian distribution (an introduction)," Annals. Maths. Statistics, vol.34, pp.152-180, 1963.

[80] J H WILKINSON, The Algebraic Eigenvalue Problem, Oxford University Press 1965, ch.2.

[81] C C KO, "The jamming rejection capability of the broadband Frost power inversion array," Proc.IEE part F, vol.128, pp. 140-151, June 81.

[82] C C KO, "The convergence behaviour of the broadband Frost power inversion array," *Second Contract Report* to the Royal Aircraft Establishment, Dept. Electrical Electronic Eng., Loughborough University of Technology, U.K., Dec.1980.